Manoeuvring Model of a Container Vessel in Coastal Waves

Manoeuvreermodel van een containerschip in ondiepwatergolven

Manasés Tello Ruíz

Promotoren: prof. dr. ir. M. Vantorre, dr. ir. G. Delefortrie
Proefschrift ingediend tot het behalen van de graad van
Doctor in de ingenieurswetenschappen: maritieme techniek

UNIVERSITEIT
GENT

Vakgroep Civiele Techniek
Voorzitter: prof. dr. ir. P. Troch
Faculteit Ingenieurswetenschappen en Architectuur
Academiejaar 2017 - 2018

ISBN 978-94-6355-120-5
NUR 969
Wettelijk depot: D/2018/10.500/38

Examining Board:

- Supervisors:
  - prof. dr. ir. Marc Vantorre
    (Ghent University)
  - dr. ir. Guillaume Delefortrie
    (Flanders Hydraulics Research, Belgium)
- Chairman:
  - prof. dr. ir. Patrick De Baets
    (Ghent University)
- Secretary:
  - prof. dr. ir. Peter Troch
    (Ghent University)
- Other members (in alphabetical order):
  - prof. dr. Bettar O. el Moctar
    (University of Duisburg-Essen, Germany)
  - prof. dr. ir. Katrien Eloot
    (Ghent University)
  - prof. dr. ir. Mia Loccufier
    (Ghent University)
  - ir. Pierre Perdon
    (Direction générale de l'armement, France)

The present work has been performed in the frame of project WL_2013_47 (Scientific support for investigating the manoeuvring behaviour of ships in waves), granted to Ghent University by Flanders Hydraulics Research, Antwerp (Department of Mobility and Public Works, Flemish Government, Belgium).

For the numerical calculations a Hydrostar licence was put at the main author's disposal by Bureau Veritas through their Antwerp and Paris offices, which is highly appreciated.

Waterbouwkundig Laboratorium
Vlaanderen is wetenschap

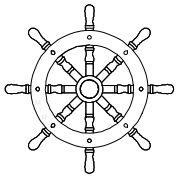

*There are only two mistakes one can make along the road to truth; not going all the way, and not starting.*

*Buddha*

# Preface

The present work summarises the last four years of research activities, constant questioning, searching for answers, learning and understanding the exciting and intrinsic world of ship hydrodynamics. The long days of running experiments and pencil leads broken while attempting to transcribe thoughts on white paper sheets (which later, most of them, turn into missiles heading towards the gash bin) have come to this very moment where these lines welcome you reader and thank you already for your natural interest.

The entire journey (or better say voyage) of research arrives now to its end with the present work. This would not have been possible without the support of Professor Marc Vantorre. To whom I cannot express only my gratitude for the given opportunity to pursue my doctoral degree but also for the enlightening discussions, comments, remarks and suggestions which enhanced every single part of the present work.

I owe a special word of gratitude to Dr. Guillaume Delefortrie for the extensive discussions during the course of the research study, for the interesting questions and meticulous remarks, and for being always ready to help as well as for the laborious work required to set and coordinate the experimental programs.

I wish to express my gratitude to the members of the jury for the consideration in taking the time out of their busy lives to take part on the journey of my doctoral degree, for their comments and suggestions to improve the context of the present work, and also for their willingness to share their knowledge and research concerns of the fascinating topic of manoeuvring in waves.

A major part of the present work includes experimental studies conducted at the Towing Tank for Confined Water at Flanders Hydraulic Research. The extensive program was diligently followed

by Mr. Luc Van Ostaeyen, to whom I thank for his enthusiasm to ensure the correct execution of the tests and for his willingness to help even if it required of him to be at work outside office hours.

The present work would not have been possible to complete without my UGent colleagues' support and collaboration. Thank you Maxim Candries and Marc Mansuy for the time shared at the office and for answering and discussing over any single question I might have. Thank you Evert Lataire, especially, for stressing the need to start writing the thesis which otherwise this very lines would have been written in a much later time. Thank you Ellen Vyncke, Thibaut Van Zwijnsvoorde, Luca Donatini, Ajie Pribadi, and Changyuan Chen for your always kind help and support.

To my (ex-)colleagues from Flanders Hydraulics Research, Emmanuel Cornet, Yvan Machiels, Jeroen Verwilligen, Stijn Vos, Stefan Geerts, Wim Van Hoydonck, and Sam Das, I am thankful for your research collaboration and cooperation as well as for your kind attention at my arrival and during my stay at FHR.

Finalmente, para ustedes mis queridos padres, hermanos, sobrinos y cuñados muchas gracias por el apoyo de siempre, por entender mis sueños y metas, y también por todas aquellas alegrías que me motivan día a día a salir a delante. Y especialmente para ti "manito" y "manita", muchas gracias por darme la oportunidad de empezar un nuevo camino en mi vida.

Finally, I wish you reader a pleasant navigation throughout the eight chapters of the book. In each chapter, you will always be welcomed on board with an eight-spokes steering wheel and thoughts that will envision you the chapter's knowledge.

Ghent, summer 2018,

Manasés

# Summary

The prediction of the ship's behaviour has always been a major focus of attention to the maritime sector, this in order to provide answers to questions regarding safety of the ship's crew and the ship itself. Throughout the ship's voyage from departure to arrival in a port, the ship will navigate, manoeuvre, under the effect of different environmental conditions such as, current, wind, waves, and shallow water, among others, the impact of which needs to be considered in the analysis.

To study the ship's behaviour it has been a common practice to separate the analysis in two different areas: the seakeeping problem and the manoeuvring problem. The first addresses the problem of ship responses to waves while navigating on a straight path in open sea; the second focuses on the behaviour of the ship in a more general curvilinear path and its ability to follow such a path in calm water. The combination of both, wave effects on the manoeuvring ship, has not been fully understood yet.

In close proximity to ports, the manoeuvring behaviour of deep drafted ships such as an Ultra Large Container Carrier (ULCC) will be influenced by shallow water effects. This is the case, for instance, when the ship approaches or leaves the port of Zeebrugge or the mouth of the Scheldt estuary giving access to the port of Antwerp or the harbour area of North Sea Port by the Scheur, the Wielingen and the Pas van het Zand access channels. Hence, manoeuvring in coastal waves is of major interest for Flanders Hydraulics Research in view of a realistic representation of manoeuvring behaviour in full mission bridge simulators.

The main objective of the present work is the development of a 6DOF manoeuvring model than can take into account the combined effect of shallow water and waves, with main focus of attention on an ultra large container vessel. In addition, the mathematical model should be suitable for implementation in the

ship manoeuvring simulators of Flanders Hydraulics Research. This requires a model running in real-time which includes phenomena such as short crested waves and squat effects.

A review of state of the art methods for manoeuvring in waves shows two different main approaches, the two-time scale method and the unified method. The first addresses the problem in a relatively simplified analysis: manoeuvring in waves is solved without any significant change on the manoeuvring model obtained for calm water, while waves are mainly accounted for as an external source of forces and moments. The second, on the other hand, requires a more comprehensive analysis of the hydrodynamic phenomena dominating manoeuvring in waves, as the aim is to unify the formulations addressing the combined hydrodynamic problems, while they are modelled differently in the seakeeping problem and the manoeuvring in calm water problem.

Since more realistic simulation scenarios are aimed at, the incorporation of the ship's vertical motions in the manoeuvring analysis is then necessary. Moreover, in a real, irregular sea scenario the ship's motion responses are not harmonically oscillating with a defined frequency. These requirements are all neglected in the two-time scale method and not in the unified methods. Hence, the present study further considers the unified method for the investigation of the manoeuvring in coastal waves problem.

Bear in mind that none of the works found in literature addresses the manoeuvring problem in waves in shallow water. Moreover with respect to the unified model, there are restrictions with respect to the forward speed dependent problem that limits its application. These are main topics which need further attention and better understanding for their modelling in a more general manoeuvring model which can account more rigorously for wave effects.

To proceed further with the study, it was necessary to restrict the analysis to the characteristics mostly encountered in coastal waves when approaching or leaving a port. To summarise, the main considerations taken into account:

- environmental conditions correspond to coastal waves;
- the ship will always move with positive longitudinal speed $u$, and positive propeller rates $n$;
- the ship speed $V$ can vary from low to intermediate speeds, e.g. Froude number $F_r < 0.125$;
- the lateral velocity $v$ of the ship will always be smaller in contrast to the longitudinal speed $u$. Thus, only small angles of drift will be considered, e.g. $|\beta| < 20$ deg.

To investigate the wave effects on manoeuvring, an extensive experimental investigation has been conducted at the Towing Tank for Manoeuvres in Confined Water at Flanders Hydraulics Research (in cooperation with Ghent University) with a scale model of an ultra large container vessel. The test program comprised semi-captive and fully captive model tests with and without waves. Harmonic yaw and steady straight line tests were conducted. Several model parameters were varied during the study, e.g. the water depth, the ship's draft, the ship's forward speed, the drift angle, the wave amplitudes and frequencies, the wave angles of encounter. Waves were selected to represent conditions commonly measured in the Belgian coastal zone of the North Sea.

From the experimental results, wave effects on the steady hull forces and moments were investigated. The effect of the hull drift angle on wave forces and moments was also considered. Further investigation took into account the evaluation of the superposition approach, in which forces and moments evaluated from manoeuvring in calm water model are superposed to respective ones obtained from the quasi-steady evaluation of the seakeeping problem. Moreover, the investigation of the propeller and rudder behaviour working under the effect of waves was also examined.

The experimental evaluation revealed (within the limits of the study) that the steady hull forces and moments as observed in calm water do not significantly change when studied in waves (especially at higher speeds). Wave forces and moments were found to be insignificantly affected when hull drift angles were considered, this for both, the first and mean second order effects. In the case of the mean second order effects, the influence of the ship motions and the ship's forward speed was found to be negligible for wave lengths smaller than $0.5L_{PP}$.

Results obtained from the experiments were also compared against numerical computations (carried out in Hydrostar). For the first order forces and moments insignificant improvements were found when the diffraction problem was included in the analysis. For the mean second order forces and moments, numerical estimations were found to agree well for wave lengths smaller than $0.4L_{PP}$ only. The superposition approach was also investigated; the results suggest that such approximation can be used for further evaluation of the ship manoeuvring in waves.

The unification of the hydrodynamic forces and moments as modelled in the seakeeping and the manoeuvring in calm water has also been studied. This has been conducted with main focus of attention to the radiation problem. Expressions relating the frequency dependent coefficients in manoeuvring and seakeeping have been derived. The final expressions of these relationships are given in the time domain as a form of impulse response function (IRF). An additional analysis has been conducted to solve the forward speed dependence problem of the IRF, which resulted in the division of the IRF in two sub IRFs, both speed independent.

Taking into account the observations mentioned above regarding wave forces and moments, the superposition approach, and the limits of the numerical method; a more suitable tool for the implementation of wave forces and moments aiming at simulation purposes has been developed. The method considers a constantly varying hull wetted surface which needs to be defined each time

step. For this purpose the hull surface is defined three-dimensionally by flat panels which are redefined each time step. The computations incorporate a nonlinear approach for the Froude-Krylov and hydrostatic forces and moments.

# Samenvatting

De voorspelling van het scheepsgedrag op zee is een uiterst belangrijk aandachtspunt van de maritieme sector, omwille van het rechtstreeks verband met de veiligheid van de opvarenden en van het schip zelf. Tijdens een scheepsreis van vertrek tot bestemming vaart en manoeuvreert het schip onder wisselende omgevingsomstandigheden en moet terdege rekening gehouden worden met de impact van stromingen, wind, golven, ondieptes.

Het is gebruikelijk om de studie van het scheepsgedrag op te splitsen in twee verschillende deelaspecten: het zeegangsgedrag en het manoeuvreergedrag. Het eerste behandelt het probleem van de responsie van het schip op golven terwijl het een rechtlijnig traject aflegt in open zee; het tweede focust op het gedrag van een schip om een gekromde baan en diens vermogen om een dergelijke baan te volgen in kalm water. De combinatie van beide, de invloed van golven op een manoeuvrerend schip, is nog steeds niet volledig doorgrond.

In de nabijheid van havens wordt het manoeuvreergedrag van diepgeladen schepen zoals een ULCC (Ultra Large Container Carrier) beïnvloed door ondiep-watereffecten. Dit is bijvoorbeeld het geval wanneer een schip vaart van of naar de haven van Zeebrugge, of de monding van de Westerschelde die toegang geeft tot de havens van Antwerpen en North Sea Port via de gebaggerde vaargeulen Scheur, Wielingen en Pas van het Zand. Het zijn dergelijke situaties die van belang zijn voor het Waterbouwkundig Laboratorium met het oog op een zo realistisch mogelijke weergave van het manoeuvreergedrag in brugsimulatoren.

De belangrijkste doelstelling van dit werk bestaat uit de ontwikkeling van een wiskundig manoeuvreermodel met zes vrijheidsgraden dat het gecombineerde effect van ondiep water en golven in rekening brengt, met de focus op de grootste containerschepen (ULCC's). Dit wiskundige model dient geschikt te

zijn voor implementatie in de scheepsmanoeuvreersimulatoren van het Waterbouwkundig Laboratorium. Dit vereist een model dat kan werken in reële tijd en fenomenen zoals kortkammige golven en squat-effecten aankan.

Uit een overzicht van de bestaande methodes voor manoeuvreren in golven blijkt dat er twee verschillende benaderingen in de literatuur te vinden zijn: de twee-tijdsschalenmethode (*two-time scale method*) en de gecombineerde methode (*unified method*). De eerste behandelt het probleem op basis van een relatief vereenvoudigde analyse: manoeuvreren in golven wordt aangepakt zonder noemenswaardige verandering aan het manoeuvreermodel voor kalm water, terwijl de golven beschouwd worden als een externe bron van krachten en momenten. De tweede aanpak daarentegen vereist een diepgaander analyse van de hydrodynamische fenomenen die het manoeuvreren van een schip in golven beheersen, daar het doel erin bestaat één enkele formulering voor het gecombineerde probleem op te stellen, in plaats van de afzonderlijke, afwijkende formuleringen voor beide deelproblemen.

Om meer realistische scenario's te kunnen simuleren dienen de verticale scheepsbewegingen verwerkt te worden in de manoeuvreeranalyse. Bovendien verlopen in realistische onregelmatige zeeën de scheepsresponsies niet harmonisch met een welbepaalde frequentie. Dergelijke vereisten worden in een twee-tijdsschalenmethode verwaarloosd, in tegenstelling tot de gecombineerde methode. De huidige studie zal zich bijgevolg verder toespitsen op de *unified method* voor het modelleren van manoeuvres in ondiep-watergolven.

Het dient benadrukt dat in de literatuur geen enkele bron scheepsmanoeuvres in ondiep-watergolven behandelt. Bovendien vertonen de beschreven gecombineerde modellen beperkingen met betrekking tot de voorwaartse snelheid van het schip. Deze beschouwingen verdienen de nodige aandacht bij het opstellen

van een algemener manoeuvreermodel dat op een afdoende wijze rekening houdt met golfeffecten.

De studie beperkt zich verder tot omstandigheden die zich voordoen in kustzones in toegangsgeulen tot havens, wat leidt tot de volgende beperkingen:

- als omgevingsfactoren wordt rekening gehouden met ondiep-watergolven;
- het schip beweegt steeds met positieve langsscheepse snelheid $u$, en positief schroeftoerental $n$;
- de scheepssnelheid $V$ kan variëren tussen lage en matige snelheden, met typische Froudegetallen $F_r < 0.125$;
- de dwarsscheepse snelheid $v$ van het schip is klein in verhouding tot de langsscheepse snelheidscomponent $u$. Bijgevolg nemen de drifthoeken beperkte waarden aan, typisch $|\beta| < 20$ deg.

Om de invloed van golven op manoeuvres te onderzoeken werd een uitgebreid experimenteel programma uitgevoerd op de Sleeptank voor Manoeuvres in Beperkt Water (samenwerking Waterbouwkundig Laboratorium – Universiteit Gent) met een schaalmodel van een ULCC (containerschip). Dit programma bevatte half-gedwongen en volledig gedwongen modelproeven met en zonder golven. Er werden zowel harmonische gierproeven als stationaire driftproeven uitgevoerd. Verscheidene parameters werden gevarieerd: de waterdiepte, de diepgang, de voorwaartse scheepssnelheid, de drifthoek, de golfamplitude en -frequentie, de invalshoek van de golven. De golfkarakteristieken werden geselecteerd in functie van het golfklimaat zoals waargenomen in het Belgische gedeelte van de Noordzee.

Op basis van de experimentele resultaten werd de invloed van golven op de stationaire krachten en momenten op de scheepsromp onderzocht. De invloed van de drifthoek op golfkrachten en -momenten werd eveneens in beschouwing genomen. Verder werd ook de geldigheid van het

superpositieprincipe onderzocht, dat ervan uitgaat dat krachten en momenten zoals ze zich voordoen in kalm water gesuperponeerd mogen worden op de krachten die volgen uit een quasi-stationaire benadering van het zeegangsprobleem. Bovendien werd ook de werking van roer en schroef onder golfactie onderzocht.

Binnen de beperkingen van het onderzoek toonden de experimentele resultaten aan dat de stationaire krachten en momenten in stil water niet significant veranderen onder invloed van de golven, vooral niet bij hogere snelheid. De golfkrachten en -momenten worden ook niet significant beïnvloed door drifthoeken, en dit geldt zowel voor effecten van eerste als van tweede orde. De invloed van scheepsbewegingen en de voorwaartse scheepssnelheid op de gemiddelde tweede-orde krachten bleek verwaarloosbaar van golflengten kleiner dan $0.5L_{pp}$.

De proefresultaten werden ook vergeleken met numerieke berekeningen uitgevoerd met Hydrostar. Voor de krachten en momenten van de eerste orde bleek de inbreng van het diffractieprobleem geen significante verbetering teweeg te brengen. Voor de gemiddelde krachten en momenten van tweede orde vertoonden numerieke resultaten enkel voor golflengten kleiner dan $0.4L_{pp}$ een goede overeenkomst. Het superpositieprincipe werd ook onderzocht; de resultaten suggereren dat een dergelijke aanpak gebruikt kan worden voor scheepsmanoeuvres in golven.

De gecombineerde aanpak van de hydrodynamische krachten en momenten in zeegang en tijdens manoeuvres werd eveneens onderzocht, met bijzondere aandacht voor het radiatieprobleem. Er werden uitdrukkingen afgeleid die het verband weergeven tussen frequentie-afhankelijke coëfficiënten voor zeegang en manoeuvreren. De uiteindelijke uitdrukkingen worden uitgedrukt in het tijdsdomein onder de vorm van impulsresponsfuncties (IRF). Een bijkomende analyse werd uitgevoerd om het probleem van de snelheidsafhankelijkheid van de IRF's op te lossen, wat uiteindelijk

leidde tot de opsplitsing van de IRF in twee sub-IRF's, die beide snelheidsonafhankelijk zijn.

Rekening houdend met de vermelde beschouwingen wat betreft krachten en momenten, het superpositieprincipe en de grenzen van het numerieke model, werd een geschikte berekeningstool ontwikkeld voor de implementatie van golfkrachten en -momenten in een manoeuvreersimulatiemodel. De methode neemt een permanent variërend nat oppervlak in beschouwing dat op elke tijdsstap gedefinieerd dient te worden. Daartoe wordt het oppervlak van de scheepsromp driedimensionaal gedefinieerd door vlakke panelen die bij elke tijdsstap geherdefinieerd worden. De berekeningen leiden tot het invoeren van niet-lineaire Froude-Krylov en hydrostatische krachten en momenten in de manoeuvreersimulaties.

# Table of Contents

# Nomenclature

## Latin alphabet

| | | |
|---|---|---|
| $\mathbf{A}$ | – | State matrix |
| $\boldsymbol{A_{jk}}$ | – | Generalised added inertia matrix |
| $\vec{\boldsymbol{a}}^{\boldsymbol{b}}_{\boldsymbol{P/O_0}}$ | (m/s²) | Linear ship's acceleration vector |
| $\boldsymbol{A_W}$ | (m²) | Waterplane area |
| $\mathbf{B}$ | – | State space input matrix |
| $\mathbf{B}$ | (m) | Ship's breadth |
| $\boldsymbol{B_{jk}}$ | – | Generalised damping matrix |
| $\mathbf{C}$ | – | State space output matrix |
| $\mathbf{C_B}$ | (–) | Block coefficient |
| $\boldsymbol{C_{DR}}$ | (–) | Rudder's drag coefficient |
| $\boldsymbol{C_{jk}}$ | – | Generalised restoring matrix |
| $\boldsymbol{C_{LR}}$ | (–) | Rudder's lift coefficient |
| $\mathbf{c_s}$, $\mathbf{c_\theta}$ | (–) | Squat sinkage and trim coefficients |
| $\mathbf{C_{33}}$ | (N/m) | Restoring coefficients in heave |
| $\mathbf{C_{44}}$ | (Nm) | Restoring coefficient in roll |
| $\mathbf{C_{55}}$ | (Nm) | Restoring coefficients in pitch |
| $\mathbf{D}$ | – | State space transmission matrix |
| $\mathbf{D}$ | (m) | Ship's depth |
| $\boldsymbol{D}$ | (m) | Propeller diameter |
| $\mathbf{ds}$ | (m²) | Infinitesimal surface area |
| $\vec{\boldsymbol{F}}$ | (N) | Force vector |
| $\mathbf{f}$ | (Hz) | Frequency |
| $\boldsymbol{F_j}$ | – | Generalised wave forces |
| $\boldsymbol{F_{NR}}$ | (N) | Rudder normal force |
| $\boldsymbol{F_{TR}}$ | (N) | Rudder tangential force |
| $\mathbf{F_r}$ | (–) | Froude number |
| $\boldsymbol{F_{r_h}}$ | (–) | Froude depth based number |
| $\mathbf{g}$ | (m/s²) | Gravity constant of the Earth |
| $\overline{\boldsymbol{GM}}$ | (m) | Transverse metacentre height |
| $\overline{\boldsymbol{GM}}_{\boldsymbol{L}}$ | (m) | Longitudinal metacentre height |
| $\vec{\boldsymbol{H}}$ | (kgm²/s) | Angular momentum vector |
| $\mathbf{H^V}$ | – | Speed dependent impulse response functions |

| | | |
|---|---|---|
| $H^*$, $H$ | – | Speed independent impulse response functions |
| $H_R$ | (m) | Rudder height |
| Hs | (m) | Significant wave height |
| $I, J, K$ | (–) | Unitary vectors in the E-frame |
| $\hat{i}', \hat{j}', \hat{k}$ | (–) | Unitary vectors in the h-frame |
| $\hat{i}, \hat{j}, \hat{k}$ | (–) | Unitary vectors in the b-frame |
| $J$ | (–) | Advance coefficient |
| K | (Nm) | Roll moment |
| k | (–) | Wave number |
| $K_T$ | (–) | Thrust coefficient |
| $K_Q$ | (–) | Torque coefficient |
| Kv | (Nm) | Viscous roll moment |
| $Kv_p$ | ($kgm^2/s$) | Linear viscous coefficient |
| $Kv_{p\|p\|}$ | ($kgm^2$) | Nonlinear viscous coefficient |
| LOA | (m) | Length overall |
| LCF | (m) | longitudinal centre of flotation |
| $L_{PP}$ | (m) | Length between perpendiculars |
| M | (Nm) | Pitch moments |
| $\vec{M}$ | (Nm) | Moment of force vector |
| m | (kg) | Ship's mass |
| $M_{jk}$ | – | Generalised inertia matrix |
| N | (Nm) | Yaw moments |
| $n$ | (rev/s) | Propeller rate |
| $O$ | – | Big O notation |
| $O' - x'y'z'$ | (–) | Horizontal axes system, h-frame |
| $O - xyz$ | (–) | Body bound axes system, b-frame |
| $O_0 - X_0 Y_0 Z_0$ | (–) | Earth bound axes system, E-frame |
| $O_R - x_R y_R z_R$ | (–) | Rudder bound axes system, R-frame |
| $P, Q, R$ | (rad/s ) | Roll, pitch, and yaw angular velocities in the E-frame |
| $\vec{P}$ | (kgm/s) | Linear momentum vector |
| $p, q, r$ | (rad/s) | Roll, pitch, and yaw angular velocities in the b-frame |
| $Q$ | (Nm) | Propeller Torque |
| $R$ | (–) | Euler rotation matrix |
| $\vec{r}$ | (m) | Position vector |
| $R_{xx}$ | (m) | Roll radius of inertia |

| | | |
|---|---|---|
| $\mathbf{R_{yy}}$ | (m) | Pitch radius of inertia |
| $\mathbf{R_{zz}}$ | (m) | Yaw radius of inertia |
| $\boldsymbol{S}$ | ($m^2$) | Actual hull wetted surface |
| $\boldsymbol{S_0}$ | ($m^2$) | Mean wetted surface |
| $\mathbf{S_\zeta}$ | – | Directional wave spectrum. |
| $\boldsymbol{t}$ | (–) | Thrust deduction fraction |
| $\boldsymbol{T}$ | ($kgm^2/s^2$) | Kinetic energy of the fluid |
| $\boldsymbol{T}$ | (N) | Propeller thrust |
| $\boldsymbol{T_{jk}}$ | – | Generalised radiation forces and moments in the $j$th mode per unit motion in the $k$ mode. |
| $\mathbf{T_M}$ | (m) | Draft at midship |
| $\boldsymbol{T_{u_h}}$ | (–) | Tuck's parameter |
| $\mathbf{Tz}$ | (s) | Zero crossing wave period |
| $\mathbf{T_\zeta}$ | (s) | Wave period |
| $\vec{\boldsymbol{V}}$ | (m/s) | Linear ship's velocity vector |
| $\boldsymbol{U, V, W}$ | (m/s) | Surge, sway and heave linear velocities in the E-frame |
| $\boldsymbol{u, v, w}$ | (m/s) | Surge, sway and heave linear velocities in the b-frame |
| $\boldsymbol{V_R}$ | (m/s) | Inflow velocity at the rudder |
| $\boldsymbol{w_T}$ | (–) | wake fraction by thrust identity |
| $\mathbf{W_T}$ | (m) | Width of the towing tank |
| $\boldsymbol{w_Q}$ | (–) | wake fraction by torque identity |
| $\mathbf{X}$ | (N) | Surge forces |
| $\mathbf{X}$ | – | State space variable |
| $\mathbf{Y}$ | (N) | Sway forces |
| $\mathbf{Z}$ | (N) | Heave forces |

## Greek alphabet

| | | |
|---|---|---|
| $\vec{\boldsymbol{\alpha}}$ | ($rad/s^2$) | Angular acceleration vector |
| $\boldsymbol{\alpha_R}$ | (deg) | Effective rudder angle |
| $\boldsymbol{\alpha_W}$ | (deg) | Phase angle of the incident wave |
| $\boldsymbol{\beta}$ | (deg) | hull drift angle |
| $\boldsymbol{\beta, \gamma, \chi}$ | (deg) | Hydrodynamic angles |
| $\boldsymbol{\Xi}$ | (rad) | Linear Euler angles |
| $\boldsymbol{\epsilon}$ | (–) | small order of magnitude where $\epsilon \ll 1$. |
| $\boldsymbol{\delta_R}$ | (deg) | Rudder angles |

| | | |
|---|---|---|
| $\boldsymbol{\Delta}$ | (N) | displacement |
| $\boldsymbol{\xi_1, \xi_2, \xi_3}$ | (m) | Surge, sway and heave motions in the h-frame |
| $\boldsymbol{\xi_4, \xi_5, \xi_6}$ | (deg) | Roll, pitch, and yaw motions in the h-frame |
| $\boldsymbol{\eta}$ | (deg) | The wave angle relative to the E-frame |
| $\boldsymbol{\eta^*}$ | (-) | Propeller diameter to rudder height ratio |
| $\boldsymbol{\lambda}$ | (m) | Wave length |
| $\boldsymbol{\mu}$ | (deg) | Angle of wave encounter |
| $\boldsymbol{\vec{\nabla}}$ | (-) | Gradient vector |
| $\boldsymbol{\nabla}$ | ($m^3$) | Ship's volume of water displacement |
| $\boldsymbol{\omega_E}$ | (rad/s) | Frequency of wave encounter |
| $\boldsymbol{\omega_W}$ | (rad/s) | Wave frequency |
| $\boldsymbol{\omega_0}$ | (rad/s) | Incident wave frequency |
| $\boldsymbol{\phi, \theta, \psi}$ | (rad) | Roll, pitch and yaw Euler angles |
| $\boldsymbol{\Phi}$ | ($m^2/s$) | Velocity potential |
| $\boldsymbol{\phi_T}$ | ($m^2/s$) | Unsteady velocity potential |
| $\boldsymbol{\phi_I}$ | ($m^2/s$) | Incident wave potential |
| $\boldsymbol{\phi_D}$ | ($m^2/s$) | Diffraction potential |
| $\boldsymbol{\phi_j}$ | ($m^2/s$) | Radiation potential |
| $\boldsymbol{\psi}$ | (deg) | Ship's heading angle |
| $\boldsymbol{\psi_A}$ | (deg) | Amplitude of the harmonic oscillation test |
| $\boldsymbol{\psi_T}$ | (deg) | Period of the harmonic oscillation test |
| $\boldsymbol{\rho}$ | ($kg/m^3$) | Density of the water |
| $\boldsymbol{\Theta}$ | (rad) | Euler angles |
| $\boldsymbol{\zeta_\omega}$ | (rad/s) | Wave frequency |
| $\boldsymbol{\zeta_a}$ | (m) | Wave amplitude |
| $\boldsymbol{\omega_0}$ | (rad/s) | Wave frequency |
| $\boldsymbol{\omega}$ | (rad/s) | Frequency of oscillation |
| $\boldsymbol{\vec{\Omega}}$ | (rad/s) | Angular velocity vector |

## Subscripts:

| | |
|---|---|
| *AW* | Added wave resistance |
| *D* | Drag |
| *D* | Diffraction |
| *D* | Mean second order wave (drift ) effects |
| *Ext* | External effects |
| *FK* | Froude-Krylov forces and moments |
| *G* | Ship's centre of gravity |
| *H* | Hull |
| *hyd* | Hydrostatic |
| *id* | Ideal fluid |
| *L* | Lift |
| *P* | Propeller |
| *R* | Rudder |
| *R* | Ship's resistance |
| *ret* | Retardation |
| *T* | Tangential |
| *N* | Normal |
| *2nd* | Second order wave forces and moments |

## Accents:

| | |
|---|---|
| $\dot{}$ | Time derivative |
| $\sim$ | Oscillatory frequency dependent |
| $\rightarrow$ | Vector |

## Superscripts:

| | |
|---|---|
| *b* | Body axes frame |
| *E* | Earths axes frame |
| *h* | Horizontal axes frame |
| *T* | The transpose of a matrix |
| $\infty$ | Infinity |

Abbreviations:

| | |
|---|---|
| ***AIS*** | Automatic Identification System |
| ***BVP*** | Boundary Value Problem |
| ***CFD*** | Computational Fluid Dynamics |
| ***CW*** | Calm Water |
| ***EFD*** | Experimental Fluid Dynamics |
| ***FFT*** | Fast Fourier Transformation |
| ***FHR*** | Flanders Hydraulics Research |
| ***Hs*** | Hydrostar |
| ***IRF*** | Impulse Response Function |
| ***ITTC*** | International Towing Tank Conference |
| ***KVLCC2*** | KRISO Very Large Crude Carrier 2 |
| ***LC*** | Load Cell |
| ***NED*** | North-East-Down |
| ***P*** | Potentiometer |
| ***PIANC*** | Permanent International Association for Navigation Congresses (The World Association for Waterborne Transport Infrastructure) |
| ***PMM*** | Planar Motion Mechanism |
| ***RW*** | Regular Waves |
| ***S*** | Strain gauge |
| ***SRC*** | Scheldt Radar Chain |
| ***SS*** | State Space |
| ***St*** | Steady straight line test |
| ***UKC*** | Under Keel Clearance |
| ***ULCC*** | Ultra Large Container Carrier |
| ***WG*** | Wave Gauge |
| ***3D*** | Three-dimensional |
| ***2D*** | Two-dimensional |
| ***3DOF*** | Three degrees of freedom |
| ***4DOF*** | Four degrees of freedom |
| ***6DOF*** | Six degrees of freedom |

# MANOEUVRING IN COASTAL WAVES



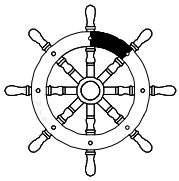

*It is not because things are difficult that we dare not venture. It is because we dare not venture that they are difficult*.

*Seneca*

# 1

# Introduction

## 1.1 The research context

### 1.1.1 Two different paths to study the ship behaviour

The understanding and prediction of the ship response to its environmental conditions has always been a major question of interest to the maritime sector, mainly because of the concern regarding the safety of the ship's crew and the ship itself. In the lifetime operation of the ship, it will be subjected to effects such as wind, current, and waves which will in overall impair the ship's navigability and increase the probability of hazardous conditions. Moreover, if one considers the scenarios of confined waters, the limited water depth then becomes also an important constraint because of shallow water effects.

The complex nature of the fluid phenomena involved in the general analysis of the ship's hydrodynamics, to some extent, requires then a level of simplification. This has been achieved by taking into account the different ship's behaviour observed at open sea and in restricted waters. See for example the different character of trajectories developed by ships in each independent scenario as shown in Figure 1.1 and Figure 1.2, respectively. In

open seas a straight line path of the voyages are observed, while in restricted waters the ship trajectories are generally curvilinear. This clear distinction between the ship's behaviour lead to a subdivision of the problem in two independent fields, the fields of seakeeping and the field of manoeuvring.

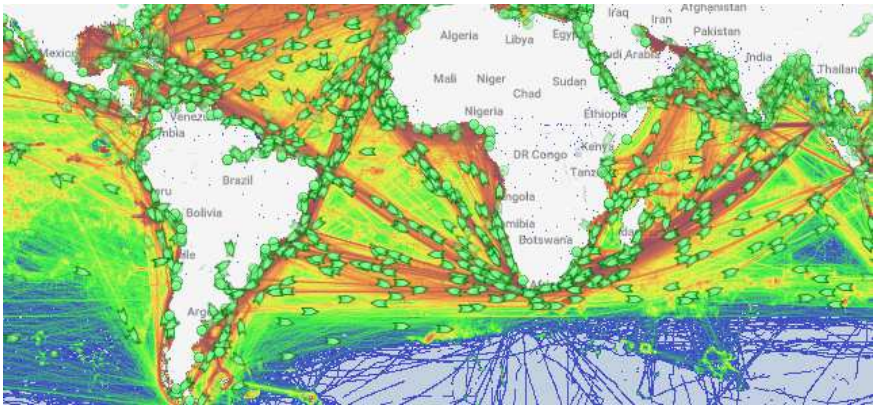


Figure 1.1 Density map of marine traffic of ships (green arrow markers) across the Atlantic and Indian Ocean. Trajectories are mostly in a straight line. The intensity of the traffic is depicted by the colours scale varying from red to green for more to less dense traffic, respectively.

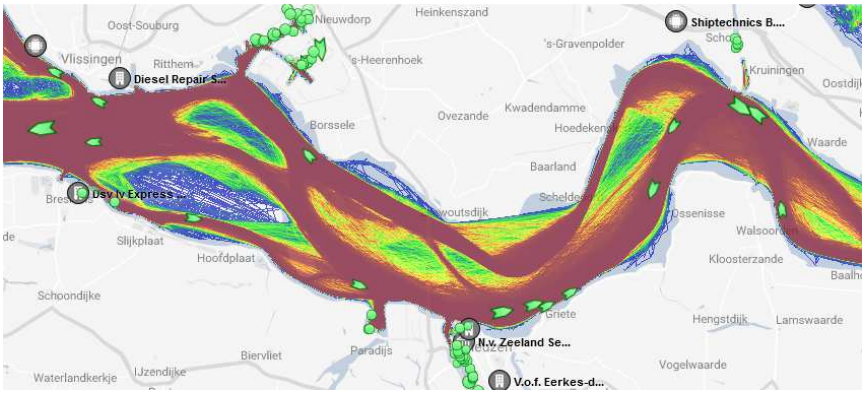


Figure 1.2 Density map of marine traffic of ships (green arrow markers) across the Scheldt River in the Netherlands and Belgium. Ship trajectories are mostly curvilinear with river bends as main obstacles. The intensity of the traffic is depicted by the colours scale varying from red to green for more to less dense traffic, respectively.

Seakeeping studies consider the ship sailing in open sea with a constant forward speed, constant heading, and under the effect of waves. Propeller and rudder effects are neglected from the analysis. The hydrodynamic problem, and the respective forces and moments, are then considered to be dependent only on the hull forms, the ship speed, and the wave main characteristics. Because of the dominant effects of waves, viscous effects are neglected (further corrections are required especially for roll motion) and the study is further conducted by using potential theory. Seakeeping studies are mostly carried out in the frequency domain, assuming only regular waves, and are related to the actual seas by means of spectral analysis as proposed in St. Denis and Pierson (1953).

Taking into account the calm water restriction, in manoeuvring studies the ship is assumed to move horizontally only. This simplified the study from a general six-degrees of freedom (6DOF) to a more simple three-degrees of freedom (3DOF). Surge, sway and yaw motions are mostly considered, extension to a 4DOF analysis, including roll motion can also be found in literature. Propeller and rudder effects are important, hence they are accounted for. Although a 3DOF analysis simplifies the problem greatly, the hydrodynamic study still remains complex. Forces and moments are dependent on different phenomena among then the most important, viscous, lift, cross flow effects, and resistance.

In manoeuvring in calm water further considerations are still necessary to reduce the complexity of the hydrodynamic problem. This is the main reason why mathematical models have been developed specifically suited for particular purposes, for instance, in literature models suited for different forward speed ranges or as function of the drift angle can be found. An example of the large variety which can be encountered in literature are the models in Norrbin (1971), Oltmann and Sharma (1984), and Kobayashi (1987). For a more extensive discussion on the type of models and their selection, the reader is referred to the work in Eloot (2006).

### 1.1.2 The need for a more realistic scenario

The clear subdivision of the ship's hydrodynamic problem in two separate analyses, seakeeping on one hand and manoeuvring in calm water on the other, is not always possible. This is especially the case when the ship manoeuvres in coastal zones approaching or leaving a port, being subjected to incident waves. Manoeuvring in such condition is by no means similar to the one in calm water, however, for simplicity in the analysis, it has been commonly accepted to neglect the effect of waves.

A common scenario where the ship manoeuvres in waves can be found, for instance, when the ship approaches or leaves the port of Zeebrugge or the mouth of the Scheldt estuary giving access to the port of Antwerp or the harbour area of North Sea Port by the Scheur, the Wielingen and the Pas van het Zand access channels, see Figure 1.3.

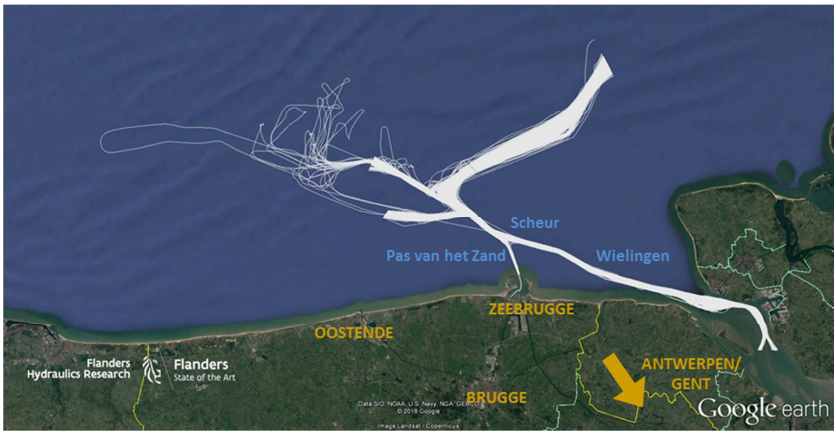


Figure 1.3 View of ships main trajectories when approaching or leaving the ports of Antwerp and Zeebrugge by the access channels of the Scheur, Wielingen and Pas van het Zand. Adapted from Verwilligen et al. (2014).

Manoeuvring in such scenarios will be, in addition, subjected to shallow water effects due to the limited water depths. This is especially the case for Ultra Large Container Carriers (ULCC) which is the type of ship studied in the present work (see Figure 1.4 and Figure 1.5).

Taking into account the water depth restrictions in combination with wave effects can result in critical hazardous conditions, such as increasing the bottom touching probability. Moreover, wave effects could alter the ship manoeuvring characteristics observed in calm water, such as directional stability and the turning ability.

Therefore implementation of wave effects in the manoeuvring analysis is relatively important, not only from the point of view of safety, design and feasibility studies, but also from the point of view of training activities in simulators which require always more realistic scenarios.


Figure 1.4 Morten Maersk Triple-E class ULCC arriving to the port of Antwerp on January 2015 (photo retrieved from maritiemnieuws.nl).


Figure 1.5 The ULCC CMA CGM Antoine de Saint Exupéry, expected to arrive in the port of Zeebrugge on 24 March 2018 (photo retrieved from www.meretmarine.com).

### 1.1.3 Research opportunities

The study of wave effects on ship manoeuvring has recently received more attention. To the author's best knowledge, one of the first works addressing the subject was presented by Hirano et al. (1980), Ankudinov (1983), and later by McCreight (1986). More recent works are, to cite few, Bailey et al. (1998), Yasukawa (2006a), Sutulo and Guedes Soares (2006a), Skejic and Faltinsen (2008), Seo and Kim (2011), and Zhang et al. (2017). For a more extensive discussion the reader is referred to Chapter 3.

When the ship manoeuvres in waves, it will in general be subject to two types of forces and moments: the first one is an oscillating excitation while the second one is a steady contribution. They are commonly referred to as the first order effects and the mean second order effects, respectively. The names assigned are related to the level of approximation in the solution of the numerical calculation of potential theory. For purposes of brevity, this will not be further discussed in here, but the reader can consult Chapter 2 for more insight on this topic.

From the literature review, it can be observed that when dealing with the problem of manoeuvring in waves, mostly the main focus of attention is with respect to the mean second order wave forces and moments. Such steady effects will displace the ship from its expected course in calm water, as was observed by Hirano et al. (1980) and Yasukawa (2006a) in their studies with free running model test in waves. Because of their relative importance, the mean second order wave effects have been extensively studied during the last decade. This has been conducted mainly with numerical methods arising from potential theory developed for seakeeping studies. However, it is important to stress that in literature, only a limited number of experimental studies have been performed to validate such methodologies.

Another common approach on the analysis of manoeuvring in waves is that only few consider it as a full 6DOF problem (e.g. Ankudinov, 1983; and Bailey et al., 1998). In fact, almost no

current studies have addressed the problem as such, and most works use only a 4DOF manoeuvring model (see, Seo and Kim, 2011; Zhang et al. 2017). The vertical excitations on the manoeuvring analysis are neglected or solved partly in parallel quasi steady seakeeping evaluations. To the author's opinion, this can be mainly addressed to the deep water characteristics assumed in their analysis; which if neglected, can substantially simplify the manoeuvring analysis.

When considering full 6DOF, as shown in Ankudinov (1983), and Bailey et al. (1998), the complexity of the problem is significantly increased. The ship oscillatory motions are then considered, which bring additional questions regarding the ship's wave generation problem (radiation problem), an effect that is generally neglected in calm water manoeuvring models. Although their analysis was more correct, some simplifications were considered. In Ankudinov (1983) the radiation problem was simplified by assuming a polynomial expansion as a function of the encounter frequency; similar assumption were conducted for the first order and second order effects. In Bailey et al. (1998) a more accurate treatment of the radiation problem was introduced by convolution integral terms (see, Cummins, 1962), but with respect to wave exiting forces and moments, only first order effects were considered.

It is important to mention that in spite of the aimed more accurate treatment of the radiation problem in the studies of Ankudinov (1983), and Bailey et al. (1998), the forward speed dependence of the radiation problem will be a major constraint to its applicability. As mentioned by Skejic and Faltinsen (2008), because of the speed loss experienced while manoeuvring, the radiation problem will require a continuous evaluation which would impair the numerical simulation. To overcome this problem, in Ankudinov (1983) the speed dependence has been neglected because of the low speeds considered in his study. In Bailey et al. (1998) this was not further discussed because a constant forward speed was assumed.

From the literature study, some additional observations can be made:

- none of studies take into account the restriction of finite water depths. Shallow water effects might be an important constraint in the analysis considering access channels such as the ones of the Belgian coast of the North Sea (see Figure 1.3) and the dimensions of ULCC ships;
- in spite of the introduction of advanced methods for the mean second order wave effects, their validation against experimental results is rather scarce;
- there are few studies addressing the effects of waves on the propeller and rudder behaviour;
- in general there is a lack of experimental studies on the effect of the waves on the manoeuvring forces on the hull.

An additional remark which can be made is regarding the simplifications assumed for the speed dependence of the radiation problem. For a manoeuvring ship in a real sea scenario this might be an important constraint to its incorporation in the analysis because of the speed loss caused by manoeuvring.

It is also important to stress that in spite of the relevance of the steady effects of waves on manoeuvring, accounting only for them and neglecting other effects such as the induced harmonic motions and forces might be insufficient. As mentioned earlier, for instance, in coastal areas characterised by limited water depths and channel widths as well as by the dense traffic at the entrance to ports, motion responses represent an important constraint to safe ship operations. Therefore they must be accounted.

Bear in mind that research works on the topic of manoeuvring in waves in shallow water are rather scarce. Such a combination is undoubtedly a new discipline that requires further attention.

### 1.1.4 Research studies at FHR and UGent

Manoeuvring studies, with especial attention to shallow water, have been a main focus of studies at Flanders Hydraulics Research (FHR), in Antwerp, Belgium, in close cooperation with the Maritime Technology Division of Ghent University.

Different topics of research concerning manoeuvring in calm water have been addressed during the last decades, for instance, on "the accuracy consideration and optimisation when selecting captive manoeuvres test with ship models" in Vantorre (1989), on "the selection, experimental determination and evaluation of a mathematical model for ship manoeuvring in shallow water" in Eloot (2006), on the "evaluation of manoeuvring behaviour of container vessel in muddy navigation areas" in Delefortrie (2007), and on the "experiment based mathematical modelling of ship-bank interaction" in Lataire (2014).

Bear in mind that at Flanders Hydraulics Research, the evaluation of a ship's seagoing behaviour in Belgian coastal zone of the North Sea has also been conducted. For instance, in Vantorre and Journee (2003), the validation of seakeeping code in very shallow water has been studied; and in Vantorre et al. (2012), a probabilistic study for risk analysis for adverse events such as slamming, overtaking of water on board, etc., have been investigated for so-called estuary vessels. As the main purpose of these works, however, was to evaluate the seakeeping behaviour of ships, no particular attention was drawn to the effect of waves on the manoeuvring problem.

The influence of waves on manoeuvring is recognised without doubt as a new research topic that needs to be addressed at Flanders Hydraulics Research. This is mainly because ships in the approach channels to the ports of Antwerp and Zeebrugge (Figure 1.3) already manoeuvre under the presence of wave actions.

Research activities on this topic are currently being addressed at FHR in the project WL_2013_47 (Scientific support for investigating the manoeuvring behaviour of ships in waves), which has been

granted to Ghent University by Flanders Hydraulics Research, Antwerp (Department of Mobility and Public Works, Flemish Government, Belgium). The present work has been conducted within the frame of this project.

## 1.2 Objectives of the present work

### 1.2.1 Main Objective

From the discussion in the section above it can be observed that to incorporate wave effects into the analysis of manoeuvring is a fairly new discipline that still mainly is in a research and development phase. Research topics on this problem are even scarcer in literature if one considers a 6DOF manoeuvring problem in combination with shallow water. Taking into account these research opportunities, the main objective of the present work is the development of a 6DOF manoeuvring model than can take into account the combined effect of shallow water and waves. In addition, the mathematical model should be suitable for implementation in the simulators of Flanders Hydraulics Research.

It is important to mention that the wave climate in the Belgian coastal area of the North Sea is in general characterized by moderate wave heights. In addition, shipping traffic is interrupted in very adverse weather conditions. Hence, extreme wave events are therefore not the subject of the present study.

### 1.2.2 Secondary objectives

#### *1.2.2.1Experimental studies*

From the literature review, it has also been observed that mostly studies have been validated against results obtained from free running model tests. Forces and moments, however, have only been compared independently against experimental results obtained from manoeuvring in calm water or seakeeping, and not with tests in manoeuvring in waves.

The limited number of available experiments is not really surprising considering the large number of parameters involved, such as the ship's speed, water depth, the frequency and amplitude of waves, the ship's motions, etc. Taking into account these limitations, the present work aims to provide a significant amount of test results that can be used for better understanding of the wave induced phenomena on the manoeuvring problem, and also for further validation of the mathematical models.

For this purpose the experimental study will be conducted with a scale model of an ULCC container ship at the Towing Tank for Manoeuvres in Confined Water (TTCW) at Flanders Hydraulics Research. Tests comprise semi-captive and fully captive tests, both executed at different ship's forward speeds with and without waves, in head and following waves, with and without drift angle. Propeller and rudder action will be also investigated under the influence of waves.

During the tests, forces and moments will be measured in all directions. In addition, wherever possible, the motion responses and the propeller and rudder performance in waves will be evaluated.

#### *1.2.2.2Validation of numerical methods*

For the purpose of the implementation of wave exciting forces and moments, the estimation of the first order as well as the second order effects by numerical methods must be validated against the experimental results. This is especially the case for the second order effects which require more specialised approaches such as the 3D potential panel methods.

The limitations of the numerical methods when drift angles are accounted for, which are commonly observed while manoeuvring, questions their indiscriminate use in the analysis. It is then of relevance to investigate their applicability against the experimental results from model tests. In the present work, the numerical computation of motions, first and mean wave drift forces and moments will be obtained from Hydrostar mostly, which is a 3D boundary element method that incorporates the speed effects by employing the so-called "encounter-frequency" approximation based on the use of the Green function associated to the encounter frequency, see Bureau Veritas (2012).

#### *1.2.2.3Investigation on the superposition principle*

In literature, in spite of the significant differences encountered within the studies, a general consensus has been observed to assume that the wave forces and moments can be simply added as

an external effect in the manoeuvring model. This is the so-called "superposing approach", the investigation of which will also be a major objective of research in the present study. The evaluation of such method will be conducted by comparing models tests results and using numerical estimations from potential theory.

#### *1.2.2.4Numerical studies for the radiation problem*

A unification of the radiation problem, similar to the ones found in literature using the full 6DOF analysis, is an important objective of the present work. However, different from those approaches, the aim of the present study is to obtain impulse response functions which are independent of the ship's forward speed. For these purposes, some assumptions will be required which are based on the Ogilvie (1964) approximations between frequency domain and time domain solutions, and the forward speeds approximation for the radiation problem used in Salvesen et al. (1970). Because of these relationships are given in a different frame than the one used to solve the manoeuvring analysis, axes transformations will be required.

#### *1.2.2.5Numerical studies for wave forces*

When the ship manoeuvres in waves and in shallow water, the ship's hull wetted surface will change continuously because of the wave-induced ship's motion and squat-induced ship's sinkage and trim. Since the wetted surface is important for the evaluation of the hydrodynamic pressure around the hull, forces and moments due to waves are then expected to change accordingly. For this purpose an in house numerical tool that can estimate wave forces and moments is desired.

Due to the complexity of the problem, as a first step, the objective will be to account for a more exact (from the point of view of the simplification usually considered with the hull surface, e.g. two dimensional strips in strip theory) estimation of the Froude-Krylov forces and moments. For this purpose a more realistic estimation of the actual wetted surface is required. Hence, a three-dimensional representation of the hull surface, by flat panels, will be used.

## 1.3 Some aspects regarding the thesis

### 1.3.1 Chapters outline

In Chapter 2 an extensive discussion on the different axes frames used in the analysis of the ship's rigid body dynamics is introduced. The axes transformations by the common Euler angles are outlined. In addition, a brief discussion of the literature review with respect to seakeeping and manoeuvring in calm water studies is presented. For purposes of clarity, the state of the art review of manoeuvring in waves has been comprehensively discussed in a separate Chapter 3.

The extensive experimental study conducted at the towing tank of FHR can be found in Chapter 4. In addition, the challenges encountered while performing such experiments are also commented in Chapter 4. The results obtained for hull, propeller and rudder forces and moments, as well as the ship motions with and without the influence of waves are discussed in Chapter 5.

In Chapter 6, the proposed mathematical method for the analysis of the ship manoeuvring in waves in six degrees of freedom is presented. The evaluation of the ship radiation problem and the representation by steady and unsteady terms are proposed. Wave forces and moments are studied by using the superposition principle.

Chapter 7 presents a more detailed discussion of the numerical analysis carried out for the evaluation of the impulse response functions (IRFs), their equivalent representations in the body-fixed axes frame, and the relationships between the zero and non-zero speeds IRFs. The latter allow a representation of the IRFs which is independent of the forward speed. In addition, in Chapter 7, an in house developed numerical approach for the evaluation of the Froude-Krylov forces and moments which accounts for the actual wetted surface of the hull will be discussed.

Finally, in Chapter 8 the general conclusions and recommendation for further work are presented.

### 1.3.2 General definitions

Most of the terms used in the present work follow the ITTC definitions which can be encountered in the Dictionary of Hydrodynamics Alphabetic ITTC (2011a). For purposes of clarity some of the terms' definitions will be given below.

Shallow water and medium deep water manoeuvres are defined based on the water depth ($h$) to the ship's draft ($T_M$) ratio $h/T_M$, for medium water depths this is restricted by $3 > h/T_M > 1.5$, and for shallow water this is given by, $1.5 > h/T_M > 1.2$. The present definition has been retrieved form PIANC (2012).

Shallow, intermediate and deep water waves are defined as a function of the ratio between the water depth and the wave length ($\lambda$) $h/\lambda$. For deep water waves $h/\lambda > 1/2$, and for shallow water waves $h/\lambda < 1/20$. Waves with a water depth to wave length ratio between the values mentioned above are classified as intermediate water waves.

Froude-Krylov forces and moments are resulting from the integration of the pressure due to undisturbed incident wave potential on the hull surface.

The radiation problem concerns with the evaluation of the waves generated by the ship oscillatory motion on the water surface.

Manoeuvring, according to ITTC, is the process of executing various voluntary evolutions with a ship, such as starting, stopping, backing, steering, turning, diving, rising, circling, zigzagging, dodging and the like.

Manoeuvrability is that quality which determinates the ease with which the speed, attitude and direction of motion of a body can be changed or maintained by its control devices.

Seakeeping the study of the behaviour and performance of ship in a seaway. As an adjective, a term signifying a ship's ability to maintain normal functions at sea.

Drift angle is the horizontal angle between the instantaneous direction of motion of the centre of gravity of a ship and its longitudinal axis. It is positive in the positive sense of rotation about the vertical body's axis.

Velocity potential, in irrotational motion of a fluid, the velocity at any point may be derived from a single function $\phi$ such that its derivative with respect to distance in any direction is equal to the velocity component in that direction.

Beam waves is a condition in which a ship and waves, or the predominant wave components, advance at right angles, or nearly so.

Bow waves is a condition in which a ship and the waves, or the predominant wave components, advance at oblique angles. This condition covers the direction between a head sea and beam sea.

Following waves is a condition in which ship and the waves, or predominant wave components, advance in the same, or nearly the same direction.

Head waves is a condition in which a ship and the waves, or the predominant components, advance in opposite, or nearly opposite directions.

Quartering waves is a condition in which a ship and the waves, or the predominant wave components, advance at oblique angles. This condition covers the directions between a beam sea and a following sea.

# MANOEUVRING IN COASTAL WAVES



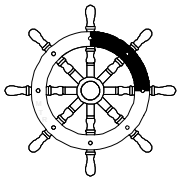

*He who loves practice without theory is like the sailor who boards ship without a rudder and compass and never knows where he may cast.*

*Leonardo da Vinci*

# 2

# Ship dynamics and hydrodynamics

## 2.1 General discussion

To simplify the variables' representation during the analysis, the following definitions are adopted: for positions ($\vec{r}^{f}_{pa/rp}$), and linear velocities ($\vec{v}^{f}_{pa/rp}$) the subscript indicates the position/velocity of the point under analysis ($pa$) with respect to the point of reference($rp$), for angular velocities ($\vec{\Omega}^{f}_{fa/rf}$) the subscript indicates the angular velocity of the frame under analysis ($fa$) with respect to the reference frame ($rf$); finally, for forces ($\vec{F}^{f}_{pa}$) and moments ($\vec{M}^{f}_{pa}$) the subscript only indicates the point of application (pa).

For all variables the superscript (e.g. $f$) indicates the frame of reference in which the vector is given.

The linear/angular accelerations follow the same representation of the linear/angular velocities. In cases where the frame of reference (superscript) is omitted the given representation is valid for any reference frame.

## 2.2 Rigid body dynamics

### 2.2.1 Frames of reference

To describe the ship behaviour three different axes systems are required, the Earth-bound axis system ( $O_0 - X_0 Y_0 Z_0$ ), the horizontal-bound axes system ($O' - x'y'z'$), and the ship-bound axes system ($O - xyz$). All axes systems are right handed and North-East Down (NED) oriented. They are shown in Figure 2.1.

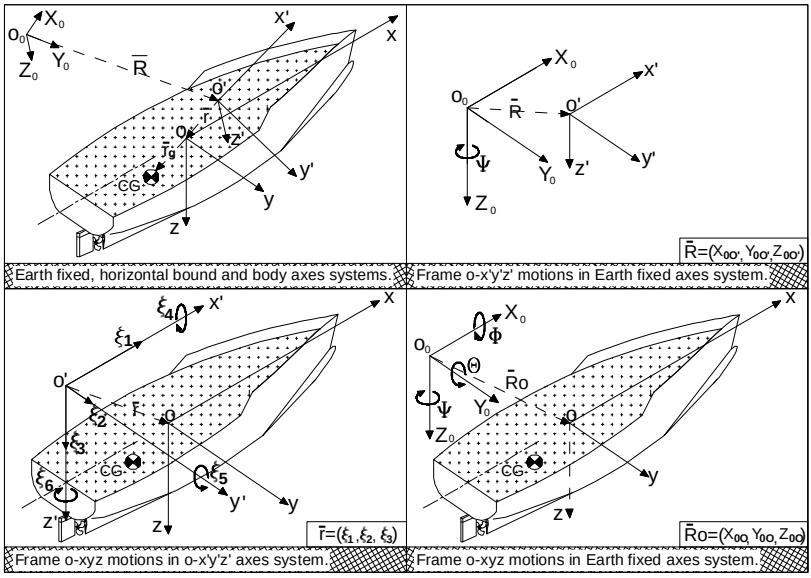


Figure 2.1 Axes systems: the Earth bound (E-frame), the horizontal bound (h-frame) and the body bound (b-frame).

The Earth axes system (E-frame), $O_0 - X_0\, Y_0\, Z_0$, is fixed to the Earth surface with its axes $X_0$, $Y_0$, and $Z_0$ pointing North, East and down of the Earth's tangent plane, respectively. The plane $O_0 X_0 Y_0$ coincides with the mean water level. The unitary vectors defining the $X_0$, $Y_0$, and $Z_0$ axes are $I$, $J$, and $K$, respectively.

The horizontal axes system (h-frame), $O' - x'y'z'$, moves along the ship's path with the ship speed $V\hat{\imath}'$ and with the ship's heading angle $\psi$. The $x'$-axis is positive forwards, the $y'$-axis is positive starboard, and the $z'$-axis is positive downwards. The $x'$-axis does not necessarily coincide with the ship's centre line, an angle $\xi_6$

(yaw angle) can be defined between them (see Figure 2.2). The $x'y'$-plane is parallel to the $X_0Y_0$-plane and coincides also with the mean water level. The unitary vectors defining the $x'$,$y'$, and $z'$ axes are $i'$, $j'$, and $k'$, respectively.

The body bound axes system (b-frame), $O-xyz$, origin is fixed amidships, with its $x$-axis positive towards the bow, the $y$-axis positive starboard, and the $z$-axis positive downwards. The unitary vectors defining the $x$, $y$ and $z$ axes are $i$, $j$, and $k$, respectively. This frame moves in six degrees of freedom with linear motions, $\xi_1\hat{i}', \xi_2\hat{j}', \xi_3\hat{k}'$, and angular rotations, $\xi_4\hat{i}', \xi_5\hat{j}', \xi_6\hat{k}'$, as seen from the h-frame; and moves with the linear velocities, $u\hat{\imath}, v\hat{\jmath}, w\hat{k}$, and angular velocities, $p\hat{\imath}, q\hat{\jmath}, r\hat{k}$, expressed in the b-frame, see Figure 2.1 and Figure 2.2. At time $t = 0$ s the E-frame, the h-frame, and the b-frame are parallel to each other and their origins coincide. It is assumed that the ship moves with a slowly varying yaw angle $\psi$ and perturbation motions in all six degrees of freedom with small order of magnitudes.

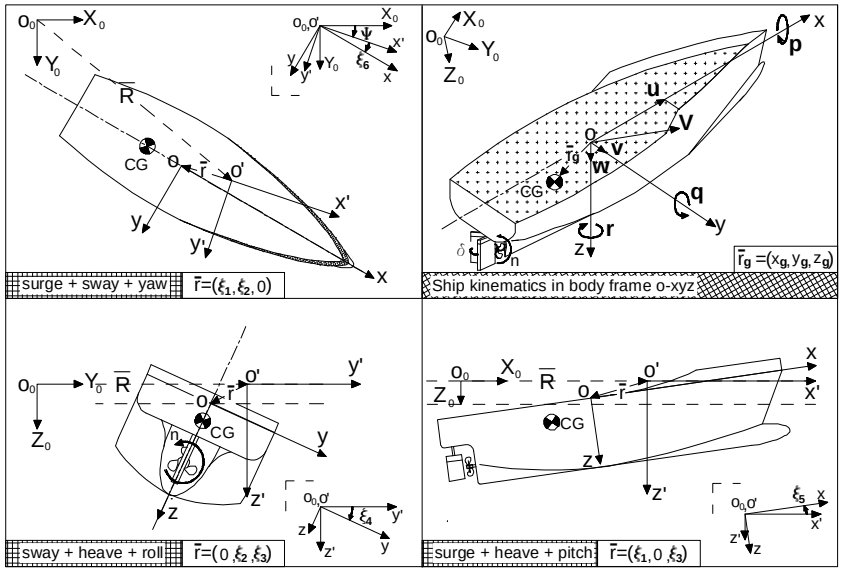


Figure 2.2 Definition of the ship's kinematical parameters, the relative motions between the axes systems, and other parameters such as rudder angle ($\delta$) and propeller rates (n).

### 2.2.2 Axes transformations

The axes system transformation used in the present study follows the Euler 321 rotation method. This refers to a sequence of finite rotations: first a yaw ($\psi$) rotation, followed by a pitch ($\theta$) rotation, and finally a roll ($\phi$) (see Figure 2.2 and Figure 2.3) rotation. This order should be respected as any other combination will give a different final orientation of the body. An illustration of the rotation steps to obtain the b-frame from the E-frame, and the h-frame are shown in Figure 2.3.

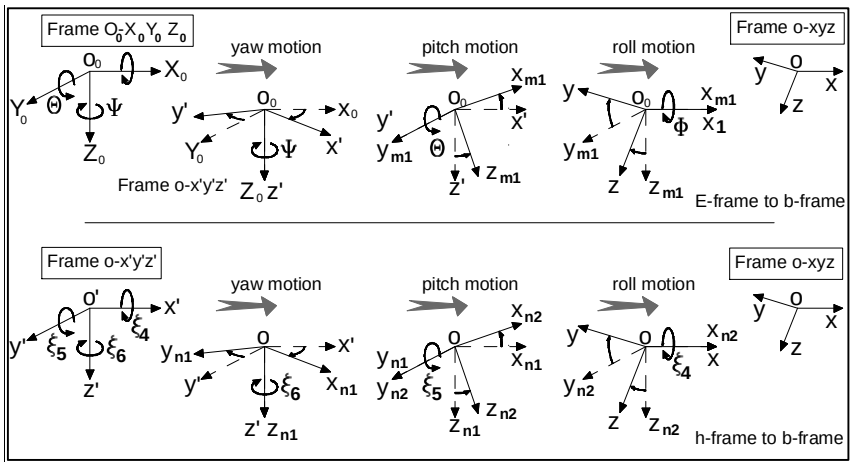


Figure 2.3 The 321 Euler axes rotation conventions for axes transformations between the E-frame to the b-frame (above) and between the h-frame and the b-frame (below).

Note that because of the three different axes used in the present analysis, three possible rotations can be obtained, a rotation from the b-frame to the E-frame, a rotation from h-frame to the E-frame, and a rotation from the b-frame to the h-frame. Notice that the h-frame can be obtained by only a yaw($\psi$) rotation of the E-frame.

#### *2.2.2.1 b-frame to E-frame transformation*

The rotation matrix for the transformation of any vector defined in the b-frame to the E-frame is given by:

$$R_b^E(\Theta) = \begin{bmatrix} c\phi c\theta & -s\psi c\phi + c\psi s\theta s\phi & s\psi s\phi + c\psi c\phi s\theta \\ s\psi c\theta & c\psi c\phi + s\phi s\theta s\psi & -c\psi s\phi + s\theta s\psi c\phi \\ -s\theta & c\theta s\phi & c\theta c\phi \end{bmatrix} \tag{2.1}$$

The notations $c$ and $s$ refer to the trigonometric cosine and sine functions, respectively. $R_b^E$ indicates the rotation is being performed from the b-frame to the E-frame. and $\Theta = (\phi, \theta, \psi)$ represents the Euler angles.

An additional matrix which relates the angular velocities defined in the b-frame to the Euler angles is given by:

$$T_\Theta(\Theta) = \begin{bmatrix} 1 & 0 & -s\theta \\ 0 & c\phi & c\theta s\phi \\ 0 & -s\phi & c\theta c\phi \end{bmatrix} \tag{2.2}$$

Note that $R_b^E$ and $T_\Theta$ are orthogonal and non-orthogonal matrices, respectively.

In Eq. (2.1) and Eq. (2.2) only for the purpose of better illustration, the trigonometric cosine and sine functions have been represented by the letters $c$ and $s$, respectively.

Using the matrices defined above, for instance, a force $\vec{F}^b$ and the angular velocity $\vec{\Omega}^b$ both expressed in the b-frame can be expressed in the E-frame by applying the following relationships:

$$\vec{F}^E = R_b^E(\Theta)\vec{F}^b \tag{2.3}$$

$$\vec{\Omega}_{b/E}^E = R_b^E(\Theta)\vec{\Omega}_{b/E}^b = R_b^E(\Theta)T_\Theta(\Theta)\begin{bmatrix} \dot{\phi} \\ \dot{\theta} \\ \dot{\psi} \end{bmatrix} \tag{2.4}$$

#### 2.2.2.1.1 Linear R and T matrices

If now the Euler angles $\delta\Theta = (\delta\phi, \delta\theta, \delta\psi)$ are considered to be of small order of magnitude, the linearization of the $R_b^E$ and $T_\Theta$matrices can be applied which results in:

$$R_b^E(\Theta) = \begin{bmatrix} 1 & -\delta\psi & \delta\theta \\ \delta\psi & 1 & -\delta\phi \\ -\delta\theta & \delta\phi & 1 \end{bmatrix} \tag{2.5}$$

$$T_\Theta(\Theta) = \begin{bmatrix} 1 & 0 & -\delta\theta \\ 0 & 1 & \delta\phi \\ 0 & -\delta\phi & 1 \end{bmatrix} \tag{2.6}$$

#### *2.2.2.2 h-frame to E-frame transformation*

The h-frame can be obtained by applying only a yaw rotation to the E-frame (see Figure 2.3). Replacing $\Psi = (0,0,\psi)$ as the Euler angles in Eq. (2.1) and (2.2), the R and T matrices are defined as:

$$R_h^E(\Psi) = \begin{bmatrix} 1 & -s\psi & 0 \\ s\psi & c\psi & 0 \\ 0 & 0 & 1 \end{bmatrix} \tag{2.7}$$

$$T_\Psi(\Psi) = \begin{bmatrix} 1 & 0 & 0 \\ 0 & 1 & 0 \\ 0 & 1 & 1 \end{bmatrix} \tag{2.8}$$

$\Psi$, over a time period equal to a wave period, can be assumed equal to the change in heading ($\bar{\psi}$) as observed in calm water manoeuvring. This is because of the smaller magnitudes of the high frequency oscillations in yaw, which can be assumed negligible in comparison to $\bar{\psi}$.

#### *2.2.2.3 b-frame to h-frame transformation*

By using Eq. (2.1) and Eq. (2.2) with the Euler angles given by $\Theta^* = (\phi^*, \theta^*, \psi^*)$, the matrices, $R_b^h(\Theta^*)$ and $T_{\Theta^*}(\Theta^*)$, defining the transformations from the b-frame to the h-frame can be obtained.

The matrices $R_b^h(\Theta^*)$ and $T_{\Theta^*}(\Theta^*)$, however, can be expressed in terms of the Euler angles($\Theta$) which defined the b-frame to the E-frame transformations. Recalling that the h-frame rotates with respect to the E-frame with a yaw angle $\psi$, see Figure 2.3. It can be observed that only the yaw rotation of the b-frame to the E-frame differs from the b-frame to the h-frame. The Euler angles $\Theta^*$and $\Theta$ hold the following relationships:

$$\phi^* = \phi \tag{2.9}$$

$$\theta^* = \theta \tag{2.10}$$

$$\psi^* = \psi - \overline{\psi} = \delta\psi \tag{2.11}$$

where the average yaw rotation over a wave period $T$ is given by: $\overline{\psi} = \frac{1}{T}\int_t^{t+T} \psi(\tau)d\tau$.

Replacing $\Theta^* = (\phi^*, \theta^*, \psi^*)$ by $\Theta^* = (\phi, \theta, \delta\psi)$, and considering that $cos(\delta\psi) \approx 1$ and $sin(\delta\psi) \approx \delta\psi$, the matrices defining the transformation from the b-frame to h-frame can be expressed as:

$$R_b^h(\Theta^*) = \begin{bmatrix} c\phi c\theta & -\delta\psi c\phi + s\theta s\phi & \delta\psi s\phi + c\phi s\theta \\ \delta\psi c\theta & c\phi + \delta\psi s\phi s\theta & -s\phi + \delta\psi s\theta c\phi \\ -s\theta & c\theta s\phi & c\theta c\phi \end{bmatrix} \tag{2.12}$$

$$T_{\Theta^*}(\Theta^*) = \begin{bmatrix} 1 & 0 & -s\theta \\ 0 & c\phi & c\theta s\phi \\ 0 & -s\phi & c\theta c\phi \end{bmatrix} \tag{2.13}$$

#### 2.2.2.3.1 Linear R and T matrices

If now the Euler angles are assumed of small order of magnitude, $\Theta^* = \delta\Theta^* = (\delta\phi, \delta\theta, \delta\psi)$, and taking into account the linear transformation matrices obtained in Eq. (2.5) and Eq. (2.6) and the relationship in Eq. (2.4), the ship's angular velocity $\vec{\Omega}_b^h = (\dot{\xi}_4, \dot{\xi}_5, \dot{\xi}_6)$ can be related to the Euler angles by:

$$\vec{\Omega}_{b/h}^h = R_b^h(\Theta^*)T_{\Theta^*}(\Theta^*)[\delta\dot{\phi} \quad \delta\dot{\theta} \quad \delta\dot{\psi}]^T \tag{2.14}$$

Neglecting higher order terms in the equation above yields:

$$\vec{\Omega}_{b/h}^h = [\dot{\xi}_4 \quad \dot{\xi}_5 \quad \dot{\xi}_6]^T = [\delta\dot{\phi} \quad \delta\dot{\theta} \quad \delta\dot{\psi}]^T \tag{2.15}$$

From Eq. (2.15) it can be observed that for small angles of rotation the Euler angles $\Theta^* = (\delta\phi, \delta\theta, \delta\psi)$ can be replaced by $\Xi = (\xi_4, \xi_5, \xi_6)$, which are the ship's roll, pitch and yaw, respectively, as observed from the h-frame. Considering this new notation, the $R_b^h(\Xi)$ and $T_\Xi(\Xi)$ matrices can be expressed as:

$$R_b^h(\Xi) = \begin{bmatrix} 1 & -\xi_6 & \xi_5 \\ \xi_6 & 1 & -\xi_4 \\ -\xi_5 & \xi_4 & 1 \end{bmatrix} \tag{2.16}$$

$$T_\Xi(\Xi) = \begin{bmatrix} 1 & 0 & -\xi_5 \\ 0 & 1 & \xi_4 \\ 0 & -\xi_4 & 1 \end{bmatrix} \tag{2.17}$$

### 2.2.3 Kinematic analysis

#### *2.2.3.1 Kinematics analysis in the b-frame*

The position of a point P, fixed in the ship, with respect to the origin ($O_0$) of the E-frame can be expressed as:

$$\vec{r}_{P/O_0} = \vec{r}_{O/O_0} + \vec{r}_{P/O} \tag{2.18}$$

The linear velocity of the same point can be obtained by taking the derivative of Eq. (2.18) with respect to time.

$$\vec{V}_{P/O_0}^b = \frac{d\vec{r}_{P/O_0}}{dt} = \frac{d\vec{r}_{O/O_0}}{dt} + \frac{d\vec{r}_{P/O}}{dt} \tag{2.19}$$

The right hand side terms in Eq. (2.19) are the ship's linear velocity and the relative velocity as seen by an observer located at the b-frames origin ($O$). They can be expressed as:

$$\frac{d\vec{r}_{O/O_0}^h}{dt} = u\hat{\imath} + v\hat{\jmath} + w\hat{k} \tag{2.20}$$

$$\frac{d\vec{r}_{P/O}^b}{dt} = \vec{\Omega}_{b/E}^b \times \vec{r}_{P/O}^b \tag{2.21}$$

The ship's angular velocity, $\vec{\Omega}_{b/E}^b$, and the position, $\vec{r}_{P/O}$, in the b-frame axes system are, respectively:

$$\vec{\Omega}_{b/E}^b = p\hat{\imath} + q\hat{\jmath} + r\hat{k} \tag{2.22}$$

$$\vec{r}_{P/O}^b = x_P\hat{\imath} + y_P\hat{\jmath} + z_P\hat{k} \tag{2.23}$$

Replacing Eq. (2.21) and (2.23) in Eq. (2.19) the velocity of the point P fixed on the ship can be obtained by:

$$\vec{V}^b_{P/O_0} = \begin{bmatrix} u + qz_P - ry_P \\ v - pz_P + rx_P \\ w + py_P - qx_P \end{bmatrix} \tag{2.24}$$

Taking the derivative of Eq. (2.24) and Eq. (2.22) with respect to time, the linear acceleration, $\vec{a}^b_{P/O_0}$, and the angular acceleration $\vec{\alpha}^b_{b/E}$ expressed by their components are, respectively:

$$\vec{a}^b_{P/O_0} = \begin{bmatrix} \dot{u} - vr + wq - x_P(r^2 + q^2) + y_P(pq - \dot{r}) + z_P(pr + \dot{q}) \\ \dot{v} - wp + ur - y_P(p^2 + r^2) + z_P(qr - \dot{p}) + x_P(pq + \dot{r}) \\ \dot{w} - uq + vp - z_P(p^2 + q^2) + x_P(pr - \dot{q}) + y_P(qr + \dot{p}) \end{bmatrix} \tag{2.25}$$

$$\vec{\alpha}^b_{b/E} = \begin{bmatrix} \dot{p} \\ \dot{q} \\ \dot{r} \end{bmatrix} \tag{2.26}$$

### *2.2.3.2Kinematics analysis in the h-frame*

Taking into account the three reference frames, the instantaneous position of the point P, analysed in the section above, can also be expressed as:

$$\vec{r}_{P/O_0} = \vec{r}_{O\prime/O_0} + \vec{r}_{O/O\prime} + \vec{r}_{P/O} \tag{2.27}$$

Taking the derivative of Eq. (2.27) with respect to time, the velocity of the point P can be obtained.

$$\vec{V}^h_{P/O_0} = \frac{d\vec{r}_{P/O_0}}{dt} = \frac{d\vec{r}_{O'/O_0}}{dt} + \frac{d\vec{r}_{O/O'}}{dt} + \frac{d\vec{r}_{P/O}}{dt} \tag{2.28}$$

Where the right hand side terms, expressed in the h-frame, are given by:

$$\frac{d\vec{r}^h_{O\prime/O_0}}{dt} = U\hat{\imath}' + V\hat{\jmath}' \tag{2.29}$$

$$\frac{d\vec{r}^h_{O/O\prime}}{dt} = \frac{\partial\vec{r}^h_{O\prime/O}}{\partial t} + \vec{\Omega}^h_{h/E} \times \vec{r}^h_{O\prime/O} \tag{2.30}$$

$$\frac{d\vec{r}^h_{P/O}}{dt} = \vec{\Omega}^h_{b/E} \times \vec{r}^h_{P/O} \tag{2.31}$$

Replacing Eq. (2.29) to Eq. (2.31) in Eq. (2.28) the velocity of a point P, fixed on the ship and given in the h-frame axes system, can be obtained by:

$$\vec{V}^h_{P/O_0} = U\hat{\imath}' + V\hat{\jmath}' + \frac{\partial \vec{r}^h_{O'/0_0}}{\partial t} + \vec{\Omega}^h_{h/E} \times \vec{r}^h_{O'/0_0} + \vec{\Omega}^h_{b/E} \times \vec{r}^h_{P/O} \tag{2.32}$$

Recalling that from the definitions, the reference positions $\vec{r}^h_{O'/O}$ and $\vec{r}^h_{P/O}$, and the angular velocity $\vec{\Omega}^h_{b/E}$, are given by:

$$\vec{r}^h_{O/O'} = \xi_1\hat{\imath}' + \xi_2\hat{\jmath}' + \xi_3\hat{k}' \tag{2.33}$$

$$\vec{r}^h_{P/O} = R^h_b(\Theta^*)(x_P\hat{\imath} + y_P\hat{\jmath} + z_P\hat{k}) \tag{2.34}$$

$$\vec{\Omega}^h_{b/E} = \vec{\Omega}^h_{h/E} + \vec{\Omega}^h_{b/h} \tag{2.35}$$

where:

$$\vec{\Omega}^E_{h/E} = R^E_b(\Psi)T_\Psi(\Psi)\begin{bmatrix}0\\0\\\dot{\psi}\end{bmatrix} = (0,0,\dot{\psi}) \tag{2.36}$$

$$\vec{\Omega}^h_{b/h} = R^h_b(\Theta^*)T_{\Theta^*}(\Theta^*)\begin{bmatrix}\phi\\\theta\\\delta\psi\end{bmatrix} \tag{2.37}$$

The linear acceleration and the angular acceleration of the point P can be obtained by deriving Eq. (2.32) and Eq. (2.35) with respect to time, respectively.

$$\vec{a}^h_{P/O_0} = \frac{\partial \vec{V}^h_{p/O_0}}{\partial t} + \vec{\Omega}^h_{h/E} \times \vec{V}^h_{P/O_0} \tag{2.38}$$

$$\vec{\alpha}^h_{b/E} = \frac{\partial \vec{\Omega}^h_{h/E}}{\partial t} + \frac{\partial \vec{\Omega}^h_{b/h}}{\partial t} + \vec{\Omega}^h_{h/E} \times \vec{\Omega}^h_{b/h} \tag{2.39}$$

#### 2.2.3.2.1 Linear kinematic analysis in the h-frame

Considering that the induced ship motions by the waves are of small order of magnitude, Eq. (2.32) and Eq. (2.38) can be further simplified. This by adopting a linear analysis, hence, neglecting terms of higher order.

Considering the linear analysis, the ship's angular velocity becomes $\vec{\Omega}_{b/h}^{h} = (\dot{\xi}_4, \dot{\xi}_5, \dot{\xi}_6)$, and the rotation matrices $R_b^h(\Theta^*)$ and $T_{\Theta^*}(\Theta^*)$ are defined by $R_b^h(\Xi)$ and $T_{\Xi}(\Xi)$, respectively. The Euler angles are given by $\Xi = (\xi_4, \xi_5, \xi_6)$, see 2.2.2.3.1. Replacing these relationships in Eq. (2.34) and (2.35) yields:

$$\vec{r}_{P/O}^{h} = (x_P - \xi_6 y_P + \xi_5 z_P)\,\hat{\imath}' + (y_P + \xi_6 x_P - \xi_4 z_P)\,\hat{\jmath}' + (z_P - \xi_5 x_P + \xi_4 y_P)\hat{k}' \tag{2.40}$$

$$\vec{\Omega}_{b/E}^{h} = \dot{\xi}_4\hat{\imath}' + \dot{\xi}_5\hat{\jmath}' + (\dot{\xi}_6 + \dot{\psi})\hat{k}' \tag{2.41}$$

Recall that the angular velocity of the h-frame with respect the E-frame, given in the h-frame, is given by $\vec{\Omega}_{h/E}^{h} = \dot{\psi}\hat{k}$.

Replacing $\vec{r}_{O/O'}^{h} = \xi_1\hat{\imath}' + \xi_2\hat{\jmath}' + \xi_3\hat{k}'$, Eq. (2.40) and (2.41) in Eq.(2.30) and Eq. (2.31) gives, respectively:

$$\frac{d\vec{r}_{O/O'}^{h}}{dt} = (\dot{\xi}_1 - \dot{\psi}\xi_3)\hat{\imath}' + (\dot{\xi}_2 + \dot{\psi}\xi_1)\hat{\jmath}' + \dot{\xi}_3\hat{k}' \tag{2.42}$$

$$\frac{d\vec{r}_{P/O}^{h}}{dt} = (\dot{\xi}_4\hat{\imath}' + \dot{\xi}_5\hat{\jmath}' + (\dot{\xi}_6 + \dot{\psi})\hat{k}') \times \vec{r}_{P/O}^{h} \tag{2.43}$$

$\vec{V}_{P/O_0}^{h}$ components $v_{x'}^{h}, v_{y'}^{h}, v_{z'}^{h}$, then becomes:

$$v_{x'}^{h} = U + \dot{\xi}_1 - \dot{\psi}\xi_3 - x_P\left(\dot{\xi}_5\xi_5 + \dot{\xi}_6\xi_6 + \dot{\psi}\xi_6\right) + y_P\left(\dot{\xi}_5\xi_4 - \dot{\xi}_6 - \dot{\psi}\right) + z_P(\dot{\xi}_5 + \dot{\xi}_6\xi_4 + \dot{\psi}\xi_4) \tag{2.44}$$

$$v_{y'}^{h} = V + \dot{\xi}_2 + \dot{\psi}\xi_1 + x_P\left(\dot{\xi}_4\xi_5 + \dot{\xi}_6 + \dot{\psi}\right) - y_P\left(\dot{\xi}_4\xi_4 + \dot{\xi}_6\xi_6 + \dot{\psi}\xi_6\right) + z_P(\dot{\xi}_6\xi_5 - \dot{\xi}_4 + \dot{\psi}\xi_5) \tag{2.45}$$

$$v_{z'}^{h} = \dot{\xi}_3 + x_P(\dot{\xi}_4\xi_6 - \dot{\xi}_5) + y_P(\dot{\xi}_4 + \dot{\xi}_5\xi_6) - z_P(\dot{\xi}_4\xi_4 + \dot{\xi}_5\xi_5) \tag{2.46}$$

Neglecting terms of order $O(\epsilon^3)$ ($\epsilon \ll 1$) and smaller, Eq. (2.44) to Eq. (2.46) can be written as:

$$v_{x'}^{h} = U + \dot{\xi}_1 - x_P\left(\dot{\xi}_5\xi_5 + \dot{\xi}_6\xi_6\right) - y_P(\dot{\xi}_6 - \dot{\xi}_5\xi_4) + z_P(\dot{\xi}_5 + \dot{\xi}_6\xi_4) \tag{2.47}$$

$$v_{y'}^{h} = V + \dot{\xi}_2 + x_P(\dot{\xi}_6 + \dot{\xi}_4\xi_5) - y_P\left(\dot{\xi}_4\xi_4 + \dot{\xi}_6\xi_6\right) - z_P(\dot{\xi}_4 - \dot{\xi}_6\xi_5) \tag{2.48}$$

$$v_{z'}^{h} = \dot{\xi}_3 - x_P(\dot{\xi}_5 - \dot{\xi}_4\xi_6) + y_P(\dot{\xi}_4 + \dot{\xi}_5\xi_6) - z_P(\dot{\xi}_4\xi_4 + \dot{\xi}_5\xi_5) \tag{2.49}$$

The acceleration of the point P can be obtained by:

$$\vec{a}_{P/O_0}^{h} = \frac{\partial v_{x'}^{h}}{\partial t}\hat{\imath}' + \frac{\partial v_{y'}^{h}}{\partial t}\hat{\jmath}' + \frac{\partial v_{z'}^{h}}{\partial t}\hat{k}' + \vec{\Omega}_{h/E}^{h} \times (v_{x'}^{h}\hat{\imath}' + v_{y'}^{h}\hat{\jmath}' + v_{z'}^{h}\hat{k}') \tag{2.50}$$

where $\vec{a}_{p/O_0}^{h}$ expressed in terms of its components $\vec{a}_{x'}^{h}, \vec{a}_{y'}^{h}$, and $\vec{a}_{z'}^{h}$ is given by:

$$\vec{a}_{x'}^{h} = \ddot{\xi}_1 - \dot{\psi}V - x_P\left(\dot{\xi}_5^2 + \dot{\xi}_6^2 + \ddot{\xi}_6\xi_6 + \ddot{\xi}_5\xi_5\right) - y_P\left(\ddot{\xi}_6 - \ddot{\xi}_5\xi_4 - \dot{\xi}_5\dot{\xi}_4\right) + z_P(\ddot{\xi}_5 + \ddot{\xi}_6\xi_4 + \dot{\xi}_6\dot{\xi}_4) \tag{2.51}$$

$$\vec{a}_{y'}^{h} = \ddot{\xi}_2 + \dot{\psi}U + x_P\left(\ddot{\xi}_6 + \ddot{\xi}_4\xi_5 + \dot{\xi}_4\dot{\xi}_5\right) - y_P\left(\dot{\xi}_6^2 + \dot{\xi}_4^2 + \ddot{\xi}_4\xi_4 + \ddot{\xi}_6\xi_6\right) - z_P(\ddot{\xi}_4 - \ddot{\xi}_6\xi_5 - \dot{\xi}_6\dot{\xi}_5) \tag{2.52}$$

$$\vec{a}_{z'}^{h} = \ddot{\xi}_3 - x_P\left(\ddot{\xi}_5 - \ddot{\xi}_4\xi_6 - \dot{\xi}_4\dot{\xi}_6\right) + y_P\left(\ddot{\xi}_4 + \ddot{\xi}_5\xi_6 + \dot{\xi}_5\dot{\xi}_6\right) - z_P(\dot{\xi}_4^2 + \dot{\xi}_5^2 + \ddot{\xi}_4\xi_4 + \ddot{\xi}_5\xi_5) \tag{2.53}$$

Assuming the ship speed is low to moderated O($\epsilon$), and that the ship's lateral velocity (V) is smaller compared to the ship's longitudinal velocity (U), hence V/U<<1, Eq. (2.47) to Eq. (2.53) can be further simplified taking into account linear terms only. The resulting velocity and acceleration terms of the point P fixed in the ship are:

$$\vec{V}_{P/O_0}^{h} = \left(U + \dot{\xi}_1 - y_P\dot{\xi}_6 + z_P\dot{\xi}_5\right)\hat{\imath}' + \left(V + \dot{\xi}_2 - z_P\dot{\xi}_4 + x_P\dot{\xi}_6\right)\hat{\jmath}' + (\dot{\xi}_3 - x_P\dot{\xi}_5 + y_P\dot{\xi}_4)\hat{k}' \tag{2.54}$$

$$\vec{a}_{P/O_0}^{h} = \left(\ddot{\xi}_1 - y_P\ddot{\xi}_6 + z_P\ddot{\xi}_5\right)\hat{\imath}' + \left(\ddot{\xi}_2 - z_P\ddot{\xi}_4 + x_P\ddot{\xi}_6\right)\hat{\jmath}' + (\ddot{\xi}_3 - x_P\ddot{\xi}_5 + y_P\ddot{\xi}_4)\hat{k}' \tag{2.55}$$

Similarly, applying the same restrictions angular velocity, $\vec{\Omega}_{b/E}^{h}$, and acceleration, $\vec{\alpha}_{b/E}^{h}$, their linear approximation can be written as:

$$\vec{\Omega}_{b/E}^{h} = \dot{\xi}_4\hat{\imath}' + \dot{\xi}_5\hat{\jmath}' + (\dot{\xi}_6 + \dot{\psi})\hat{k}' \approx \dot{\xi}_4\hat{\imath}' + \dot{\xi}_5\hat{\jmath}' + \dot{\xi}_6\hat{k}' \tag{2.56}$$

$$\vec{\alpha}_{b/E}^{h} = (\ddot{\xi}_4 - \dot{\psi}\dot{\xi}_5)\hat{\imath}' + (\ddot{\xi}_5 + \dot{\psi}\dot{\xi}_4)\hat{\jmath}' + \left(\ddot{\xi}_6 + \ddot{\psi}\right)\hat{k}' \approx \ddot{\xi}_4\hat{\imath}' + \ddot{\xi}_5\hat{\jmath}' + \ddot{\xi}_6\hat{k}' \tag{2.57}$$

#### *2.2.3.3 Linear kinematic relationships between the h-frame and the b-frame*

To find an equivalence between the b-frame and the h-frame kinematic representations lets first consider the point P fixed on the ship to be located at the b-frame's origin $O$. Hence, the coordinates, $x_P$, $y_P$, $z_P$, become $x_O = y_O = z_O = 0$.

Replacing $x_O = y_O = z_O = 0$ in Eq. (2.54) to Eq. (2.57), the linear velocity and accelerations of the point $O$ can be written as:

$$\vec{V}^h_{O/O_0} = \left(U + \dot{\xi}_1\right)\hat{\imath}' + \left(V + \dot{\xi}_2\right)\hat{\jmath}' + \dot{\xi}_3\hat{k}' \tag{2.58}$$

$$\vec{a}^h_{O/O_0} = \ddot{\xi}_1\hat{i}' + \ddot{\xi}_2\hat{j}' + \ddot{\xi}_3\hat{k}' \tag{2.59}$$

Bear in mind that the equations above have been obtained taking into account that the instantaneous position of the b-frame's origin with respect to the h-frame's origin, which coincide at rest, is given only by the ship motions $\vec{r}^h_{O/O'} = \xi_1\hat{\imath}' + \xi_2\hat{\jmath}' + \xi_3\hat{k}'$, where the coordinates $\xi_1$, $\xi_2$ and $\xi_3$ are relative small, of order O($\epsilon$). If now this distance $\vec{r}^h_{O/O'}$ does not coincide at rest and it is of order O($\epsilon$) the relationships described above will not be applicable to relate the h—frame and b-frame kinematical relationships.

By assuming an intermediate b'-frame, who's origin coincide with the h-frame's origin at rest, and parallel to the b-frame and at the distance given by:

$$\vec{r}^b_{O'/O} = x_{o'}\hat{\imath} + y_{o'}\hat{\jmath} + z_{o'}\hat{k} \tag{2.60}$$

where $x_{O'}$, $y_{O'}$, $z_{O'}$ are assumed constant or quasi-steadily changing in time (e.g. due to squat), and replacing the point P coordinates in Eq. (2.24) and Eq. (2.25) by $O'$, the linear velocity and accelerations of the b'-frames origin (which approximately coincided with 0') can be written as:

$$\vec{V}^b_{O/O_0} = \begin{bmatrix} u + qz_{O'} - ry_{O'} \\ v - pz_{O'} + rx_{O'} \\ w + py_{O'} - qx_{O'} \end{bmatrix} \tag{2.61}$$

$$\vec{a}^{b}_{O/O_0} = \begin{bmatrix} \dot{u} - vr + wq - x_{O'}(r^2 + q^2) + y_{O'}(pq - \dot{r}) + z_{O'}(pr + \dot{q}) \\ \dot{v} - wp + ur - y_{O'}(p^2 + r^2) + z_{O'}(qr - \dot{p}) + x_{O'}(pq + \dot{r}) \\ \dot{w} - uq + vp - z_{O'}(p^2 + q^2) + x_{O'}(pr - \dot{q}) + y_{O'}(qr + \dot{p}) \end{bmatrix} \quad (2.62)$$

Note that in the notations $\vec{V}^{b}_{O/O_0}$ and $\vec{a}^{b}_{O/O_0}$ the letter $O$ has been used to represent the origin of the b'-frame in order to make a clearer link between the Eq. (2.61), Eq. (2.62) and Eq. (2.58), Eq. (2.59), respectively.

Using the rotation matrices $R^{h}_{b}(\Xi)$ and $T_{\Xi}(\Xi)$ defined in (2.16) and Eq. (2.17), Eq. (2.61), and Eq. (2.62) can be rotated to the h-frame which yields the following relationships for the linear velocity and acceleration terms between the h-frame and b-frame:

$$\begin{bmatrix} \dot{\xi}_1 \\ \dot{\xi}_2 \\ \dot{\xi}_3 \end{bmatrix} = \begin{bmatrix} \delta u + z_{O'}\delta q - y_{O'}\delta r \\ \delta v + U\xi_6 + x_{O'}r - z_{O'}\delta p \\ \delta w - U\xi_5 + y_{O'}\delta p \ - x_{O'}\delta q \end{bmatrix} \quad (2.63)$$

$$\begin{bmatrix} \ddot{\xi}_1 \\ \ddot{\xi}_2 \\ \ddot{\xi}_3 \end{bmatrix} = \begin{bmatrix} \delta \dot{u} + z_{O'}\delta \dot{q} - y_{O'}\delta \dot{r} \\ \delta \dot{v} + U\delta r + x_{O'}\delta \dot{r} - z_{O'}\delta \dot{p} \\ \delta \dot{w} - Uq + y_{O'}\delta \dot{p} - x_{O'}\delta \dot{q} \end{bmatrix} \quad (2.64)$$

The lateral velocity $V$ has been neglected from Eq.(2.63) and Eq. (2.64) because of its small order of magnitude O($\epsilon$). Note as well that in the above relationships the following is assumed: $u = U + \delta u$,$v = V + \delta v$, and $w = \delta w$

Using the $R^{h}_{b}(\Xi)$ and $T_{\Xi}(\Xi)$ matrices the angular velocity and acceleration can also be related as:

$$\begin{bmatrix} \dot{\xi}_4 \\ \dot{\xi}_5 \\ \dot{\xi}_6 \end{bmatrix} = \begin{bmatrix} \delta p \\ \delta q \\ \delta r \end{bmatrix} \quad (2.65)$$

$$\begin{bmatrix} \ddot{\xi}_4 \\ \ddot{\xi}_5 \\ \ddot{\xi}_6 \end{bmatrix} = \begin{bmatrix} \delta \dot{p} \\ \delta \dot{q} \\ \delta \dot{r} \end{bmatrix} \quad (2.66)$$

### 2.2.4 Dynamic analysis

Now considering the ship as a rigid body, where external forces $\vec{F}_G$ and moments $\vec{M}_G$ are applied to the ship, the linear momentum $\vec{P}_G$ and the angular momentum $\vec{H}_G$ are related to these forces and moments by:

$$\vec{F}_G = \frac{d\vec{P}_G}{dt} = m\frac{d\vec{V}_G}{dt} \tag{2.67}$$

$$\vec{M}_G = \frac{d\vec{H}_G}{dt} \tag{2.68}$$

In general the point of reference for the analysis differs from the centre of gravity. This point, hereafter named $O$, is in general chosen located amidships. The ship's velocity, the angular momentum, and the external moment defined at the ship's centre of gravity, in the equations above, can be expressed with respect to a frame of reference with its origin located at $O$ by:

$$\vec{V}_G = \vec{V}_O + \frac{d\vec{r}_{G/O}}{dt} = \vec{V}_O + \vec{\Omega} \times \vec{r}_{G/O} \tag{2.69}$$

$$\vec{H}_G = \vec{H}_O - m\,\vec{r}_{G/O} \times \left(\vec{\Omega} \times \vec{r}_{G/O}\right) \tag{2.70}$$

$$\vec{M}_G = \vec{M}_O - \vec{r}_{G/O} \times \vec{F}_G \tag{2.71}$$

Taking into account Eq. (2.69) to Eq. (2.71) in Eq. (2.67) and Eq. Eq. (2.68), the forces and moments can be expressed:

$$\vec{F}_O = m\frac{d\vec{V}_O}{dt} = m\left(\frac{d\vec{V}_G}{dt} + \frac{d\left(\vec{\Omega} \times \vec{r}_{G/O}\right)}{dt}\right) \tag{2.72}$$

$$\vec{M}_O = \frac{d\vec{H}_G}{dt} + m\,\vec{r}_{G/O} \times \frac{d\vec{V}_G}{dt} \tag{2.73}$$

Recall that the angular momentum ($\vec{H}_G$) with respect to the centre of gravity is given by:

$$\vec{H}_G = \begin{bmatrix} h_x \\ h_y \\ h_z \end{bmatrix} = \begin{bmatrix} I_x & -I_{xy} & -I_{zx} \\ -I_{yx} & I_y & -I_{yz} \\ -I_{zx} & -I_{zy} & I_z \end{bmatrix} \begin{bmatrix} \Omega_x \\ \Omega_y \\ \Omega_z \end{bmatrix} = I_G\vec{\Omega} \tag{2.74}$$

$I_G$ is the inertia tensor and $\overrightarrow{\Omega}$ is the angular velocity, all given in the body fixed reference frame.

From the relationship defined in 2.2.3.1 and taking into account that the position of the ship's centre of gravity is given by $\vec{r}^{\,b}_{G/O} = x_G\hat{\imath} + y_G\hat{\jmath} + z_G\hat{k}$, the resulting dynamic equation of the rigid body in six degrees of freedom can be written as:

$$\begin{bmatrix} X \\ Y \\ Z \\ K \\ M \\ N \end{bmatrix} = \begin{bmatrix} m\big(\dot{u} - vr + wq - x_G(r^2 + q^2) + y_G(pq - \dot{r}) + z_G(pr + \dot{q})\big) \\ m\big(\dot{v} - wp + ur - y_G(p^2 + r^2) + z_G(qr - \dot{p}) + x_G(pq + \dot{r})\big) \\ m(\dot{w} - uq + vp - z_G(p^2 + q^2) + x_G(pr - \dot{q}) + y_G(qr + \dot{p})) \\ \dot{h}_x + qh_z - rh_y + m(y_G\dot{w} - z_G\,\dot{v} + y_G(vp - uq) - z_G(ur - wp)) \\ \dot{h}_y + rh_x - ph_z + m\big(z_G\dot{u} - x_G\dot{w} + z_G(wq - vr) - x_G(vp - uq)\big) \\ \dot{h}_z + ph_y - qh_x + m\big(x_G\dot{v} - y_G\dot{u} + x_G(ur - wp) - y_G(wq - vr)\big) \end{bmatrix} \quad (2.75)$$

Where X, Y, Z are forces in surge, sway and heave, and K, M, N are the moments in roll, pitch and yaw, respectively.

# 2.3 Hydrodynamics of ideal fluids

## 2.3.1 Generalities

Because of the use of this concept in both independent fields of seakeeping and manoeuvring, it is necessary to describe the main characteristics of ideal fluids and their effects on the ship hull. Although the application might differ in both fields, the present discussion aims to provide more insight in the physics of ideal fluids, and the reason of inertial terms in the final equations of manoeuvring and seakeeping. Part of this discussion is also extended in 6.1.2.

It is important to mention that the present analysis uses two different frames, the E-frame, and the b-frame, which follow the conventions described in 2.2.1.

## 2.3.2 Moving body in an unbounded fluid

It has been shown in Lamb (1945) that the fluid kinetic energy ($T$) can be expressed as a function of the potential velocity $\phi$ by:

$$2T = -\rho \iint \phi \frac{d\phi}{dn} ds \tag{2.76}$$

The kinetic energy $T$ associated to the potential flow $\phi$, as shown by Kirchhoff (1869), can be expressed in terms of the instant angular, $p$, $q$, $r$, and the translational $u$, $v$, $w$, velocities, by:

$$\phi = u\phi_1 + v\phi_2 + w\phi_3 + p\phi_4 + q\phi_5 + r\phi_6 \tag{2.77}$$

Replacing this expression in Eq. (2.76), as shown in Imlay (1961), see also Lamb (1945), Milne-Thomson (1962) and Norrbin (1971), the kinetic energy $T$ can be written as a function of the velocities and a total of 21 coefficients.

$$\begin{aligned} 2T = &-X_{\dot{u}}u^2 - Y_{\dot{v}}v^2 - Z_{\dot{w}}w^2 - K_{\dot{p}}p^2 - M_{\dot{q}}q^2 - N_{\dot{r}}r^2 - 2Y_{\dot{w}}vw - 2X_{\dot{w}}wu \\ &- 2X_{\dot{v}}uv - 2M_{\dot{r}}qr - 2K_{\dot{r}}rp - 2K_{\dot{q}}pq \\ &- 2p\left(X_{\dot{p}}u + Y_{\dot{p}}v + Z_{\dot{p}}w\right) - 2q\left(X_{\dot{q}}u + Y_{\dot{q}}v + Z_{\dot{q}}w\right) \\ &- 2r(X_{\dot{r}}u + Y_{\dot{r}}v + Z_{\dot{r}}w) \end{aligned} \tag{2.78}$$

The fluid forces will be a result of the variation of the kinetic energy $T$. In Imlay (1961), the derivation of these forces and moments expressed in the body bound axes system, (the b-frame) are given by:

$$X_{id} = -\frac{d}{dt}\frac{\partial T}{\partial u} - q\frac{\partial T}{\partial w} + r\frac{\partial T}{\partial v} \tag{2.79}$$

$$Y_{id} = -\frac{d}{dt}\frac{\partial T}{\partial v} - r\frac{\partial T}{\partial u} + p\frac{\partial T}{\partial w} \tag{2.80}$$

$$Z_{id} = -\frac{d}{dt}\frac{\partial T}{\partial w} - p\frac{\partial T}{\partial v} + q\frac{\partial T}{\partial u} \tag{2.81}$$

$$K_{id} = -\frac{d}{dt}\frac{\partial T}{\partial p} - q\frac{\partial T}{\partial r} + r\frac{\partial T}{\partial q} - v\frac{\partial T}{\partial w} + w\frac{\partial T}{\partial v} \tag{2.82}$$

$$M_{id} = -\frac{d}{dt}\frac{\partial T}{\partial q} - r\frac{\partial T}{\partial p} + p\frac{\partial T}{\partial r} - w\frac{\partial T}{\partial u} + u\frac{\partial T}{\partial w} \tag{2.83}$$

$$N_{id} = -\frac{d}{dt}\frac{\partial T}{\partial r} - p\frac{\partial T}{\partial q} + q\frac{\partial T}{\partial p} - u\frac{\partial T}{\partial v} + v\frac{\partial T}{\partial u} \tag{2.84}$$

Replacing Eq. (2.78) in the equations above, and taking into account a body of symmetry with respect to the $xz$ −plane, yields:

$$X_{id} = X_{\dot{u}}\dot{u} + X_{\dot{w}}\dot{w} + X_{\dot{q}}\dot{q} + X_{\dot{w}}uq - Y_{\dot{v}}vr - Y_{\dot{r}}r^2 + Z_{\dot{w}}wq + Z_{\dot{q}}q^2 \tag{2.85}$$

$$Y_{id} = Y_{\dot{v}}\dot{v} + Y_{\dot{p}}\dot{p} + Y_{\dot{r}}\dot{r} - X_{\dot{w}}(up - wr) + X_{\dot{u}}ur + X_{\dot{q}}qr - Z_{\dot{w}}wp - Z_{\dot{q}}pq \tag{2.86}$$

$$Z_{id} = X_{\dot{w}}\dot{u} + Z_{\dot{w}}\dot{w} + Z_{\dot{q}}\dot{q} - X_{\dot{u}}uq + X_{\dot{w}}wq - X_{\dot{q}}q^2 + Y_{\dot{v}}vp + Y_{\dot{r}}rp + Y_{\dot{p}}p^2 \tag{2.87}$$

$$K_{id} = Y_{\dot{p}}\dot{v} + K_{\dot{p}}\dot{p} + K_{\dot{r}}\dot{r} + X_{\dot{w}}uv - (Y_{\dot{v}} - Z_{\dot{w}})vw - \left(Y_{\dot{r}} + Z_{\dot{q}}\right)wr - Y_{\dot{p}}wp - X_{\dot{q}}ur + \left(Y_{\dot{r}} + Z_{\dot{q}}\right)vq + K_{\dot{r}}pq - (M_{\dot{q}} - N_{\dot{r}})qr \tag{2.88}$$

$$M_{id} = X_{\dot{q}}(\dot{u} + wq) + Z_{\dot{q}}(\dot{w} - uq) + M_{\dot{q}}\dot{q} - X_{\dot{w}}(u^2 - w^2) - (Z_{\dot{w}} - X_{\dot{u}})wu + Y_{\dot{p}}vr - Y_{\dot{r}}vp - K_{\dot{r}}(p^2 - r^2) + \left(K_{\dot{p}} - N_{\dot{r}}\right)rp \tag{2.89}$$

$$N_{id} = Y_{\dot{r}}\dot{v} + K_{\dot{r}}\dot{p} + N_{\dot{r}}\dot{r} - (X_{\dot{u}} - Y_{\dot{v}})uv - X_{\dot{w}}vw + \left(X_{\dot{q}} + Y_{\dot{p}}\right)up + Y_{\dot{r}}ur$$

$$+ Z_{\dot{q}}wp - \left(X_{\dot{q}} + Y_{\dot{p}}\right)vq - \left(K_{\dot{p}} - M_{\dot{q}}\right)pq - K_{\dot{r}}qr \qquad (2.90)$$

In the expressions above, symmetry considerations allow to reduce the 21 coefficients in Eq. (2.78) to only 12.

$$2T = -X_{\dot{u}}u^2 - Y_{\dot{v}}v^2 - Z_{\dot{w}}w^2 - K_{\dot{p}}p^2 - M_{\dot{q}}q^2 - N_{\dot{r}}r^2 - 2X_{\dot{w}}wu - 2K_{\dot{r}}rp$$

$$- 2q\left(X_{\dot{q}}u + Z_{\dot{q}}w\right) - 2p\left(Y_{\dot{p}}v\right) - 2r(Y_{\dot{r}}v) \qquad (2.91)$$

The analysis of added inertial terms has been an important focus of studies since the pioneering work of Kirchhoff (1869). However, as described by Imlay (1961) this concept has been lost to many researchers and the use of given formulations have been generally accepted valid without questioning their applicability.

### 2.3.3 Moving body on the water surface

For a body moving on the water surface, the results of the ideal fluid will incorporate additional coefficients depending linearly on the ship velocities. The latter, is because of the wave generation problem, known as the radiation problem.

When studying manoeuvring in calm water, the ideal fluid terms which are linearly dependent on the velocity are generally neglected. This is a common approach because of the small amplitudes of the radiated waves. In seakeeping studies, however, the radiated waves need to be accounted for, and consequently the ideal fluid problem is then expressed in terms of inertial terms and additional damping coefficients as linear functions of the velocities, see 2.5.

As mentioned by Newman, (1977) the different nature of the fluid problem will introduce fundamental differences between added inertial terms, encountered independently in the fields of manoeuvring in calm water and seakeeping, although they address the same hydrodynamic phenomena. Several authors have worked on the analysis in order to unify the concepts, see for instance Bishop et al. (1973), Bailey, et al. (1998), and Bishop et al. (1977).

## 2.4 Manoeuvring in calm water

### 2.4.1 Definitions and Coordinate systems

The ships manoeuvrability as defined in ITTC (2011a) is *that quality which determinates the ease with which the speed, attitude and direction of motion of a body can be changed or maintained by its control devices.* The ship is not restricted to any particular path and any curvilinear motion is expected. Because of the latter, the ship dynamic analysis will incorporate centripetal and Coriolis terms; this has already been studied in the general analysis of the rigid body dynamic analysis conducted in section 2.

To investigate the ship dynamics and hydrodynamics, two coordinates systems are used, the Earth axes system (the E-frame, $O_0 - x_0\, y_0\, z_0$), and the body-bound axes system (the b-frame, $O - xyz$). Their definitions have been given in 2.2.1.

### 2.4.2 Hydrodynamic phenomena: hull forces

The hull surface will be subjected to fluid forces which can be assumed to be composed of normal and tangential stresses due the pressure change in the fluid domain and the due to friction. Pressures and tangential stresses will cause phenomena such as lift, cross flow and resistance, and the effect of these phenomena is relevant for the analysis of manoeuvring ships because they are more important than effects such as vortex shedding and the accompanying memory effects. The discussion of these main concepts will be briefly given in the sections below. For a more extended analysis the reader might consult, for instance, Norrbin, (1971), Motora et al. (1971), Newman, (1979), and Oltmann and Sharma, (1984).

#### *2.4.2.1Ideal fluids*

As mentioned earlier in 2.3, an important contribution of the pressure changes can be modelled by the assumption of ideal fluid. Assuming the flow to be incompressible, irrotational and without viscosity, inertial terms are derived as a function of the acceleration parameter, $\dot{u}$, $\dot{v}$, $\dot{w}$, $\dot{p}$, $\dot{q}$, and $\dot{r}$. In manoeuvring it is common to restrict the analysis to the horizontal plane only. This

is a reasonable approach as the vertical motions are rather negligible in calm water manoeuvring.

#### *2.4.2.2Hull lifting effects*

Because of the steady flow velocity to the fluid at small angles of drift, the ship will act similar to a hydrofoil. Lift and drag forces will be subjected to the ship in the direction perpendicular and parallel to the fluid flow, respectively. Because of the application point of the lift and drag, a yawing moment will be also induced.

Lift can be understood as the net circulation along the hull. In a real flow, according to Munk (1924), the circulation will increase and consequently the lift because of the vortices generated at the rear of the hull.

These forces and moments are in general modelled as proportional to the velocity components $uv$. Because of the yaw velocity, one can also define a local lift as a function of the product of the yaw and the surge velocities, $ur$. These terms are averaged over the entire length, see e.g. Oltmann and Sharma, (1984).

#### *2.4.2.3Cross flow*

For large angles of drift, the ship will experience forces that are generated mainly because of the large pressure difference from the side of the upstream flow to the side of the downstream flow. These large forces will be mainly dominated by pressure forces because of the low relative velocities of the fluid and the rather blunt shape of the ship in the transversal direction. They can be modelled according to Norrbin (1978) by:

$$Y_{HC} = -\frac{\rho}{2}\int_{-x_a}^{x_f} T(x)C_{CFD}(x)(v + rx)|v + rx|dx \tag{2.92}$$

$$N_{HC} = -\frac{\rho}{2}\int_{-x_a}^{x_f} T(x)C_{CFD}(x)(v + rx)|v + rx|xdx \tag{2.93}$$

where $T(x)$ and $C_{CFD}(x)$ are the local draft and the cross flow drag coefficient, and the integrals are carried out from the position of

$x_a$ to the $x_f$, in general $x_a = x_f = \frac{L_{PP}}{2}$. Some level of simplification can be achieved by considering the draft $T(x)$ as constant and expressing $C_{CFD}(x)$ as a polynomial, see Oltmann and Sharma (1984).

#### 2.4.2.4 Resistance

According to the ITTC the ship's resistance can be written as a sum of a viscous and the wave resistance.

$$C_T = \frac{R}{\frac{1}{2}\rho S u^2} = (1+k)C_F(R_n) + C_W(F_r) \tag{2.94}$$

where $C_F$ is the frictional coefficient, $(1+k)$ is the form factor, and $C_W$ is the wave resistance. In ITTC 1978, the terms $C_A$ and $C_{AA}$ are added to the right hand side of Eq. (2.94) to incorporate the hull roughness and global air resistance components, respectively.

The frictional resistance is given, according to ITTC 1957, by:

$$C_F = \frac{0.075}{(log_{10}Rn - 2)^2} = \tag{2.95}$$

As mentioned in Oltmann and Sharma (1984), for purposes of simulations the ship resistance is modelled by a polynomial expansion to avoid numerical problems with the term $C_F(R_n)$ near zero forward speed.

$$R(u) = R_{Tu}u + R_{Tu|u|}u|u| + R_{Tuuu}u^3 \tag{2.96}$$

The model including linear, quadratic, and cubic terms allow to incorporate a large range of ship speeds. According to Oltmann and Sharma (1984) this formulation can also be applied for forward and backward motions without any change in the coefficients, and any serious induced error. However, if higher precision is required, different coefficients can be estimated for the backward motion ($u$<0).

### 2.4.3 Manoeuvring model in 3DOF

In the conventional manoeuvring analysis, the influence of waves and any other factor that might subject the ship to vertical motions is neglected. Neglecting the ship's vertical motions, and considering the ship's symmetry with respect to the vertical plane ($y_G = 0$), Eq. (2.75) can be simplified greatly.

$$\begin{bmatrix} m(\dot{u} - vr - x_G r^2) \\ m(\dot{v} + ur + x_G \dot{r}) \\ \dot{h}_z + m(x_G \dot{v} + x_G ur) \end{bmatrix} = \begin{bmatrix} X \\ Y \\ N \end{bmatrix} \tag{2.97}$$

The right hand side of Eq. (2.97) is associated to forces and moments resulting from the hydrodynamic effects on the hull, propeller effects, and rudder effects.

In literature different models have been proposed for the evaluation of the surge forces ($X$), the sway forces ($Y$) and the yaw moments ($N$). They can be distinguished in two main groups: formal mathematical models and modular mathematical models. The present discussion will only focus on modular approach as they allow a more detailed representation of the physical phenomena. For a more extensive discussion on the two types of models, see Eloot (2006).

In the modular approach, the forces are subdivided in four main components as:

$$\begin{bmatrix} X \\ Y \\ N \end{bmatrix} = \begin{bmatrix} X_H + X_P + X_R + X_{EXT} \\ Y_H + Y_P + Y_R + Y_{EXT} \\ N_H + N_P + N_R + N_{EXT} \end{bmatrix} \tag{2.98}$$

The subscripts H, P, R, and EXT represent the hull, propeller, rudder, and external forces and moments.

Bear in mind that wave action will also influence the ship forces on the hull, this will be extensively discussed in Chapter 5 and 6.

#### 2.4.3.1Hull effects

The hydrodynamic forces on the hull can be assumed to be mainly determined by fluid phenomena which are considered dominant. In literature, these fluid forces are commonly divided in: ideal fluid effects, lift effects, cross flow effects and viscous drag and pressure drag effects associated to ship resistance.

The modelling of the hydrodynamic forces and moments in general varies depending on the application of the model itself. This is the main reason why several models can be found in literature and also because of the simplifications that can be applied. These considerations depend mainly of two ships parameters, the ship's speed regime, low and high Froude numbers, and smaller and larger drift angles.

Considering mainly the regime speed and smaller drift angles, polynomial mathematical models based on a 2nd order regression model, commonly known as a Norrbin model, can be found in literature. For instance, in Vantorre (1997), the hull forces can be expressed as:

$$X_H = X_{\dot{u}}\dot{u} + X_{u|u|}u|u| + X_{vv}v^2 + X_{rr}r^2 + X_{vr}vr \tag{2.99}$$

$$Y_H = Y_{\dot{v}}\dot{v} + Y_{\dot{r}}\dot{r} + Y_{uv}uv + Y_{ur}ur + Y_{v|v|}v|v| + Y_{r|r|}r|r| + Y_{v|r|}v|r| + Y_{r|v|}r|v|$$

$$N_H = N_{\dot{v}}\dot{v} + N_{\dot{r}}\dot{r} + N_{uv}uv + N_{ur}ur + N_{v|v|}v|v| + N_{r|r|}r|r| + N_{v|r|}v|r| + N_{r|v|}r|v| \tag{2.101}$$

In Eq. (2.99) and Eq. (2.101) the ideal fluid ($H_{id}$) effects are given by the acceleration terms:

$$X_{H_{id}} = X_{\dot{u}}\dot{u} \tag{2.102}$$

$$Y_{H_{id}} = Y_{\dot{v}}\dot{v} + Y_{\dot{r}}\dot{r} \tag{2.103}$$

$$N_{Hid} = N_{\dot{v}}\dot{v} + N_{\dot{r}}\dot{r} \tag{2.104}$$

The remaining sixteen terms, $X_{u|u|}$, to $N_{r|v|}$, are constant terms and depend only on the ship's velocity components.

Models especially suited for full manoeuvring bridge simulator require a more complex approach. In general different sub models are used to cover the wide range of speeds: low speed models, intermediate speed models, and higher speed models. In Kobayashi (1987), in addition sub models are introduced as a function of the drift angle ($\beta$).

Intermediate and higher speed models are mostly of the type described above. Different from those, low speed manoeuvring models involve large drift angles. This is because they can be used to simulate a broad range of manoeuvres including crash ahead stop, and turning at zero speed. Models as such are the works of Oltmann and Sharma (1984), Kobayashi (1987), and Khattab (1987). Although their respective expressions may differ, the hydrodynamic effect due to lift, drag, and cross flow effects are commonly considered.

In Eloot (2006) and most recently in Delefortrie et al. (2016a) the models using tabular functions for the hydrodynamic forces on the hull, given in here only for 3DOF, can be written as:

$$X_H = X_{\dot{u}}\dot{u} + \frac{1}{2}\rho L_{PP} T_M X'(\beta)(u^2+v^2) + \frac{1}{2}\rho L_{PP} T_M X'(\gamma)(u^2+v_P^2) + \frac{1}{2}\rho L_{PP} T_M X'(\chi)(v^2+v_P^2) \quad (2.105)$$

$$Y_H = Y_{\dot{v}}\dot{v} + Y_{\dot{r}}(\beta)\dot{r} + \frac{1}{2}\rho L_{PP} T_M Y'(\beta)(u^2+v^2) + \frac{1}{2}\rho L_{PP} T_M Y'(\gamma)(u^2+v_P^2) + \frac{1}{2}\rho L_{PP} T_M Y'(\chi)(v^2+v_P^2) \quad (2.106)$$

$$N_H = N_{\dot{v}}\dot{v} + N_{\dot{r}}(\beta)\dot{r} + \frac{1}{2}\rho L_{PP}^2 T_M N'(\beta)(u^2+v^2) + \frac{1}{2}\rho L_{PP}^2 T_M N'(\gamma)(u^2+v_P^2) + \frac{1}{2}\rho L_{PP}^2 T_M N'(\chi)(v^2+v_P^2) \quad (2.107)$$

where $\rho$, $L_{PP}$, $T_M$, $u$, and $v$ are the water density, the ship's length, the ship's draft, and the ship's longitudinal and lateral velocity, respectively. $v_{\mathrm{P}}$ is a reference lateral velocity, function of the angular velocity in yaw ($r$), and is given by:

$$v_{\mathrm{P}} = rL_{PP}/2 \tag{2.108}$$

In Eq. (2.105) to Eq. (2.107) the tabular nine coefficients $X'(\beta)$ to $N'(\chi)$ are the tabular functions. They are given as function of the hydrodynamic angles:

$$\beta = \arctan\left(\frac{-v}{u}\right) \tag{2.109}$$

$$\gamma = \arctan\left(\frac{v_P}{u}\right) \tag{2.110}$$

$$\chi = \arctan\left(\frac{v_P}{v}\right) \tag{2.111}$$

The ideal fluid effects in Eq. (2.105) to Eq. (2.107) are accounted by the same components of the polynomial model given in Eq. (2.102) to Eq. (2.104). In the current approach, however, $Y_{\dot{r}}(\beta)$ and $N_{\dot{r}}(\beta)$ are dependent on the drift angle $\beta$. This drift dependency of the forces is because of the physical background lying behind ideal fluid effects. They represent work needed to be done to change the current kinetic energy of the fluid, see 2.3. Since the flow is different with and without drift angle, consequently the added masses and moments will change. This dependency has been pointed out by Imlay (1961) and will also be discussed extensively in the present work in Chapter 6.

Notice that ideal fluid effects in the models above are only a function of acceleration terms. From the discussion in 2.3, the ship's velocities $u$ and $v$ will also introduce a destabilizing $(X_{\dot{u}} - Y_{\dot{v}})uv$ term in yaw. This term is also known as the Munk moment. Because the same parameters define lift effects, in most mathematical models they are modelled together, see for instance the terms $N_{uv}uv$ in Eq. (2.101) and $N'(\beta)$ in Eq. (2.107).

The modelling of the lift and Munk moments by a common term is also justified when considering a real fluid. This is because as mentioned by Munk (1924), due to the viscosity of the fluid vortices will be produced at the rear of the moving body that will increase local lift and decrease the Munk moment. Hence, the correct estimation of the Munk contribution in a real fluid and its distinction with respect to lift effects is more complicated. Thus modelling them together is relatively simple and more convenient.

### *2.4.3.2Hydrodynamic forces induced by the propeller*

#### 2.4.3.2.1 Propeller thrust

Manoeuvring models for full bridge simulations include positive and negative ship longitudinal speeds $u$ and propeller rates $n$, the combination of which yield to four possible arrangements known as quadrants. The first quadrant corresponds to positive $u$ speeds and $n$ rates. The present section focuses only on this quadrant as the present study of manoeuvring in waves is restricted to positive values for $u$ and $n$ only. An extensive discussion on the other quadrants and methods to compute propeller forces can be found in Vantorre (1997) and more recently in Eloot (2006).

The forces on the hull due to the propeller action will depend on the propeller thrust, which is in turn a function of the propeller rate and is given by:

$$T = \rho D^4 n^2 K_T \tag{2.112}$$

The thrust coefficient $K_T$, can be assumed to be defined by a polynomial function (see e.g. Kijima, 1987) dependent on the advance coefficient.

$$K_T(J) = a_0 + a_1 J + a_2 J^2 \tag{2.113}$$

$J$ can be expressed as:

$$J = \frac{u(1-w)}{nD} \tag{2.114}$$

where $w$ is the wake fraction which expresses the free flow speed $u$ reduction at the location of the propeller due to the presence of the ship. The wake fraction in Kobayashi (1987) is expressed as:

$$(1-w) = (1-w_0) + C_1 v' + C_2 r' + C_3 v'^2 + C_4 v' r' + C_5 r'^2 \tag{2.115}$$

The terms incorporating the non-dimensional ship velocities $v'$ and $r'$ take into account the effect of sway and yaw motions on the wake, and the respective coefficients $C_1$ to $C_5$ are constant values determined experimentally. The first term in Eq. (2.115) expresses the wake fraction when the ship moves in a straight path and it is given by:

$$(1-w_0) = b_0 + b_1 J^* \tag{2.116}$$

$J^*$ is the apparent advance number defined assuming open water, hence, no interference of the free flow $u$.

$$J^* = \frac{u}{nD} \tag{2.117}$$

#### 2.4.3.2.2 Propeller forces on the ship

In spite of the different approaches to estimate the wake fraction, in literature all models express the longitudinal force on the hull due to the propeller action as:

$$X_P = (1-t)T \tag{2.118}$$

The term $t$ is the thrust deduction fraction, which is generally understood as an increase of the ship's resistance due to the presence of the working propeller.

The thrust deduction fraction can be found experimentally and can be expressed as a function of the apparent advance number $J^*$. In literature, is also common to replace the advance number $J$ by the hydrodynamic advance angle $\varepsilon$, defined by:

$$\varepsilon = \arctan\left(\frac{J}{0.7\pi}\right) \tag{2.119}$$

The lateral force and yaw moment due to the propeller are in general small. Because of these small magnitudes, In Kijima (1987), for instance, they are neglected. Other authors, however, still account for them, e.g. Kobayashi (1987), Oltmann and Sharma (1984) and Vantorre and Eloot (1996).

The formulations available in literature for the lateral force and yaw moment differ from one author to another, in Oltmann and Sharma (1984), fo instance the sway forces and yaw moment are determined by the constant coefficients $Y_{PT}$ and $N_{PT}$, respectively and are function of the propeller thrust.

$$Y_P = Y_{PT}T \tag{2.120}$$

$$N_P = N_{PT}T \tag{2.121}$$

In Vantorre and Eloot (1996), the propeller lateral force and yawing moment are modelled as a modification of the flow field due to propeller action. This can be expressed as:

$$Y_P = Y(\beta)C_n(\beta)\left(\frac{n^2}{n_0}\right) \tag{2.122}$$

$$N_P = x_Y(\beta)Y_P \tag{2.123}$$

where $Y(\beta)$ is the sway forces without propeller action, and the coefficients $C_n(\beta)$ and $x_Y(\beta)$ change as function of the drift angle $\beta$. $n$ and $n_0$ are the actual and nominal maximum propeller rate, respectively.

In Kobayashi (1987) the sway force $Y_P$ and yaw moment $N_P$ are given as tabular function of the advance number $J$.

### *2.4.3.3 Hydrodynamic forces induced by the rudder*

#### 2.4.3.3.1 Forces on the rudder in open water

Rudder forces can be obtained by composing the lift force $F_L$ and drag force $F_D$ which are dependent on the inflow velocity $V_R$ and the inflow angle $\alpha_R$. These forces can also be expressed in the rudder frame of reference $O_R - x_R\, y_R\, z_R$ (R-frame) as the tangential force $F_{TR}$ and the normal force $F_{NR}$. In Figure 2.4 these parameters

are illustrated for better understanding. Rudder forces, expressed in R-frame, can be further transformed to the b-frame axes by a single rotation using the rudder angle $\delta_R$, this is given by:

$$\begin{bmatrix} F_X \\ F_Y \end{bmatrix} = \begin{bmatrix} cos\delta_R & -sin\delta_R \\ sin\delta_R & cos\delta_R \end{bmatrix} \begin{bmatrix} F_{TR} \\ F_{NR} \end{bmatrix} \tag{2.124}$$

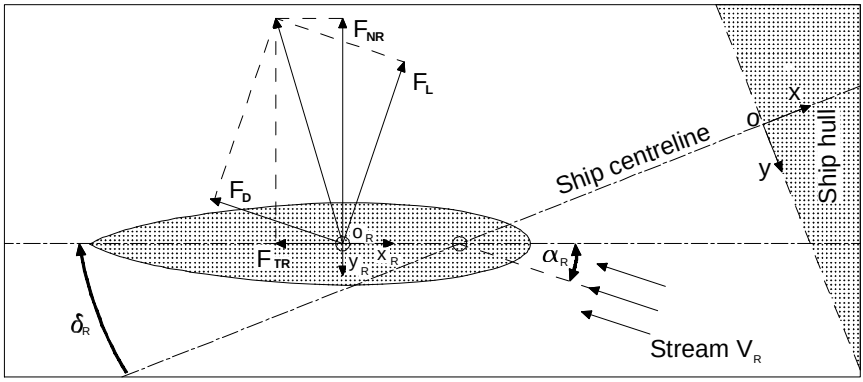


Figure 2.4 Top view of the rudder behind the ship and definitions of the rudder angle, inflow angle, drag forces, lift forces, normal forces and tangential forces. Normal and tangential forces given in the rudder reference frame $O_R - x_R\, y_R\, z_R$.

The tangential and normal rudder forces can be expressed as function of the lift $C_{LR}$ and drag $C_{DR}$ coefficients by:

$$\begin{bmatrix} F_{TR} \\ F_{NR} \end{bmatrix} = \frac{1}{2}\rho A_R V_R^2 \begin{bmatrix} -cos\alpha_R & sin\alpha_R \\ sin\alpha_R & cos\alpha_R \end{bmatrix} \begin{bmatrix} C_{DR}(\alpha_R) \\ C_{LR}(\alpha_R \end{bmatrix} \tag{2.125}$$

Introducing Eq. (2.125) in Eq. (2.124), the rudder forces, given as function of the drag and lift coefficients, can be found by:

$$\begin{bmatrix} F_X \\ F_Y \end{bmatrix} = \frac{1}{2}\rho A_R V_R^2 \begin{bmatrix} cos\delta_R & -sin\delta_R \\ sin\delta_R & cos\delta_R \end{bmatrix} \begin{bmatrix} -cos\alpha_R & sin\alpha_R \\ sin\alpha_R & cos\alpha_R \end{bmatrix} \begin{bmatrix} C_{DR}(\alpha_R) \\ C_{LR}(\alpha_R \end{bmatrix} \tag{2.126}$$

#### 2.4.3.3.2 Forces on the rudder behind the ship

The rudder forces on the b-frame axes can also be expressed as function of the lift and drag coefficients by a relative simplified relationship given by:

$$\begin{bmatrix} F_X \\ F_Y \end{bmatrix} = \frac{1}{2}\rho A_P V_R^2 \begin{bmatrix} -cos\beta_R & sin\beta_R \\ sin\beta_R & cos\beta_R \end{bmatrix} \begin{bmatrix} C_{DR}(\alpha_R) \\ C_{LR}(\alpha_R \end{bmatrix} \tag{2.127}$$

The lift $C_{LR}(\alpha_R)$ and drag $C_{DR}(\alpha_R)$ coefficients in Eq. (2.127), different from the previous expressions, are given as function of a modified inflow angle $\alpha_R$, defined by:

$$\alpha_R = \delta_R + \delta_0 + \beta_R \tag{2.128}$$

$\delta_0$ is a correction of flow asymmetry (see, Delefortrie 2009), and it is defined at the condition where the normal force satisfy:

$$\delta_0 = -\delta_R(F_{NR} = 0) \tag{2.129}$$

in Eq. (2.127) the angle $\beta_R$ is the local drift angle defined by the local longitudinal speed $u_R$ and lateral speed $v_R$ components of the inflow velocity $V_R$ (given in the b-frame), $\beta_R$ can be found by:

$$\beta_R = \arctan\left(\frac{-v_R}{u_R}\right) \tag{2.130}$$

The transversal velocity $v_R$ at the rudder can be obtained by:

$$v_R = k_{HR}(v + rx_R) \tag{2.131}$$

The variables $k_{HR}$ and $x_R$ refer to the straightening coefficient and the longitudinal position of the rudder axis. More details on these parameters can be found in Vantorre (1989).

The longitudinal speed $u_R$ can be estimated by a weighted average of the free flow $u_{R0}$ and the flow due to the propeller action $u_{RP}$.

$$u_R = \sqrt{\eta^* u_{RP}^2 + (1 - \eta^*)u_{R0}^2} \tag{2.132}$$

The velocity $u_{R0}$, similar to the case of the propeller, is reduced because of the presence of the ship by the wake fraction $w_R$.

$$u_{R0} = u(1 - w_R) \tag{2.133}$$

The variable $\eta^*$, in the equation above, is the propeller diameter $D$ to rudder height $H_R$ratio ($\eta^* = D/H_R$).

The velocity $u_{RP}$ can be estimated based on the momentum theory (Brix, 1993) by:

$$u_{RP} = u_{R0} + K_m u_P \left( \sqrt{1 + \frac{8K_T}{\pi J^2}} - 1 \right) \tag{2.134}$$

where $u_P$ is the flow axial velocity at the propeller location, given by $u(1-w)$, and $K_m$ is a factor taking into account the propeller jet contraction at the rudder location. $K_m$can vary between 0.5 to 0.96 according to Brix (1993), and is given as function of the distance between the rudder stock and the propeller blade tips.

#### 2.4.3.3.3 Rudder forces on the ship

The rudder longitudinal and lateral forces, as well as the yaw moment contribution on the hull can be obtained by:

$$X_R = (1 - t_R)F_X \tag{2.135}$$

$$Y_R = (1 + a_H)F_Y \tag{2.136}$$

$$N_R = x_R F_Y + x_H a_H F_Y \tag{2.137}$$

the parameters $t_R$, $a_H$, and $x_H$ can be understood as the interaction coefficients due to presence of the hull.

The parameter $x_R$ is the point of application of the rudder force $F_Y$, which can be considered equal to half the length between perpendiculars ($0.5L_{PP}$). Similarly to the case of $x_R$ the parameter $x_H$ can be considered as the application point for the additional lateral force $a_H F_Y$.

The coefficients parameters $t_R$, $a_H$, and $x_H$ can be considered as constant but in literature they have been found to be dependent on the propeller loading, and the sway and yaw velocities of the ship. An extensive discussion on these ship parameters can be found, for instance, in Eloot (2006), and Delefortrie (2007).

### 2.4.4 Manoeuvring model in 6DOF

#### *2.4.4.1General discussion*

Mathematical models for 6DOF manoeuvring motion, for surface ships, are rather scarce in literature. Models have been mostly extended to 4DOF (3+1), to include roll motion only. In the present work the 6DOF model presented by Delefortrie et al. (2016a) will be discussed. Bear in mind that the present representations might differ with the ones presented in Delefortrie et al. (2016a), this is done in order to have a clear distinction of the nature of the hydrodynamic forces which are actually accounted for in the model.

The ship's dynamic equation, assuming the ship's centre of gravity located in the vertical plane of symmetry ($y_G = 0$), is given by:

$$\begin{bmatrix} X \\ Y \\ Z \\ K \\ M \\ N \end{bmatrix} = \begin{bmatrix} m\left(\dot{u} - vr + wq - x_G(r^2 + q^2) + z_G(pr + \dot{q})\right) \\ m(\dot{v} - wp + ur + x_G(pq + \dot{r}) + z_G(qr - \dot{p})) \\ m\left(\dot{w} - uq + vp + x_G(pr - \dot{q}) - z_G(p^2 + q^2)\right) \\ \dot{h}_x + qh_z - rh_y - mz_G(\,\dot{v} + ur - wp) \\ \dot{h}_y + rh_x - ph_z + m\left(-x_G(\dot{w} + vp - uq) + z_G(\dot{u} + wq - vr)\right) \\ \dot{h}_z + ph_y - qh_x + mx_G(\dot{v} + ur - wp) \end{bmatrix} \tag{2.138}$$

where X, Y, and Z represent the forces in surge, sway and heave, while K, M, and N stand for the roll, pitch and yaw moments, respectively, defined in the ship bound axes system (b-frame).

Similar to the case of the 3DOF modular approach discussed above, see 2.4.3.1, the forces and moments acting on the ship are also treated by the following modules:

$$\begin{bmatrix} X \\ Y \\ Z \\ K \\ M \\ N \end{bmatrix} = \begin{bmatrix} X_H + X_P + X_R + X_{EXT} \\ Y_H + Y_P + Y_R + Y_{EXT} \\ Z_H + Z_P + Z_R + Z_{EXT} \\ K_H + K_P + K_R + K_{EXT} \\ M_H + M_P + M_R + M_{EXT} \\ N_H + N_P + N_R + N_{EXT} \end{bmatrix} \tag{2.139}$$

The subscripts H, P, R, and EXT, stand for the hull effects, propeller effects, rudder effects, and external effects, respectively.

#### 2.4.4.2 Hull forces

Hydrodynamic forces and moments on the hull can be assumed to be composed of ideal fluid terms (id), retardation terms (ret), hydrostatic terms (hyd), and finally additional fluid terms which, to the author (because of the similarity to the 3DOF tabular models), can be understood as the contribution of lift, cross flow and viscous effects.

The contributions to forces and moments due to the ideal terms are given as:

$$X_{id} = X_{\dot{u}}\dot{u} \tag{2.140}$$

$$Y_{id} = Y_{\dot{v}}\dot{v} + Y_{\dot{r}}\dot{r} \tag{2.141}$$

$$Z_{id} = Z_{\dot{w}}\dot{w} + Z_{\dot{q}}\dot{q} \tag{2.142}$$

$$K_{id} = K_{\dot{v}}\dot{v} + K_{\dot{p}}\dot{p} + K_{\dot{r}}\dot{r} \tag{2.143}$$

$$M_{id} = M_{\dot{u}}\dot{u} + M_{\dot{w}}\dot{w} + M_{\dot{q}}\dot{q} \tag{2.144}$$

$$N_{id} = N_{\dot{v}}\dot{v} + N_{\dot{r}}\dot{r} \tag{2.145}$$

Notice that in Delefortrie et al. (2016a), the ideal fluid contributions described above, are given together with the ship's inertial terms and centripetal terms in the right hand side of Eq. (2.138).

The retardation terms, or memory terms, are given for heave and pitch only by:

$$Z_{ret} = Z_{\dot{u}}\dot{u} + Z_{\dot{v}}|\dot{v}| + Z_{\dot{r}}|\dot{r}| \tag{2.146}$$

$$M_{ret} = M_{\dot{v}}|\dot{v}| + M_{\dot{r}}|\dot{r}| \tag{2.147}$$

In Delefortrie et al. (2016a) the other degrees of freedom are assumed to be free of retardation terms. In addition, the term $M_{\dot{u}}\dot{u}$ in Eq. (2.144) is also considered as retardation contribution but is left outside of Eq. (2.147).

Notice that the terms such as $Z_{\dot{u}}\dot{u}$ should not be considered as memory terms. They are instead impulsive responses of the fluid due to the ship's accelerations. Acceleration terms as such have

been discussed in 2.3, terms as a function of $\dot{v}$, and $\dot{r}$, however, do not appear for heave and pitch.

The linearised hydrostatic terms, assuming that angles and vertical motion are small, are given by:

$$Z_{hyd} = -\rho g A_W z \tag{2.148}$$

$$K_{hyd} = -\Delta \overline{GM}_T \phi \tag{2.149}$$

$$M_{hyd} = -\Delta \overline{GM}_L \theta \tag{2.150}$$

The total hydrodynamic forces on the hull can be written as:

$$X_H = X_{id} + \frac{1}{2}\rho L_{PP} T_M X'(\beta)(u^2 + v^2) + \frac{1}{2}\rho L_{PP} T_M X'(\gamma)(u^2 + v_P^2) + \frac{1}{2}\rho L_{PP} T_M X'(\chi)(v^2 + v_P^2) \tag{2.151}$$

$$Y_H = Y_{id} + \frac{1}{2}\rho L_{PP} T_M Y'(\beta)(u^2 + v^2) + \frac{1}{2}\rho L_{PP} T_M Y'(\gamma)(u^2 + v_P^2) + \frac{1}{2}\rho L_{PP} T_M Y'(\chi)(v^2 + v_P^2) \tag{2.152}$$

$$Z_H = Z_{id} + Z_{ret} + Z_{hyd} + \Delta T_{u_h} Z'(\beta) + \frac{1}{2}\rho L_{PP} T_M Z'(\gamma)(u^2 + v_P^2) + \frac{1}{2}\rho L_{PP} T_M Z'(\chi)(v^2 + v_P^2) + Z_w w + Z_q q \tag{2.153}$$

$$K_H = K_{id} + K_{hyd} + \frac{1}{2}\rho L_{PP} T_M^2 K'(\beta)(u^2 + v^2) + \frac{1}{2}\rho L_{PP} T_M^2 K'(\gamma)(u^2 + v_P^2) + \frac{1}{2}\rho L_{PP} T_M^2 K'(\chi)(v^2 + v_P^2) + \left(|\phi|\sqrt{\Delta \overline{GM}_T\left(-K_{\dot{p}} + I_{xx}\right)}\right)p + K_p p + K_{up} up \tag{2.154}$$

$$M_H = M_{id} + M_{ret} + M_{hyd} + \Delta L_{PP} T_{u_h} M'(\beta) + \frac{1}{2}\rho L_{PP} T_M^2 M'(\gamma)(u^2 + v_P^2) + \frac{1}{2}\rho L_{PP} T_M^2 M'(\chi)(v^2 + v_P^2) + M_w w + M_q q \tag{2.155}$$

$$N_H = N_{id} + \frac{1}{2}\rho L_{PP} T_M^2 N'(\beta)(u^2 + v^2) + \frac{1}{2}\rho L_{PP} T_M^2 N'(\gamma)(u^2 + v_P^2)$$
$$+ \frac{1}{2}\rho L_{PP} T_M^2 N'(\chi)(v^2 + v_P^2) \quad (2.156)$$

Notice that in Eq. (2.151) to Eq. (2.156) the hull forces in surge and sway, and the yaw moment are the same as the ones described in 3DOF tabular model in Eq. (2.105) to Eq. (2.107),

The heave forces and pitch forces are also given as function of the Tuck's parameter, which is defined as:

$$T_{u_h} = \frac{F_{r_h}}{\sqrt{1 - F_{r_h}^2}} \quad (2.157)$$

where the ship speed, given as the depth based Froude number, is defined as:

$$F_{r_h} = \frac{V}{\sqrt{gh}} \quad (2.158)$$

g is the gravity acceleration constant and h is the water depth.

In the representation for the heave force and the pitch moment, terms such as $Z_w w$ , $Z_q q$, $M_w w$ , $M_q q$ can be observed. These terms can be associated to the wave generation problem associated to the ship motions in heave and pitch.

In roll motion, Eq. (2.154), the term in parenthesis involve the ship's displacement, $\Delta$ ,the transversal metacentric height, $\overline{GM}_T$ , and the added roll added mass, $K_{\dot{p}}$ , and is assumed to be a nonlinear correction of the linear damping coefficient $K_p$ .In addition a term $K_{up}$ takes into account the ship forward speed influence in the damping factor. Notice that a similar nonlinear correction have been proposed in Himeno (1981) roll motion; however, in this case the nonlinear term $K_{p|p|}$ is proportional to $p|p|$ ($K_{p|p|}p|p|$) and $K_p$ is assumed to be composed of a constant term and one proportional to ship speed.

It is important to mention that the above equations do not consider the coupled inertia terms in surge $X_{\dot{w}}$, $X_{\dot{q}}$, in sway $Y_{\dot{p}}$, in heave $Z_{\dot{u}}$, in roll $K_{\dot{r}}$ and in yaw, $N_{\dot{p}}$.

#### *2.4.4.3Hydrodynamic effects due to propeller action*

The propeller thrust characteristics in open water and behind the ship follow the same analysis as described in 2.4.3.2.1. Hence, they are omitted in the current discussion. The propeller forces and moments, however, differ to some extent. They include also heave forces, roll moments, and pitch moments, apart from the forces in surge and sway, and yaw moments.

##### 2.4.4.3.1 Propeller forces on the ship

The longitudinal forces on the ship are given as function of the thrust forces and the thrust deduction fraction ($t$) by:

$$X_P = (1 - t(\varepsilon^*, \phi^*, \gamma^*))T \tag{2.159}$$

$t$ is defined as function of the propeller loading angles, $\varepsilon^*$, $\phi^*$, $\gamma^*$.

$$t = f(\varepsilon^*) + q_1(\varepsilon^*)\phi^* \, \mathrm{E}_1 + q_3(\varepsilon^*)\phi^* \, \mathrm{E}_3 + q_4(\varepsilon^*)\phi^* \, \mathrm{E}_4 \tag{2.160}$$

where $\varepsilon^*$ has been already defined in Eq. (2.119), and $\phi^*$ and $\gamma^*$ are given by:

$$\phi^* = arctan\left(\frac{|v|}{0.7\pi nD}\right) \tag{2.161}$$

$$\gamma^* = arctan\left(\frac{|v_p|}{0.7\pi nD}\right) \tag{2.162}$$

The terms $q_j(\varepsilon^*)$ in Eq. (2.160) are equal to one in their respective quadrant $j$, and are zero otherwise.

The remaining forces and moments applying on the ship have three different causes according to Delefortrie et al. (2016a). Firstly, the propeller action affects the hydrodynamic (inertial) derivatives. Secondly, a constant force is induced depending on the propeller thrust, $T(\varepsilon^*)$, yaw, $\gamma$, and drift angle, $\beta$. In the third place, an oscillation with frequency $\omega(\varepsilon^*)$ will occur in the even quadrants as function of the propeller loading $\varepsilon^*$.

With the considerations stated above, the forces and moments on the ship due to propeller action are given by:

$$Y_P = \left|\frac{n}{n_0}\right| (Y_{\dot{v}}^n \dot{v} + Y_{\dot{r}}^n \dot{r}) + K_1 T \left(Y_{PT}(\beta, \varepsilon^*) + Y_{PT}(\gamma, \varepsilon^*)\right) + K_2 T Y_{PTA} cos\left(\omega(\varepsilon^*)t + \phi_Y(\varepsilon^*)\right) \quad (2.163)$$

$$Z_P = K_3 T\left(Z_{PT}(\beta, \varepsilon^*) + Z_{PT}(\gamma, \varepsilon^*)\right) + K_2 T Z_{PTA} cos\left(\omega(\varepsilon^*)t + \phi_Z(\varepsilon^*)\right)$$

$$K_P = \left|\frac{n}{n_0}\right| (K_{\dot{v}}^n \dot{v} + K_{\dot{r}}^n \dot{r}) + T_M T\left(K_{PT}(\beta, \varepsilon^*) + K_{PT}(\gamma, \varepsilon^*)\right) + K_2 T_M T K_{PTA} cos\left(\omega(\varepsilon^*)t + \phi_K(\varepsilon^*)\right) \quad (2.165)$$

$$M_P = L_{PP} T\left(M_{PT}(\beta, \varepsilon^*) + M_{PT}(\gamma, \varepsilon^*)\right) + K_2 L_{PP} T M_{PTA} cos\left(\omega(\varepsilon^*)t + \phi_M(\varepsilon^*)\right) \quad (2.166)$$

$$N_P = \left|\frac{n}{n_0}\right| (N_{\dot{v}}^n \dot{v} + N_{\dot{r}}^n \dot{r}) + L_{PP} T\left(N_{PT}(\beta, \varepsilon^*) + N_{PT}(\gamma, \varepsilon^*)\right) + K_2 L_{PP} T\, N_{PTA} cos\left(\omega(\varepsilon^*)t + \phi_N(\varepsilon^*)\right) \quad (2.167)$$

where $T$, $Y_{PTA}$, $Z_{PTA}$, $K_{PTA}$, $M_{PTA}$, $N_{PTA}$, are all functions of $\varepsilon^*$.

#### *2.4.4.4Hydrodynamic effects due rudder action*

##### 2.4.4.4.1 Rudder forces on the ship

The analysis of the rudder characteristics are similar to the case studied in 2.4.3.3. The main differences of the present model are in the forces and moments applied to the ship. They are given by:

$$X_R = F_X \quad (2.168)$$

$$Y_R = (1 + a_H(\varepsilon^*, \beta))F_Y \quad (2.169)$$

$$K_R = -(z_R + a_H(\varepsilon^*, \beta) Z_H(\beta))F_Y \quad (2.170)$$

$$M_R = z_{HX}(\beta)F_X \quad (2.171)$$

$$N_R = x_R F_Y + x_H a_H(\beta) a_H(\varepsilon^*, \beta) F_Y \quad (2.172)$$

The longitudinal force is accounted without reduction due to interaction with the hull. Heave forces are not affected by the rudder action according to Delefortrie et al. (2016a).

## 2.5 Seakeeping

### 2.5.1 General discussion

In literature, different methods to study the ship's seakeeping behaviour can be found. They can be distinguished from different points of view, to mention the most important: from the domain of analysis (frequency or time domain), from the level of complexity of the hull surface description (two-dimensional methods or three-dimensional methods), and from the wave amplitude and ship induced motion magnitudes (small or large).

Most of the studies have been conducted in the frequency domain, and perhaps the most common study to researchers is the strip theory method of Salvesen et al. (1970). Frequency domain methods have been further extended to include more accurately the three-dimensional shape of the body geometry. The problems arising when considering the ship's forward speed, however, are not yet fully solved. Time domain methods such as the Rankine panel method are perhaps the most advanced methodology but their relative advantages for the prediction of wave loads are not conclusive, and with respect to ship motions almost no differences are attained.

It is not possible to cover all aspects of the developed and proposed methods for seakeeping analysis, hence, the present discussion will mainly focus on the frequency domain analysis because of its relative practical use. A time domain analysis is also discussed in the present work but has been presented separately in Chapter 6 and Chapter 7 for better understanding of the problem.

### 2.5.2 Definitions and coordinate systems

In seakeeping the ship is considered to move on a straight path with a constant forward speed $V$. Waves relative to the ship speed have an angle $\mu$, which is known as the wave angle of encounter, see Figure 2.5 for better understanding on the definitions. Moreover, it is important to mention that generally in seakeeping the ship's propeller and rudder actions are neglected.

To analyse the ship's motion responses, and forces and moments acting on the ship, three axes systems are used, the E-frame $(0_0 - X_{0_0}, Y_{0_0}, Z_{0_0})$, the b-frame $(0 - x, y, z)$ and the h-frame $(0_0 - x', y', z')$ as defined in 2.2.1. The E-frame is fixed relative to the mean water level, the h-frame moves parallel to the mean water level with the constant speed $V$ while the b-frame is fixed to the ship. In general the origins of the h-frame and the b-frame are located at the ship's centre of gravity G. Notice that in seakeeping, different from the frames used in the rigid body analysis, both frames are oriented with their vertical axis pointed upwards.

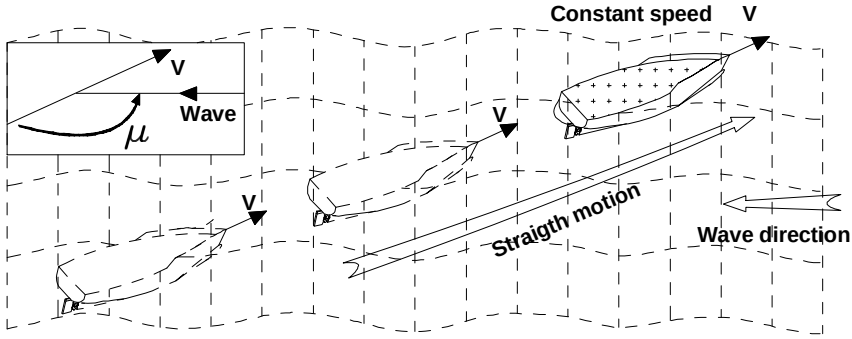


Figure 2.5 Ship moving on an straight path in waves, with an angle of encounter $\mu$.

Because of the relative motion between the ship and waves, the ship will not harmonically oscillate with the wave frequency. This frequency, however, will be a function of the angle of encounter $\mu$, the ship speed $V$, and the wave main parameters, and is given by:

$$\omega_E = \omega_W - kgVcos(\mu) \tag{2.173}$$

where $g$ is the gravity acceleration constant, k the wave number and $\omega_W$ the wave frequency.

### 2.5.3 Dynamics of the rigid body

From the linear analysis between the b-frame and the h-frame, see 2.2.3.3, and assuming that both coincide at the centre of gravity G, with the ship performing harmonic oscillatory motions

$\xi_k e^{i\omega_E t}$ at the frequency of encounter $\omega_E$, the dynamic equation, in a summarised version, can be written as:

$$\sum_{K=1}^{6}\left[-\omega_E^2\left(M_{jk}+A_{jk}\right)+i\omega_E B_{jk}+C_{jk}\right]\xi_k = F_j \tag{2.174}$$

Notice that because of the linearity of the equation due to the assumption of small oscillatory motions, the distinction between the h-frame and the b-frame are lost in the simplifications.

The variables $M_{jk}$ , $A_{jk}$, $B_{jk}$ $C_{jk}$ and $F_j$ are the matrices representing the inertia terms, the added masses terms, the damping coefficients, the restoring terms and the wave exciting forces, respectively. The matrices $M_{jk}$, $A_{jk}$, and $B_{jk}$, for a ship with a lateral symmetry, are:

$$M_{jk} = \begin{bmatrix} m & 0 & 0 & 0 & mz_G & 0 \\ 0 & m & 0 & -mz_G & 0 & 0 \\ 0 & 0 & m & 0 & 0 & 0 \\ 0 & -mz_G & 0 & I_{xx} & 0 & -I_{xz} \\ mz_G & 0 & 0 & 0 & I_{yy} & 0 \\ 0 & 0 & 0 & -I_{xz} & 0 & I_{zz} \end{bmatrix} \tag{2.175}$$

$$A_{jk} = \begin{bmatrix} A_{11} & 0 & A_{13} & 0 & A_{15} & 0 \\ 0 & A_{22} & 0 & A_{24} & 0 & A_{26} \\ A_{31} & 0 & A_{33} & 0 & A_{35} & 0 \\ 0 & A_{42} & 0 & A_{44} & 0 & A_{46} \\ A_{51} & 0 & A_{53} & 0 & A_{55} & 0 \\ 0 & A_{62} & 0 & A_{64} & 0 & A_{66} \end{bmatrix}, \quad (or\ B_{jk}) \tag{2.176}$$

For now, it is only useful to define these parameters, in a later subsection the mathematical treatment to obtain $A_{jk}$, $B_{jk}$, $C_{jk}$ and $F_j$ will be discussed in more detail.

### *2.5.3.1Hydrodynamic phenomena*

In seakeeping analysis three main assumptions are considered for the fluid: it must be incompressible, irrotational, and inviscid. These assumptions allow to consider the fluid as ideal, which allows the use of the potential theory. Although viscosity is initially neglected from the analysis, it should be noticed that further

corrections are introduced to account for it, the most obvious case being the use of a viscous damping correction for roll motion.

The fluid forces in the analysis can be mainly considered as composed of two different sources, the body reaction forces and the wave exciting forces. The body reaction forces, also known as the radiation problem are forces arising due to the ship motion in the fluid; because the ship is to move at the water surface, waves will be generated in all directions. The radiation problem is commonly solved separately assuming the ship to move in otherwise calm water. The wave exciting forces and moments arise due to the presence of waves changing the flow, hence, the pressure along the hull. The wave exciting forces are usually solved on the body restrained, hence no motions are allowed. The mathematical solution of this problem yields two different sub problems, the Froude-Krylov forces and moments and the diffraction forces and moments.

The diffraction problem is a result of the boundary condition applied of the hull surface, necessary to attain no net flow flux through the hull surface. The pressure integration of this potential yields the respective forces and moments.

The Froude-Krylov problem is perhaps the most practical to solve from the entire analysis. This requires the integration of the pressure due to the incident waves on the hull surface assuming that the incident wave is not disturbed by the presence of the ship's hull. No change of the incident wave potential is needed.

Because of the nature of the problem, further simplifications are used in the study of the ship hydrodynamic forces, for instance assuming constant wetted hull surfaces, and waves and ship motions with small amplitudes of oscillations.

### 2.5.4 Potential flow general considerations

Although the different approaches may differ, they all are based on the fundaments of ideal fluids. They all assume the fluid to be incompressible, irrotational, and inviscid, and define a velocity potential $\Phi$ which must satisfy the following conditions:

Laplace or continuity equations.

$$\nabla^2\Phi = \frac{\partial^2\Phi}{\partial \mathrm{x}^2} + \frac{\partial^2\Phi}{\partial \mathrm{y}^2} + \frac{\partial^2\Phi}{\partial \mathrm{z}^2} = 0 \tag{2.177}$$

Free Surface Boundary Conditions (FSBC),

$$\frac{Dp}{Dt} = -\rho\frac{D}{Dt}\left(\frac{\partial\Phi}{\partial t} + \frac{1}{2}|\nabla\Phi|^2 + gz\right) = 0 \tag{2.178}$$

at the unknown free surface defined by: $z = \zeta(x, y, t)$, and where $\frac{D}{Dt}$ is the substantial derivative given by: $\frac{D}{Dt} = \frac{\partial}{\partial t} + \nabla\phi.\nabla$.

Sea bed boundary condition.

$$\frac{\partial\Phi}{\partial \mathrm{z}} = 0 \qquad \text{for } z = -h \tag{2.179}$$

where $h$ is the water depth.

Radiation at infinity condition.

$$\lim_{R\to\infty} \Phi = 0 \qquad \text{for } z = -h \tag{2.180}$$

$R$ is the distance from the ship to a point in the fluid domain.

Additional boundary conditions are set on the body surface of the ship to comply with the ship motions, for instance for a ship with zero forward speed, it will be:

$$\frac{\partial\Phi}{\partial \mathrm{n}} = 0 \tag{2.181}$$

Other boundary conditions are also taken into account depending on the level of approximations of the solutions, see for instance, Salvesen, et al. (1970), and Ogilvie (1964).

### *2.5.4.1Newman-Kelvin linearization*

When the ship moves with a forward speed, the analysis requires further approximations. It is in general accepted to assume the velocity potential $\Phi(x', y', z', t)$ is separated into two main parts:

$$\Phi(x', y', z', t) = [-Vx' + \phi_s(x', y', z')] + \phi_T(x', y', z')e^{i\omega_E t} \quad (2.182)$$

one time independent steady contribution, $-Vx' + \phi_s(x', y', z')$, due to the forward motions of the ship, and the other the time dependent part associated with the incident wave system and the unsteady body motion, $\phi_T(x', y', z')e^{i\omega_E t}$ . $\phi_T$ is the complex amplitude of the unsteady potential, and $\omega_E$ is the frequency of encounter in the moving reference frame (h-frame).

Further simplification can be applied by assuming the potential unsteady contribution $\phi_T$ to be given by:

$$\phi_T = \phi_I + \phi_D + \sum_{j=1}^{6} \xi_J \phi_J \quad (2.183)$$

a linear superposition of the incident wave potential $\phi_I$ , the diffraction potential, $\phi_D$, and the radiation potential $\xi_J \phi_J$.

The radiation potential is considered different from the case described above in 2.3.2. In here, this is defined by the ship harmonic motion amplitudes given by $\xi_j$, where $j$=1, 2, 3, 4 , 5, 6 refer to surge, sway, heave, roll, pitch and yaw, respectively. Bear in mind that because of the new definition the radiation potential must satisfy on the hull surface:

$$\frac{\partial \phi_j}{\partial n} = i\omega_E n_j + V m_j \quad (2.184)$$

where $n_j$ is the generalized normal given by:

$$(n_1, n_2, n_3) = n \qquad \textit{and} \qquad (n_4, n_5, n_6) = r \times n \quad (2.185)$$

$n$ is the outward unit vector and $r$ is the position vector with respect to the origin of coordinates. $m_j = 0$, for $j$ =1, 2, 3, 4, and $m_5 = n_3$, and $m_6 = n_2$.

Further simplification can be achieved by assuming the radiation potential to be given by:

$$\phi_j = \phi_j^0 + \frac{V}{i\omega_E}\phi_j^U \tag{2.186}$$

which yields:

$$\frac{\partial \phi_j^0}{\partial n} = i\omega_E n_j \tag{2.187}$$

$$\frac{\partial \phi_j^U}{\partial n} = i\omega_E m_j \tag{2.188}$$

The relationships above allow to find relationships between the zero speed and the non-zero speed radiation problem. These expressions are given below:

$$\phi_j = \phi_j^0 \qquad \textit{for} \qquad j = 1,2,3,4 \tag{2.189}$$

$$\phi_5 = \phi_5^0 + \frac{V}{i\omega_E}\phi_3^0 \tag{2.190}$$

$$\phi_6 = \phi_6^0 - \frac{V}{i\omega_E}\phi_2^0 \tag{2.191}$$

### 2.5.5 Radiation and wave exciting forces and moments

To find the forces on the ship hull, the integration of the pressure around the hull should be obtained. The latter can be obtained based on the Bernoulli principle, given by:

$$p = -\rho\left(\frac{\partial \phi}{\partial t} + \frac{1}{2}\left(\vec{\nabla}\phi\right)^2 + gz\right) \tag{2.192}$$

The equation above can be simplified by considering only the linear terms of the Taylor expansion around the mean wetted surface of the hull $S_0$. The linearised pressure, taking into account the Newman-Kelvin relationship, is given by:

$$p = -\rho\left(i\omega_E - V\frac{\partial}{\partial x}\right)\phi_T e^{i\omega_E t} - pg\left(\xi_3 + \xi_4 y' - \xi_5 x'\right)e^{i\omega_E t} \tag{2.193}$$

The second term in the equation above gives the restoring terms which can be separately computed, hence dropped from the present equations. The hydrodynamic forces can be finally computed by:

$$\boldsymbol{F_{Hj}^{h}} = \left( -\rho \iint\limits_{S_0} \boldsymbol{n_j} \left( i\omega - V\frac{\partial}{\partial x} \right) \phi_T ds \right) e^{i\omega_E t} \tag{2.194}$$

Replacing the potential $\phi_T$ by its approximation given in Eq. (2.183), the forces and moments can decomposed in the components given by the radiation, diffraction forces and Froude-Krylov effects. The later will be grouped as wave exciting forces.

### *2.5.5.1Radiation forces and moments.*

The radiation forces and moments can be obtained from Eq. (2.194) by:

$$\boldsymbol{F_{Rj}^{h}} = -\rho \iint\limits_{S_0} \boldsymbol{n_j} \left( i\omega_E - V\frac{\partial}{\partial x} \right) \sum_{K=1}^{6} \xi_k \phi_k \, ds = \sum_{K=1}^{6} T_{jk} \xi_k \tag{2.195}$$

Where a new term $T_{jk}$ has been introduced representing the hydrodynamic forces and moments in the $j$th direction per unit oscillatory displacement in the $k$th mode. $T_{jk}$ is defined as:

$$T_{jk} = -\rho \iint\limits_{S_0} \boldsymbol{n_j} \left( i\omega_E - V\frac{\partial}{\partial x} \right) \phi_k ds \tag{2.196}$$

Because of the nature of the complex potential terms in the equations above, $T_{jk}$ can be split as:

$$T_{jk} = \omega_E^2 A_{jk} - i\omega_E B_{jk} \tag{2.197}$$

Where the A terms are proportional to accelerations, and B terms are proportional to velocities. Recall the motions are defined as $\xi_k e^{i\omega_E t}$, hence velocities and accelerations are given by, $i\omega_E \xi_k e^{i\omega_E t}$ and $-\omega_E^2 e^{i\omega t}$, respectively.

Notice that the surface integration above, is carried out over the mean surface $S_0$.

Eq. (2.196) can be further simplified taking into account the Eq. (2.186) to Eq. (2.191), as shown by Salvesen, et al. (1970).

$$T_{jk} = -\rho i\omega_E \iint\limits_{S_0} \boldsymbol{n_j}\phi_k ds + V\rho \iint\limits_{S_0} \boldsymbol{m_j}\phi_k ds - V\rho \int_{\boldsymbol{C_A}} \boldsymbol{n_j}\phi_k dl \tag{2.198}$$

The integrals terms where further defined as:

$$T_{jk}^0 = -\rho i\omega_E \iint\limits_{S_0} \boldsymbol{n_j}\phi_k^0 ds \qquad t_{jk} = -\rho i\omega_E \int_{\boldsymbol{C_A}} \boldsymbol{n_j}\phi_k^0 ds \tag{2.199}$$

where $t_{jk}$ refers to the line integral at the aftermost ship section.

The following relationships were further obtained:

for $j,k$=1, 2, 3, 4

$$T_{jk}^V = T_{kj}^0 + \frac{V}{i\omega_E} t_{jk}^A \tag{2.200}$$

for $j$=5, 6, and $k$=1, 2, 3, 4

$$T_{5k}^V = T_{5k}^0 - \frac{V}{i\omega_E} T_{3k}^0 + \frac{V}{i\omega_E} t_{5k}^A \tag{2.201}$$

$$T_{6k}^V = T_{6k}^0 + \frac{V}{i\omega_E} T_{2k}^0 + \frac{V}{i\omega_E} t_{6k}^A \tag{2.202}$$

for $j$=1, 2, 3 and $k$=5, 6

$$T_{j5}^V = T_{j5}^0 + \frac{V}{i\omega_E} T_{j3}^0 + \frac{V}{i\omega_E} t_{j5}^A - \left(\frac{V}{\omega_E}\right)^2 t_{j3}^A \tag{2.203}$$

$$T_{j6}^V = T_{j6}^0 - \frac{V}{i\omega_E} T_{j2}^0 + \frac{V}{i\omega_E} t_{j6}^A + \left(\frac{V}{\omega_E}\right)^2 t_{j2}^A \tag{2.204}$$

for $j = k$=5, 6

$$T_{55}^V = T_{55}^0 + \left(\frac{V}{\omega_E}\right)^2 T_{33}^0 + \frac{V}{i\omega_E} t_{55}^A - \left(\frac{V}{\omega_E}\right)^2 t_{53}^A \tag{2.205}$$

$$T_{66}^V = T_{65}^0 + \left(\frac{V}{\omega_E}\right)^2 T_{22}^0 + \frac{V}{i\omega_E} t_{66}^A + \left(\frac{V}{\omega_E}\right)^2 t_{62}^A \tag{2.206}$$

Expressing the relationships described above in terms of the added masses and damping coefficients, see Eq. (2.197), the terms A and B are given by:

for $jk$=1, 2, 3, , 4

$$A_{jk}^V = A_{kj}^0 \qquad B_{jk}^V = B_{kj}^0 \tag{2.207}$$

for $j$=1,3, $k$=3, 5

$$A_{j5}^V = A_{j5}^0 - \frac{V}{\omega_E^2} B_{j3}^0 \qquad B_{j5}^V = B_{j5}^0 + V A_{j3}^0 \tag{2.208}$$

for $j$=2,4, $k$=2, 6

$$A_{j6}^V = A_{j6}^0 + \frac{V}{\omega_E^2} B_{j2}^0 \qquad B_{j6}^V = B_{j6}^0 - V A_{j2}^0 \tag{2.209}$$

for $j$=5,3, $k$=1, 3

$$A_{5k}^V = A_{5k}^0 + \frac{V}{\omega_E^2} B_{3k}^0 \qquad B_{5k}^V = B_{5k}^0 - V A_{3k}^0 \tag{2.210}$$

for $j$=2,6, $k$=2, 4

$$A_{6k}^V = A_{6k}^0 - \frac{V}{\omega_E^2} B_{2k}^0 \qquad B_{6k}^V = B_{6k}^0 + V A_{2k}^0 \tag{2.211}$$

for $j = k$=5

$$A_{55}^U = A_{55}^0 + \left(\frac{V}{\omega_E}\right)^2 A_{33}^0 \qquad B_{55}^U = B_{55}^0 + \left(\frac{V}{\omega_E}\right)^2 B_{33}^0 \tag{2.212}$$

for $j = k$=6

$$A_{66}^U = A_{66}^0 + \left(\frac{V}{\omega_E}\right)^2 A_{22}^0 \qquad B_{66}^U = B_{66}^0 + \left(\frac{V}{\omega_E}\right)^2 B_{22}^0 \tag{2.213}$$

Notice that in the above relationships the "end terms", given by $t_{jk}^A$, have been neglected. As discussed in Fonseca and Guedes Soares (2004), because of their relatively small immersed transom sections, their added masses and damping magnitudes are very small compared to the corresponding ones of entire hull.

### 2.5.5.2Wave exiting forces and moments.

Wave forces and moments can be obtained from Eq. (2.194) by considering only the diffraction and the radiation potential.

$$\boldsymbol{F_j^h} = \left( -\rho \iint\limits_{S_0} \boldsymbol{n_j} \left( i\omega_E - V\frac{\partial}{\partial x} \right) (\phi_I + \phi_D)\, ds \right) e^{i\omega_E t} \tag{2.214}$$

Splitting them in their components, the diffraction part is given by

$$\boldsymbol{F_{Dj}^h} = \left( -\rho \iint\limits_{S_0} \boldsymbol{n_j} \left( i\omega_E - V\frac{\partial}{\partial x} \right) \phi_D ds \right) e^{i\omega_E t} \tag{2.215}$$

and the Froude-Krylov by:

$$\boldsymbol{F_{FKj}^h} = \left( -\rho \iint\limits_{S_0} \boldsymbol{n_j} \left( i\omega_E - V\frac{\partial}{\partial x} \right) \phi_I ds \right) e^{i\omega_E t} \tag{2.216}$$

The Froude-Krylov can be rearranged by considering the incident potential defined as:

$$\phi_I = \frac{ig\zeta_a}{\omega_W} \frac{\cosh \mathrm{k}(h+z)}{\cosh(kh)}\, e^{-ik(x' cos\mu - y' sin\mu)} \tag{2.217}$$

and the encounter frequency defined in Eq. (2.173) which yields:

$$\boldsymbol{F_{FKj}^h} = \left( -\rho i\omega_W \iint\limits_{S_0} \boldsymbol{n_j} \phi_I ds \right) e^{i\omega_E t} \tag{2.218}$$

In Salvesen et al. (1970) an alternative formulation of the diffraction forces and moments is obtained based on the radiation and incident potentials as:

$$\boldsymbol{F_{Dj}^h} = \left( \rho \iint\limits_{S_0} \left( \phi_j^0 - \frac{V}{i\omega_E}\phi_j^V \right) \frac{\partial \phi_I}{\partial n} ds + \frac{\rho V}{i\omega_E} \int_{C_A} \phi_j^0 \frac{\partial \phi_I}{\partial n} dl \right) e^{i\omega_E t} \tag{2.219}$$

Recall that $C_A$ refer to the aftermost section of the ship and that $S_0$ is the mean wetted hull surface.

### 2.5.6 Wave drift forces and moments

The derivation of the wave exciting forces and moments, obtained above, has been found by considering some simplifications. For instance, the ship does not develop motions, hence waves approach the restrained ship, and only linear terms in the pressure have been taken into account.

Second order forces and moments will arrive by considering the ship moving with the first order oscillatory motions, the pressure is computed in the actual wetted surface and up to second order terms in their expansion are considered. As in the previous analysis, the wave amplitudes and ship's motion amplitudes are considered to be of small order of magnitudes. Moreover, it is assumed that the ship moves only in response to the first order forces and moments.

It is important to point out that the present representation uses the same coordinate axes described earlier in this section, the Earth frame (E-frame), the horizontal frame (h-frame) and the body-bound axes frame (the b-frame).

The following subsection provides a brief discussion of the methods known as the pressure integration method. This allows getting better insight in the nature of the second order forces. For an extended discussion on this topic, the reader can consult the works of Faltinsen and Løken (1979), Journée and Massie (2001), Chen (2004), and Chen (2007).

#### *2.5.6.1 Pressure integration method (near field)*

The main approach of the present methods is to account for a more correct estimation of the pressure forces and integrate them on the actual wetted surface.

To address the present problem, the perturbation method, Taylor expansion of the ship motion, normal vectors around the hull surface, pressure, forces, fluid potential are assumed. This can be summarised as:

$$X = X^{(0)} + \epsilon X^{(1)} + \epsilon^2 X^{(2)} + \cdots \tag{2.220}$$

where the variable $X$ represent the fluid properties or ship characteristics mentioned above. $\epsilon$ is small order of magnitude where $\epsilon \ll 1$.

The potential flow ($\Phi$) and the ship motions ($\vec{X}$), forces ($\vec{F}$) and moments ($\vec{M}$) can be expressed as:

$$\Phi = \epsilon\Phi^{(1)} + \epsilon^2\Phi^{(2)} + O(\epsilon^3) \tag{2.221}$$

$$\vec{X} = \vec{X}^{(0)} + \epsilon\vec{X}^{(1)} + \epsilon^2\vec{X}^{(2)} + O(\epsilon^3) \tag{2.222}$$

$$\vec{F} = \vec{F}^{(0)} + \epsilon\vec{F}^{(1)} + \epsilon^2\vec{F}^{(2)} + O(\epsilon^3) \tag{2.223}$$

$$\vec{M} = \vec{M}^{(0)} + \epsilon\vec{M}^{(1)} + \epsilon^2\vec{M}^{(2)} + O(\epsilon^3) \tag{2.224}$$

Where the superscripts (0), (1), and (2), refer to the static terms, the first order terms, and the second order terms, respectively.

Notice that considering the notation used in the description of the rigid body dynamics, see 2.2, the position vector described in Eq. (2.222) can be written as, $\vec{X} = (\mathrm{x}_0,\ \mathrm{y}_0,\ \mathrm{z}_0) = \vec{r}^{\,E}_{P/O_0}$, where:

$$\vec{r}^{\,E}_{P/O_0} = \vec{r}^{\,h}_{G/O_0} + R^E_b(\Theta)\vec{r}^{\,b}_{P/G} \tag{2.225}$$

Where $R^h_b(\Theta)$ is the linear rotation matrix from the b-frame to the E-frame. Because of the small motion oscillations, $R^h_b(\Theta)$ can be given by the rotation from the b-frame to the h-frames as:

$$R^h_b(\Theta) = R^h_b(\Xi) = \begin{bmatrix} 1 & -\xi_6 & \xi_5 \\ \xi_6 & 1 & -\xi_4 \\ -\xi_5 & \xi_4 & 1 \end{bmatrix} \tag{2.226}$$

In Journée and Massie (2001) $\Phi$ is shown to be decomposed in:

$$\Phi = \Phi^{(1)}_I + \Phi^{(1)}_D + \Phi^{(1)}_R + \Phi^{(2)}_D + \Phi^{(2)}_I \tag{2.227}$$

where the second order potential $\Phi^{(2)}$ in Eq. (2.221) is given by:

$$\Phi^{(2)} = \Phi^{(2)}_D + \Phi^{(2)}_I \tag{2.228}$$

$\Phi_D^{(2)}$ is an ordinary potential and $\Phi_I^{(2)}$ may be regarded as a second order equivalent of the incoming wave potential $\Phi_I^{(1)}$. Terms with superscript (1) are first order potentials, as discussed earlier.

The remaining part of the analysis is to compute the pressure and integrate it on the actual hull wetted surface. From the Bernoulli equation,

$$p = -\rho g z_0 - \rho \frac{\partial \phi}{\partial t} - \frac{1}{2}\rho\left(\vec{\nabla}\phi\right)^2 \tag{2.229}$$

and assuming also a Taylor expansion up to the second order only,

$$p = p^{(0)} + \epsilon p^{(1)} + \epsilon^2 p^{(2)} \tag{2.230}$$

the following pressures can be identified.

a hydrostatic pressure

$$p^{(0)} = -\rho g z_0^{(0)} \tag{2.231}$$

a first order pressure

$$p^{(1)} = -\rho g z_0^{(1)} - \rho \frac{\partial \phi^{(1)}}{\partial t} \tag{2.232}$$

and a second order pressure

$$p^{(2)} = -\rho \frac{1}{2}\left(\nabla\phi^{(1)}\right)^2 - \rho \frac{\partial^2 \phi^{(2)}}{\partial t^2} - \rho\left(\vec{X}^{(1)} \cdot \vec{\nabla}\frac{\partial \phi^{(1)}}{\partial t}\right) \tag{2.233}$$

The forces and moments on the actual surface S, can be obtained by:

$$\vec{F} = -\iint_S p \cdot \vec{N} \cdot dS \tag{2.234}$$

$$\vec{M} = -\iint_S p \cdot \left(\vec{X}' \times \vec{N}\right) \cdot dS \tag{2.235}$$

where $\vec{N}$ is the normal to the hull surface S.

Notice thatthe integration is carried out over the entire whole wetted surface S. This is a constantly changing surface due to the first order motions of the ship.

#### 2.5.6.2Wave drift forces and moments: other methods

In literature the momentum theory, also known as far field method, proposed by Maruo (1960) can be found. In this method, the second order problem is solved by applying the conservation principle of linear and angular momentum to the fluid domain bounded by the body surface $S$, the free surface $F$ and the control surface $S_\infty$. The later assumed to be at a greater distance from the body.

In Maruo (1960) only the horizontal forces have been analysed, this has been later extended by Newman (1967) including the momentum around the vertical axis. In Chen (2007) Newman's formulations are presented as:

$$\mathrm{F}_D^x = \langle \iint_{S_\infty} (\rho \Phi_n \Phi_x + p n_1)\, ds + \frac{\rho g}{2} \oint_{\Gamma_\infty} \eta^2 n_1 dl \rangle \tag{2.236}$$

$$\mathrm{F}_D^y = \langle \iint_{S_\infty} \left(\rho \Phi_n \Phi_y + p n_2\right) ds + \frac{\rho g}{2} \oint_{\Gamma_\infty} \eta^2 n_2 dl \rangle \tag{2.237}$$

$$\mathrm{M}_\mathrm{D}^z = \langle \iint_{S_\infty} \left(\rho \Phi_n \left[x_0\, \Phi_y - y_0\, \Phi_x\right] + p n_2\right) ds + \frac{\rho g}{2} \oint_{\Gamma_\infty} \eta^2 n_2 dl \rangle \tag{2.238}$$

The symbol "⟨ ⟩" means the average over one period of oscillations, and $\Gamma_\infty$ is the boundary touching vertically the mean free surface $F$. The line integral is the result from the pressure integral between the mean and the instantaneous position of the free surface included in the compact form of the control-surface integral.

The pressure $p$ is given by the Bernoulli equation, as before, by

$$p = -\rho g \mathrm{z}_0 - \rho \frac{\partial \phi}{\partial t} - \frac{1}{2} \rho \left(\vec{\nabla} \phi\right)^2 \tag{2.239}$$

In Chen (2007) modified formulations for the near field and the far field methods are presented. In addition a new middle field method is proposed. These new modified formulations are part of the numerical software Hydrostar from Bureau Veritas (2012).

Notice that the above formulations, except for the first order forces and moments, do not account for the forward speed effects. In Bureau Veritas (2012) an approximation is made based on the Green function associated with the encounter frequency. Other possible solutions are to account for the wave-current approximation made for the first order forces and moments. Because of the complexity and extensive discussion required to describe these relationships, to extend the present work discussion on this topic falls out of the main scope of the present work, hence it is not included; the reader might consult the work of Chen (2004), for instance, for a more detail discussion on this topic.

# MANOEUVRING IN COASTAL WAVES



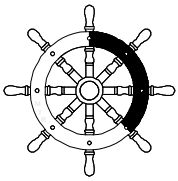

*If one does not know to which port one is sailing, no wind is favourable.*

*Seneca*

# 3

# State of the art

## 3.1 Methods available in literature

### 3.1.1 General discussion

In literature several works addressing the topic of manoeuvring in waves can be found, to mention some of them: Hirano et al. (1980), Ankudinov (1983), McCreight (1986), Ottoson and Bystrom (1991), Bailey et al. (1998), and more recent the works of Skejic (2008), Seo and Kim (2011), Otzen and Simonsen (2012), Carrica et al. (2012), Mousaviraad et al. (2012), and Yasukawa (2015).

It is important to notice that in spite of the different works presented within this topic, only a limited number of methods can be differentiated. These methods can be arranged in three main groups as: a unified method, a two-time scale method, and studies conducted by using computational fluid dynamics. The first two are considered in ITTC (2014) as the unified method because both merge the seakeeping and the manoeuvring problem; however, one must bear in mind the different approaches in the merging process, hence, the distinction made in the present work.

In addition to the methods mentioned above, experimental studies have been conducted to obtain the wave forces and moments on the ship. The results have either been directly used for manoeuvring models, or have first been employed to tune theoretical prediction of wave loads for later use in manoeuvring models.

The methodology to account for wave forces and moments in the experimental studies do not differ significantly from the ones already mentioned above; e.g. Otzen and Simonsen (2012) used experimental studies to tune their seakeeping program which was later used in their manoeuvring model, and Hirano et al. (1980) used the measured second order forces as input to the manoeuvring problem. Although they differ in the estimation of the wave effects, both can be classified as variants of the two-time scale described in Skejic (2008). Therefore, experimental studies will not be considered as a separate methodology. Experimental studies will, however, be considered in the present chapter with special attention on the state of the art methods for the evaluation of wave effects on ship manoeuvring.

For a better illustration of the different topics, the state of the art will be arranged in two sub sections: the first, with the main focus on numerical studies, and the second, with the main focus on experimental studies. The first will discuss mainly the different methodologies available in literature aiming especially on simulation purposes, while the last will focus on the experimental methods for the estimation of wave effects on manoeuvring.

As the main purpose of the present work is to develop a method for simulation purposes, an extended discussion of the two-time scale method and the unified methods will be presented in sub sections 3.2 and 3.3, respectively.

### 3.1.2 Numerical studies

In the two-time scale method the analysis is conducted similar to the case of manoeuvring in calm water, with the only additional consideration that wave effects are introduced in the analysis as

an external source of forces and moments only. Hence, the seakeeping problem must be solved along with the manoeuvring problem. The separation in two independent problems is made based on the assumption of a rapidly varying time scale of the wave problem and the slowly varying time scale associated with the manoeuvring motion.

To calculate the respective wave effects, the ship's position and orientation are provided from the solution of the manoeuvring problem. Then, the wave forces and moments are computed for and introduced in the manoeuvring equation for the next time step solution. It is important to mention that wave forces and moments acting on the manoeuvring problem account only for the mean second order wave forces and moments.

The work of Hirano et al. (1980), although not theoretical, made use of such subdivision of the problem introducing directly the mean wave drift forces in the manoeuvring model. This method has been widely used during the last years by researchers such as Ueno et al. (2003), Skejic (2008) and Seo and Kim (2011). Yasukawa and Nakayama (2009), and Yasukawa (2015). Other studies such as the ones of McCreight (1986), McCreight (1991), and Zhang et al. (2017) can be also included within this classification.

In the unified method the main purpose is to integrate the hydrodynamic phenomena associated to the body reaction forces and moments (radiation problem). The unification of this problem is mostly conducted based on the application of the Cummins equations (Cummins, 1962) using time domain impulse response functions. To the author's knowledge, this methodology was first introduced in the manoeuvring problem in waves by Ankudinov (1983). In Ankudinov (1983); however, an equivalent form expressed by a set of ordinary differential equations was used.

In Bailey et al. (1998), the convolution integral representation was introduced with additional corrections to account for viscous

influence. A detailed analysis of the equivalence between the manoeuvring and seakeeping representation of the radiation problem was also presented. However, problems associated to the forward speed are the main constraint of the model. In addition, only forces and moments linear in terms of velocities and accelerations were considered.

Other approaches such as the works of Lee (2000), Nishimura and Hirayama (2003), Ayaz, et al. (2006), Sutulo and Guedes Soares (2006a), Araki et al. (2011), and the work of Subramanian and Beck (2015) fall into the classification of unified methods. However, in their approach the use of the convolution integral is bypassed by directly computing the radiation problem each time step in the time domain.

It is important to mention that wave exciting forces and moments (first and second order effects) in the unified method are computed mostly in the frequency domain.

CFD studies are perhaps one of the most promising approaches to understand the hydrodynamic problem of manoeuvring in waves, within a good level of detail. CFD has been enhanced significantly in recent years and numerous studies have been presented for steady problems such as resistance and stationary manoeuvres. Only recently, CFD studies have addressed the problem of non-steady conditions such as direct manoeuvring simulation in calm water (Carrica et al., 2012; Carrica et al, 2016), tests in oblique waves (Akimoto, 2010).

It is obvious that manoeuvring in waves is a more time and resources demanding problem because of the complex nature of the fluid problem. From the literature the work of Mousaviraad et al. (2012) and Wang and Wan (2018) are examples of such works. As mentioned in Skejic (2013), the progress of CFD studies for manoeuvring cases is clear; however, considering the required resources and level of complexity of the problem, CFD studies with an accurate prediction in real time (for implementation in

simulators) are not yet foreseen in the near future, certainly not for manoeuvring in shallow water.

### 3.1.3 Experimental studies

Scale model experiments are the most suitable method to investigate the effect of wave forces on manoeuvring. One of the first publications on experimental studies of manoeuvring ships in waves is the work of Hirano et al. (1980), who studied the turning trajectory of a ro-ro ship in regular waves. Because of the growing concern regarding safety of ships in open sea Hirayama and Kim (1994) performed zig-zag tests in irregular waves with a tanker model. Ueno et al. (2003) carried out a more extensive experimental program including straight course, turning and stopping tests in regular waves with a VLCC ship model. Yasukawa (2006a, 2006b) performed similar studies for straight course and turning motion in regular and irregular waves with a S-175 ship model, and recently, Yasukawa (2015) conducted zig-zag and turning tests in irregular waves using a KVLCC2 ship model.

All the previous works were conducted with free running model tests for deep water scenarios and all have been motivated by studying the manoeuvring characteristics in the presence of waves. In spite of the importance of such works, the question regarding how the wave forces are subjected to the ship is quite unclear. To answer this question would require captive model tests during which the forces can be measured, and the effect of the water depth should be taken into account. Unfortunately, in literature, only a limited number of studies have been conducted, and all of them are in deep water (none in shallow water), e.g. Ueno et al. (2000), Yasukawa and Adnan (2006), and Sung et al. (2012). Ueno et al. (2000) studied captive model tests in oblique and turning motion in regular waves for a VLCC ship model; Yasukawa and Adnan (2006) investigated the ship's motions and induced steady drifting forces on an oblique moving ship in regular waves, and in Sung et al. (2012) a study, consisting of harmonic sway, harmonic yaw and stationary drift tests with a KCS ship model, was performed in following waves for one moderate

forward speed. In Sung et al. (2012) no clear second order wave effects in the sway force and yaw moments were reported, and they suggested that tests at low speed would be able to capture these effects in a more pronounced way.

## 3.2 The two-time scale method

### 3.2.1 General discussion

Several works can be classified within the two-time scale approach, for instance the work of McCreight (1986) however, works as such will not be considered in the present discussion because they accounted for the first order wave forces and moments only.

### 3.2.2 Coordinate systems

It is important to recall that the manoeuvring in calm water and the seakeeping analyses are in general conducted in the b-frame and the h-frame, respectively. Both analyses use also the Earth fixed E-frame. These frames have been presented in Chapter 2, mind that in seakeeping the E-frame and the h-frame are in general oriented with their vertical axis pointed upwards.

As mentioned earlier, no modification of the hydrodynamic problem arising on manoeuvring in calm water and seakeeping methods have been considered within this approach, and the solution to each independent problem has been obtained in their respective frames. This implies that for the data exchange process, both solutions would require an axes transformation before its incorporation in the next simulation step.

In literature, one can find that all methods using the two-time scale approach differ mostly in the choice of the axes orientations, which can be North-East-Down (NED), or right handed with their vertical axis pointed upwards. For instance, in Skejic and Faltinsen (2008) and Seo and Kim (2011), the axes systems are of the second type. Notice, however, that the axes transformation in Seo and Kim (2011) was not required because the seakeeping problem was solved on the body-fixed frame. In Yasukawa and Nakayama

(2009), Hamamoto and Kim (1993) the NED orientation for the three axes systems were used.

It can be also noticed from the literature that even if the methods differ with respect to the orientation of their axes systems they all mostly consider the h-frame's origin located only at the vertical distance from the ship's centre of gravity G. The main advantage of this representation it that no terms related to the longitudinal position of the centre of gravity need to be accounted for, see for instance, Seo and Kim (2011) and Yasukawa and Nakayama (2009).

### 3.2.3 Rigid body dynamic equations

A general agreement while dealing with the manoeuvring and the seakeeping problems is to treat the independent fields as a 4DOF manoeuvring problem where surge, sway, yaw and roll motions are considered, and a full 6DOF seakeeping problem. Although the simplification of a 4DOF manoeuvring model will be less accurate than a full 6DOF, according to Skejic and Faltinsen (2008) the results can be accepted as a practical solution for simulation of the ship manoeuvring in waves.

Taking into account that in most works the ship's centre of gravity is located only at the b-frame's origin, hence, $x_G = y_G = z_G = 0$, the manoeuvring rigid body equations, expressed in the b-frame, are given by:

$$\begin{bmatrix} X \\ Y \\ K \\ N \end{bmatrix} = \begin{bmatrix} m(\dot{u} - vr) \\ m(\dot{v} + ur) \\ I_{xx}\dot{p} \\ I_{zz}\dot{r} \end{bmatrix} \tag{3.1}$$

where $X$, $Y$, $K$, $N$ are the surge forces, sway forces, roll moments and yaw moments, respectively. $m$ is the ship mass, $I_{xx}$ and $I_{zz}$ are moments of inertia with respect to the longitudinal and vertical axes, respectively.

The seakeeping rigid body equations, expressed in the h-frame, and considering only linear motions, can be written as:

$$\sum_{k=1}^{6}\left[\left(M_{jk}+A_{jk}\right)\ddot{\xi}_k+B_{jk}\dot{\xi}_k+C_{jk}\xi_k\right]=F_j e^{i\omega_E t} \tag{3.2}$$

where $M_{jk}$, $A_{jk}$, $B_{jk}$, $C_{jk}$, $F_j$ are the matrices corresponding to the ship inertia, the added inertia, the damping coefficients, the restoring coefficients, and the wave exciting forces, respectively. $\xi_k$ refers to the ship's linear motions. For a more extended discussion on these terms see Chapter 2.

It is important to mention that in literature different methods are used for the solution of the manoeuvring and the seakeeping problems. Those methods, to the author's opinion, are rather as function of their availability, rather than to their suitability. With respect to the mathematical approach for modelling of the forces, not to the solution of it, it is however, a general common practice to use the modular approach, where the forces and moments are subdivided as:

$$\begin{bmatrix}X\\Y\\K\\N\end{bmatrix}=\begin{bmatrix}X_H+X_P+X_R+X_W\\Y_H+Y_P+Y_R+Y_W\\K_H+K_P+K_R+K_W\\N_H+N_P+N_R+N_W\end{bmatrix} \tag{3.3}$$

The subscripts H, R, P, and W, indicates the contribution of the hull, rudder, propeller and wave effects. The wave contribution can be replaced by external (EXT) contribution to account for additional effects such as wind forces and moments.

### 3.2.4 Differences between the proposed methods

Apart from the different choice of the axes frames encountered within this approach (see 3.2.2), other main differences encountered between the works using the two-time scale approach can be summarised as: (a) the method used for the estimation of the slow motion derivatives, (b) the method used to obtain the wave forces and moments, and finally, (c) the time scales for the data exchange between the manoeuvring and the seakeeping modules.

The distinction between one method and the other can be extensive if one attempt to cover in detail all works proposed. For the purpose of brevity, the following discussion will only consider the works of Skejic and Faltinsen (2008), Yasukawa and Nakayama (2009), and Seo and Kim (2011) because, to the author's opinion, they are the most representative analysis for the two-time scale methods.

#### *3.2.4.1 The manoeuvring models*

The manoeuvring model employed by Skejic and Faltinsen (2008) is based on the 3DOF (surge, sway and yaw) model of Söding (1982) with modifications to include roll motion. The added inertia terms were computed at zero frequency by using slender body theory and approximations given by Söding (1982). Cross flow, lift and resistance, propeller and rudder effects were also accounted for, however, by using semi-empirical methods.

In Yasukawa and Nakayama (2009), the model description for the low frequency problem is based on the work of Hamamoto and Kim (1993). The representations used for the hydrodynamic forces and moments are, however, based on Yasukawa (2006a) where added inertial terms are given at zero frequency and hull forces are accounted for by differential coefficients (Taylor series expansion) to deal with lift and cross flow effects on the hull. All of these terms are found experimentally. Propeller and rudder effects are accounted for by the thrust fraction, lift and drag effects, respectively. The latter are similar to the analysis described in Chapter 2 for the propulsion and rudder effects in calm water studies.

The work of Seo and Kim (2011) uses also the mathematical model for the hull forces proposed in Yasukawa (2006a). However, different from Yasukawa and Nakayama (2009), the numerical code developed by Seo and Kim (2011) allows the estimation of the added inertial terms, and partially the lift effects; for viscous effects contribution the methods presented in the work of

Yasukawa (2006a) are used. In the case of the propeller and rudder effect, they are also modelled as in Yasukawa (2006a).

#### 3.2.4.2 The seakeeping methods

The major difference between the referred works is related to the chosen approaches for the seakeeping analysis. While Skejic and Faltinsen (2008) and Yasukawa and Nakayama (2009) employed a frequency time domain based, Seo and Kim (2011), solved directly the seakeeping problem in time domain.

Apart from the differences with respect to the domain solution, the methods employed may differ on the type of solution itself of the Boundary Value Problem (BVP) of seakeeping. Strip theory, where the ship is representing entirely by two-dimensional sections, have been used in Skejic and Faltinsen (2008), and Yasukawa and Nakayama (2009). In Seo and Kim (2011), however, a Rankine panel method, where the ship is represented in three-dimensional surface panels, has been used.

Solving the seakeeping problem in the frequency domain, would require further transformation to the time domain, especially due to the radiation forces and the memory effects associated to it. Hence, the incorporation of memory terms would require the convolution integral equations proposed by Cummins (1962). Memory effects are, however, neglected in the analyses of Skejic and Faltinsen (2008) and Yasukawa and Nakayama (2009). This is because of the quasi-steady assumption of the manoeuvring in waves problem. Hence, first order waves forces and moments over a time equal to one period of oscillation will have a zero mean, and the main wave effects will be of second order because of their non-zero mean values.

In literature, different methods for the estimation of the mean second order wave forces and moments can be found. The direct pressure integration method (near field, see. e.g. Faltinsen and Løken, 1979), the momentum conservation method (far field, e.g. Maruo, 1957) and other methods especially designed for the short wave length range (see e.g. Faltinsen et al., 1980). In Skejic and

Faltinsen (2008) all these methods have been used depending on their suitability as a function of the ship speed V and the wave length range. In Yasukawa and Nakayama (2009), the results obtained from strip theory have been corrected with empirical formulations.

Although the evaluation of the seakeeping forces and moments used by Seo and Kim (2011) is expected to give better prediction because of its more accurate treatment of the Boundary Value Problem (BVP), they have used only the pressure integration method. To the author's best knowledge the advantages with respect to the methods mentioned above are not found in literature. This may be an important subject of further study.

#### *3.2.4.3The time scales*

To calculate the respective wave effects, the ship's position and orientation are provided from the solution of the manoeuvring problem. Then, the wave forces and moments are computed for and introduced in the manoeuvring equation for the next time step solution. The degree of information exchange varies slightly in literature. Two main approaches are found; they are classified, in here, as the parallel and sequential approaches. Figure 3.1 illustrates both time scale approaches.

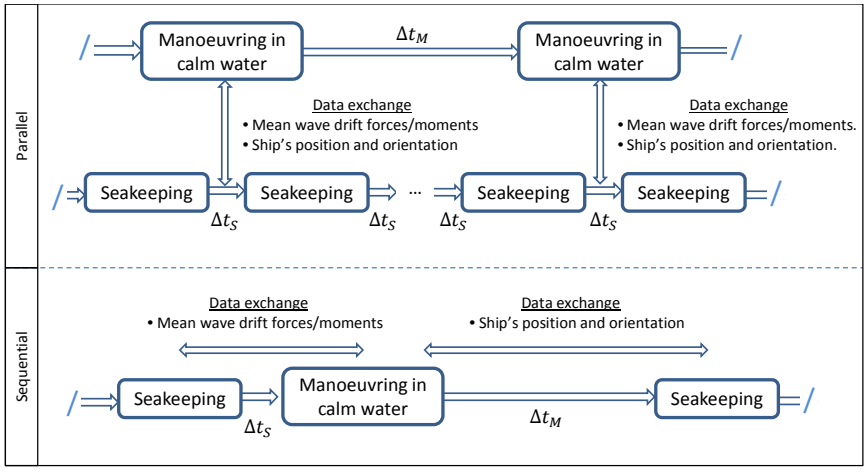


Figure 3.1 Different approaches used in the two-time scale method, (top) the parallel evaluation and (bottom) the sequential evaluation.

The main difference between the parallel and the sequential approaches is that the first one requires several evaluations of the seakeeping problem while the manoeuvring problem is evaluated only once, while in the sequential evaluation the seakeeping computations are only carried out after a time equivalent to a significant change in ship heading has been achieved. Examples of the latter type are the works of Skejic and Faltinsen (2008), Skejic (2008) and Yasukawa and Nakayama (2009), and of the first type of study, see for instance, Seo and Kim (2011).

It is clear that the parallel approach of Seo and Kim (2011) will require higher computational time, not only because the seakeeping computations are carried out each time step, but as well because the solution of the potential flow analysis is also obtained each time step.

## 3.3 The unified method

### 3.3.1 General discussion

As mentioned in 3.1.2, the present classification considers only all mathematical approaches aiming for the unification of the manoeuvring model's added inertial terms with the more general representation of added inertia and damping coefficients of seakeeping analysis. Methods which incorporate wave effects computed by a seakeeping model running in parallel can be considered as a variant of the two-time scale methods (see McCreight 1991), hence they will not be addressed in the present discussion.

In the present section, only a selected number of works will be used for further discussion, they are the works of Bailey et al. (1998), Ayaz et al. (2006a,b) and Sutulo and Guedes Soares (2006a). These methods are considered relevant for the present discussion because of their distinct approach within the unified method.

Other works found in literature can be also considered a variation of the ones previously mentioned, for instance, the work of Letki and Hudson (2005) follow the study proposed by Bailey et al. (1998), in Sutulo and Guedes Soares (2006b) and their later work Sutulo and Guedes Soares (2008) the same approach used in Sutulo and Guedes Soares (2006a) is also presented, and in the work of Schoop-Zipfel and Abdel-Maksoud (2011) their approach is to some extend similar to the one of Ayaz et al. (2006a).

### 3.3.2 Coordinate systems

The analysis requires initially the consideration of three axes systems, the Earth axes system (E-frame), the horizontal axes system (h-frame), and the body-bound axes system (b-frame). These axes systems are the same as described in Chapter 2. Only in Bailey et al. (1998) the orientation of these frames is upright contrary to the NED orientation used in Ayaz et al. (2006a) and Sutulo and Guedes Soares (2006a). According to Bailey et al.

(1998), the upright orientation allows for a simplified relationship between the manoeuvring and seakeeping expressions.

Although three coordinate systems are initially used, the solution of the problem is only conducted in the b-frame in Bailey et al. (1998) and Sutulo and Guedes Soares (2006a), and in the h-frame in Ayaz et al. (2006a). The latter claims a better suitability of h-frames for the incorporation of large angles of pitch motion.

Some additional differences between the b-frame and the h-frame axes representations are related to the motions of the horizontal frames. In Ayaz et al. (2006a) the h-frame is allowed to move in the horizontal and vertical planes while in Bailey et al. (1998) and Sutulo and Guedes Soares (2006a) the h-frame moves only in the horizontal plane, parallel to the mean water surface. Moreover, the origin of the h-frame and the b-frame coincided in the centre of gravity (G) in Ayaz et al. (2006a), while in Bailey et al. (1998) and Sutulo and Guedes Soares (2006a) the h-frame is located above the ship's centre of gravity.

### 3.3.3 Rigid body dynamic equations

The methods of Bailey et al. (1998), Ayaz et al. (2006a) and Sutulo and Guedes Soares (2006a) address the problem of manoeuvring in waves directly with the full 6DOF ship rigid body dynamics. The respective representation of the ship dynamic equation does not only differs from the point of view of the axes frame used for the solution of the problem, but also from the point of view of simplification accounted for.

The ship rigid body dynamic equations in Bailey et al. (1998) are:

$$X = m\dot{u}$$

$$Y = m(\dot{v} + ur)$$

$$Z = m(\dot{w} - uq)$$

$$K = I_{xx}\dot{p} - I_{xz}\dot{r} \qquad (3.4)$$

$$M = I_{yy}\dot{q}$$

$$N = -I_{xz}\dot{p} + I_{zz}\dot{r}$$

and in Sutulo and Guedes Soares (2006a) are:

$$X = m\big(\dot{u} - vr + wq - x_G(r^2 + q^2) + z_G(pr + \dot{q})\big)$$

$$Y = m\big(\dot{v} - wp + ur + z_G(qr - \dot{p}) + x_G(pq + \dot{r})\big)$$

$$Z = m\big(\dot{w} - uq + vp - z_G(p^2 + q^2) + x_G(pr - \dot{q})\big)$$

$$K = -mz_G\,\dot{v} + I_{xx}\dot{p} - I_{xz}\dot{r} + \big(I_{zz} - I_{yy}\big)rq - mz_G(ur - wp) \qquad (3.5)$$

$$M = mz_G\dot{u} - mx_G\dot{w} + I_{yy}\dot{q} + (I_{xx} - I_{zz})pr + I_{xz}(p^2 - r^2) + mz_G(wq - vr) - mx_G(vp - uq)$$

$$N = mx_G\dot{v} - I_{xz}\dot{p} + I_{zz}\dot{r} + I_{xx}\dot{p} + mx_G ur - mx_G wp + \big(I_{yy} - I_{xx}\big)pq + I_{xz}qr$$

X,Y,Z and K,N,M are the corresponding surge, sway and heave forces and the roll, pitch and yaw moments, respectively. $u$, $v$, $w$, are ship's linear velocities and $p$, $q$, $r$ are the angular velocities, $m$ is the ship mass and $I_{xx}$, $I_{yy}$, and $I_{zz}$ are moments of inertia and $I_{xz}$ is the product of inertia.

The representation of the rigid body dynamic equation given in Ayaz et al. (2006a) is slightly more complicated. This will not be presented in the section for purposes of simplicity; moreover the description of such equations is not believed to add substantial difference in the further discussion of the unified method. See Ayaz et al. (2006a) for more detail information.

### 3.3.4 Differences between the proposed methods

#### *3.3.4.1Manoeuvring models*

With respect to the modelling for the forces and moments, all works separate the effects of the hull, propeller and rudder. In Ayaz et al. (2006a) their modular approach is given by:

$$X = X_H + X_P + X_R + X_{EXT}$$

$$Y = Y_H + Y_P + Y_R + Y_{EXT}$$

$$Z = Z_H + Z_{EXT}$$

$$K = K_H + K_P + K_R + K_{EXT} \tag{3.6}$$

$$M = M_H + M_{EXT}$$

$$N = N_H + N_P + N_R + N_{EXT}$$

The subscripts H, R, P, and W, indicates the contribution of the hull, rudder, propeller and wave effects. The wave contribution can be replaced by external (EXT) contribution to account for additional effects such as wind forces and moments.

In Ayaz et al. (2006a), the propeller, rudder and hull effects due to manoeuvring are estimated by using the Japanese Ship Manoeuvring Mathematical Modelling Group (MMG, see Ogawa and Kasai, 1978) and the pitch and heave radiation contribution by the empirical formulation of Tasai (1961). In Sutulo and Guedes Soares (2006a), a variation of the method given by Inoue et al. (1981) was used for the manoeuvring forces in 4DOF, roll damping estimations where made based on the Ikeda et al. (1977) approach. In Bailey et al. (1998), contrary to the works mentioned above, a simplified model based only on linear derivatives was used (this will be discussed in more detail in the following subsection 3.3.4.2), and rudder and propeller effects were not properly considered. The latter is mainly because their main objective was the unification of the hull effects. Because this is the main objective of the present approach, further discussions will be restricted to hull and wave effects only.

#### *3.3.4.2Hull models*

The representation of the hull forces and moments, as initially given by the manoeuvring approach in Bailey et al. (1998) is:

$$X_H = X_{\dot{u}}\dot{u} + X_u u + X_{\dot{w}}\dot{w} + X_w w + X_{\dot{q}}\dot{q} + X_q q$$

$$Y_H = Y_{\dot{v}}\dot{v} + Y_v v + Y_{\dot{p}}\dot{p} + Y_p p + Y_{\dot{r}}\dot{r} + Y_r r$$

$$Z_H = Z_{\dot{u}}\dot{u} + Z_u u + Z_{\dot{w}}\dot{w} + Z_w w + Z_{\dot{q}}\dot{q} + Z_q q$$

$$K_H = K_{\dot{v}}\dot{v} + K_v v + K_{\dot{p}}\dot{p} + K_p p + K_{\dot{r}}\dot{r} + K_r r \tag{3.7}$$

$$M_H = M_{\dot{u}}\dot{u} + M_u u + M_{\dot{w}}\dot{w} + M_w w + M_{\dot{q}}\dot{q} + M_q q$$

$$N_H = N_{\dot{v}}\dot{v} + N_v v + N_{\dot{p}}\dot{p} + N_p p + N_{\dot{r}}\dot{r} + N_r r$$

In Sutulo and Guedes Soares (2006a) this representation is:

$$X_H = -X_{\dot{u}}\dot{u} + (Y_{\dot{v}} + X_{vr})vr + X(u)$$

$$Y_H = -Y_{\dot{v}}\dot{v} - X_{\dot{u}}ur + Y_{H0}(v,r) + Y_{H1}(v,r,\phi)$$

$$K_H = K_{\dot{p}}\dot{p} + K_p p \tag{3.8}$$

$$N_H = -N_{\dot{r}}\dot{r} + N_{H0}(v,r) + N_{H1}(v,r,\phi) + \big(Y_{H0}(v,r) + Y_{H1}(v,r,\phi)\big)x_H$$

For more detail of the coefficients $Y_{H0}(v,r)$, $Y_{H1}(v,r,\phi)$, $N_{H0}(v,r)$, $N_{H1}(v,r,\phi)$ and other parameters, see Inoue et al. (1981).

In Ayaz et al. (2006a) the hull forces and moments are represented as follows:

$$X_H = X_{\dot{u}}\dot{u} - Y_{\dot{v}}vr + \frac{u}{|u|}Y_{\dot{r}}r^2 + X_{vr}vr - R_T(u)$$

$$Y_H = Y_{\dot{v}}\dot{v} + Y_{\dot{r}}\dot{r} + Y_v v + \frac{u}{|u|}Y_r r + Y_{v|v|}v|v| + Y_{r|r|}r|r|$$

$$Z_H = Z_{\dot{w}}\dot{w} + Z_w w + Z_{\dot{q}}\dot{q} + Z_q q$$

$$K_H = K_{\dot{p}}\ddot{\phi} + C\big(\dot{\phi}\big) - z_y Y_H \tag{3.9}$$

$$M_H = M_{\dot{w}}\dot{w} + M_w w + M_{\dot{q}}\dot{q} + M_q q$$

$$N_H = N_{\dot{v}}\dot{v} + N_{\dot{r}}\dot{r} + N_r r + \frac{u}{|u|}N_v v + N_{vvr}vvr + N_{rrv}rrv$$

In the equations above, the terms linearly proportional to velocities and acceleration are also considered as the zero frequency problem because of their slowly varying nature.

It can be seen that in Bailey et al. (1998) the manoeuvring approach is linear, while in the case of Sutulo and Guedes Soares (2006a) and Ayaz et al. (2006a) nonlinear manoeuvring representations are used. It is important to mention, however, that

the terms in Eq. (3.7) can mostly be considered as due to the contribution by ideal fluid and partially by viscous effects. Adding to this model, mainly viscous components, will lead to nonlinear methods as presented in Eq. (3.8) and in Eq. (3.9).

Bear in mind that in the present discussion, the hull resistance, given in Eq. (3.8) by $X(u)$ and in Eq. (3.9) by $R_T(u)$, is left out of the analysis.

In Ayaz et al. (2006a), when dealing with the unification problem, only the linear terms were considered. Hence, even though they used a nonlinear representation for the hull forces, their unification method will be similar to the one of Bailey et al. (1998). For this main reason, further discussion is only restricted to the approach of Bailey et al. (1998) and Sutulo and Guedes Soares (2006a).

#### 3.3.4.3 Unification method

In Bailey et al. (1998) the main goal is to replace the zero frequency coefficients of Eq. (3.8) by the time domain responses. This can be done by using the time domain convolution integral equation given in Cummins (1962), which can be expressed as:

$$\boldsymbol{F} = \boldsymbol{A}\ddot{\boldsymbol{X}} + \boldsymbol{B}\dot{\boldsymbol{X}} + \int_{-\infty}^{+\infty} \boldsymbol{H}(\boldsymbol{t}-\boldsymbol{\tau})\,\dot{\boldsymbol{X}}(\boldsymbol{\tau})\boldsymbol{d\tau} \tag{3.10}$$

Where $\boldsymbol{F}$, $\boldsymbol{A}$, $\boldsymbol{B}$, $\boldsymbol{H}$, and $\dot{\boldsymbol{X}}$ are the 6DOF forces, added inertia, damping, impulse response function, and velocity matrices, respectively.

In Bishop et al. (1973) an extensive discussion on the application of the integral-differential equation for the manoeuvring velocity and accelerations derivatives is presented.

The use of Eq. (3.10) would require first the evaluation of the impulse response function (IRF) $\boldsymbol{H}$. The latter, however, can be obtained by evaluating first the frequency domain responses of seakeeping and then using the relationships derived in Ogilvie

(1964). In Bailey et al. (1998), an additional correction to the IRFs is applied in order to account for the viscous influence measured in the manoeuvring derivatives.

The use of the IRF, however, is in general found to be time consuming because of their frequency and speed dependence. To overcome this difficulty, for example, in Ayaz et al. (2006a) the values of the added inertia terms and the damping coefficients have been stored every 10 deg of heading change of angle varying between 0 to 360 deg. During simulations they are interpolated for a particular wave heading. An alternative solution could be to represent the convolution terms by a set of ordinary differential equation (ODEs). The set of ODEs have already been used in field of seakeeping, however, the speed dependence for the IRF is a major problem. The evaluation of possible simplifications that can allow a more direct use of the convolution integral approach is then an interesting topic of future research.

In Sutulo and Guedes Soares (2006a), their unification approach also claims considering nonlinear terms, such as $X_{\dot{u}}ur$ in Eq. (3.8). For this purpose, they proposed that the manoeuvring forces and moments in waves should be computed as:

$$F(W,M) = F_{WM}(W,M) - F_{WM}(0,M) + F_M(M) \tag{3.11}$$

where $F_{WM}(W,M)$ is the theoretical external forces while manoeuvring in waves, $F_{WM}(0,M)$ is the forces predicted by the theory in calm water, and $F_M(M)$ is the forces predicted by the selected experimentally determine manoeuvring model.

In Eq. (3.11) the subtraction of the potential forces for zero wave amplitude, $F_{WM}(0,M)$, is considered as a correction to remove potential effects already accounted for when computing the manoeuvring coefficients of in Eq. (3.8). Hence, the Eq. (3.8) will only account for the viscous contribution while the model $F_{WM}(W,M)$ will incorporate potential effects.

In Sutulo and Guedes Soares (2006a), although their method is more elaborate, the main unified parameters, the acceleration derivatives, are also replaced by a approach similar to the convolution integral. However, a simplified representation was used by applying the inverse Fourier transform to the radiation problem; this allowed to express the radiation problem in a set of ODEs. The latter, however, are still functions of the ship speed.

#### 3.3.4.4Wave effects models

The wave excitation forces can be subdivided similar to the convention analysis of seakeeping in (a) Froude-Krylov forces and moments (b) diffraction forces and moments, and (c) of second order forces.

In Bailey et al. (1998) only linear forces due to the Froude-Krylov and the diffraction forces are mentioned; they are, however, expressed in a convolution integral form. In Ayaz et al. (2006a), different from Bailey et al. (1998), the Froude-Krylov forces and moments are computed over the exact wetted surface (see also Schoop-Zipfel and Abdel-Maksoud, 2011), and an approximation for long waves is used for the diffraction contribution. In Sutulo and Guedes Soares (2006a), a more accurate treatment is included by integration the pressure, similar to the near field method (see Chapter 2), over the actual wetted surface. All of the methods above are based on a two-dimensional approach of the wetted surface and none have incorporated the evaluation with three-dimensional consideration of the hull surface.

## 3.4 Discussion on the available methods

From the discussion above, it can be observed that the two methods (the two-time scale model and the unified model) are based on the general assumption that the fluid effects on a ship manoeuvring in waves can be, to some extent, separated into two main components. A contribution from the seakeeping problem which is dominated by potential flow, and a contribution from calm water manoeuvring which is also affected by viscous flow. However, from the point of view of the incorporation of these effects, the treatment of the problem is different.

In the two-time scale method, the 6DOF problem is mostly simplified in a 4DOF problem, the effects of the first order wave contributions are neglected, and only wave second order forces and moments are accounted for. The choice of the manoeuvring model is found to be irrelevant, as authors have chosen indistinctively from Taylor expansion models, the MMG model and the model described in Söding (1982). The major difference in the application of the two-time scale method, between the different authors, is in the consideration of the mean wave drift forces, a major shift from two-dimensional strip theory methods to three-dimensional panel methods has been observed. With this respect the Rankine panel method applied by Seo and Kim (2011) seems to be a better choice.

In the Unified method a full 6DOF manoeuvring problem is aimed at. Although, only a slight modification of the 4DOF conventional manoeuvring models (MMG, Inoue et al., 1981) is presented, the attempt to include all six degrees of freedom is a common practice. With respect to the unification of the fluid effects, mostly the linear velocity and acceleration derivatives are used, and only few works deal with the nonlinear terms accounting for hydrodynamic phenomena such as lift effects. Wave forces are mostly considered as linear and to some extend nonlinear by the incorporation of Froude-Krylov forces and moments.

The use of convolution terms as proposed in Bailey et al. (1998), seems a practical approach because of the simple evaluations required to find the respective IRFs, which can be obtained from any conventional seakeeping code. However, according to Skejic (2008), their accuracy depends strongly on the asymptotic behaviour of either the encounter frequency-dependent added inertia terms or damping coefficients. Moreover, the presence of the forward speed (loss) introduces additional difficulties in the evaluation of the retardation functions. Because they change with changing encounter frequency and encounter heading angle, the IRFs evaluation will be frequently executed, consequently increasing computational time. This, however, has not been reported in their study. To the author, a possible simplification of the convolution approach seems applicable, and has been presented in chapter 7.

An important observation about all the methods within the unified approach, is that none of them incorporates a more accurate estimation of the second order wave effects. The omission of the steady fluid components will lead to a wrong prediction for manoeuvring characteristics such as turning cicle and zigzag manoeuvres. However, to the author's opinion, a significant improvement will be to consider wave exciting forces and moments as conducted in the two-time scale method.

In both methods no general consensus is observed regarding the type of models used for the calm water manoeuvring problem and the seakeeping approach. However, a major agreement between both methods is the use of a modular approach for the incorporation of hull, propeller, rudder, and wave forces and moments.

From the discussion of the methods, it can also be noticed that all manoeuvring methods for the hull forces are to some extent based on nonlinear polynomial expansion and none have used a tabular approach. For the two-time scale method this is rather indifferent; for the unified approach, however, such a representation in a more

physical based analysis is required to allow further unification of the fluid effects.

Bear in mind that in the present literature study, manoeuvring in waves in shallow water is hardly addressed, nor the two-time scale or the unified methods have been studied in such limited water depths. Only the works presented by the author in Tello Ruiz et al. (2016a) and in Tello Ruiz et al. (2018) can be found addressing partially this problem.

It is important to mention that from the point of view of manoeuvring in shallow water, the incorporation of the mean wave second order wave effects is equally important for the first order wave effects. This is because in limited water depths, the ship's oscillatory motions together with squat effects could result in hazardous conditions such as bottom touch. The incorporation of the first order forces, which will induce ship motions, can also be important from the point of view of the propeller and rudder behaviour, which has been hardly addressed in literature. To the author's best knowledge, only the work of Taskar (2017) has addressed this topic for the manoeuvring in waves in deep water.

It is also important to mention that, similar to the analysis in manoeuvring studies, some levels of restriction are required in order to solve the problem. The decision on which phenomena to be accounted will depend mostly on the dominant character on its contribution to the total forces. This will depend on several parameters, such as the ship's type and loading condition, as well as the environmental factors, which depend on the characteristics of the operational areas. Thus, this must be investigated.

# MANOEUVRING IN COASTAL WAVES



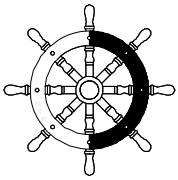

Ideas do not always come in a flash but by diligent trial-and-error experiments that take time and thought.

Charles K. Kao

# 4

# Experimental study

## 4.1 General discussion

During the course of the present work, four experimental test campaigns have been conducted in the Towing Tank for Manoeuvres in Confined Water (co-operation Flanders Hydraulics Research – Ghent University) in Antwerp.

The different test programs are further referred to as: test program 2014, test program 2015, test program 2016, and finally test program 2017. Test programs 2014, 2015 and 2016 have been conducted with the same scale model of an Ultra Large Container Carrier (ULCC), hereafter referred as C0W, while model tests executed in 2017 were carried out with a different ship model, the MOERI Container Ship (KCS), see SIMMAN 2008.

The test program conducted in 2016 is the most extensive of all, an approximate of +3000 tests have been conducted. These tests can be identified in two main groups, fully captive model tests and semi captive model tests. Model tests conducted in 2014 and 2015 comprised only semi captive tests which differ with the 2016 program in the model's loading condition.

During the execution of test program 2014, restrictions due to the tank main dimensions, wave generation, and interference with the instrumentation were not accounted for; as a consequence, test results were impaired qualitatively and quantitatively. Because of these problems, an optimization of the model test procedures in waves was required. This in order to avoid several problems, starting from the most fundamental ones such as wave reflection from the beach (because of the poor wave damping by the beach) to the determination of a region along the tank where waves could be assumed regular and constant in magnitude.

The encountered (unanticipated) difficulties mentioned above, turned the analysis of test program 2014 tedious, time consuming, and in most cases impossible. In 2015 a great amount of time and effort was dedicated to the investigation of waves, and their propagation and behaviour along the tank. The analysis of these results were partially presented in Delefortrie et al. (2016b), and also in Tello Ruiz et al. (2016b). To have a better idea of the main challenges encountered, only the most relevant problems related to the side wall interaction and wave generation, as well as regarding the post processing analysis will be discussed in the present chapter. A more recent extension of the limitations during tests has been presented in Tello Ruiz et al. (2017).

The test program 2016 has been conducted taking into account all problems encountered in 2014 and studied in test program 2015. Because in 2015 a large amount of time has been used to the optimization of the test procedure in waves, only few tests in waves were conducted. They will not be further discussed in the present work because they provide limited information in contrast to test program 2016. Moreover, the discussion of test program 2016 allows the direct comparison of fully captive and semi captive tests which will allow to investigate the effects of ship motions on the manoeuvring characteristics.

Model tests with an additional ship model have been conducted in 2017. Only few experiments have been post processed up to now.

This is because, although the selection of test parameters has been optimised, a careful study and post processing analysis is still required. The difficulties regarding the post processing analysis has been reported in Mansuy et al. (2017). For this reason, tests conducted in 2017 will not be addressed in the present work, but they can be used in later studies for validation purposes.

The present chapter presents an overview of the main wave characteristics and ship model parameters chosen for test program 2016. Additionally, a brief discussion of the main problems encountered which impaired model tests are also presented; their importance, and solutions, are also discussed.

## 4.2 Test parameter selection

The parameters of the experimental investigation have been selected to represent the most common conditions experienced by the ULCC ship when approaching or leaving a port. These environmental conditions, and the ship's attained state while manoeuvring define the problem of manoeuvring in coastal waves, as seen from the present point of view.

To further proceed with the present work, the environmental conditions corresponding to the access channels to the mouth of the Western Scheldt and to Zeebrugge have been selected, and the ship's main constraints are summarised as:

a) The wave scenario has to correspond to typical conditions observed in the Belgian coastal zone of the North Sea (see Figure 4.1).
b) The ship will always navigate with a positive forward speed $u$, and positive propeller rates ($n$).
c) The ship speed can vary from low to intermediate values, e.g. Froude number ($F_r$) less than 0.125, which correspond to ship speeds up to 15 knots for a ship of length around 400 m.
d) The lateral velocity ($v$) of the ship will always be small in comparison with the longitudinal speed ($u$). Thus, only small

drift angles ($\beta$) can be achieved, smaller than 20 deg (see Figure 4.2).

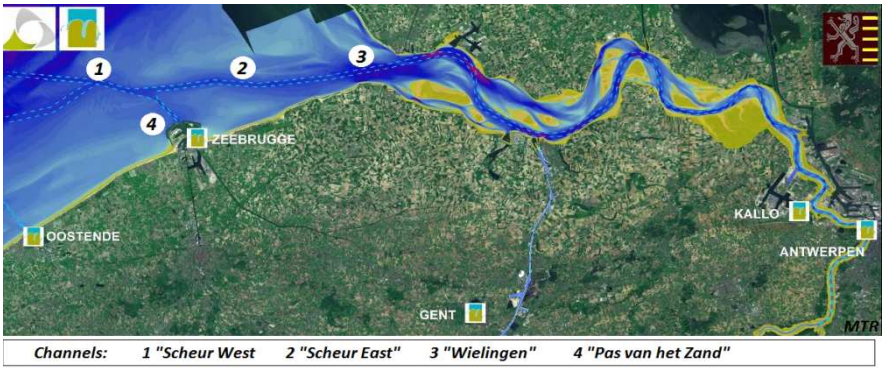


Figure 4.1 Access channels to the mouth of the Western Scheldt river and to the port of Zeebrugge.

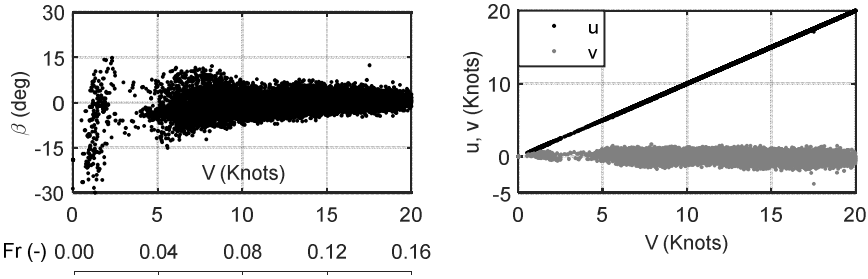


Figure 4.2 Ship speed and drift angle (left), and speed components $u$ and $v$ (right) attained by ULCC vessel when navigating throughout the access channels towards (or away from) the mouth of the Western Scheldt river and to the port of Zeebrugge. A sample of 40 ULCC ships have been analysed using AIS-data obtained during the period of 35 days from Scheldt Radar Chain (SRC).

To get a better idea of the wave characteristics in these areas, examples of the wave spectra are presented in Figure 4.3. Additionally, a scatter diagram of the wave records measured at the Scheur and Wielingen channels (see 1, 2 and 3 in Figure 4.1) is presented in Table 2. The scatter diagram is given as a function of the significant wave height (Hs) and the zero crossing wave period (Tz).

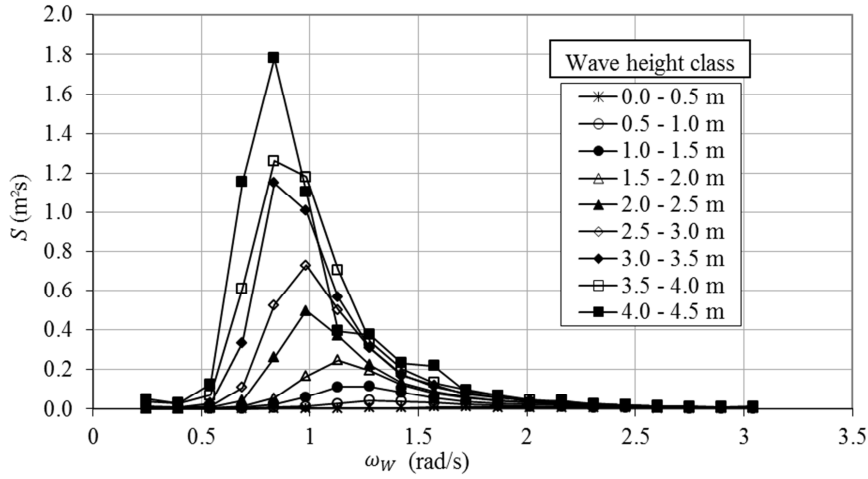


Figure 4.3 Typical wave spectra in the Flemish banks region. Retrieved from Vantorre and Journée (2003).

The wave records presented in Figure 4.3 are concentrated in a range of frequencies ( $\zeta_\omega$ ) situated between 0.5 rad/s and 2.0 rad/s. Lower and higher frequencies are still present but their energy density ($S$) is significantly smaller. From Table 4.1, it can be seen that waves up to 2.0 m Hs have a high probability to occur, of around 93 %, and if Hs is increased to 3 m the probability increases to 99 %. For Tz up to 6.5 s a similar probability, of 99 %, is found.

Table 4.1 Scatter diagram near the Scheur/Wielingen channel (at Bol Van Heist location). Retrieved from the Flemish Banks Monitoring Network (1984–2004).

| Tz (s) | Hs (m) | | | | | | | | | | | | | P(Tz) | P(≤Tz) |
|---|---|---|---|---|---|---|---|---|---|---|---|---|---|---|---|
| | <=0.25 | 0.25 0.50 | 0.5 1.0 | 1.0 1.5 | 1.5 2.0 | 2.0 2.5 | 2.5 3.0 | 3.0 3.5 | 3.5 4.0 | 4.0 4.5 | 4.5 5.0 | 5.0 5.5 | 5.5 6.0 | | |
| <=2.5 | 0.22 | 2.96 | 1.59 | 0.07 | 0 | 0 | - | - | - | - | - | - | - | 4.8 | 4.8 |
| 2.5 - 3.5 | 1.85 | 12.2 | 18.1 | 3 | 0.17 | 0.01 | 0 | - | - | - | - | - | - | 35.3 | 40.2 |
| 3.5 - 4.5 | 1.07 | 4.96 | 15.6 | 13.3 | 3.97 | 0.49 | 0.03 | 0.01 | 0 | - | - | - | - | 39.4 | 79.6 |
| 4.5 - 5.5 | 0.02 | 0.75 | 2.94 | 4.32 | 5.35 | 2.97 | 0.78 | 0.1 | 0.01 | 0 | - | - | - | 17.2 | 96.8 |
| 5.5 - 6.5 | - | 0.02 | 0.26 | 0.25 | 0.31 | 0.74 | 0.82 | 0.48 | 0.11 | 0.01 | 0 | 0 | - | 3.0 | 99.8 |
| 6.5 - 7.5 | - | - | 0 | 0.01 | 0 | 0.01 | 0.02 | 0.05 | 0.04 | 0.02 | 0 | - | - | 0.2 | 100.0 |
| 7.5 - 8.5 | - | - | - | - | - | - | - | - | 0 | 0 | 0 | - | - | 0.0 | 100.0 |
| P(Hs) | 3.2 | 20.9 | 38.5 | 21.0 | 9.8 | 4.2 | 1.7 | 0.6 | 0.2 | 0.03 | 0.0 | 0.0 | 0.0 | | |
| P(≤Hs) | 3.2 | 24.0 | 62.5 | 83.5 | 93.3 | 97.5 | 99.1 | 99.8 | 99.9 | 100.0 | 100.0 | 100.0 | 100.0 | | |

The limits on Hs and Tz do not imply that higher periods (longer waves) are absent, it only indicates that such waves have relatively smaller amplitudes in contrast to shorter waves, hence they cannot be distinguished in the scatter diagram shown in Table 4.1.

Taking into account the wave environment described above, the range of wave frequencies ($\zeta_\omega$) varying from 0.3 rad/s to 2.0 rad/s (corresponding to wave periods, $T_\zeta$, varying from 3.0 s to 20.9 s) and wave heights (H) up to 3 m are chosen as limits for the present study. Bear in mind extreme waves are out of the scope for the present study. Although they may occur, their probability of occurrence is rather small, as shown in Table 4.1.

## 4.3 Experimental set-up

### 4.3.1 The towing tank

The experiments were conducted at the Towing Tank for Manoeuvres in Confined Water at Flanders Hydraulics Research (FHR) in Antwerp, Belgium (co-operation with Ghent University). The towing tank has a total length of 87.5 m, a width of 7.0 m and a maximum water depth of 0.5 m. Because of the presence of the harbour and the wave maker, the useful towing tank length is limited to 68.0 m. See Figure 4.4 for better illustration.

The towing tank carriage mechanisms consist of a main carriage, a lateral carriage, a yawing table and a roll mechanism, allowing all possible movements in the horizontal plane and roll motion. The carriage mechanism allows the execution of both captive and free running tests by using two different setups. The towing tank is equipped with a wave generator. Both regular and irregular long-crested waves can be generated. An extensive discussion on the towing tank can be found in Delefortrie et al. (2016c).

During tests, the ship's position and orientation along the tank are defined by using two coordinate systems, an Earth-fixed coordinate system $O_0\ x_0\ y_0\ z_0$ and a body-fixed coordinate system $Oxyz$; both are North-East-Down (NED) oriented. The longitudinal axis of the Earth axes system coincides with the towing tank's centre line and is positive towards the wave maker. For the body axis system, the longitudinal $x-$axis is aligned with the ship's centreline, positive towards the bow.

For brevity purposes, the Earth-bound, and the ship-bound axes systems are referred as the E-frame and the b-frame (see Chapter 2), respectively. To define the ship's relative position during tests in waves, parameters such as wave angle of encounter ($\mu$), hull drift angle ($\beta$), and ship's heading angle ($\psi$) are used. The wave angle ($\eta$) relative to the E-frame axes is always 180 deg. These definitions are sketched in Figure 4.4.

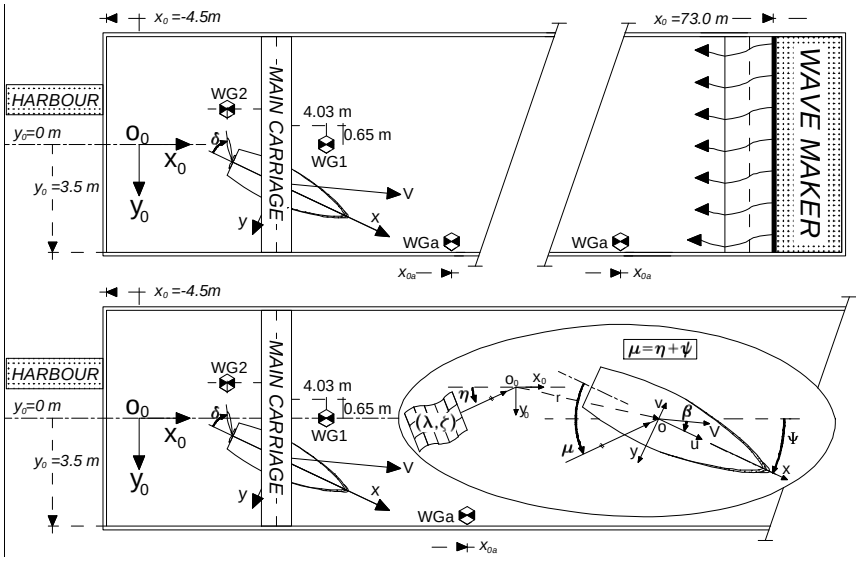


Figure 4.4 Towing tank main dimensions and parameters defining the ship's disposition along the tank during model tests.

To further study the ship model response in waves obtained during tests, the wave propagation along the tank, as well as the waves the ship model encounters must be recorded. For this purpose, wave gauges were located fixed relative to the tank (WGa and WGb) and fixed relative to the carriage (WG1 and WG2). In Figure 4.4 the general arrangement of the wave gauges is shown. Previous to tests with the ship model, WGa and WGb were set at the towing tank's centre line ($y_0 = 0$ m) to verify the wave's main parameters without the influence from the ship model.

### 4.3.2 The ship model

Model tests were conducted with a $1/90$ scale model of an ULCC containership C0W. The main parameters in model and full scale are presented in Table 4.2. A cross sectional view, a perspective view and a profile view of the ship hull are shown in Figure 4.5.

As mentioned earlier, two different test types have been conducted in 2016, semi captive tests and fully captive tests. Different beam frames attached to the carriage were used for this

purpose which resulted in a slight change of the longitudinal position of the centre of gravity ($x_G$), see Table 4.2.

Table 4.2 Main particulars of the containership model C0W at model scale and full scale.

| Item | Model scale (1/90) | | Full scale | | Remarks |
|---|---|---|---|---|---|
| | Value | Units | Value | Units | |
| $L_{OA}$ | 4418 | (mm) | 397.6 | (m) | |
| $L_{\mathrm{PP}}$ | 4191 | (mm) | 377.2 | (m) | |
| $B$ | 627 | (mm) | 56.4 | (m) | |
| $D$ | 330 | (mm) | 29.7 | (m) | |
| $T_M$ | 145.6 | (mm) | 13.1 | (m) | |
| $Cb$ | 0.6 | (–) | 0.6 | (–) | |
| $m$ | 226.4 | (kg) | 165046 | (ton) | |
| $R_{xx}$ | 212 | (mm) | 19.1 | (m) | -- |
| $R_{yy}$ | 1029 | (mm) | 92.6 | (m) | -- |
| $R_{zz}$ | 1054 | (mm) | 94.9 | (m) | -- |
| $x_G$ | -108 | (mm) | -9.7 | (m) | Frame A |
| $x_G$ | -94 | (mm) | -8.5 | (m) | Frame B |
| $y_G$ | 0 | (mm) | 0.0 | (m) | -- |
| $z_G$ | 0 | (mm) | 0.0 | (m) | -- |

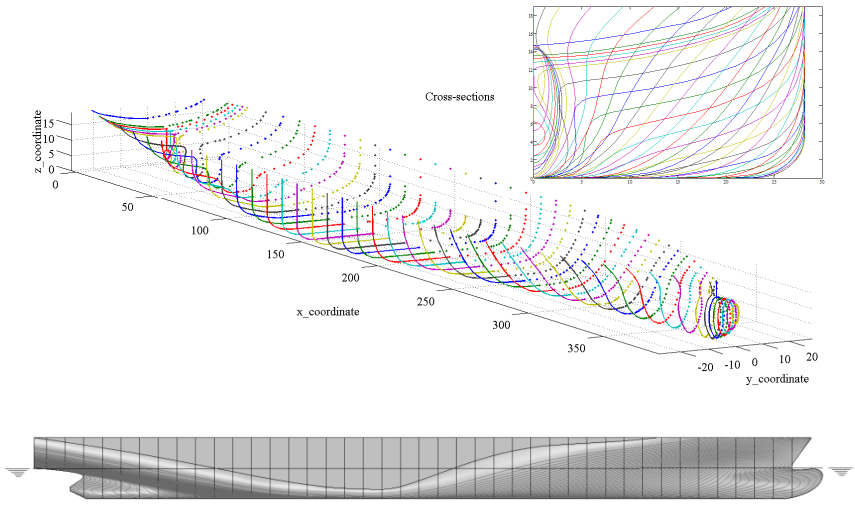


Figure 4.5 Cross sectional view, perspective view and profile view of the container ship C0W, dimensions are given in full scale.

#### 4.3.2.1 Propeller and rudder appendages

The ship model was implemented with a single propeller and a single rudder. The propeller geometry was designed according to the Wageningen B-series, with six blades, and the rudder is a semi-balance design. Figure 4.6 show both of them as installed on the model, and their main particulars are given in Table 4.3.

Figure 4.6 Single propeller and single rudder installed on the ship model.

Table 4.3 Propeller and rudder main characteristics. Dimensions are given at model scale.

| Single propeller | | Units | Single rudder | | Units |
|---|---|---|---|---|---|
| Rotation direction | Right | (-) | Height | 150 | (mm) |
| Number of blades | 6 | (-) | Cord above | 72 | (mm) |
| Diameter | 107 | (mm) | Cord middle | 106 | (mm) |
| Pitch ratio (mean) | 0.954 | (-) | Cord below | 90 | (mm) |
| Blade area ratio | 0.964 | (-) | Thickness above | 23 | (mm) |
| Propeller rate, maximum, $n_0$ | 949 | (RPM) | Thickness middle | 21 | (mm) |
| | | | Thickness below | 16 | (mm) |
| | | | Area | 0.012 | ($m^2$) |

### 4.3.3 Beam frame units

Model tests have been conducted with two different beam frames, which connect the ship to the main carriage mechanism. The frames are referred to as frame A and frame B and are related to semi-captive tests and fully captive tests, respectively. Frame A is commonly used at FHR (see Delefortrie et al., 2016a), while the frame B has been rented from MARIN.

#### *4.3.3.1Beam frame A*

Beam frame A comprises a set of two different instruments: two load cells LC1and LC2 which measure longitudinal and transversal forces, and four potentiometers, P1 to P4, to measure vertical motions. A roll and pitch mechanism is also implemented which can be locked or unlocked to restrain roll or pitch or both of them if needed. During experiments the model was set free to move in pitch and roll. Heave motion was also allowed by a vertical guidance system. Figure 4.7 illustrates the general arrangement of the instrumentation.

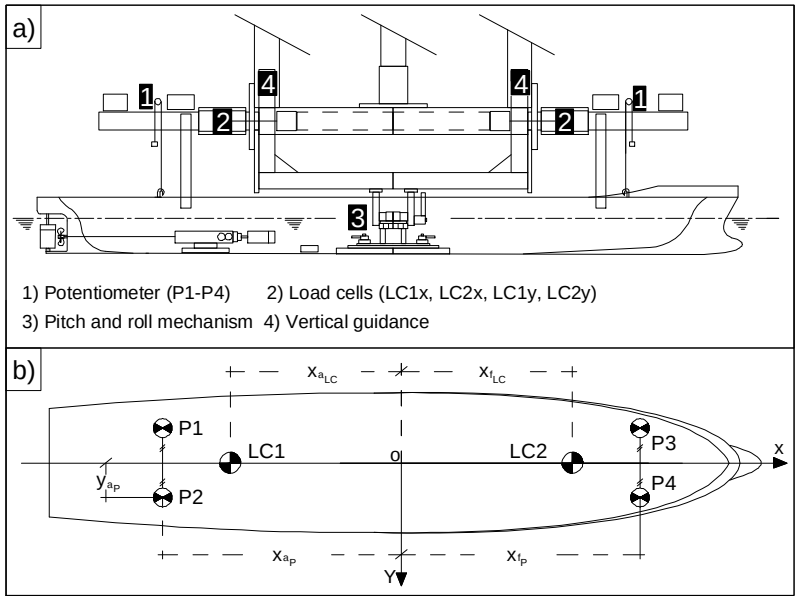


Figure 4.7 Beam frame A, (a) mounted on the ship model and (b) a respective position of the instrumentation relative to amidships and the model's centreline.

From the load cells LC1 and LC2 records, surge and sway forces, as well as yaw moments (in the b-frame) can be derived by:

$$\begin{bmatrix} X \\ Y \\ N \end{bmatrix} = \begin{bmatrix} 1 & 1 & 0 & 0 \\ 0 & 0 & 1 & 1 \\ 0 & 0 & x_{a_{\mathrm{LC}}} & x_{f_{\mathrm{LC}}} \end{bmatrix} \begin{bmatrix} X_{\mathrm{LC1}} \\ X_{\mathrm{LC2}} \\ Y_{\mathrm{LC1}} \\ Y_{\mathrm{LC2}} \end{bmatrix} \tag{4.1}$$

where $x_{a_{\mathrm{LC}}}$ and $x_{f_{\mathrm{LC}}}$ are the longitudinal positions of the load cells.

From the potentiometers, P1 to P4, the ship's heave z, roll ϕ and pitch θ motions, in the b-frame, can be derived by:

$$\begin{bmatrix} z \\ \theta \end{bmatrix} = \frac{1}{2(x_{f_P} - x_{a_P})} \begin{bmatrix} x_{f_P} & x_{f_P} & -x_{a_P} & -x_{a_P} \\ 1 & 1 & -1 & -1 \end{bmatrix} [\mathrm{P1} \quad \mathrm{P2} \quad \mathrm{P3} \quad \mathrm{P4}]^T \qquad (4.2)$$

$$[\phi] = \frac{1}{4y_{a_P}} [-1 \quad 1 \quad -1 \quad 1][\mathrm{P1} \quad \mathrm{P2} \quad \mathrm{P3} \quad \mathrm{P4}]^T \qquad (4.3)$$

$x_{f_P}$ $x_{a_P}$, and $y_{a_P}$ are the longitudinal and transversal position of the potentiometers P1 to P4.

#### *4.3.3.2Beam frame B*

Beam frame B is composed of two sub-frames, both of them connected by six strain gauges S1 to S6. The beam frame installed on board the ship model, and a general arrangement of the instrumentation is illustrated in Figure 4.8.

The forces in surge, sway and heave, as well as the moments in roll, pitch and yaw, expressed on the b-frame, can be derived from the measurements obtained from the strain gauges by the following relationships:

$$\begin{bmatrix} X \\ Y \\ Z \\ K \\ M \\ N \end{bmatrix} = \begin{bmatrix} 0 & 0 & 0 & 1 & 0 & 0 \\ 0 & 0 & 0 & 0 & 1 & 1 \\ 1 & 1 & 1 & 0 & 0 & 0 \\ \frac{1}{2}b & -\frac{1}{2}b & -\frac{1}{2}b & 0 & -z_{CF} & -z_{CF} \\ 0 & \frac{1}{2}a & -\frac{1}{2}a & z_{CF} & 0 & 0 \\ 0 & 0 & 0 & 0 & -\frac{1}{2}c & \frac{1}{2}c \end{bmatrix} \begin{bmatrix} S1 \\ S2 \\ S3 \\ S4 \\ S5 \\ S6 \end{bmatrix} \qquad (4.4)$$

The constant parameters $a$, $b$, and $c$ define the relative position of the strain gauges with respect to each other (see Figure 4.8). The parameter $z_{CF}$ denotes the vertical distance of the b-frame's origin to the centre of the frame ($CF$).

Because of the limited space between the carriage and the model, the frame's B centre did not coincide with the b-frame's origin, hence, $z_{CF}$ was measured 0.078 m. The parameters $a$, $b$, and $c$ were 0.80 m, 0.22 m, and 1.45 m, respectively.

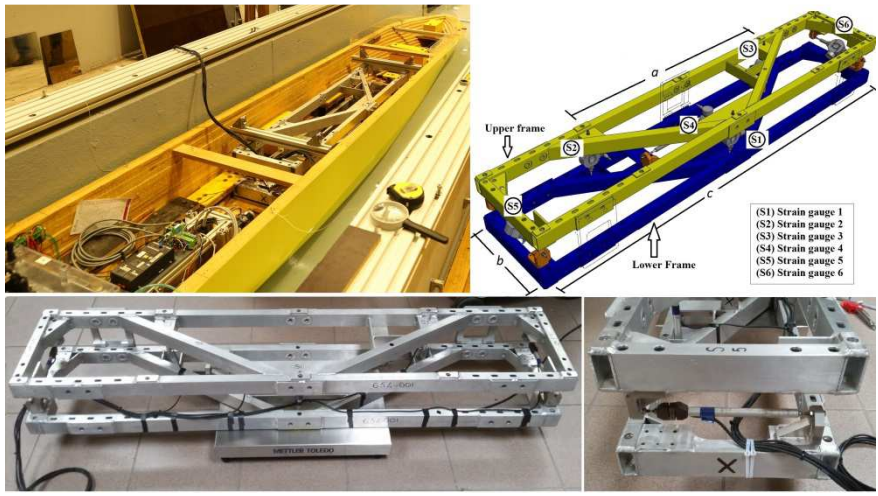


Figure 4.8 Beam frame B mounted on the model (top left figure), and general arrangement of the strain gauges and sub-frames (top right and bottom figures).

## 4.4 Test matrix

The experimental program can be separated in three main groups, steady straight line tests, harmonic yaw tests, and free roll decay tests. Steady straight line tests and harmonic yaw tests have been conducted in both in calm water and in regular waves using the beam frames frame A and frame B, described above. A few steady tests and harmonic yaw tests have been conducted using only the frame A, these tests are shown in grey shaded areas in the tables presented below.

Free roll decay tests have been only conducted in calm water using the frame A. Different from the first two test types, in this study four different water depths have been used. This was because free roll decay tests do not require longer waiting times to execute the next tests compared to tests in wave. Hence, the possibility to investigate additional water depths.

The following sub sections present the model speed, heading, drift angle, and wave angle of encounter selected for the present study. The respective signs follow the conventions established in 4.3.1.

### 4.4.1 Wave main characteristics

Seventeen regular waves have been chosen accordingly to what has been discussed in 4.2. These waves can be differentiated in two groups as a function of their wave amplitudes ($\zeta_a$), which are 11.1 mm and 15.0 mm at model scale and 1.0 m and 1.35 m at full scale, respectively. The wave main particulars are presented in Table 4.4 and they have been calculated for a water depth ($h$) of 0.218 m (19.6 m full scale) corresponding to the ship's keel to tank bottom clearance (UKC) of 50% of the ship's draft.

Bear in mind that the selected wave frequencies ($\omega_W$) have a lower limit than the 2.0 rad/s value discussed in 4.2. This is because higher limits of $\omega_W$ will imply wave lengths ($\lambda$) smaller than one fifth of the ship length ($L_{PP}$). Such waves will not subject the ship to important loads and induced motions, hence, they are omitted.

Table 4.4 Wave main particulars at water depth h=0.2183 m at model scale and 19.6 m at full scale.

| Item | ratio $L_{PP}/\lambda$ (–) | Model scale 1/90 $\lambda$ (m) | $\omega_W$ (rad/s) | $\zeta_a$ (mm) | Full scale $\lambda$ (m) | $\omega_W$ (rad/s) | $\zeta_a$ (m) |
|---|---|---|---|---|---|---|---|
| w1 | 5.00 | 0.84 | 8.26 | | 75.4 | 0.87 | |
| w2 | 3.85 | 1.09 | 6.94 | | 98.0 | 0.73 | |
| w3 | 3.13 | 1.34 | 5.95 | | 120.5 | 0.63 | |
| w4 | 2.63 | 1.59 | 5.19 | (RW1) | 143.4 | 0.55 | (RW1) |
| w5 | 2.27 | 1.85 | 4.59 | 11.1 | 166.2 | 0.48 | 1.0 |
| w6 | 2.00 | 2.10 | 4.11 | | 188.6 | 0.43 | |
| w7 | 1.67 | 2.51 | 3.49 | | 225.9 | 0.37 | |
| w8 | 1.43 | 2.93 | 3.03 | | 263.8 | 0.32 | |
| w9 | 1.25 | 3.35 | 2.67 | | 301.8 | 0.28 | |
| w10 | 5.00 | 0.84 | 8.26 | | 75.4 | 0.87 | |
| w11 | 3.85 | 1.09 | 6.94 | | 98.0 | 0.73 | |
| w12 | 3.13 | 1.34 | 5.95 | | 120.5 | 0.63 | |
| w13 | 2.63 | 1.59 | 5.19 | (RW2) | 143.4 | 0.55 | (RW1) |
| w14 | 2.27 | 1.85 | 4.59 | 15.0 | 166.2 | 0.48 | 1.35 |
| w15 | 2.00 | 2.10 | 4.11 | | 188.6 | 0.43 | |
| w16 | 1.67 | 2.51 | 3.49 | | 225.9 | 0.37 | |
| w17 | 1.43 | 2.93 | 3.03 | | 263.8 | 0.32 | |

### 4.4.2 Steady straight line tests

Steady straight line tests are conducted with the model speed components, $u$, and $v$ constant, and zero yaw velocity. Such tests can be performed as well as with a given drift angle ($\beta$) and in combination with propeller rates ($n$) and rudder angles ($\delta$).

Tests in calm water have been investigated for five main speeds in combination with different drift angles. Table 4.5 presents the respective values for these experiments.

Table 4.5 Ship speeds, drift angles, and heading angles combination during steady tests in calm water.

| Item | $F_r$ (–) | V (Knots) full scale | $\beta = \bar{\psi}$ (deg) | UKC (%) |
|---|---|---|---|---|
| St1 | 0.025 | 3 | 0,5, 10 | 50 |
| St2 | 0.050 | 6 | 0,5, 10 | 50 |
| St3 | 0.075 | 9 | 0,5, 10 | 50 |
| St4 | 0.100 | 12 | 0,5, 7.5 | 50 |
| St5 | 0.125 | 15 | 0,5 | 50 |

The respective combinations of steady tests with propeller and rudder action have been also investigated. Only few tests have been performed. The selected parameters are shown in Table 4.6.

Table 4.6 Steady tests combined with propeller rates and rudder angles.

| Item | $n/n_0$ (%) | $\delta_R$ (deg) |
|---|---|---|
| St2 | 75, 100 | 0, 35 |
| St3 | 75, 100 | 0, 35 |
| St4 | 75, 100 | 0, 35 |
| St5 | 75, 100 | 0, 35 |

The same test parameters described above have been used for the experiments in regular waves. Their respective combination with the regular wave parameters are presented in Table 4.7 and in Table 4.8.

Notice that tests with propeller and rudder action are shaded in grey indicating that they have been conducted only with the frame A, thus with the semi captive model.

Table 4.7 Steady tests, and wave angle of encounter for test in regular waves.

| Item | Regular waves | | | $\eta$ (deg) |
|---|---|---|---|---|
| St1 | w1 to w9 | and | w10 to w17 | 0,180 |
| St2 | | w1 to w9 | | 0,180 |
| St3 | w1 to w9 | and | w10 to w17 | 0,180 |
| St4 | | w1 to w9 | | 0,180 |
| St5 | w1 to w9 | and | w10 to w17 | 0,180 |

Table 4.8 Steady tests, propeller rates, rudder angles, and wave angle of encounter for test in regular waves.

| Item | Waves | $n/n_0$ (%) | $\delta_R$ (deg) | $\eta$ (deg) |
|---|---|---|---|---|
| St2 | w5, w7, w9 | 75, 100 | 0, 35 | 180 |
| St3 | w5, w7, w9 | 75, 100 | 0, 35 | 180 |
| St4 | w5, w7, w9 | 75, 100 | 0, 35 | 180 |
| St5 | w5, w7, w9 | 75, 100 | 0, 35 | 180 |

### 4.4.3 Harmonic yaw tests

Harmonic yaw tests are conducted with the model speed components, $u$ and $v$, constant during the entire run. The yaw velocity $r$, however, oscillates harmonically. The latter is a result of the harmonically changing heading with a period $\psi_T$, and the amplitude $\psi_A$. Such test can be also combined with a propeller rate and a rudder angle.

The combination of selected speeds with the ship drift angles, and period and amplitudes of the harmonic oscillations are shown in Table 4.9.

Table 4.9 Ship speeds, drift angles and periods and amplitudes of the harmonic oscillating heading in calm water.

| Item | $F_r$ (–) | Full scale V (Knots) | $\psi_T$ (s) | $\psi_A$ (deg) | $\beta$ (deg) | UKC (%) |
|---|---|---|---|---|---|---|
| PMM1 | 0.025 | 3 | 58 | 25 | 0, 5, 10 | 50 |
| PMM2 | 0.050 | 6 | 48 | 22 | 0, 5, 10 | 50 |
| PMM3 | 0.075 | 9 | 40 | 20 | 0, 5, 10 | 50 |
| PMM4 | 0.100 | 12 | 35 | 15 | 0, 5, 7.5 | 50 |
| PMM5 | 0.125 | 15 | 32 | 15 | 0, 5 | 50 |

The respective parameters for harmonic yaw tests combined with propeller and rudder actions are presented in Table 4.10.

Table 4.10 Harmonic yaw tests combined with propeller and rudder action in calm water.

| Item | $n/n_0$ (%) | $\delta_R$ (deg) |
|---|---|---|
| PMM2 | $75, 100$ | $0, 35$ |
| PMM3 | $75, 100$ | $0, 35$ |
| PMM4 | $75, 100$ | $0, 35$ |
| PMM5 | $75, 100$ | $0, 35$ |

Harmonic yaw tests have been also performed in regular waves. The above presented yaw tests combined with regular wave action are presented in Table 4.11 and Table 4.12.

Table 4.11 Harmonic yaw tests, wave angle of encounter for test in regular waves.

| Item | Regular waves | $\eta$ (deg) |
|---|---|---|
| PMM1 | $w1$ to $w9$ and $w10$ to $w17$ | $0,180$ |
| PMM2 | $w1$ to $w9$ | $0,180$ |
| PMM3 | $w1$ to $w9$ and $w10$ to $w17$ | $0,180$ |
| PMM4 | $w1$ to $w9$ | $0,180$ |
| PMM5 | $w1$ to $w9$ and $w10$ to $w17$ | $0,180$ |

Table 4.12 Harmonic yaw tests, propeller rates and rudder angles for tests in regular waves.

| Item | Waves | $n/n_0$ (%) | $\delta_R$ (deg) |
|---|---|---|---|
| PMM2 | $w5, w7, w9$ | $75, 100$ | $0, 35$ |
| PMM3 | $w5, w7, w9$ | $75, 100$ | $0, 35$ |
| PMM4 | $w5, w7, w9$ | $75, 100$ | $0, 35$ |
| PMM5 | $w5, w7, w9$ | $75, 100$ | $0, 35$ |

### 4.4.4 Free decay tests

Free oscillation tests have been performed by giving an initial heel angle to the model, which was achieved by means of wooden piece, as shown in Figure 4.9. Further, the model was hold at this initial position until the towing carriage reached its desired speed and immediately released by pulling the cord attached to the

wooden piece. The initial heeling angles, ship speeds, and combination with different UKCs are presented in Table 4.13

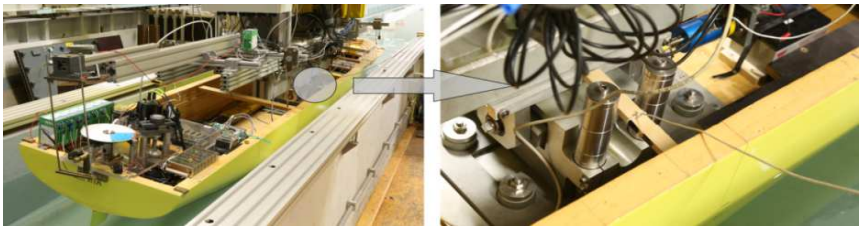

Figure 4.9 Test set up and mechanism to heel the ship and initial angle.

Table 4.13 Test matrix for the free decay test

| | $F_r$ $(-)$ | | | | | | |
|---|---|---|---|---|---|---|---|
| UKC | 0.00 | 0.025 | 0.050 | 0.075 | 0.100 | 0.125 | 0.150 |
| 10% | 2.21° | 1.6° | 1.89° | 1.54° | 1.77° | − − | − − |
| 20% | 2.70° | 3.04° | 2.71° | 3.51° | 2.74° | 2.93° | 2.35° |
| 35% | 3.11° | 3.32° | 3.27° | 2.68° | 1.95° | 3.96° | 2.74° |
| 190% | 6.96° | 6.66° | 6.45° | 5.69° | 6.23° | 6.85° | 6.64° |
| | Initial roll angles (deg) | | | | | | |

It can be noticed from Table 4.13 that initial heeling angles are rather small. Small roll angles have been selected at lower UKC to avoid bottom collision, bear in mind that the limited water depth will result in smaller clearances between the ship's bottom and the tank's bottom.

### 4.4.5 The water depth

ULCC vessels can reach small UKC values when navigating along the access channels at sea, as low as 15% of the draft. Studying wave effects in such scenarios is of major interest for the present study. However, tests at very low UKC (e.g. 35% of draft and less) have not been included in the test matrix given above. A slightly larger UKC, 50%, was chosen instead in order to reduce larger squat effects at higher speeds. Lower UKCs would have led otherwise to unrealistic test conditions with the model fully captive (frame B) and further comparison with the semi-captive model test results would not have been possible.

## 4.5 Model test limitations

### 4.5.1 Problems encountered

The experimental study of ship models in waves is not a straightforward procedure. For instance, reflection is one of the crucial problems impairing the performance of such tests. To avoid including waves reflected from the beach, an estimation based on the wave phase velocity can be carried out in order to select a proper time interval from the time record. Such an implementation is relatively easier to consider and was applied to model tests, see Tello Ruiz et al. (2015) and Van Zwijnsvoorde et al. (2018).

During the experimental program, additional challenges were encountered regarding wave generation, wave propagation along the tank, interaction with the tank side walls, the ship bottom touching probability, the different magnitude of forces to be captured (steady and unsteady forces), and the noise in the gauges. They are all only a few of the difficulties encountered.

Among all the difficulties, the wave generation and propagation along the tank, the tank side wall interaction, and the noise in the gauges were found to be the most restrictive. They are further discussed in the present subsections. A broader discussion of the problems encountered can be found in Tello Ruiz et al. (2016b), Mansuy et al. (2017) and Tello Ruiz et al. (2017).

### 4.5.2 Wave generation problem

#### *4.5.2.1General discussion*

Considering linear and nonlinear Stokes waves, it is generally expected that waves will propagate with a permanent form in space and time. However, such permanent wave propagation is not always the case despite the appropriate corrections made to account for the effect of the free wave. Such phenomenon is well-known as modulation instability (MI). Modulation instability can be easily understood, in its more simplistic version, if a medium is considered where two main wave carriers of different frequencies, $\omega_{W_1}$ and $\omega_{W_2}$, are propagating in the same direction. In such cases

frequency components $\omega_{W_1} \pm \omega_{W_2}$ will appear as a result of the interaction between the main wave carriers.

Considering the case when the two main frequencies are similar, $\omega_{W_1} \approx \omega_{W_2}$, it is then expected that the sum of frequencies leads to twice the fundamental frequency, $2\omega_{W_1}$, and the difference results in a zero frequency. Such a problem can also be observed when the main wave carriers have slightly different frequencies $\omega_W \pm \Omega$ ($\Omega \ll \omega_W$); hence, due to interaction between the waves, wave components of frequencies $2\omega_W \pm 2\Omega$ and $\pm 2\Omega$ arises. In Figure 4.10 the effect of the MI is illustrated for different locations along the propagation axes, and their respective Fourier transformation is shown at the bottom, respectively.

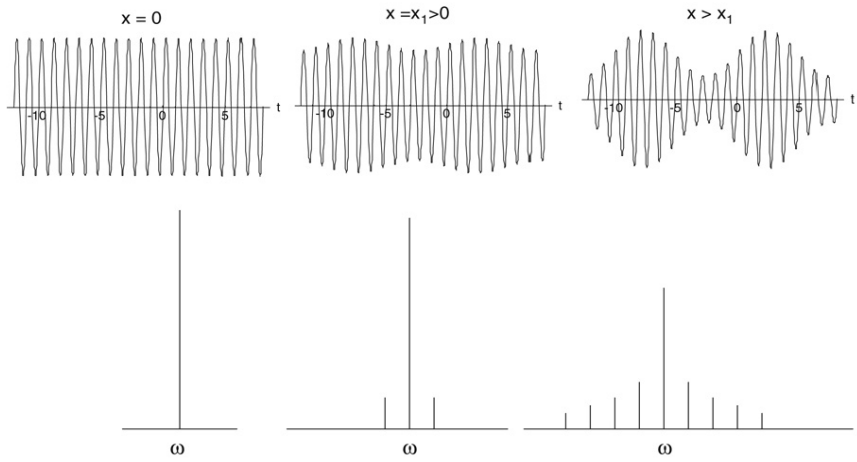


Figure 4.10 Evolution of a nonlinear wave at different position from the wave maker. Retrieved from Zakharov and Ostrovsky (2009).

As long as the generated frequencies are similar one to another, the MI will not be significant for long waves. However, a more critical scenario occurs for shorter Stokes waves in deep water. A disintegration of the wave elevation at long distance from the wave maker occurs and in the most particular events the modulation disappears and the regular wave appears again. The disintegration of waves has been studied by Benjamin and Feir

(1967) and they concluded that such a phenomenon appears for $kh > 1.363$.

Figure 4.11 shows the experiments performed by Benjamin and Feir (1967) where disintegration of waves was recorded in photographs.

Results from the Fourier analysis shown in Figure 4.10 indicate also the presence of several frequencies although only one main wave carrier was generated. In general, a range of wave frequencies will be obtained when applying Fourier analysis to the time series, this because other spurious frequencies will appear due to the fact that the rigid wave board cannot match perfectly the required water particles displacements. This required further investigation which was extensively discussed by the author in Delefortrie et al. (2016b). A brief discussion regarding this aspect is presented in the following subsection.

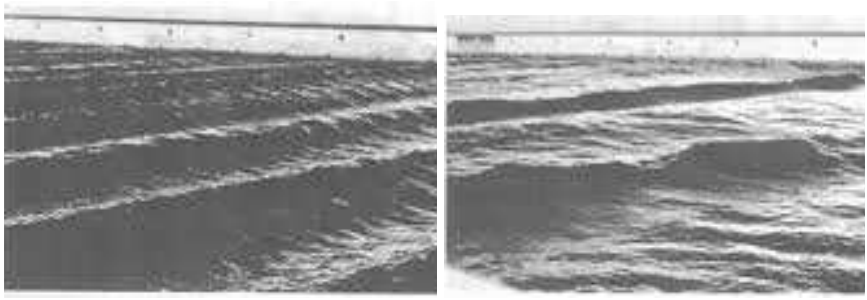

Figure 4.11 Disintegration of a Stokes regular wave propagating along a tank. Photographs of wave trains illustrating wave breaking due to the instability. Left and right photographs taken near and at $60\,m$ from the wave maker, respectively. Retrieved from Benjamin and Feir (1967).

#### *4.5.2.2Study on the wave propagation along the towing tank*

For the investigation of the wave propagation along the tank, regular wave tests were performed with several combinations of water depth and wave period. A summary of the selected test parameters is presented in Table 4.14, more details can be found in Delefortrie et al. (2016b).

Table 4.14 Test matrix of wave periods and water depths used in the analysis of wave propagation along the towing tank at FHR.

| Wave period $T_W$ (s) | | | | | | | | Water depth h (m) |
|---|---|---|---|---|---|---|---|---|
| 0.35 | 0.4 | 0.5 | 0.6 | 0.7 | 0.8 | 0.9 | 1.0 | 0.4, 0.28, 0.26, |
| 1.25 | 1.50 | 1.75 | 2.0 | 2.50 | 3.0 | 3.50 | 4.0 | 0.22, 0.16 |

Waves profiles were recorded at different locations along the tank, in total eleven wave gauges have been used, WG 1 to WG 11, distributed longitudinally and transversally along the tank as shown in Figure 4.12. The configuration allows to investigate the variation of the wave at different sections of the tank, as well as at offsets from the tank centre line.

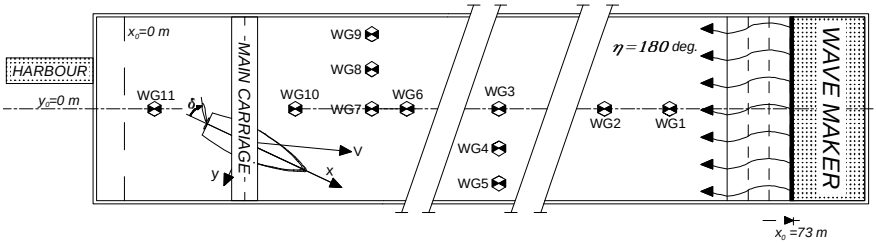


Figure 4.12 Illustration of the location of the wave gauges along the towing tank at FHR.

Examples of the records are presented in Figure 4.13 and Figure 4.14. The evolution of the wave profile can be observed in time and space. For better illustration purposes of the wave propagation along the towing tank, they are displaced vertically. In addition, three different circle markers, for each wave gauge, are also displayed: white circles showing the starting and end of the wave, red circles indicating when reflection from the beach occur, and green circles are plotted if one of the conditions are satisfied, the water surface has displaced vertically larger than 25% of the desired wave amplitude or after three wave lengths of the first white circle. The position in time of the white and red circles for each wave gauge has been estimated based on the initial and end times motion orders given to the wave maker, the wave phase velocity, the distances between each wave gauge and to the beach.

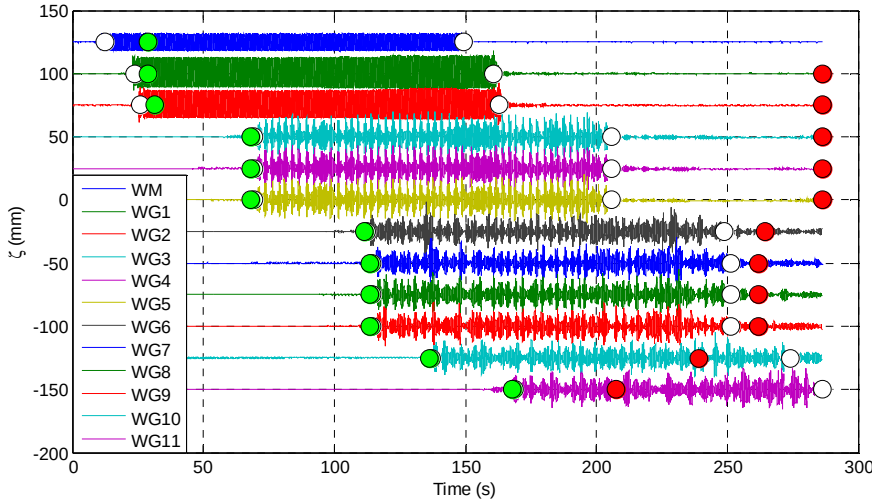


Figure 4.13 Wave records obtained at $T_W = 0.50$ s and $\zeta_a = 15$ mm, and $\mathrm{h} = 0.4$ m showing instabilities in the wave propagation. Records are offset vertically, and circles show the estimated start and end of wave action (white circle), reflection from the beach (red circle) and a reference of wave action (green circle).

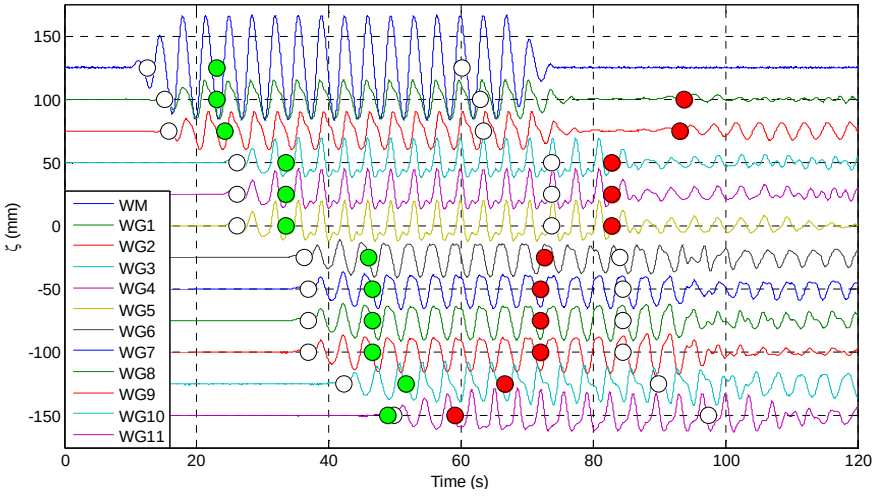


Figure 4.14 Wave records for regular wave tests at $T_W = 3.5$ s and $\zeta_a = 15$ mm, $\mathrm{h} = 0.40$ m. Modulation occur due to free wave. Records are offset vertically, and circles show the estimated start and end of wave action (white circle), reflection from the beach (red circle) and a reference of wave action (green circle).

From Figure 4.13 a regular behaviour of waves can be observed in WG1 and WG2 only. Starting from WG3 instabilities appear and the regular behaviour is no longer observed. This phenomenon is highly nonlinear and little can be done to restrict it other than limit the length of the towing tank available for such tests.

An additional problem was also found for the longer wave range. This is better observed in Figure 4.14. Waves profiles change their form as they propagate along the tank, see for instance, the profile at WG2 is different than the one seen observed at WG9.

Such differences in the wave profile according to Daugaard (1972), Fontanet (1961), Hansen and Svendsen (1974), and Shäffer (1996) can be related to a secondary wave generated at the wave maker. This is mainly because of the kinematical boundary condition which is not satisfied at the wave board. To overcome this problem, a second harmonic motion having an opposite phase of the secondary wave has been applied to the wave maker. The phase and amplitude have been chosen based on the study of Madsen (1971).

The wave profiles before and after the correction using Madsen (1971) approach are presented in Figure 4.15. For better illustration purposses only three wave gauges, WG2, WG3, and WG4 are shown. It can be seen that before the correction was applied, the wave form does not seems regular and changes in form, in contrast, the corrected wave has a regular form and preserves its shape as it propagates along the tank.

During the studies, waves were found to change in amplitude along the longitudinal and transversal direction along the tank. This has been reported in Delefortrie et al. (2016b). Considering the ship moving in a region in the tank, it is then needed to define a region were waves have approximately a constant amplitude (5% can be considered as a reference)

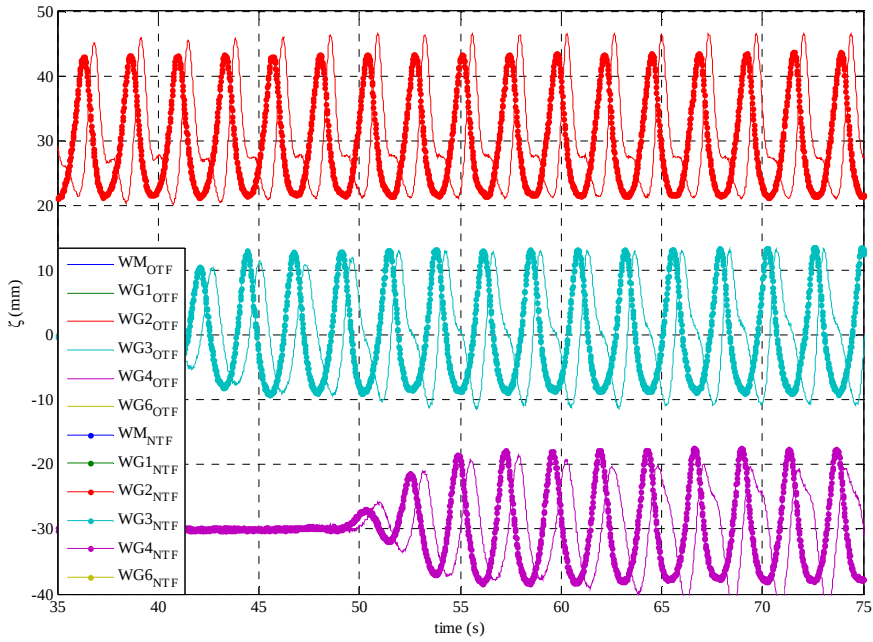


Figure 4.15 Wave records comparison after Madsen (1971) correction for the secondary wave profile. Test at $T_W = 2.35$ s, $\zeta_a = 11.1$ mm, and h = 0.22 m.

From the observations made during the experiments a region where the wave amplitudes change is less than 5% has been defined. This region is delimited by the longitudinal positions ($x_0$) of 28 m and 68 m, and the lateral positions ($y_0$) of −2.0 m and 2.0 m. This is valid for all waves defined in Delefortrie et al. (2016b). It is important to mention that the selected waves for the present study (selected in 4.4.1, Table 4.4), are within these limits.

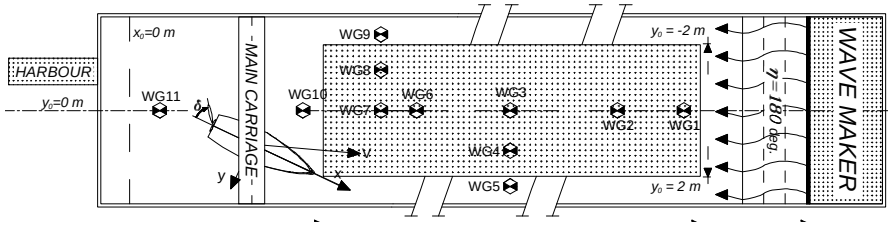


Figure 4.16 Region along the tank where waves have approximately constant amplitude, $h = 0.4$ m and $h = 0.22$ m.

### 4.5.3 Side wall effects

Ship speeds in shallow water are in general low. This is because of the limitations arising due to the finite water depth. The speeds are then chosen to be lower than the critical speed given by:

$$F_{r_{crit}} = \sqrt{g\mathrm{h}} \tag{4.5}$$

g being the gravity acceleration constant and h the water depth.

The speed limits in shallow water is an important constraint when evaluating the ship model behaviour in waves. This is mainly due to the problem resulting from the waves generated by the model which are reflected back to the model by the tank walls, this is known as side wall interaction. A reasonable higher speed is then needed to sail away from the reflected waves.

In ITTC (2011b) guidelines to avoid side wall interaction are provided as a function of the wave period (given by $\omega_0$ for clarity purposes), the model length ($L_{\mathrm{PP}}$) and the tank width ($W_T$). Those relationships are, however, more generic for deep water waves and are limited for finite water depth. The later is mainly due to the wave dispersion relationship which is still dependent of the water depth. For such cases, it is yet possible to establish speeds limits, but are specific for a given ship model length and a tank width.

The speed limits defining whether side wall interaction occur in finite water depth can be found (assuming the ship to be positioned at the centre line of the towing tank) based on the relationships presented by LLoyd (1989). They are the result of equating the time needed for the radiated waves to travel back and forth ($t_r$), and the time needed for the ship ($t_s$) to move one ship length. $t_r$ and $t_s$ can be obtained by:

$$C_r = \frac{g}{\omega_r} tanh(k_r h) \tag{4.6}$$

$$\omega_E = \omega_0 - kVcos(\mu) \qquad \omega_r = \omega_E \tag{4.7}$$

$$t_r = \frac{W_T}{C_r} \qquad t_s = \frac{L_{PP}}{V} \tag{4.8}$$

where $C_{r_{crit}}$ is the phase speed of the ship radiated waves, $V$ is the ship speed, $\mu$ is the wave angle of encounter, and $k$ is the wave number.

For a test to be free of interaction with the tank side walls, the basic requirement is then $t_r > t_s$. These boundaries, defining when interaction occurs, have been estimated for two different water depths, 100% UKC and 50% UKC for the ship model C0W (as a n example given at $T_M$ of 14.5 m). The resulting tank's width to ship length ratio ($W_T$ /$L_{\mathrm{PP}}$) is 1.67. Figure 4.17 shows the speed limits for both head and following waves as function of the non-dimensional wave frequency $\omega_0'$ ($\omega_0' = \omega_0/\sqrt{gL_{\mathrm{PP}}}$).

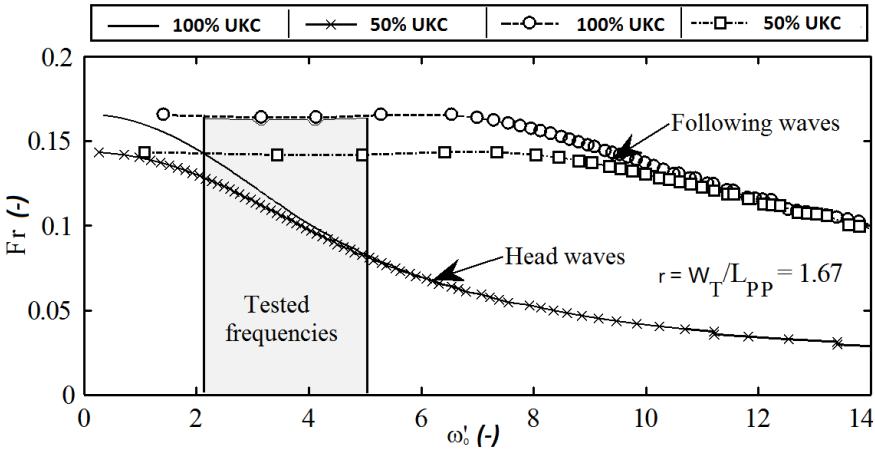


Figure 4.17 Regions where side wall interaction occur in head and following waves for the ship model C0W.

From Figure 4.17 one can identify two different regions, the regions below and above the curves indicate where interaction is expected or not, respectively.

Taking into consideration the range of selected wave frequencies (Table 4.4) and ship speeds (Table 4.5 and Table 4.9), see grey area in Figure 4.17, tank side wall interaction is expected to occur. To avoid such a problem, speeds should be higher than the ones given by the limiting curves. The latter is, however, not possible due to the critical speed in shallow water given in Eq. (4.5).

In spite of the importance of the above analysis, side wall interaction for certain wave frequencies might not be significant. This has been investigated by comparing the results for surge and sway forces from two different model tests conducted at zero speed. Wave frequencies $\omega_0' = 3.63$ and $\omega_0' = 2.06$ and their respective $\zeta_{\omega_0} = 32.8$ and $\zeta_{\omega_0} = 10.1$ mm have been selected. The results are presented in Figure 4.18.

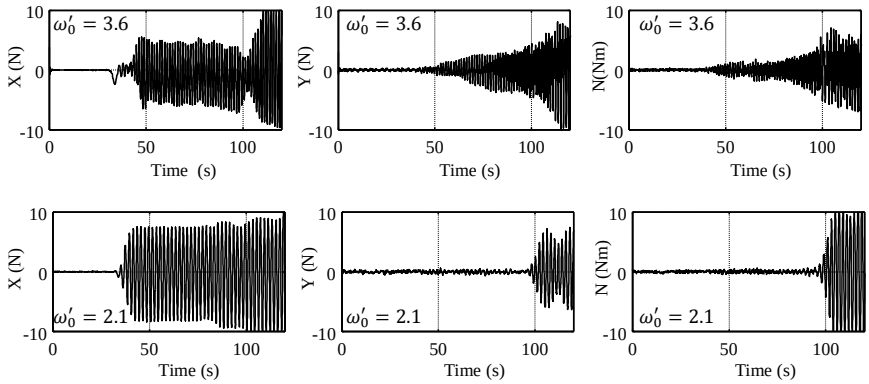


Figure 4.18 Surge and sway forces, and yaw moments during tests at zero speed, $F_r = 0$, in heading waves, $\mu = 180$ deg. At $\zeta_a = 32.8$ mm (top figure) with tank side wall interaction, and $\zeta_a = 10.1$ mm (bottom figure) with no tank side wall interaction.

From Figure 4.18 it can be observed that for $\omega_0'$ of 3.63, the measured sway force and yaw moment build up immediately after the surge force begins to oscillate harmonically. Such a response is not observed for $\omega_0'$ of 2.06. At the lower frequency both sway force and yaw moment remain in the same order as their initial values, and only after time of 100 s they experiences larger magnitudes. This delayed response indicates a time window with negligible interaction with the tank's side walls.

The influence of the tank wall at the lower frequency can be also attributed to the smaller wave amplitude. The smaller the wave amplitude the smaller the induced loads and induces ship motions; hence, the ship wave generation will be less significant.

The less significant wave generation by the ship at smaller wave amplitudes is also advantageous for the present study of the ship C0W in the Belgian coastal zone of the North Sea. Recall that the wave amplitudes are constrained to a maximum of 15.0 mm (1.35 m at full scale). In spite of the importance of the present observations, one should bear in mind that the above results (shown in Figure 4.17 and Figure 4.18) have been obtained for a ship moving along the tank centre line, with no drift angle, or offsets with respect to the tank centre line, a careful examination of the results should be taken in such cases.

In order to get a better idea of the side wall interaction problem when the tanks width to ship length changes a numerical investigation was conducted in Tello Ruiz et al. (2017).

The numerical study was conducted using the CFD software package FINE™/Marine. Two different tank widths were used, the water depth was set to correspond to 50% UKC , and the ship speed was set to $F_r = 0.075$ (9 knots at full scale). Figure 4.19 illustrates the numerical arrangements and Table 4.15 presents the respective parameters. For more details of the computational setup, see Tello Ruiz et al. (2017).

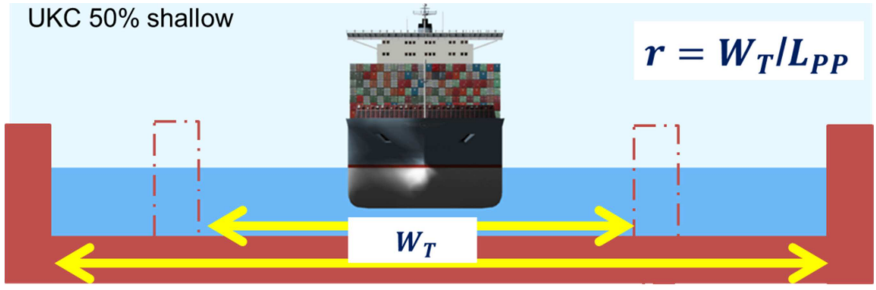


Figure 4.19 Model ship arrangement for the numerical tests, at 50% UKC.

Table 4.15 CFD tests parameters for the analysis of the ship C0W at water depth 0.242 m (21.8 m at full scale).

| r2 (–) | r1 (–) | $F_r$ (–) | $F_{rh}$ (–) | $\lambda/L_{PP}$(–) | $L_{PP}/\lambda$ (-) | $\zeta_a$ (mm) |
|---|---|---|---|---|---|---|
| 3.97 | 1.67 | 0.075 | 0.33 | 0.45 | 2.22 | 20 |

It is important to mention that the ratio r1 correspond to the actual width of the tank at FHR. The second ration r2 correspond to a width of the tank which has been chosen based on Eq. (4.6) to Eq. (4.8) to ensure no tank side wall interaction.

The comparison of the results obtained for the two different ratios are presented in Figure 4.20. Because the study has been conducted in head waves, only surge forces, heave and pitch motions are presented. In addition, a similar plot as presented in Figure 4.17, delimiting the regions of interactions, is shown at the top left figure.

From the top left figure in Figure 4.20, one can observe that the tests are located below the limiting curve of interaction (blue line). Hence, one can expect that for the lower tank width to ship length ratio, r1, interaction will be present. For the larger ratio, r2, the limiting curve (green line) is below the tests, hence, no interference is expected.

From the results presented in Figure 4.20, one can observe that insignificant differences are obtained when both results are compared. Only the surge forces seem to be different but such deviations are rather negligible.

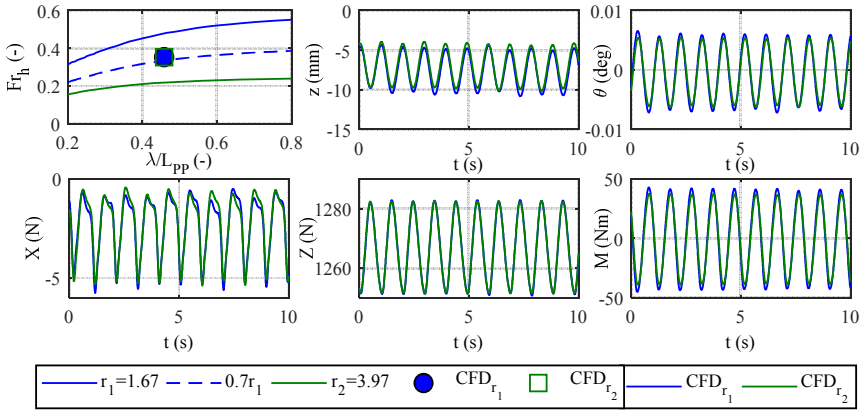


Figure 4.20 Ship model critical speeds (top left), and surge forces and motions responses obtained from numerical studies conducted with two different tank widths.

To get a quantitative idea of the results, a Fourier analysis has been performed by fitting the data to Eq.(4.9) using a least square method with eight unknown parameters $(a_0, a_1, b_1, a_2, b_2, a_3, b_3, \omega_1)$.

$$f(a_j, b_j, \omega_1) = a_0 + \sum_{j=1}^{3} a_j \cos(j\omega_1 t) + b_j \sin(j\omega_1 t) \tag{4.9}$$

$a_0$ is the mean value, and the fundamental frequency is given by $\omega_1$. The amplitude of the harmonics are given by $G_j = \sqrt{a_j^2 + b_j^2}$.

The results for the mean, the height, and the period for both analyses are presented independently in Table 4.16 and Table 4.17 for the ratio r1 and r2, respectively.

Table 4.16 Fourier analysis of the CFD computations with the C0W ship model for tank's width to ship lengths ratio r1.

| Items | $z$ (mm) | $\theta$ (deg) | $X$ (N) | $Z$ (N) | $M$ (Nm) |
|---|---|---|---|---|---|
| $a\_0$ | −6.8 | 0.00 | −2.25 | 1267.1 | 0.0 |
| $H$ | 5.8 | 0.01 | 4.42 | 31.6 | 84.0 |
| $T\ (s)$ | 1.6 | 1.6 | 1.6 | 1.6 | 1.6 |

Table 4.17 Fourier analysis of the CFD computations with the C0W ship model for the tank's width to ship lengths ratio r2.

| Items | $z$ (mm) | $\theta$ (deg) | $X$ (N) | $Z$ (N) | $M$ (Nm) |
|---|---|---|---|---|---|
| $a\_0$ | −6.3 | 0.0 | −2.19 | 1267.1 | 0.0 |
| $H$ | 5.7 | 0.01 | 4.46 | 30.9 | 76.1 |
| $T\ (s)$ | 1.6 | 1.6 | 1.6 | 1.6 | 1.6 |

From the results presented in Table 4.16 and Table 4.17 it can be confirmed that both tests yield similar results. Hence, side wall effects might be present but have no significant influence.

A particular observation can be drawn with respect to the limiting speeds shown at the top left figure in Figure 4.20. It can be observed that if one restrains the limits found with the ratio r1 to approximately 70% (shown by the dashed blue line), the interference with the tank side walls is no longer present. This has been further investigated experimentally in Tello Ruiz et al. (2017)

with a scale model of the MOERI Container Ship, the KCS. Similar to the C0W ship, the results show that a reduction to a 70% of the limits based on Eq. (4.6) to Eq. (4.8) can be used for further studies.

It has been seen that interaction with the tank side wall can occur at several conditions and that depends on several parameters such at the model speed $F_r$, the width of the tank $W_T$, the ship length $L_{\mathrm{PP}}$, and the water depth h, the wave length $\lambda$, the wave amplitude $\zeta_a$, and also the UKC. It would be advised to perform model tests in waves in wider tanks but wide enough is not always possible.

The problems encountered with respect to side wall interaction, however, shed some light in the possibility to perform model test in waves where such interactions are present but can be neglected. Much more work is yet needed in this field and can be regarded as future topic of research.

It is also important to notice, that the analysis above has been conducted with the ship in steady straight run conditions and cannot be applied nor extrapolated to tests with drift angles and harmonic tests.

### 4.5.4 Post-processing analysis

Experimental results are always subjected to noise. An example of the derived surge and sway forces including noise in the signals are presented in Figure 4.21. Such results cannot be directly used and a level of post processing is needed.

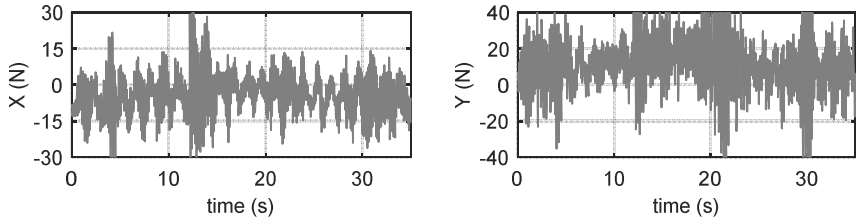


Figure 4.21 Example of the surge (left) and sway (right) forces recorded during fully captive test, at 50% UKC, $F_r = 0.100$, $L_{PP}/\lambda = 1.43$, $\beta = 7.5$ deg, $\zeta_a = 11.1$ mm, $\mu = 180$ deg.

For the post processing analysis different methods can be applied, a simple Fourier analysis or a more complex analysis including a combination of Fourier and a nonlinear least square regression, see Eq.(4.9). Such methods have been also studied by the author and were published in Mansuy et al. (2017).

Depending on the characteristics of the responses needed to measure e.g. mean values in steady tests as the one shown in Figure 4.20, even a simple average method can be used when the time records are long enough. Because of the limitation in length of the towing tank, and other problems associated with the main dimensions (tank side wall interaction), the available length of the sample is rather short, hence, simple mean or running averages cannot be applied.

For steady tests in waves, the combination of a band pass filter with a Fourier regression, see Eq.(4.9), was found to be the more reliable and suited even for short time records.

The most difficult tests, in terms of noise, were found to be the harmonic yaw tests, see Figure 4.21. In these tests, one cannot clearly differentiate the harmonic behaviour of the response to waves. For sway forces the plotted responses do not even show any indication of being influenced by waves. It was then necessary to investigate a different approach.

For harmonic yaw tests, applying a filter resulting of a combination of a low pass, and a band pass filter was found to be useful. The filter however requires first the use of a hamming window (Mansuy et al. 2017) to reduce the “leakage” (numerical frequencies arising due to the non-periodicity of the sample signal).

An example of the spectral analysis, the low pass filter and the band bass filter, as well as the post processed signal are shown in Figure 4.22. This has been obtained from the analysis of the same test presented in Figure 4.21. The results are shown for all forces and moments.

From Figure 4.22 it can be observed that the surge forces, and roll, pitch and yaw moments show a clear influence of the waves. Contrary, forces in sway as expected show a large influence of noise. This is also observed for the heave forces, although with slightly less significant magnitudes.

When the filter is applied, it is still possible to differentiate the sway force dependency of the wave, although it is not possible to separate the noise at that particular frequency. This has limited greatly a large amount of the experiments and made tedious and laborious the post processing analysis.

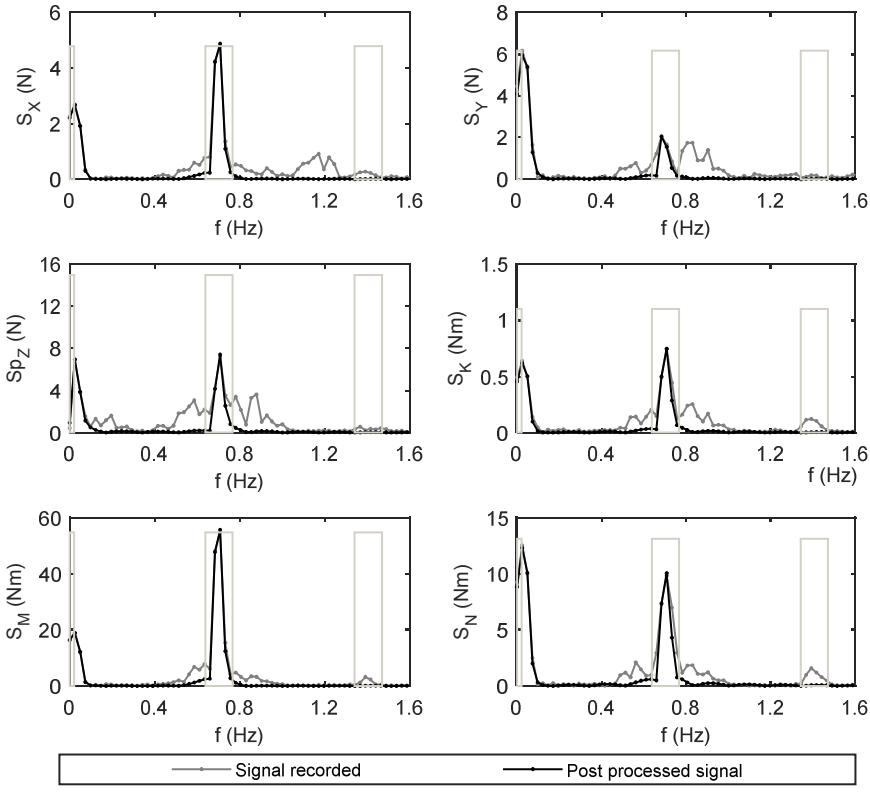


Figure 4.22 Spectral analysis for the all forces and moments recorded during test with the model fully captive, at 50% UKC, $F_r = 0.100$, $L_{PP}/\lambda = 1.43$, $\beta = 7.5$ deg, $\zeta_a = 11.1$ mm, $\mu = 180$ deg. Rectangles (in light grey) show the low pass and band pass filter.

The respective time records obtained before and after filtering are presented in Figure 4.23 for all forces and moments. After filtering, the wave frequency dependency can be clearly observed, even for the sway forces and the heave forces. The filtering process has been also applied to the wave gauge as a verification of the filtering analysis to not distort the fundamental energy of the main frequency carrier.

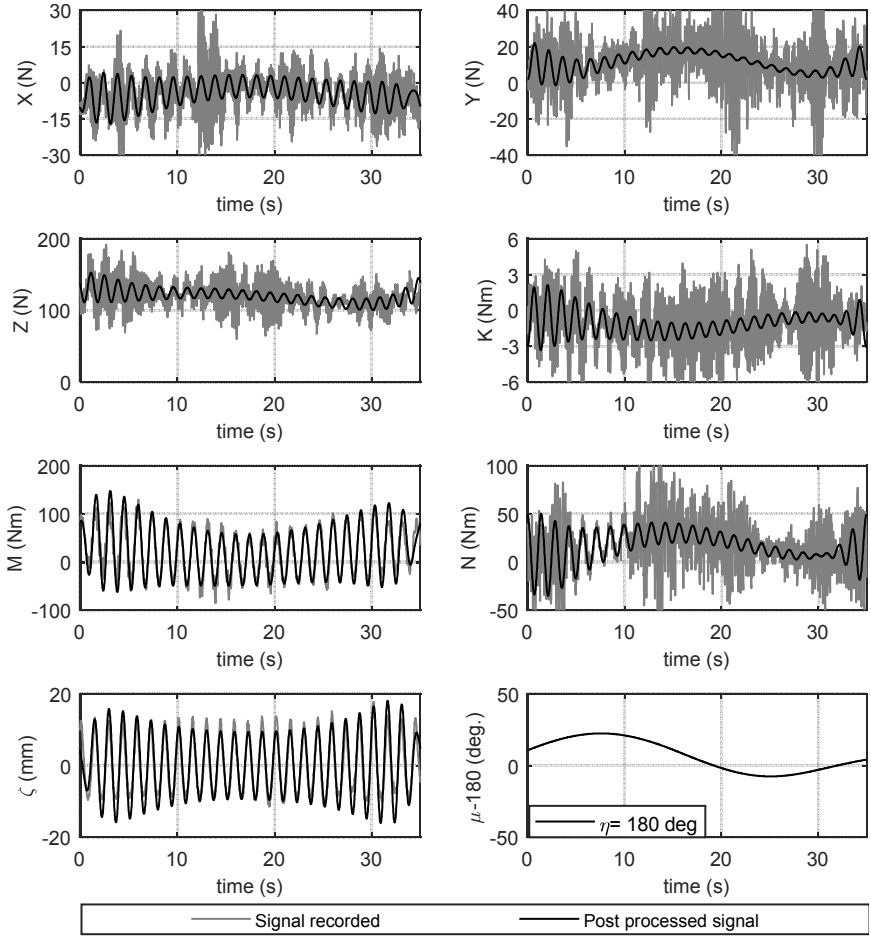


Figure 4.23 Post processed signal for all forces and moments, test at 50% UKC, $F_r = 0.100$, $L_{PP}/\lambda = 1.43$, $\beta = 7.5$ deg, $\zeta_a = 11.1$ mm, $\mu = 180$ deg.

### 4.5.5 Uncertainty analysis

An uncertainty analysis has been conducted only for the steady tests performed with the model fully captive (frame B). It is important to mention that the present uncertainty study accounts for the precision of the measurements only; bias sources have not been considered for due to the complexity of the model set up and the experimental difficulties mentioned in section 4.5.1-4.5.3. Nevertheless, the present results can be considered as representative of the numerical errors in the measurements.

Table 4.18 and Table 4.19 present the respective uncertainty estimations for the forces and moments. Taking into consideration the large number of parameters involved in the analysis, only nine runs per test have been conducted which are, however, considered sufficient for the present purposes. The tests in here discussed correspond to a steady drift test (St3, see Table 4.5) with Froude number of 0.075.

From Table 4.18 and Table 4.19, it can be observed that only surge forces and roll moments present the largest uncertainty values, both of around 2%. The influence of drift angles on the uncertainty seems negligible. The latter is also observed for the other forces and moments.

Notice that in spite of the small magnitudes of the moments measured in roll, the respective uncertainties remain always smaller. This guarantees that the results of the experiments, at least for the steady tests, can be considered as useful. The latter can be assumed to be valid for the other test conditions studied in the present work. It would have been of great interest to extend the analysis of uncertainty for other speeds, including tests in wave and also harmonic yaw tests; however, an extension of this study was not feasible in the scope of the present work.

Table 4.18 Precision uncertainty analysis for the forces measured during steady tests with the ship model fully captive (frame B). Tests conducted at Fr = 0.075, 50% UKC and $T_M$ = 13.1 m (at full scale) in calm water.

| $\beta$ (deg) | X (N) | U(X) (%) | Y (N) | U(Y) (%) | Z (N) | U(Z) (%) |
|---|---|---|---|---|---|---|
| 0 | $-1.88 \pm 0.04$ | 2.0 | -- | -- | $51.76 \pm 0.35$ | 0.7 |
| 5 | $-2.27 \pm 0.04$ | 1.8 | $2.25 \pm 0.03$ | 1.4 | $57.32 \pm 0.29$ | 0.5 |
| 10 | $-2.22 \pm 0.04$ | 1.8 | $8.63 \pm 0.03$ | 0.4 | $74.44 \pm 0.39$ | 0.5 |

Table 4.19 Precision uncertainty analysis for the moments measured during steady tests with the ship model fully captive (frame B). Tests conducted at Fr = 0.075, 50% UKC and $T_M$ = 13.1 m (at full scale) in calm water.

| $\beta$ (deg) | K (Nm) | U(K) (%) | M (Nm) | U(M) (%) | N (Nm) | U(N) (%) |
|---|---|---|---|---|---|---|
| 0 | -- | -- | $14.68 \pm 0.10$ | 0.7 | -- | -- |
| 5 | $-0.43 \pm 0.01$ | 2.1 | $13.10 \pm 0.08$ | 0.6 | $5.31 \pm 0.03$ | 0.5 |
| 10 | $-0.75 \pm 0.01$ | 1.3 | $11.17 \pm 0.12$ | 1.0 | $11.11 \pm 0.04$ | 0.3 |

# MANOEUVRING IN COASTAL WAVES



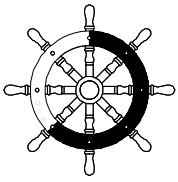

*The proper method for inquiring after the properties of things is to deduce them from experiments.*

*Isaac Newton*

# 5

# Wave effects on manoeuvring

## 5.1 General discussion

The present section is a discussion of the experimental study conducted in the Towing Tank for Manoeuvres in Confined Water at FHR (co-operation Flanders Hydraulics Research – Ghent University) in Antwerp, Belgium with a scale model of an Ultra Large Container Carried (ULCC). The test matrix, ship loading condition and parameter selection can be found in Chapter 4.

Due to the experimental limitations encountered during the experiments, only a limited number of combinations of the test parameters have been studied. These limitations are with respect to the ship model orientation in the tank, the ship model forward speed, the hull drift angle, the yaw velocity, and environmental conditions, such as wave angle of encounter, wave period and amplitude. However the difficulties encountered, it was found possible to optimise and enhance the tests results which concern the most for the present purpose of the study (see Chapter 4, Mansuy et al., 2017, and Tello Ruiz et al., 2017).

The present work does not neglect the importance of uncertainties in the measured quantities which are believed to be important in any experiments. In the present work only the precision uncertainty has been analysed for a steady test conducted with the model fully captive in calm water (see, 4.5.5). The results showed smaller uncertainty magnitudes which have been assumed to be representative for all fully captive test results. It was not possible to perform a similar study with the model semi-captive within the scope of the present work. It should be stressed that the main purpose of the present study is to propose a model for manoeuvring in waves in 6DOF. Hence, finding tendencies and identifying dominant fluid effects are believed to be more important than the accuracy of the results itself.

For the purpose of brevity and better comparison between the tests results, the results obtained from the test program conducted in 2016 are discussed, mainly (see Chapter 4). In addition, this test program allowed the possibility to compare tests with the ship model fully captive and semi captive. Where found necessary, results corresponding to the test program 2014 will be also displayed.

The test program conducted in 2016 comprised a combination of fifteen regular waves, four drift angles, one water depth and five different ship's forward speeds. Tests were performed in head and following waves with the use of two different set of beam frames, beam frame A (model semi captive), and beam frame B (model fully captive). Two types of tests have been performed, stationary tests and harmonic yaw tests, both in calm water and in waves. The main wave parameters have been selected to represent typical waves encountered by ships at the Belgian coastal zone of the North Sea. For a more detailed explanation of the experiments see Chapter 4.

It is important to mention the decomposition of the forces and moments (first order and second order) as well as the ship motion responses (mean and oscillatory responses) follow the same

analysis as described in Chapter 4, in subsections 4.5.1 and 4.5.2. An extensive discussion of these methodologies can also be found in Mansuy et al. (2017), and Tello Ruiz et al. (2017).

## 5.2 Hull forces

### 5.2.1 First order forces

The first harmonics of the forces measured with beam frame B in head ($\eta = 180$ deg) and following waves ($\eta = 0$ deg), for three different drift angles and four forward speeds are shown in Figure 5.1 to Figure 5.4. In addition, numerical results computed with Hydrostar (a 3D potential code), are plotted also for comparison. Notice that Hydrostar results do not account for drift angles.

From Figure 5.1 to Figure 5.4 it can be observed that in general the results coincide with each other showing that the influence of drift angles on the first order quantities is small. This holds true for both head and following waves. Although there is a slightly larger difference for drift angles with respect to surge forces in following waves (see Figure 5.1 and Figure 5.2) but it remains small. This difference becomes insignificantly at higher speeds.

Comparison of the numerical results (obtained from Hydrostar) against the experimental ones shows that Hydrostar results compare better for head waves than for following waves. Although the discrepancies in following waves are larger, it can be stated that generally the agreement is quite satisfactory. Because of the limited variation of the result as a function of the drift angle and the fair agreement with experiments, the influence of drift angles can be considered as negligible.

From Figure 5.1 to Figure 5.4, in addition, it can be also observed that the difference between the experimental and numerical results, including the diffraction problem (FT) and when considering the Froude Krylov forces and moments (FK) only, are less important in following waves. A similar observation can be made as the forward speed increases.

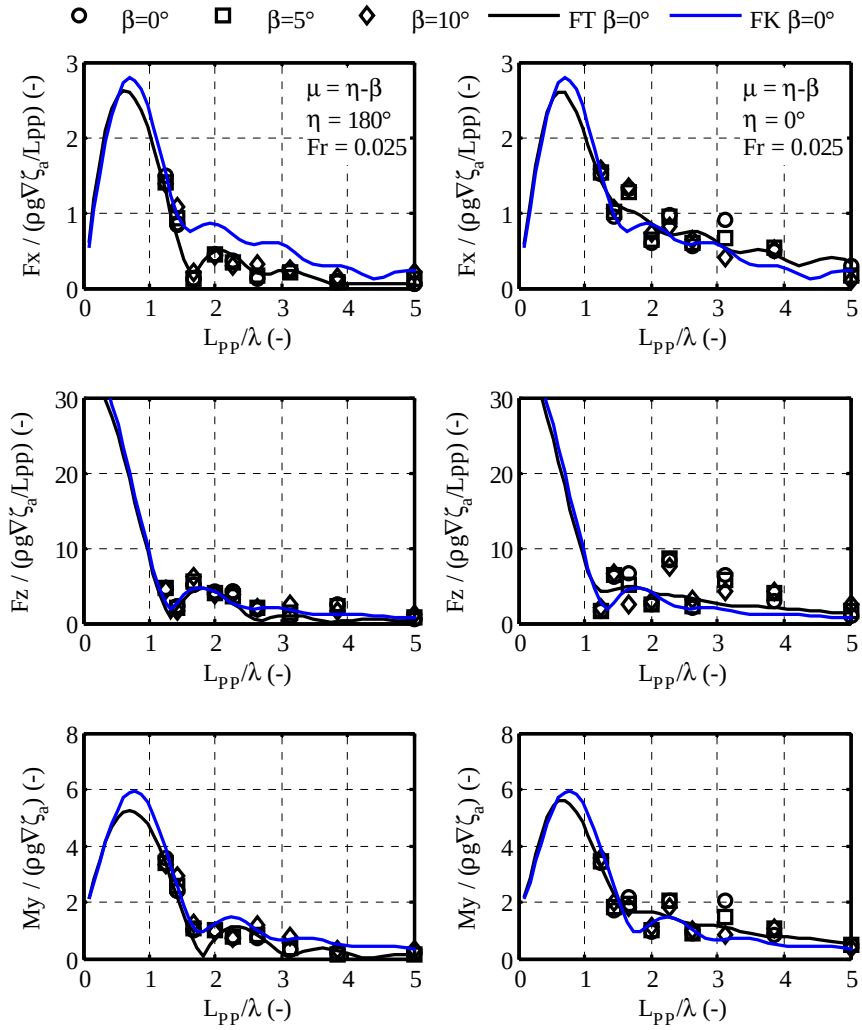


Figure 5.1 First order wave forces and moments for head (left) and following (right) waves at $F_r = 0.025$, $T_M = 13.1$m, 50% UKC, and $\zeta_a = 1$m. Tests results are shown in black markers for different hull drift angles. Numerical results ( $\beta = 0$ deg) are plotted in continuous lines, in black for FT (Froude-Krylov + diffraction) and in blue for FK (Froude-Krylov only).

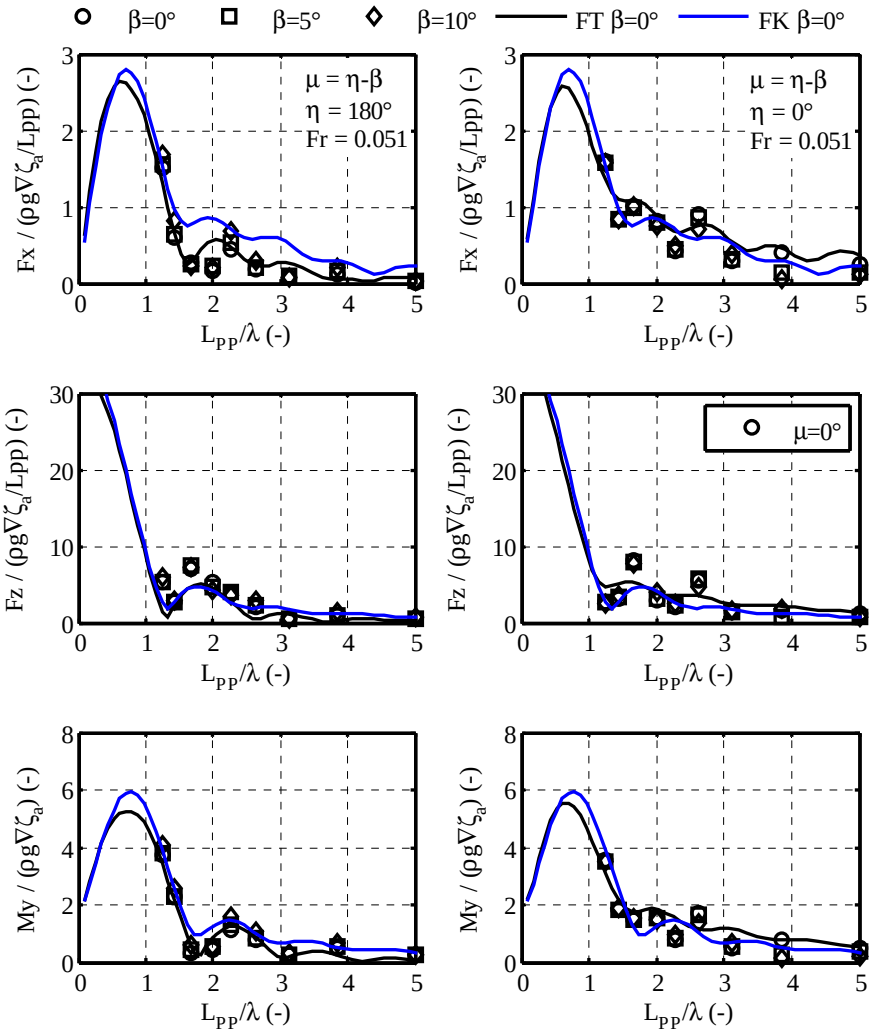


Figure 5.2 First order wave forces and moments for head (left) and following (right) waves at $F_r = 0.050$, $T_M = 13.1$m, 50% UKC, and $\zeta_a = 1$m. Tests results are shown in black markers for different hull drift angles. Numerical results ( $\beta = 0$ deg) are plotted in continuous lines, in black for FT (Froude-Krylov + diffraction) and in blue for FK (Froude-Krylov only).

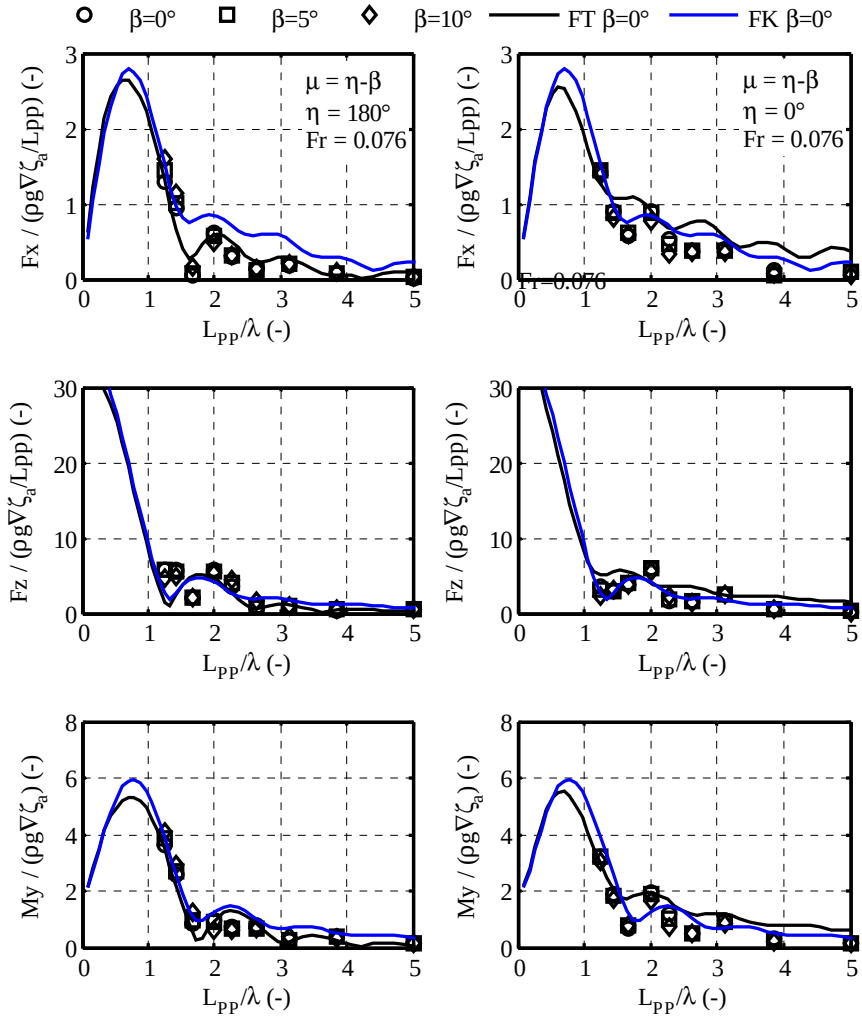


Figure 5.3 First order wave forces and moments for head (left) and following (right) waves at $F_r = 0.075$, $T_M = 13.1\text{m}$, 50% UKC, and $\zeta_a = 1\text{m}$. Tests results are shown in black markers for different hull drift angles. Numerical results ( $\beta = 0$ deg) are plotted in continuous lines, in black for FT (Froude-Krylov + diffraction) and in blue for FK (Froude-Krylov only).

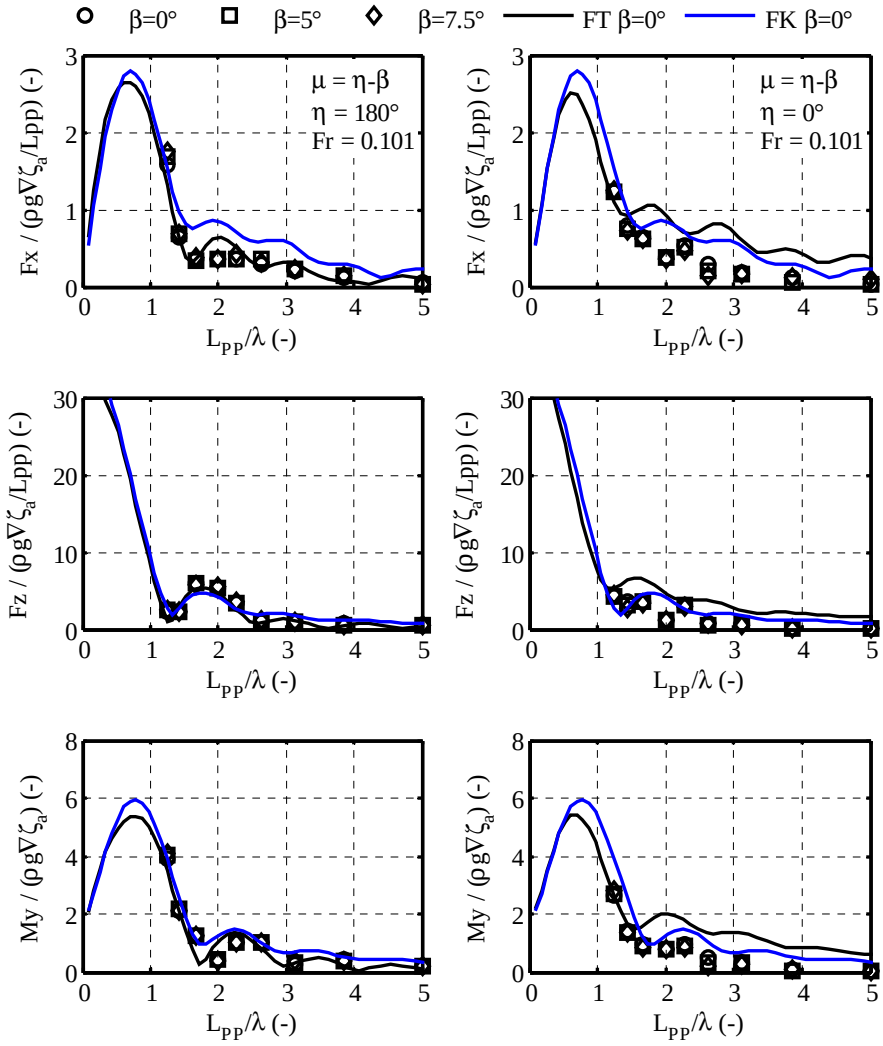


Figure 5.4 First order wave forces and moments for head (left) and following (right) wave at $F_r = 0.101$, $T_M = 13.1\text{m}$, 50% UKC, and $\zeta_a = 1\text{m}$. Tests results are shown in black markers for different hull drift angles. Numerical results ( $\beta = 0$ deg) are plotted in continuous lines, in black for FT (Froude-Krylov + diffraction) and in blue for FK (Froude-Krylov only).

### 5.2.2 Second order forces

The second order forces have been obtained by computing the mean forces in waves and subtracting it from the mean forces obtained from calm water results. The present discussion has been subdivided in two sections, dedicated to the added wave resistance in head and following waves, and to the wave mean drift forces in bow quartering waves, respectively.

#### *5.2.2.1Added wave resistance*

Results for the added wave resistance are presented in Figure 5.5 and Figure 5.6 for head and following waves, respectively. Two different wave amplitudes were used for the case of the head wave tests. In both figures, in addition, the numerical evaluations of the added wave resistance carried out with Hydrostar are also plotted.

Figure 5.5 shows fluctuations in the results which cannot be addressed to any physical meaning. These are more pronounced for the fully captive tests, at smaller wave amplitudes (RW1 in withe square markers) in contrast to the semi captive tests (RW1 in light blue square markers). These oscillations can only be addressed due to the smaller magnitudes of the added resistance (of decimal orders), as well as due to the sensitivity and noise in the frames, see Chapter 4. This can be confirmed because at larger wave amplitude (RW2) results show a more stable behaviour.

From Figure 5.5 it can be observed that results at two different amplitudes (squares and diamond markers in top and bottom left plots in Figure 5.5) coincide. This agreement between the two sets of tests (different wave amplitudes) can only mean that the differences between the mean forces in calm water and in waves are proportional to the wave amplitude square. Hence, it can be assumed that the waves considered in the present study do not alter significantly the ship's resistance as obtained from calm water.

Similarities in the results obtained for the model semi captive and fully captive for ship lengths to wave length ratios $L_{PP}/\lambda > 2$ are

also observed in Figure 5.5. This shows that the influence of ship motions can be assumed to be negligible for this wave length range. For the same range of wave lengths, the added resistance as a function of the forward speed appears to be less significant.

When experimental results are compared against the numerical ones, good agreement is found for the short wave length region. Differences found in the long wave length range ($L_{PP}/\lambda < 2$) could be addressed to the inaccuracy of the ship's motion responses estimated with Hydrostar, recall that motions responses are of great relevance when estimating the added wave resistance. This, however, will require further confirmation when the ship motions are investigated in a later subsection in this chapter.

In the case of following waves (Figure 5.6), generally the variation of the ship resistance is very small in contrast to the ones observed in head waves. The numerical estimations show this tendency also. At higher speeds ($F_r = 0.075,$ and $0.100$) and shorter wave length ($L_{PP}/\lambda > 3$), however, significant values are obtained. This particular response requires yet further attention as it seems consistent and cannot be explained at this point.

#### *5.2.2.2Mean wave drift forces*

To investigate the mean forces, taking into account the limitations of the experimental facilities at FHR (see Chapter 4), the investigation required to evaluate the harmonic yaw tests (PMM yaw test). The results plotted in Figure 5.7 and Figure 5.8 have been obtained by restricting the PMM yaw tests to the section where the maximum yaw angle has been attained. The yaw angle variations in these tests are chosen to be less than 2 deg, see Chapter 4 for more detail.

The results for the forces and moments components, surge, sway, heave, roll , pitch and yaw, represented respectively by $X_D$, $Y_D$, $Z_D$, $K_D$, $M_D$, $N_D$, are presented in Figure 5.7 and Figure 5.8. These results have been obtained from fully captive tests (beam frame B) performed with the same PMM yaw characteristics at the lower forward speed $F_r = 0.025,$ but with a different drift angle.

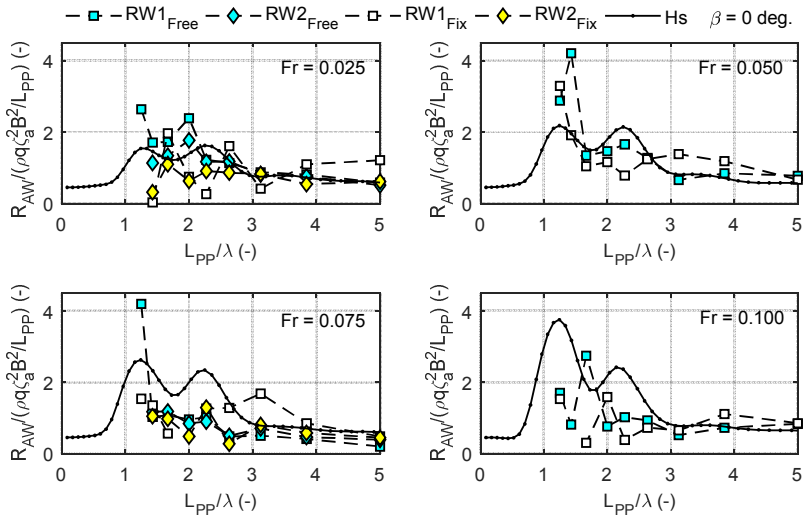


Figure 5.5 Added resistance in head waves at non-zero speed, $\beta = 0$ deg, $T_M = 13.1$m, 50% UKC, $\zeta_a = 1$m (RW1) and $\zeta_a = 1.35$m (RW2). Test results are shown in square (RW1) and in diamond (RW2) markers for the ship model semi captive (subscript "Free") and fully captive (subscript "Fix"). Numerical results are shown in continues dotted black lines.

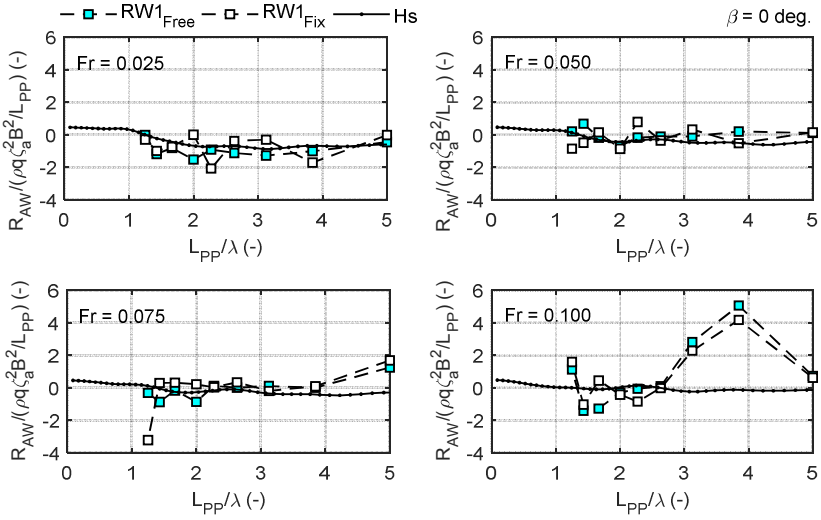


Figure 5.6 Added resistance in following waves at non-zero speed, $\beta = 0$ deg, $T_M = 13.1$m, 50% UKC, and $\zeta_a = 1$m (RW1). Test results are shown in square (RW1) markers for the ship model semi captive (subscript "Free") and fully captive (subscript "Fix"). Numerical results are shown in continues dotted black lines.

Figure 5.7 and Figure 5.8 present the results obtained at zero and non-zero drift angle respectively. Notice that the force in surge $X_D$ is also known as the added wave resistance $R_{AW}$ (discussed in 5.2.2.1). In addition, numerical results evaluated with Hydrostar have been plotted in Figure 5.7 and Figure 5.8 also.

From Figure 5.7 and Figure 5.8, once again fluctuations in the results obtained from the smaller wave amplitude (RW1) are observed, especially for the pitch and yaw moments and the surge forces. This is however not found in the case of the sway and heave forces, confirming the fluctuations observed are mainly due to the smaller magnitudes of the measured forces and moments.

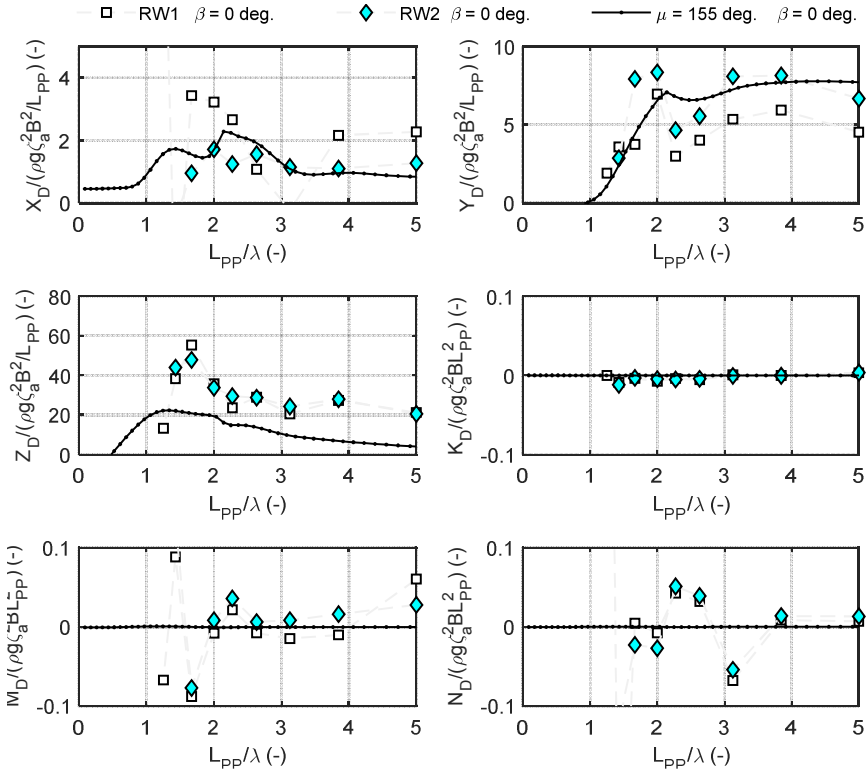


Figure 5.7 Mean wave drift forces obtained from fully captive tests at $F_r = 0.025$, $T_M = 13.1$m, 50% UKC, $\beta = 0$ deg, $\zeta_a = 1$m (RW1) and $\zeta_a = 1.35$m (RW2). Test results are shown in square (RW1) and in diamond (RW2) markers. Numerical results (at $\beta = 0$ deg) are shown in continues dotted black lines.

With respect to surge and sway forces, the influence of drift angles seems negligible for all tested wave length range. This is because the numerical results increase slightly when considering drift angles, which seems to be a function only of the increase in incoming wave angle $\mu$ , moreover, the numerical results obtained at $\beta = 0$ but at equivalent $\mu$, appear to predict fairly well.

The comparison against numerical computations shows that in general, Hydrostar agrees well with the experimental results, but underestimates the mean forces in heave and sway for the long wave range $L_{PP}/\lambda < 2$.

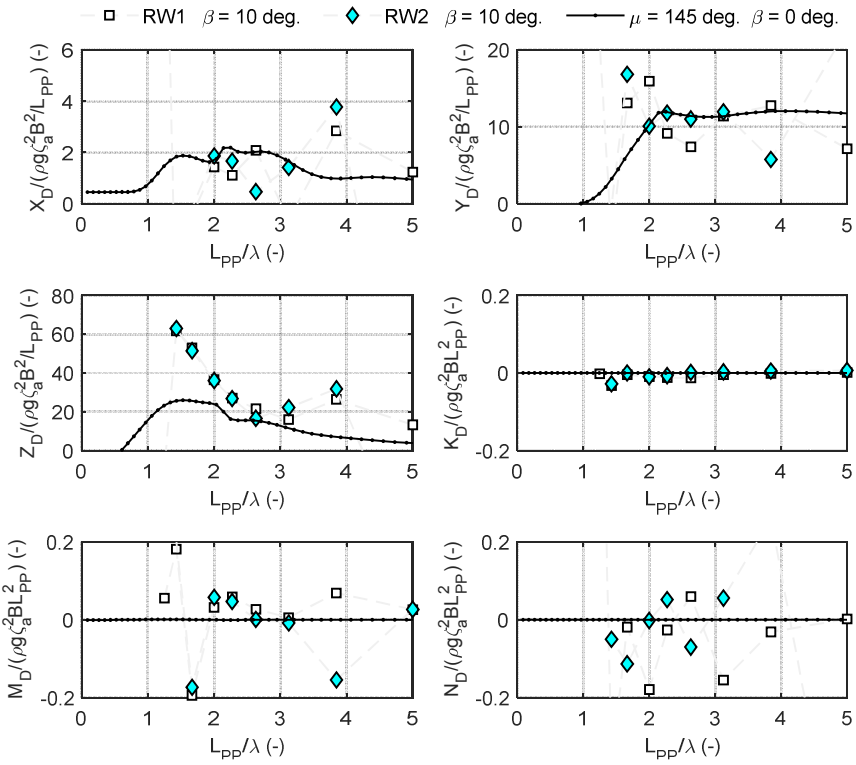


Figure 5.8 Mean wave drift forces obtained from fully captive tests at $F_r = 0.025$, $T_M = 13.1$m, 50% UKC, $\beta = 10$ deg, $\zeta_a = 1$m (RW1) and $\zeta_a = 1.35$m (RW2). Test results are shown in square (RW1) and in diamond (RW2) markers. Numerical results (at $\beta = 0$ deg) are shown in continues dotted black lines.

With respect to the mean drift moments, in roll, pitch and yaw, from Figure 5.7 and Figure 5.8 insignificant magnitudes are observed, suggesting that wave effects are rather small.

Form the results plotted in both figures, Figure 5.7 and Figure 5.8, one can state the proportionality to the wave amplitude squared holds for all the forces. This means that as previously discussed, the influence of waves on the resistance as measured from calm water, even at this low speed, can be neglected.

These observations agree with the numerical study of the added resistance conducted by Guo et al. (2012), where for wave amplitudes, corresponding to open seas, the variation of the viscous contribution was found negligible. Recall as well, that such wave amplitudes as tested in Guo et al. (2012) are larger in contrast to the ones used in the present study, and do not correspond to scenarios where the ship would commonly manoeuvre.

### 5.2.3 Mean forces in calm water and in waves

The forces discussed in the present study have been obtained from straight run tests carried out with the model fully captive (beam frame B) and semi captive (beam frame A). Tests were conducted with and without drift angles and for five different forward speeds, see Chapter 4 for better insight.

Forces and moments in the present subsection are plotted as a function of the square of the ship speed $V$ (at model scale). They are given in the $y$ −axis in a non-dimensionalised form as:

$$X^{(\beta)\prime} = \frac{X}{\frac{1}{2}\,\rho \mathrm{L}_{PP}\,\mathrm{T}_{\mathrm{M}}\mathrm{V}^2}, \quad Y^{(\beta)\prime} = \frac{Y}{\frac{1}{2}\,\rho \mathrm{L}_{PP}\,\mathrm{T}_{\mathrm{M}}\mathrm{V}^2}, \tag{5.1}$$

$$K^{(\beta)\prime} = \frac{K}{\frac{1}{2}\,\rho \mathrm{L}_{PP}^2\,\mathrm{T}_{\mathrm{M}}\mathrm{V}^2}, \quad N^{(\beta)\prime} = \frac{N}{\frac{1}{2}\,\rho \mathrm{L}_{PP}^2\,\mathrm{T}_{\mathrm{M}}\mathrm{V}^2} \tag{5.2}$$

where $\rho$ is the water density, and $L_{PP}$ and $T_M$ are the ship's length and draught, respectively.

The above non-dimensionalisation is chosen based on the calm water studies observations as the one discussed in Vantorre and Eloot (1996). Forces are expressed proportional to $V^2$ in a tabular form as function of the drift angle $\beta$. Applying the same representation for the present study will provide a better insight in the influence of waves in the calm water forces, meanwhile the evolution of the calm water forces as function of speed and drift angles is also investigated.

For better illustration and discussion purposes, test results have been split in two sub-sections, mean forces with the model fully captive and mean forces with the model semi-captive. This will allow comparison of the results obtained from the two different test setups, as well as to investigate the relative accuracy of the measurements as surge, sway and yaw forces have been recorded in both test types and can be compared directly. For heave and pitch forces and motions, their study requires an additional evaluation such as the Tuck parameter, which will be conducted in a later subsection.

To make the large number of results distinctive for the reader, the following conventions have been applied when displaying the results: tests in regular waves with smaller amplitude (RW1, in square markers) and tests with larger amplitudes (RW2, in diamond markers) are shown independently of their drift angles, but are plotted along their corresponding calm water results. The latter are in turn shown with circle markers in blue, red, yellow, and black referring to $\beta = 0$ , 5, 7.5 and 10 deg, respectively.

#### *5.2.3.1Mean forces with the model fully captive*

Test results for four different speeds, and four different drift angles are shown from Figure 5.9 to Figure 5.12. Surge forces are displayed in Figure 5.9 and Figure 5.10 for head and following waves, respectively. Results are arranged in four different subplots corresponding to their respective drift angle. Similarly, sway, roll and yaw forces and moments are plotted in Figure 5.11 and Figure 5.12 for head and following waves, respectively.

From the results plotted in Figure 5.9 it can be seen that the mean forces (expressed as function of the square of the ship speed $V^2$) remain approximately constant. This is especially the case at larger speeds, at lower speeds however a slight drop in the magnitude of the mean forces is observed.

Wave effects as seen in Figure 5.9 (RW1 and RW2), for all drift and speeds condition, seem insignificant at larger speeds, even when the larger wave amplitudes is used. At lower speeds, however, the influence seems larger and waves appear to dominate the mean forces. Recall, however, that from the previous discussion of wave added resistance (see, 5.2.2.1); wave forces at the lower speed were found to be proportional to the wave amplitude squared. Hence, the difference observed in Figure 5.9 can be addressed to wave effects only and not to a change in other fluid phenomena.

In following waves, see Figure 5.10, similar results as the ones observed in head waves are found. Calm water results are approximately constant at larger speeds and a lower magnitude is found at very low speeds. Although slightly more variations in the mean forces are obtained in waves in contrast to the calm water results, the differences still remain small except at very low speed.

With respect to the mean sway forces, roll and yaw moments in head and following waves (see Figure 5.11 and Figure 5.12), expressing them as a function of the square of the ship speed $V^2$ suggest that they can be assumed constant for larger speeds. At lower speeds, however, their results differ slightly.

Similar to the case of surge forces, in head and following waves for sway forces, roll and yaw moments (see Figure 5.11 and Figure 5.12) the influence of waves in the mean forces seems negligible at larger speeds but important at very low speeds. This, however, as previously discussed, cannot be addressed to a change in the fluid phenomena as observed in calm water because the difference obtained at low speeds remain proportional to the square of the wave amplitude (see, 5.2.2.2).

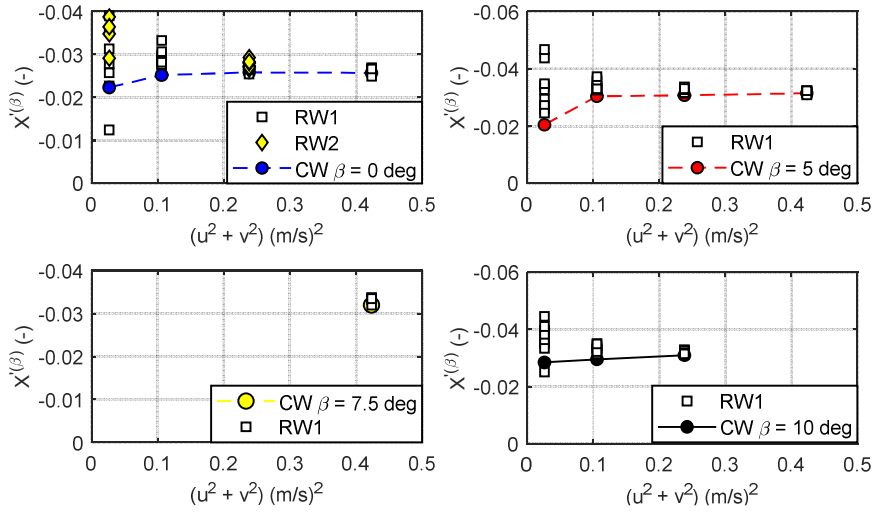


Figure 5.9 Mean surge forces in calm water (CW, in circles) and in head waves at $T_M$ = 13.1m, 50% UKC, $\zeta_a$ = 1m (RW1, in squares) and $\zeta_a$ = 1.35m (RW2, in diamonds) and at different drift angles, model fully captive. Tests results with regular waves are plotted as function of $V^2$ only (the wave length dependency has been disregarded).

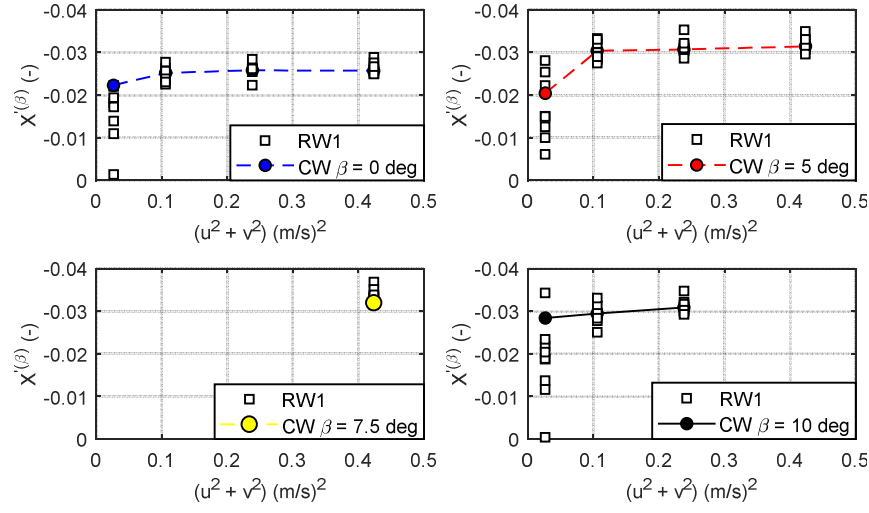


Figure 5.10 Mean surge forces in calm water (CW, in circles) and in following waves, at $T_M$ = 13.1m, 50% UKC, $\zeta_a$ = 1m (RW1, in squares) and at different drift angles, model fully captive. Tests results with regular waves are plotted as function of $V^2$ only (the wave length dependency has been disregarded).

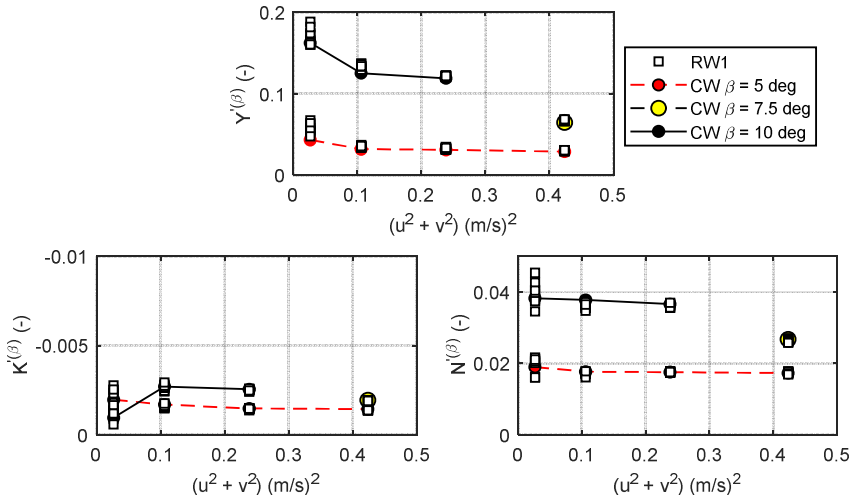


Figure 5.11 Mean sway force (top), roll moment (bottom left) and yaw moment (bottom right) in calm water (CW, in circles) and in head waves at $T_M = 13.1$m, 50% UKC, $\zeta_a = 1$m (RW1, in squares) and at different drift angles, model fully captive. Tests results with regular waves are plotted as function of $V^2$ only (the wave length dependency has been disregarded).

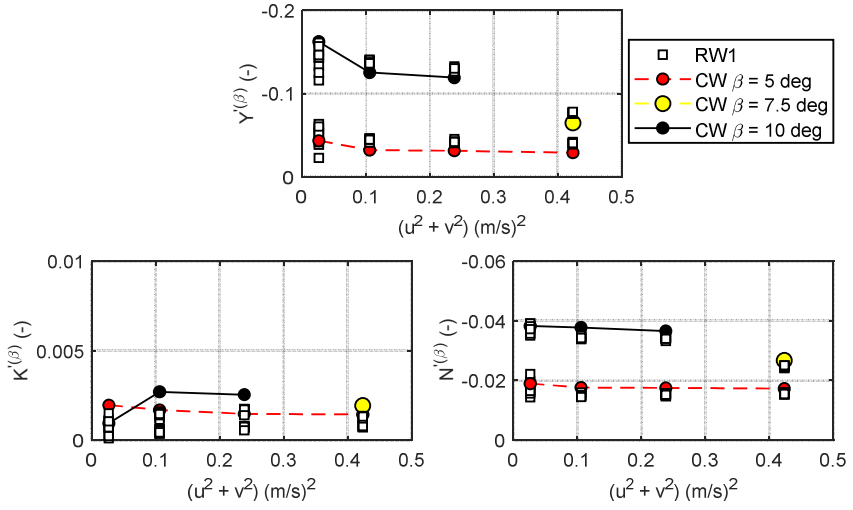


Figure 5.12 Mean sway force (top), roll moment (bottom left) and yaw moment (bottom right) in calm water (CW, in circles) and in following waves, at $T_M = 13.1$ m, 50% UKC, $\zeta_a = 1$ m (RW1, in squares) and at different drift angles, model fully captive. Tests results with regular waves are plotted as function of $V^2$ only (the wave length dependency has been disregarded).

#### *5.2.3.2Mean forces with the semi-captive model*

In the present subsection, surge and sway forces, and yaw moments are discussed only. Recall that for the study with the semi-captive model tests, heave, roll and pitch are set to move freely. Model tests with this new setup have been performed with the similar ship model, drift angles, wave incoming angles, and ship speeds combinations as carried out with the fully captive tests. However, in the present study, an additional larger forward speed was used.

Surge forces in head and following waves are displayed in Figure 5.13 and Figure 5.14, respectively. Results are arranged in four different subplots corresponding to their respective drift angle. Similarly, sway forces and yaw moments are plotted in Figure 5.15 and Figure 5.16 for head and following waves, respectively. Result for $\beta = 5$ deg, $\beta = 7.5$ deg, and $\beta = 10$ deg, are displayed together in the same subplot.

In general, results plotted in Figure 5.13 to Figure 5.16 confirm that mean surge and sway forces, and yaw moments do not vary significantly compared to the calm water results, when waves are present. At very low speed, however, the difference seems considerable. Similar trends have been found with the fully captive model tests.

Comparing the results in surge from both test setups, semi-captive and fully captive model tests, slightly larger forces are obtained for the entire range of speeds (see Figure 5.13 and Figure 5.16). These discrepancies are also observed for sway force and yaw moment, but less significant. These differences are more pronounced at lower speeds. Although the discrepancies found are in general small and can be associated to bias errors in both frames, one cannot neglect the contribution of squat effects (sinking and trimming the ship, thus changing the wetted surface and the forces associated to it), which may be of importance to explain these differences.

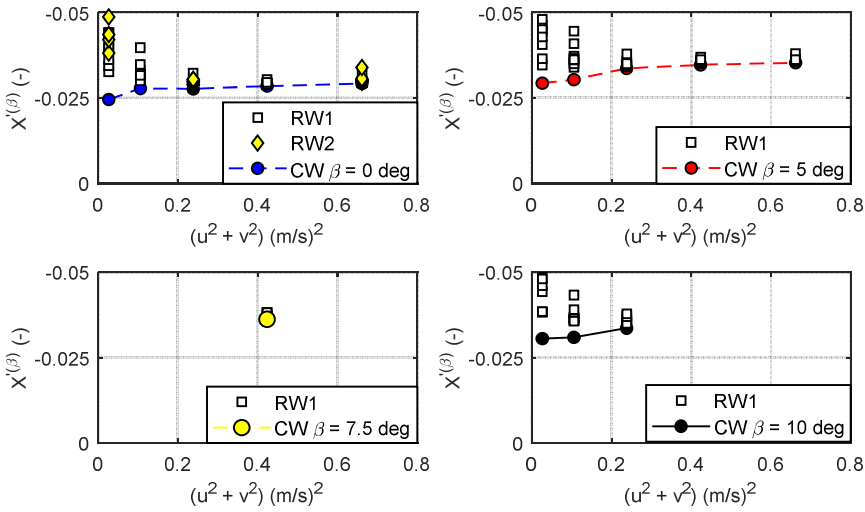


Figure 5.13 Mean surge forces in calm water (CW, in circles) and in head waves at $T_M = 13.1$m, 50% UKC, $\zeta_a = 1$m (RW1, in squares) and $\zeta_a = 1.35$m (RW2, in diamonds) and at different drift angles, model semi captive. Tests results with regular waves are plotted as function of $V^2$ only (the wave length dependency has been disregarded).

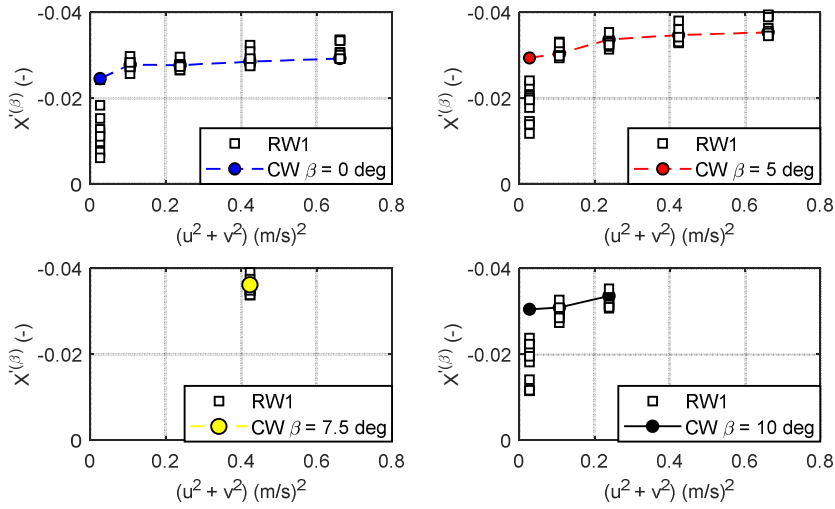


Figure 5.14 Mean surge forces in calm water (CW, in circles) and in following waves, at $T_M = 13.1$m, 50% UKC, $\zeta_a = 1$m (RW1, in squares) and at different drift angles, model semi captive. Tests results with regular waves are plotted as function of $V^2$ only (the wave length dependency has been disregarded).

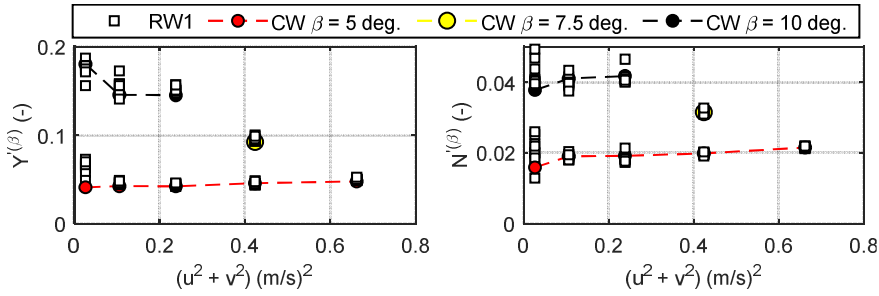


Figure 5.15 Mean sway force (left), and yaw moment (right) in calm water (CW, in circles) and in head waves, at $T_M = 13.1$m, 50% UKC, $\zeta_a = 1$m (RW1, in squares) and at different drift angles, model semi captive. Tests results with regular waves are plotted as function of $V^2$ only (the wave length dependency has been disregarded).

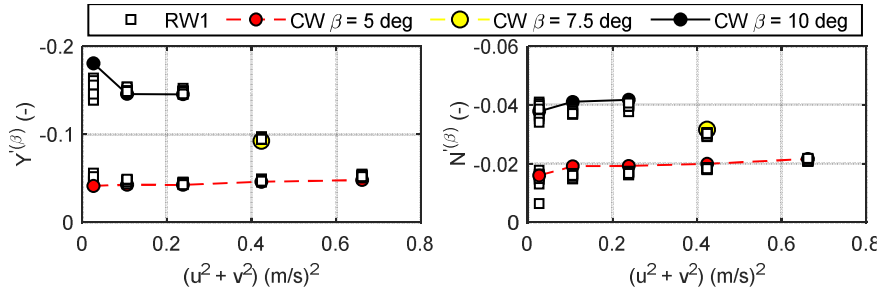


Figure 5.16 Mean sway force (left), and yaw moment (right) in calm water (CW, in circles) and in following waves, at $T_M = 13.1$m, 50% UKC, $\zeta_a = 1$m (RW1, in squares) and at different drift angles, model semi captive. Tests results with regular waves are plotted as function of $V^2$ only (the wave length dependency has been disregarded).

### 5.2.4 Squat phenomena in calm water and in waves

The effect of waves on the mean heave and pitch forces, moments, and motions are studied by using (derived by Tuck, 1966) the sinkage $z_{LCF}$ and trim $\theta_{LCF}$ expressions, given at the longitudinal centre of flotation (LCF), as:

$$z_{LCF} = c_s \frac{\nabla}{L_{PP}^2} T u_h \tag{5.3}$$

$$\theta_{LCF} = c_\theta \frac{\nabla}{L_{PP}^3} T u_h \tag{5.4}$$

where ∇ is the ship displacement and $L_{\mathrm{PP}}$ is the ship length between perpendiculars, $c_s$ and $c_\theta$ are constant coefficients, and the Tuck's parameter $Tu_h$ is given by:

$$Tu_h = \frac{F_{rh}^2}{\sqrt{1 - F_{rh}^2}} \tag{5.5}$$

where $F_{rh} = V/\sqrt{gh}$ is the depth-based Froude number, $g$ the acceleration of gravity, and $h$ the water depth.

Equations (5.3) and (5.4) are simplified formulations obtained by hydrostatic equilibrium of the heave force and pitch moment their sinkage and trim, respectively (see Tuck, 1966). Hence, they can be related back to forces and moments. Bear in mind that Eq. (5.3) and (5.4) are defined at the LCF and recall that forces and moments have been defined amidships. Hence, Eq. (5.3) and (5.4) will need to be expressed amidships, first. This, however, can be neglected because the positions of LCF ($x_{LCF}$) is smaller than the ship length ($x_{LCF} \ll L_{PP}$), hence, $Z_{Tu_h}^{(\beta)}$ and $M_{Tu_h}^{(\beta)}$ amidships can be found by:

$$Z_{Tu_h}^{(\beta)} = C_{33} Z_{Tu_h}^{\prime(\beta)} \frac{\nabla}{L_{PP}^2} Tu_h \tag{5.6}$$

$$M_{Tu_h}^{(\beta)} = C_{55} M_{Tu_h}^{\prime(\beta)} \frac{\nabla}{L_{PP}^3} Tu_h \tag{5.7}$$

Where $C_{33}$ and $C_{55}$ are the restoring coefficients in heave and pitch, respectively (see Table 5.1), and $c_s$ has been replaced by $Z_{Tu_h}^{\prime(\beta)}$ and $c_\theta$ by $M_{Tu_h}^{\prime(\beta)}$. Test results are shown dimensionless accordingly to Eq. (5.6) and (5.7) for the forces and moments, and to Eq. (5.3) and (5.4) for the sinkage and trim.

$$Z^{\prime(\beta)} = \frac{Z}{C_{33} \dfrac{\nabla}{\mathrm{L}_{PP}^2}\, \mathrm{T_{uh}}}, \quad M^{\prime(\beta)} = \frac{M}{C_{55} \dfrac{\nabla}{\mathrm{L}_{PP}^3}\, \mathrm{T_{uh}}}, \qquad \textit{Fully captive} \tag{5.8}$$

$$Z^{\prime(\beta)} = z_{LCF} \frac{\mathrm{L}_{PP}^2}{\nabla T u_h}, \quad M^{\prime(\beta)} = \theta_{LCF} \frac{\mathrm{L}_{PP}^3}{\nabla T u_h}, \qquad \textit{Semi Captive} \tag{5.9}$$

Table 5.1 Ship's heave and pitch restoring coefficients at full scale.

| Item | Value | Units |
|---|---|---|
| $C_{33}$ | $0.155x10^{9}$ | $Nm^{-1}$ |
| $C_{55}$ | $0.125x10^{13}$ | $Nm$ |

These expressions in Eq. (5.8) and (5.9) will allow comparison of the results obtained from the two different test set ups. Similar to the previous subsection, for better illustration purposes, results are subdivided in two subsections, squat effects in waves and calm water with the model fully captive, and squat effects in waves and calm water with the model semi-captive.

#### *5.2.4.1Squat effects in calm water and in waves: fully captive model*

Results obtained are displayed in Figure 5.17 and Figure 5.18. The arrangement of the figures is as follows, top figures display results for $\beta = 0$ and $5$ deg while the bottom figures display results for $\beta = 7.5$ and $10$ degrees, left and right figures shown the results for heave and pitch coefficients, respectively.

From the calm water results obtained in Figure 5.17, one can observe that the sinkage $Z'^{(\beta)}_{Tu_h}$ and trim $M'^{(\beta)}_{Tu_h}$ coefficients take approximately constant magnitudes as a function of the Tuck parameter. Only at low speeds a considerable drop in the magnitude of $M'^{(\beta)}_{Tu_h}$is found. Variations in the coefficients are also observed as a function of the drift angle, confirming their drift dependency as discussed above. With respect to wave effects, similar to the study of the mean forces and moments in surge, sway, roll and yaw, $Z'^{(\beta)}_{Tu_h}$ and $M'^{(\beta)}_{Tu_h}$ remain approximately the same as the calm water results, this is especially the case at larger speeds. This is also observed even when results obtained at larger wave amplitudes are considered. At very low speeds, however, wave effects seem important as significant variations of the coefficients can be seen.

In following waves, see Figure 5.18, although the variations in the $M'^{(\beta)}_{Tu_h}$ coefficient are slightly larger than in the case of head waves, wave effects appear to be only considerable at very low speeds.

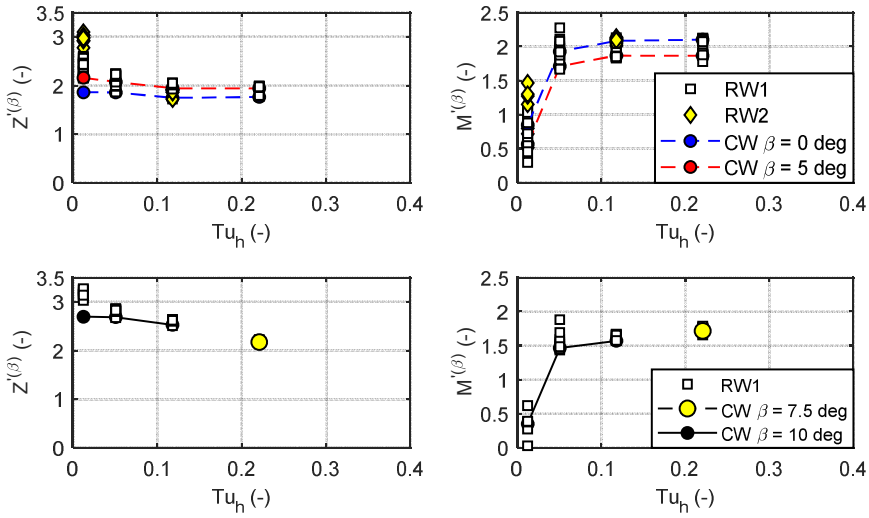


Figure 5.17 Heave (left) and pitch (right) moment coefficients in calm water (CW, in circles) and in head waves at $T_M = 13.1$m, 50% UKC, $\zeta_a = 1$m (RW1, in squares), $\zeta_a = 1.35$m (RW2, in diamonds), and at different drift angle, model fully captive. Tests results with regular waves are plotted as function of $V^2$ only (the wave length dependency has been disregarded).

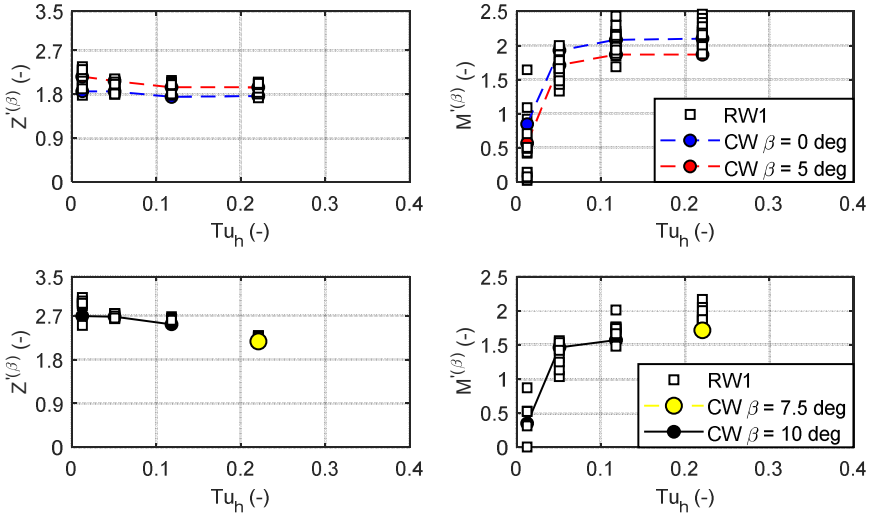


Figure 5.18 Heave (left) and pitch (right) moment coefficients in calm water (CW, in circles) and in following waves at $T_M = 13.1$m, 50% UKC, $\zeta_a = 1$ m (RW1, in squares), and at different drift angles, model fully captive. Tests results with regular waves are plotted as function of $V^2$ only (the wave length dependency has been disregarded).

The attention can be drawn to the very low speed range, but as observed in the mean wave forces analysis, also discussed in 5.2.3, the difference between the mean values obtained in calm water and in waves remains proportional to the wave amplitude squared which indicated no significant influence of waves on the forces and moments as obtained in calm water.

#### *5.2.4.2Squat effects in calm water and in waves: model semi captive*

Figure 5.19 and Figure 5.20 display the results obtained for head and following waves, respectively. Figures are arranged similar to the analysis conducted previously in 5.2.4.1.

Similarly to the case observed in the fully captive tests, the results presented in the figures below show also that wave effects at large speeds are less significant than at lower speeds for both the sinkage $Z'^{(\beta)}_{Tu_h}$ and trim $M'^{(\beta)}_{Tu_h}$ coefficients. These significant variations observed, especially for the sinkage coefficient, can be understood as the magnitude of the wave drift forces being of the same order of magnitude as calm water forces, hence, the larger fluctuations in the dimensionless values. It is important to recall that such variation in magnitudes can also be a contribution of interaction with the tank side walls. These fluctuations, as discussed in Tello Ruiz et al. (2017), can introduce a change in sinkage of around 8% with respect to the open water case.

Comparing the present results to the respective ones obtained with the fully captive tests, see Figure 5.17 and Figure 5.18, respectively, some main differences are observed. For instance, the calm water results obtained with semi captive tests (Figure 5.19 and Figure 5.20) show that sinkage coefficients slightly increase as function of the Tuck's parameter, and converge to the magnitudes obtained with fully captive tests as the speed increases. The trim coefficients however, remain approximately constant. These trends do not agree with theoretical observations, which according to Tuck (1966) and Gourlay (2008) $Z'^{(\beta)}_{Tu_h}$ and $M'^{(\beta)}_{Tu_h}$ should remain constant in open waters.

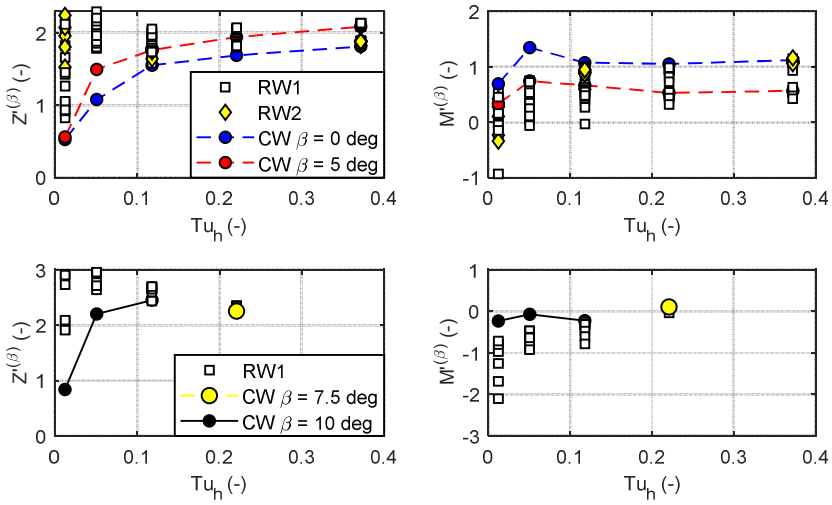


Figure 5.19 Heave (left) and pitch (right) coefficients in calm water (CW, in circles) and in head waves at $T_M = 13.1\,\mathrm{m}$, 50% UKC, $\zeta_a = 1\,\mathrm{m}$ (RW1, in squares), $\zeta_a = 1.35\,\mathrm{m}$ (RW2, in diamonds), and at different drift angle, model semi captive. Tests results with regular waves are plotted as function of $V^2$ only (the wave length dependency has been disregarded).

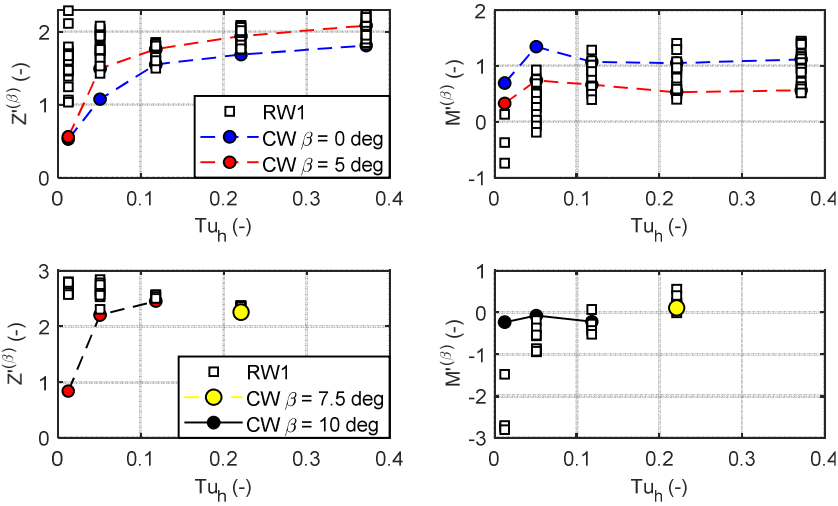


Figure 5.20 Heave (left) and pitch (right) moment coefficients in calm water (CW, in circles) and in following waves at $T_M = 13.1\,\mathrm{m}$, 50% UKC, $\zeta_a = 1\,\mathrm{m}$ (RW1, in squares), and at different drift angles, model semi captive. Tests results with regular waves are plotted as function of $V^2$ only (the wave length dependency has been disregarded).

The differences observed between the calm water results with the semi captive and fully captive tests can be partly addressed to the clearance between the hull and the tank's bottom and a sort of iterative process with the flow below the hull. At low speeds the magnitudes of the squat forces are small, hence they can be influenced by any small fluctuations in the flow produced by other effects, such as the tank's side walls, not accounted for.

### 5.2.5 Yaw motion and superposition study

The investigation of the drift angle and the ship forward speed dependence has been extensively discussed in the previous subsections. Yaw motion, however, have not been addressed yet. The separate investigation of yaw and the wave influence on the corresponding forces and moments is more complex to carry out experimentally, mainly due to the limitations with respect to width of the towing tank.

Despite these limitations, investigation of yaw motion effects and its variation when waves are present have been studied in an indirect approach. The comparison is made with the total forces as measured in both scenarios, in waves and in calm water. To allow further comparison, numerical results for the wave induced forces $\boldsymbol{F_W}$ have been superposed to the calm water hull forces $\boldsymbol{F_H}$, resulting in:

$$\boldsymbol{F = F_H + F_W} \tag{5.10}$$

Wave induced forces are decomposed in their three main components:

$$\boldsymbol{F_W = F_D + F_{FK} + F_{2nd}} \tag{5.11}$$

where $\boldsymbol{F_D}$, $\boldsymbol{F_{FK}}$ and $\boldsymbol{F_{2nd}}$ refer to the diffraction force, the Froude–Krylov force, and the mean second order wave forces.

Different from the previous analyses where mean forces have been studied only, in here all three components are estimated (using Hydrostar) and included according to Eq. (5.10). Bear in mind that numerical results do not consider drift angles; wave angles of encounter, on the other hand, have been treated accordingly.

This methodology has been applied to results obtained from harmonic pure yaw tests (PMM yaw tests). They were performed both in calm water (CW) and in regular waves (RW). A large number of tests have been conducted but only a few were selected because of drawbacks in the experiments, such as tank side wall

interaction, waves reflected from the beach, memory effects, and non-regular wave patterns, as described in Chapter 4.

Figure 5.21 and Figure 5.22 present the time records, their respective spectral analysis, and the lateral positions as well as the yaw angle for two PMM tests conducted with the model semi-captive. Results for calm water (CW) and in regular waves (RW) are plotted together with the superposed results (CW+Hs, Hs being the numerical results obtained from the potential code Hydrostar), see Eq. (5.10). Bear in mind that amplitudes of the superposed results have been considered only. A convention has been adopted for the plots: CW, RW, and CW+Hs results are plotted in red, black and blue respectively.

In Figure 5.21 and Figure 5.22, in addition, time, heading and lateral motions are displayed dimensionless by the PMM period, amplitude, and the maximum lateral deviation in the towing tank, respectively. During tests, surge and sway motions were captive and propeller rates and rudder angles were set to $n = 0\%$ and $\delta = 0$ deg, respectively. Tests presented in here correspond to the tests discussed in Tello Ruiz et al. (2015).

From Figure 5.21 and Figure 5.22 some discrepancies between the amplitudes obtained for surge and sway forces, and yaw moments can be observed. Although these discrepancies remain present for almost the entire test, they are small. Hence, in general one can state that a fair agreement is found between the superposed values (CW+Hs) and the tests in regular waves.

From the spectral analysis presented in Figure 5.21 and Figure 5.22, one can observe that the low frequency range for sway forces and yaw moments display similar results in calm water and in regular waves (head and following). This explains why the CW results appear similar to a local average of the tests in regular waves. The influence of waves is found, however, to be important at higher frequencies only.

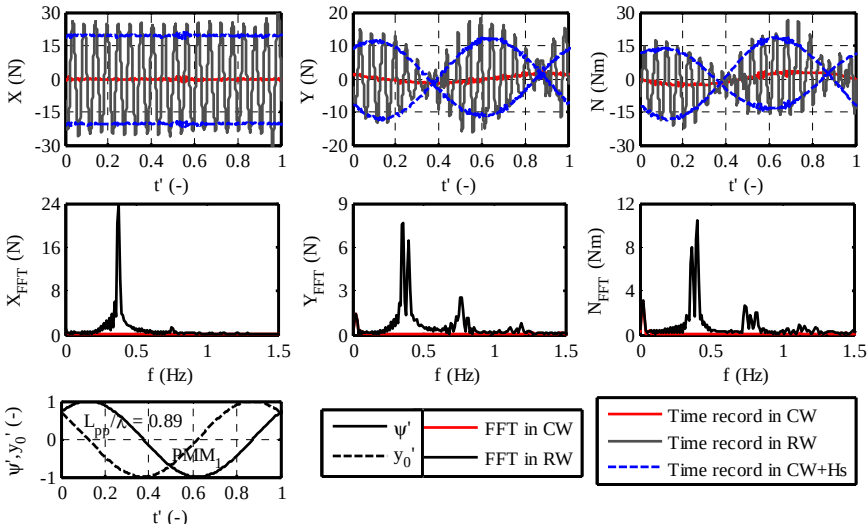


Figure 5.21 Harmonic yaw test in calm water (CW) and in head regular waves (RW), at $T_M = 14.5$ m and 50% UKC. $F_r = 0.025$, $\psi_A = 15$ deg, $\psi_T = 50$ s, $L_{PP}/\lambda = 0.89$ and $\zeta_a = 1.3$ m. Time records (above) and FFT (mid) of the longitudinal forces and yawing moment; lateral position and yaw angle during PMM (below).

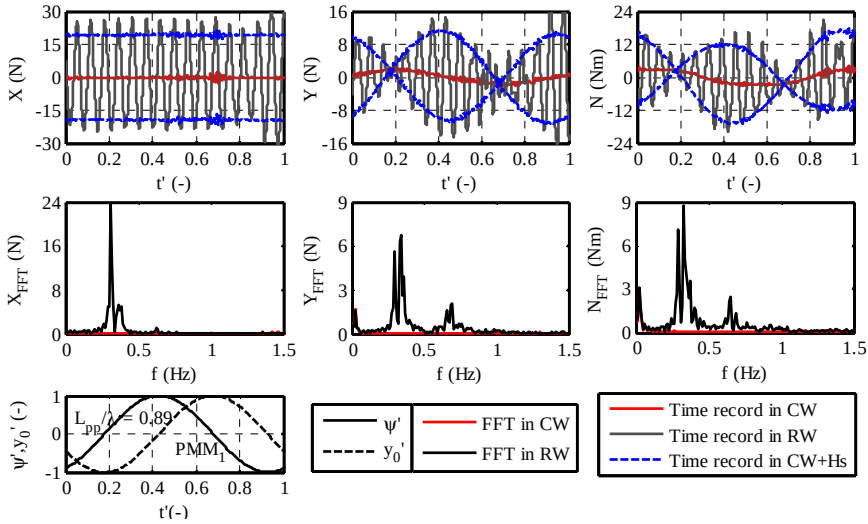


Figure 5.22 Harmonic yaw test in calm water (CW) and in following regular waves (RW), at $T_M = 14.5$ m and 50% UKC. $F_r = 0.025$, $\psi_A = 15$ deg, $\psi_T = 50$ s, $L_{PP}/\lambda = 0.89$ and $\zeta_a = 1.3$ m. Time records (above) and FFT (mid) of the longitudinal forces and yawing moment; lateral position and yaw angle during PMM (below).

The results discussed above, performed with a long wave ($L_{PP}/\lambda = 0.89$), in deep water ($100\%$ UKC) and with a low velocity, do not represent conditions usually seen in coastal zones but have been included to gain a better insight of wave effects on manoeuvring.

#### *5.2.5.1 Yaw motion and superposition study with model fully captive*

To get a better understanding of the actual situation occurring in the coastal zones, results obtained from tests conducted with the model fully captive are presented in Figure 5.23, Figure 5.24, Figure 5.25, and Figure 5.26. The first three show results for $\beta = 0$ deg, the last one displays results for $\beta = 7.5$ degrees. All body forces and moments have been measured and results are displayed for head regular waves only.

In Figure 5.23 to Figure 5.26, the same colour convention used in the figures above are used, thus, CW, RW, and CW+Hs records are shown in red, black and blue respectively. Different to previous figures, time records are compared by including the respective phase lags for each force and moment component, thus allowing a more direct comparison between the results. Time and incoming wave angles are displayed as measured during PMM yaw tests. It is important to mention that the $x-$axis is shown limited to the region of tests considered free from additional interferences such as reflected waves by the beach/harbour, see Chapter 4.

Bear in mind the complexity of the analysis when dealing with harmonic yaw tests, which involves several phenomena, e.g. interaction with the tank side walls, memory effects, and the overlapping noise and signal measurements in the gauges. Although these phenomena are all present and cannot be totally avoided, in these tests side wall effects are, for instance, expected to be substantially reduced, recall the model is fully captive.

In general, the superposed results (CW+Hs) and test results in regular waves (RW), displayed in Figure 5.23 to Figure 5.26, show fairly good agreement in trend and magnitudes for all forces and moments. This is also seen for the case when a drift angle is

included (see Figure 5.26). This agrees well with previous observations made with the model semi captive. In addition, one can also observe that the CW results follow the trend observed with RW results, similar to a local mean of forces and moments, confirming the rationality of the superposition approach.

From all forces and moments compared, only the roll moments present a phase lag between the RW and CW+Hs results. These discrepancies can be addressed to a difference in the vertical coordinate of the reference position measured in the experimental study, which do not correspond to the ones used in the numerical estimation conducted with Hydrostar. Despite these differences, from all figures it can be seen that roll moment magnitudes and trends of the time records agree fairly well with results from regular waves RW.

Results obtained at relative short wave length, $L_{PP}/\lambda = 2.27$ and $L_{PP}/\lambda = 2.0$, in Figure 5.23 and Figure 5.24, respectively, for roll and yaw tend to the CW magnitudes as the incoming wave angle tends to $\mu = 180$ degrees. These resemble head wave conditions studied in seakeeping where the oscillatory roll and yaw moments are zero. At the same ship model orientation, but now at relatively longer waves, $L_{PP}/\lambda = 1.67$ and $L_{PP}/\lambda = 1.43$, see Figure 5.25 and Figure 5.26, respectively, roll and yaw moments do not approach to the calm water results anymore. Instead, an oscillatory behaviour is observed around the CW results.

The remarks with respect to roll and yaw moments at longer waves ($L_{PP}/\lambda < 2$) can only mean that for such lengths, the time needed for one oscillation is longer than the corresponding change of heading by the model. Hence, the model never experiences a condition similar to head waves of seakeeping analysis. The observations made above are by all means contradictory to the general assumption of superposition studies where manoeuvring and seakeeping are regarded as a low frequency and high frequency problem, respectively. Hence, wave effects are considered only important by means of mean wave drift forces.

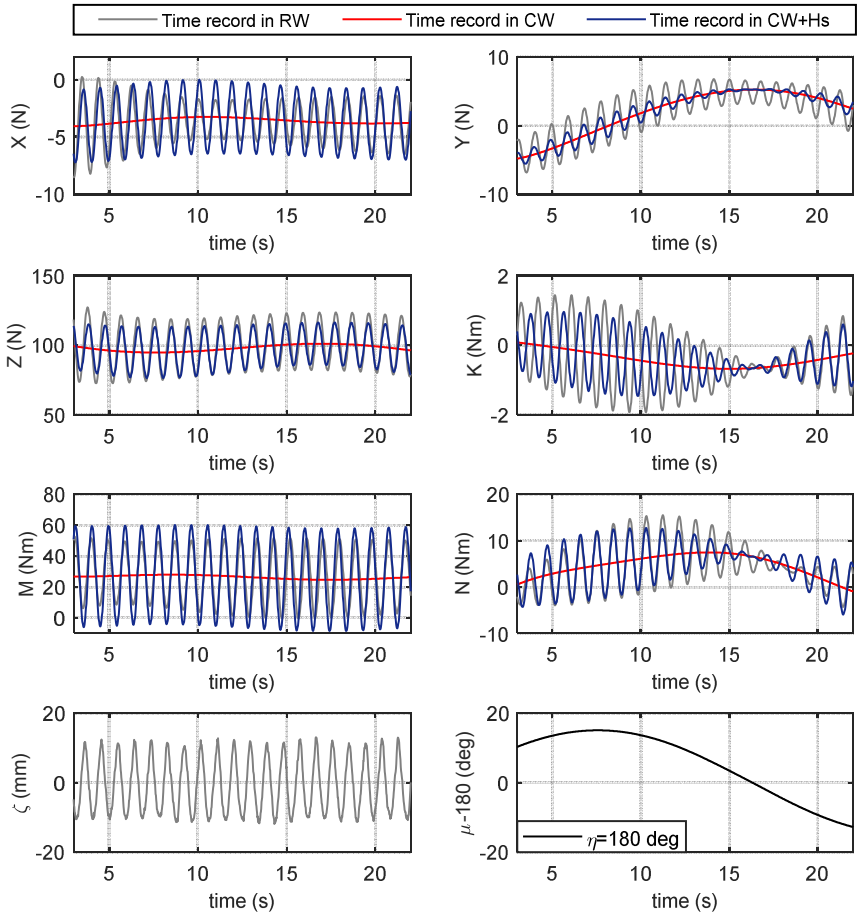


Figure 5.23 Time records of the forces and moments during harmonic yaw test in calm water (CW, in red), in head regular waves (RW, in grey) and with the superposition approach (CW + Hs, in blue). Test conducted at $Fr = 0.100$, $T_M = 13.1$ m, 50% UKC, $\psi_A = 15$ deg, $\psi_T = 35$ s, $\beta = 0$ deg, $L_{\mathrm{PP}}/\lambda = 2.27$ and $\zeta_a = 1$ m (11.1 mm at model scale). Wave (ahead the model) and yaw angle records are plotted at the bottom left and right, respectively.

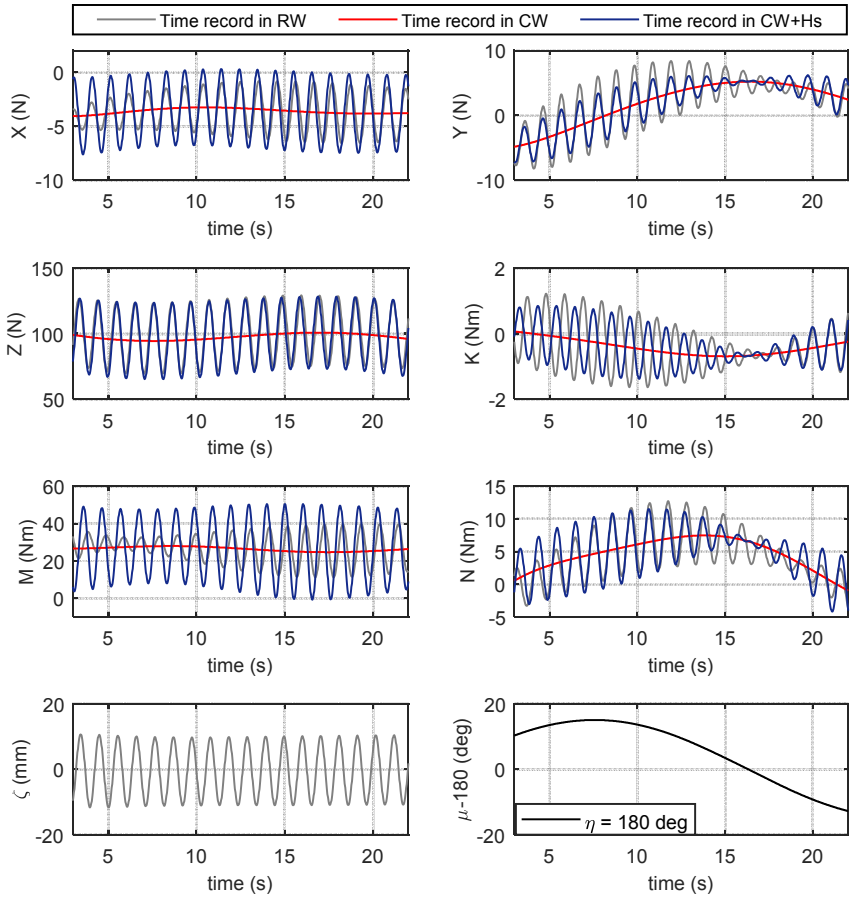


Figure 5.24 Time records of the forces and moments during harmonic yaw test in calm water (CW, in red), in head regular waves (RW, in grey) and with the superposition approach (CW + Hs, in blue). Test conducted at $Fr = 0.100$, $T_M = 13.1$ m, 50% UKC, $\psi_A = 15$ deg, $\psi_T = 35$ s, $\beta = 0$ deg, $L_{\mathrm{PP}}/\lambda = 2.0$ and $\zeta_a = 1$ m(11.1 mm at model scale). Wave (ahead the ship model) and yaw angle records are plotted at the bottom left and right, respectively.

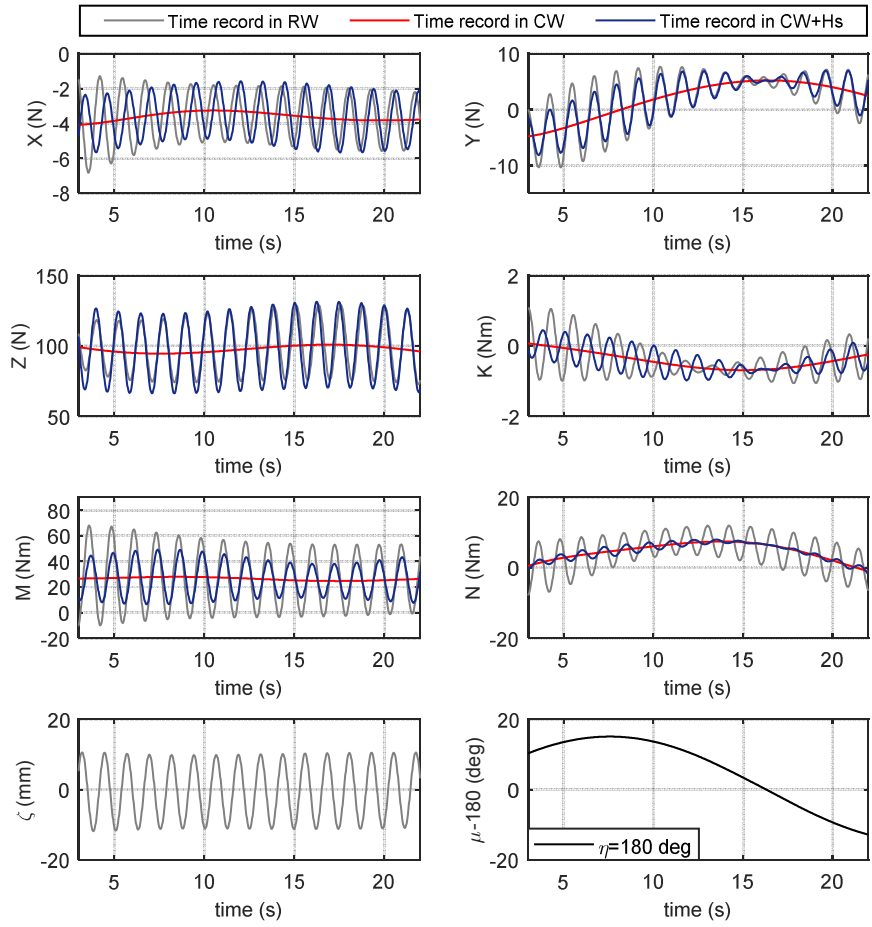


Figure 5.25 Time records of the forces and moments during harmonic yaw test in calm water (CW, in red), in head regular waves (RW, in grey) and with the superposition approach (CW + Hs, in blue). Test conducted at $Fr = 0.100$, $T_M = 13.1$ m, 50% UKC, $\psi_A = 15$ deg , $\psi_T = 35$ s, $\beta = 0$ deg, $L_{PP}/\lambda = 1.67$ and $\zeta_A = 1$ m (11.1 mm at model scale). Wave (ahead the ship model) and yaw angle records are plotted at the bottom left and right, respectively.

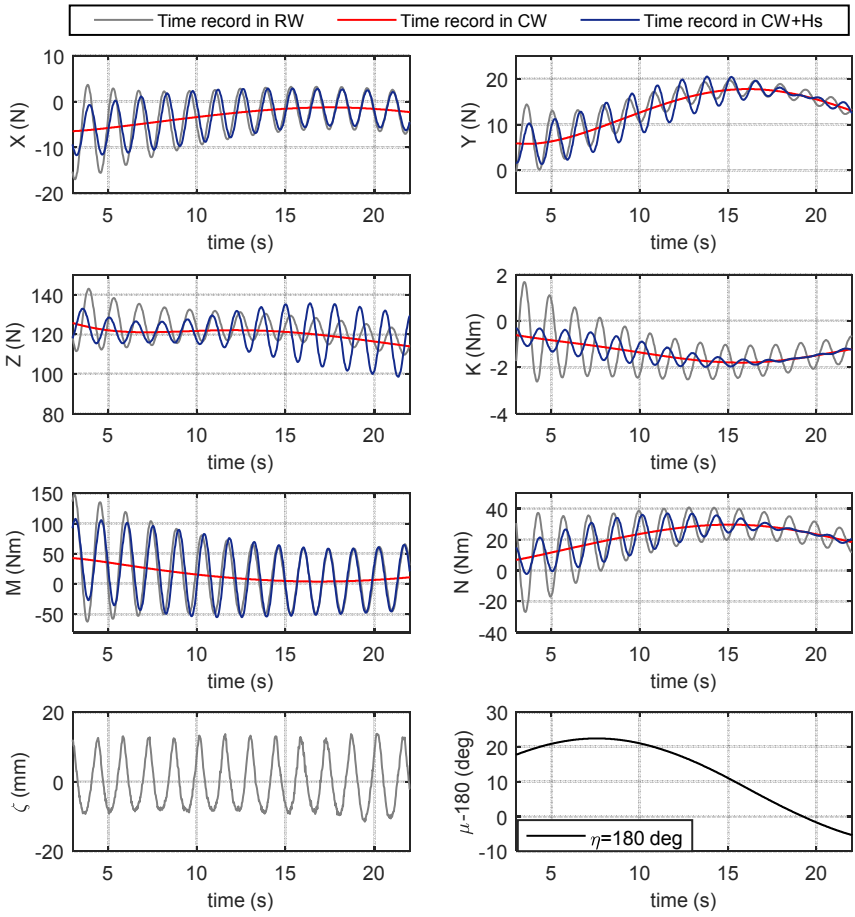


Figure 5.26 Time records of the forces and moments during harmonic yaw test in calm water (CW, in red), in head regular waves (RW, in grey) and with the superposition approach (CW + Hs, in blue). Test conducted at $Fr = 0.100$, $T_M = 13.1$ m, 50% UKC, $\psi_A = 15$ deg, $\psi_T = 35$ s, $\beta = 7.5$ deg, $L_{PP}/\lambda = 1.43$ and $\zeta_a = 1$ m ( 11.1 mm at full scale). Wave (ahead the ship model) and yaw angle records are plotted at the bottom left and right, respectively.

Results show, however, that this general assumption can only be applied for relatively short waves, and careful attention should be paid to the long wave length range where the mean of the first order forces would still play and important role. This would be especially the case for smaller ships than the one used in the present study. For the same reason, the extension of this approach for the case of the ULCC studied in the present work, and the range of wave lengths encountered in coastal zones, it is appropriate to assume that the superposition can still be applied.

## 5.3 Ship motions

The amplitudes of the motions in heave and pitch obtained from tests conducted with the model semi captive are presented in Figure 5.27, Figure 5.28, Figure 5.29 and Figure 5.30 for four different forward speeds $Fr$ of 0.025, 0.050, 0.075, and 0.100 respectively.

In each figure, results have been displayed for both head and following waves, and three different drift angles $\beta$ of 0, $5$, and 10 degrees. The figures arrangements are as follow: heave motions are plotted at the top, pitch motions are plotted at the bottom, results in head waves are shown at the left, and results in following waves are shown at the right. Results at different drift angles have been plotted together for better comparison.

In Figure 5.27 to Figure 5.30, heave and pitch motions are plotted only. Roll motions have not been displayed, their smaller magnitudes (notice that the wave angle of encounter $\mu$ is approximately 180 deg) have not allowed distinction from noise on the gauges, hence they were excluded. The attention is drawn to heave and pitch because of their more evident presence when more realistic simulations for manoeuvring in waves are aimed at.

From Figure 5.27 to Figure 5.30 it can be observed that the influence of drift angles on heave and pitch is negligible for both head and following waves. When results are compared against the numerical estimations computed with Hydrostar, a fair agreement

is obtained in head waves; in following waves the agreement is less, especially for the heave motions.

The differences found for the motions between tests and the numerical estimations can help to explain, partially, the differences seen (in the subsections above, see Figure 5.5 to Figure 5.8) for the mean wave forces in waves (e.g. added wave resistance) and their estimated ones with Hydrostar. Recall that motions are important when computing second order wave forces.

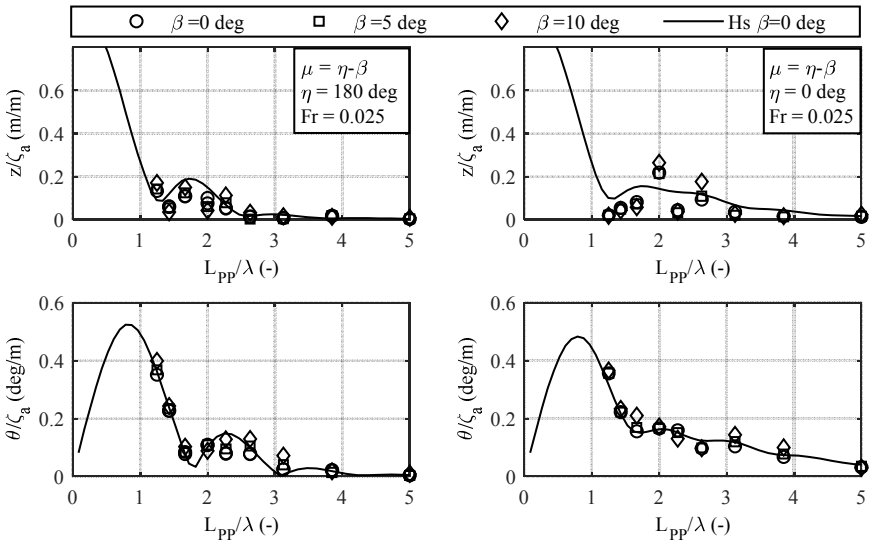


Figure 5.27 Heave (top) and pitch (bottom) motion responses in head (left) and following (right) regular waves. Test conducted at $Fr = 0.025$, $T_M = 13.1$ m, 50% UKC, $\beta = 0, 5,$ and 10 deg, and $\zeta_a = 1$ m. Test results are shown in markers and numerical ones (Hs) in continuous lines.

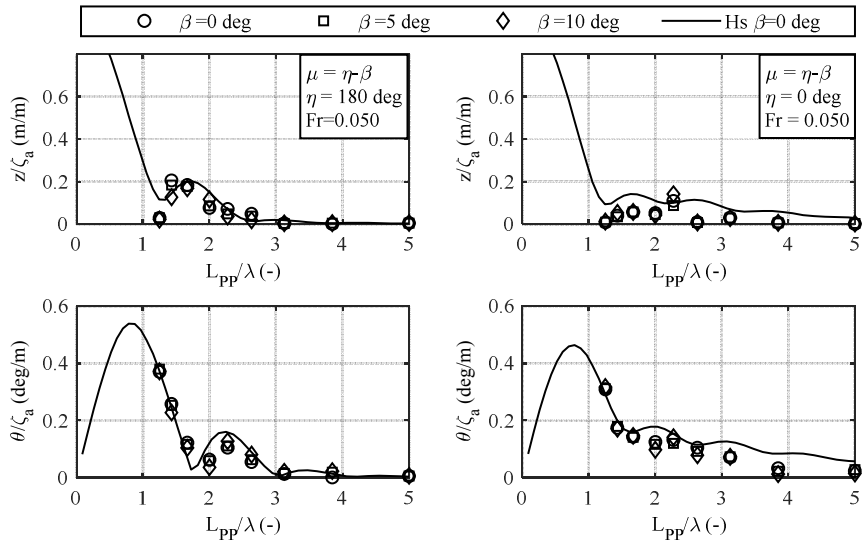


Figure 5.28 Heave (top) and pitch (bottom) motion responses in head (left) and following (right) regular waves. Test conducted at $Fr = 0.050$, $T_M = 13.1$ m, 50% UKC, $\beta = 0, 5,$ and 10 deg, and $\zeta_a = 1$ m. Test results are shown in markers and numerical ones (Hs) in continuous lines.

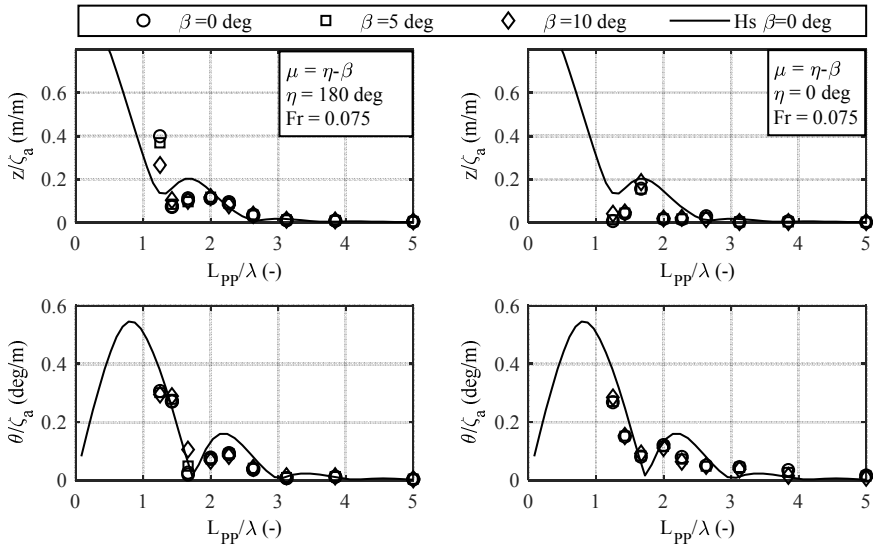


Figure 5.29 Heave (top) and pitch (bottom) motion responses in head (left) and following (right) regular waves. Test conducted at $Fr = 0.075$, $T_M = 13.1$ m, 50% UKC, $\beta = 0, 5,$ and 10 deg, and $\zeta_a = 1$ m. Test results are shown in markers and numerical ones (Hs) in continuous lines.

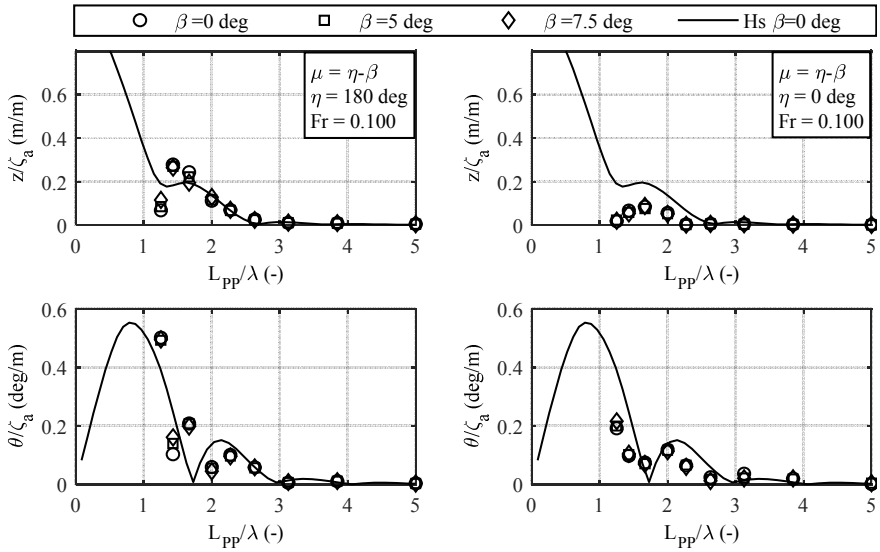


Figure 5.30 Heave (top) and pitch (bottom) motion responses in head (left) and following (right) regular waves. Test conducted at $Fr = 0.100$, $T_M = 13.1$ m, 50% UKC, $\beta = 0, 5,$ and 10 deg, and $\zeta_a = 1$ m. Test results are shown in markers and numerical ones (Hs) in continuous lines.

## 5.4 Propeller forces

To investigate the influence of waves on the propeller thrust and torque, experiments were conducted at several combinations of propeller rate and ship forward speed. An example of the time records obtained during such tests is displayed in Figure 5.31. These time records have been obtained at a propeller rate of $n = 0.75n_0$, and at a relatively long wave of ratio $L_{PP}/\lambda = 1.25$, with wave amplitude $\zeta_a = 11.1$ mm (model scale), corresponding to RW1 of test program 2016 (see Chapter 4).

From Figure 5.31 it can be seen that thrust and torque display small oscillations only at a frequency rate defined by the frequency of encounter. These oscillations are relatively small and do not represent a significant change in comparison to the mean thrust and torque. The spectral responses (mean of the signal has been subtracted) in Figure 5.31 show as well the small magnitudes of these oscillations.

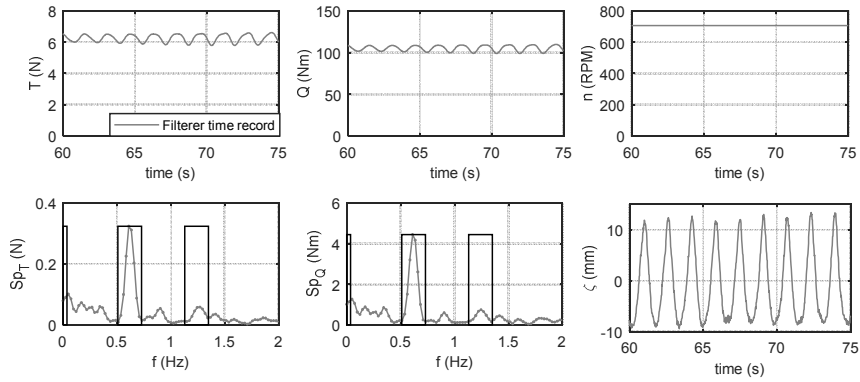


Figure 5.31 Thrust $T$ (top left), torque $Q$ (top mid), propeller rate $n$ (top right) and wave profile $\zeta$ (bottom right) in head waves. Test conducted at $T_M = 13.1$ m, 50% UKC, $n = 0.75n_0$, $L_{PP}/\lambda = 1.25$, and $\zeta_a = 1$ m (11.1 mm at model scale). Spectral results $(Sp)$ of $T$ and $Q$ are plotted below their respective time records.

To further investigate the influence of waves on the propeller, the thrust $T$ and torque $Q$ as measured in waves and in calm water have been compared by evaluating first their respective thrust $K_T$ and torque $K_Q$ coefficients. In addition, from comparison with the open water curves for $K_T$ and $K_Q$, the evaluation of the wake has also been obtained.

The thrust $K_T$ and torque $K_Q$ coefficients are given by:

$$K_T = \frac{T}{\rho D^4 n^2} \tag{5.12}$$

$$K_Q = \frac{Q}{\rho D^5 n^2} \tag{5.13}$$

where $n$ is the propeller rate, $D$ is the propeller diameter, and $\rho$ is the density of the water.

To obtain the wake factor, $K_T$ and $K_Q$ are plotted as functions of the apparent advance ratio, defined by the ship speed V, as:

$$J^* = \frac{V}{nD} \tag{5.14}$$

The wake fraction, in waves and in calm water, can be found by:

$$w_T = 1 - \frac{J}{J^*} \tag{5.15}$$

The wake factors can be found by thrust ($w_T$) or torque identity ($w_Q$), both results are plotted in Figure 5.32 as function of the apparent hydrodynamic advance angle $\varepsilon^*$, defined by:

$$\varepsilon^* = \text{atan}\left(\frac{J}{0.7\pi}\right) \tag{5.16}$$

In Figure 5.32 results have been obtained from a range of ship speeds and propeller loadings (see Chapter 4), and for three different wave lengths ($L_{PP}/\lambda = 2.27$, $1.67$, and $1.25$).

In Figure 5.32, the comparison of the thrust $K_T$ or the torque $K_Q$ coefficients obtained from tests in calm water and in waves reveals no significant change in their values. This is better observed by comparing their respective wake factors, obtained from either thrust or torque identity.

Notice that negative values are obtained for the wake factors. This is because the propeller open water curves do not correspond to water depth under study, They have been obtained for deep water. Their use, however, for the present purpose of the study is not questionable because our main interest is to investigate the propeller performance change in waves with respect to calm water.

The observations made in here correspond to conditions where the propeller rate is larger, and low to moderate ship forward speeds. It can be expected that at low propeller rates and very low forward speeds wave effects could be important because of the flow field velocities being of the same order as the orbital velocities caused by waves. To the author's opinion, such conditions are never encountered in open seas, nor do they correspond to voyages where, for instance, the ship approaches a port. Thus, they are omitted from the present study.

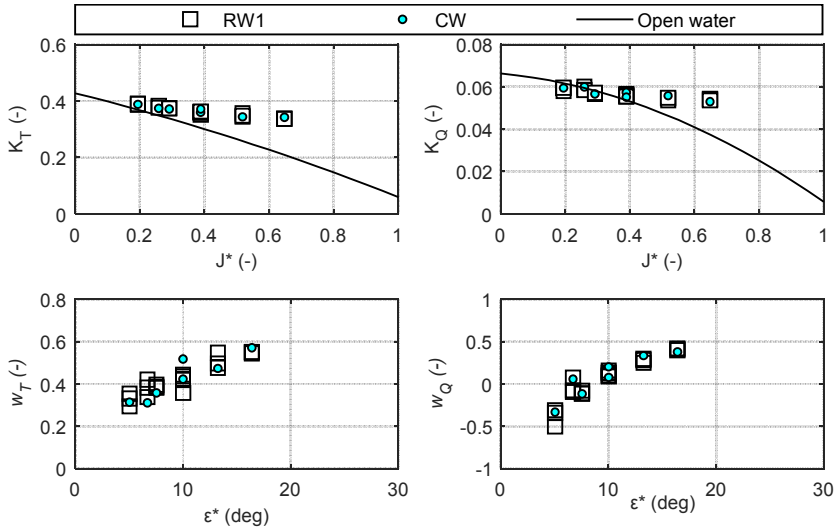


Figure 5.32 Thrust $K_T$ (top left) and torque $K_Q$ (top right) coefficients, and wake fraction from thrust $w_T$ (bottom left) and torque $w_Q$ (bottom right) identity. Test results have been obtained in calm water (CW, circles) and in head waves (RW1, in squares) at $T_M = 13.1$m, 50% UKC, $L_{PP}/\lambda = 227$, 1.67, and 1.25, and $\zeta_a = 1$ m.

## 5.5 Thrust deduction fraction

The propeller–hull interaction is investigated by computing the increase of ship resistance as a fraction of the propeller thrust, which is commonly known as the thrust deduction fraction and is given by:

$$t = \frac{T - (F + R)}{T} \tag{5.17}$$

where $F$ is the longitudinal force measured during test with the propeller action, $T$ is the propeller thrust, and $R$ is the ship's resistance.

To further investigate the influence of waves on $t$, the results obtained from model tests in calm water (CW) and in regular waves (RW) are presented in Figure 5.33 as a function of the apparent hydrodynamic advance angle $\epsilon^*$. Tests have been performed in head waves and for three different wave lengths ($L_{PP}/\lambda = 2.27$, 1.67, and 1.25, and $\zeta_A = 11.1$ mm).

In Figure 5.33 results obtained from tests in regular waves and calm water are plotted in square and circle markers, respectively (see legend above in Figure 5.33).

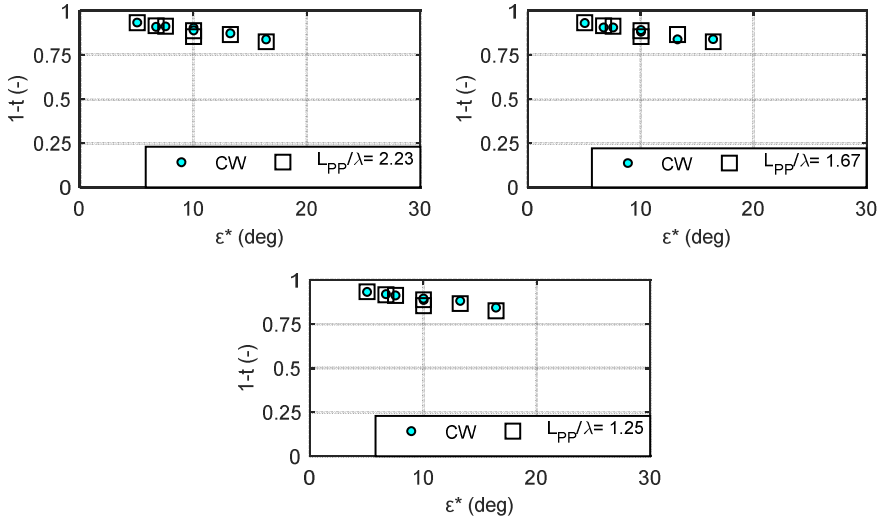


Figure 5.33 Thrust deduction fraction $t$ obtained in calm water (CW, in circles) and in head regular waves (RW1, in squares). Test conducted at $T_M = 13.1$ m, 50% UKC, and $L_{PP}/\lambda = 2.27$, $1.67$, and $1.25$, and $\zeta_A = 1$ m.

The investigation on $t$ was conducted considering longitudinal velocities $u$ only. Other parameters such as the drift angle are also important on its estimation but are not accounted in here. $t$ is strongly dependent on $u$,hence, its evaluation under this condition, in waves, is considered to be of great relevance. From Figure 5.33, the thrust deduction factor, obtained in calm water, is observed to vary slightly as a function of the hydrodynamic angle. Similar results are observed for the case in regular waves. When comparing both results, insignificant variations are observed in $t$ for all wave lengths.

## 5.6 Rudder forces

To investigate the effect of waves on rudder forces, experimental studies have been conducted in calm water and in regular waves with the fully appended ship. During the tests, propeller rates of $75\%$ and $100\%$ of the nominal propeller rate $n_0$, a rudder angle of

$\delta_R = 35$ deg, and four different ship forwards speeds, $F_r = 0.050$, $0.075$, $0.100$, and $0.125$, have been used.

An example of the time records obtained during tests is plotted in Figure 5.34. The longitudinal force $F_{TR}$, the transversal force $F_{NR}$ (as measured in the rudder axes frame, see chapter 2), and the rudder angle $\delta_R$ are displayed at the bottom of the figure.

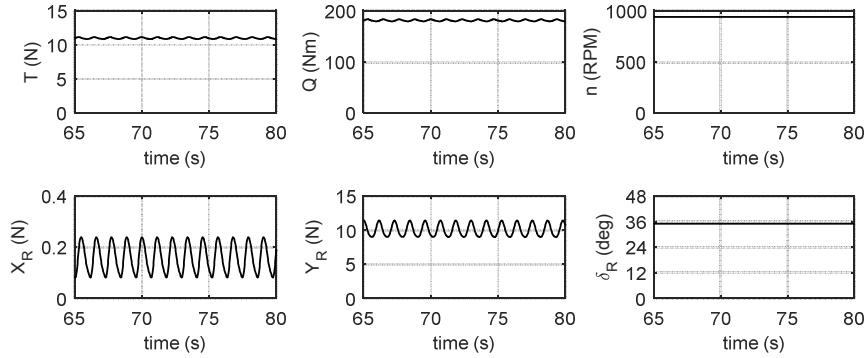


Figure 5.34 Time records during straight run tests at $T_M = 13.1$ m, 50% UKC, $\delta_R = 35$ deg, propeller rate $n = n_0$, and ship speed corresponding to $F_r = 0.125$.

From Figure 5.34, an oscillatory behaviour of the rudder forces are observed for both the tangential and normal force components. Although the oscillatory behaviour on $F_{TR}$ and $F_{NR}$ are present, they have been neglected. This is because they are generally small and will not contribute to a change of the mean behaviour of the rudder, which is considered relevant for manoeuvring.

To investigate the mean forces on the rudder, instead of investigating the tangential $F_{TR}$ and normal $F_{NR}$ forces, the rudder lift $F_{LR}$ and drag $F_{DR}$ will be discussed. To relate these two different representations of the forces, first, that the rudder forces on the hull ($b$ −frame) $X_R$, and $Y_R$ are related to the tangential and normal forces by:

$$X_R = F_{TR}cos\delta_R - F_{NR}sin\delta_R \tag{5.18}$$

$$Y_R = F_{TR}sin\delta_R + F_{NR}cos\delta_R \tag{5.19}$$

and to the lift and drag forces by:

$$X_R = \frac{\rho}{2} A_R V_R^2 (- C_{DR}(\alpha_R) cos\beta_R + C_{LR}(\alpha_R) sin\beta_R) \tag{5.20}$$

$$Y_R = \frac{\rho}{2} A_R V_R^2 ( C_{DR}(\alpha_R) sin\beta_R + C_{LR}(\alpha_R) cos\beta_R) \tag{5.21}$$

Now from Eq. (5.18) to (5.21), the lift $C_{LR}(\alpha_R)$ and drag $C_{DR}(\alpha_R)$ coefficients can be obtained as function of $F_{TR}$ and $F_{NR}$.

$$\begin{bmatrix} C_{DR}(\alpha_R) \\ C_{LR}(\alpha_R) \end{bmatrix} = \frac{2}{\rho A_R V_R^2} \begin{bmatrix} -cos\beta_R & sin\beta_R \\ sin\beta_R & cos\beta_R \end{bmatrix} \begin{bmatrix} cos\delta_R & -sin\delta_R \\ sin\delta_R & cos\delta_R \end{bmatrix} \begin{bmatrix} F_{TR} \\ F_{NR} \end{bmatrix} \tag{5.22}$$

In Eq. (5.20) and Eq. (5.21) the magnitude of the velocity $V_R$ is given by the local longitudinal $u_R$ and transversal $v_R$ velocities.

$$V_R = \sqrt{u_R^2 + v_R^2} \tag{5.23}$$

The local drift angle $\beta_R$ is defined by:

$$\beta_R = \arctan\left(\frac{-v_R}{u_R}\right) \tag{5.24}$$

The lift $C_{LR}(\alpha_R)$ and drag $C_{DR}(\alpha_R)$ coefficients are given as function of the effective inflow angle $\alpha_R$ defined by:

$$\alpha_R = \delta_R + \delta_0 + \beta_R \tag{5.25}$$

Where $\delta_0$ is a correction of flow asymmetry (see, Delefortrie 2007), and it is defined at the condition where, the normal force satisfy:

$$\delta_0 = -\delta_R (F_{NR} = 0) \tag{5.26}$$

The transversal velocity at the rudder can be obtained by:

$$v_R = k_{HR}(v + r x_R) \tag{5.27}$$

The variables $k_{HR}$ and $x_R$ refer to the straightening coefficient and the longitudinal position of the rudder axis. More details on these parameters can be found in Vantorre (1989), Eloot (2006), Delefortrie (2007).

The longitudinal speed $u_R$ can be estimated by a weighting average of the free stream $u_{R0}$ and the flow due to the propeller action $u_{RP}$, as:

$$u_R = \sqrt{\eta^* u_{RP}^2 + (1-\eta^*) u_{R0}^2} \tag{5.28}$$

In here, $\eta^* = D_P/H_R$ is the propeller diameter $D_P$ to rudder height ratio $H_R$.

For the purpose of the evaluation of the rudder behaviour, the speed $u_{RP}$ is estimated by means of the momentum theory (Brix, 1993) given by:

$$u_{RP} = u_{R0} + K_m u_P \left( \sqrt{1 + \frac{8K_T}{\pi J^2}} - 1 \right) \tag{5.29}$$

where $u_P$ is the flow axial velocity at the propeller location, and $K_m$ is a factor taking into account the propeller jet contraction at the rudder location. $K_T$ and $J$ are the thrust coefficient and the propeller advance ratio, respectively.

For the test described above, see also Chapter 4, propulsion tests, $\eta^* = 0.71$ and $K_m = 0.95$, and $v_R = 0$. The lateral velocity is zero because model tests have been conducted without drift angles $\beta$ or yaw velocities $r = 0$.

The results obtained for both, drag $C_{DR}$ and lift $C_{LR}$ coefficients have been plotted as a function of the square of the inflow velocity ($V_R$) to the rudder in Figure 5.35. Both results, in calm water and in regular head waves are displayed together for comparison.

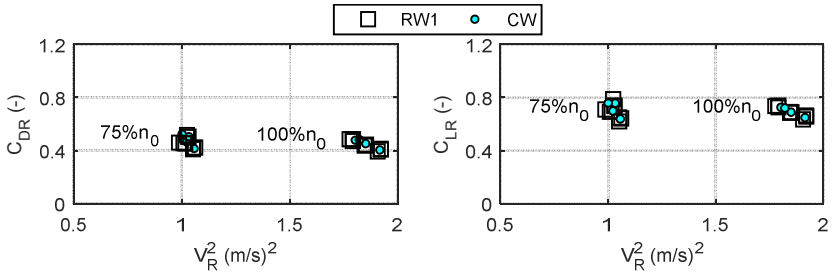


Figure 5.35 Drag and lift coefficients obtained in calm water (CW, in circles) and in head regular waves (RW1, in squares) at $T_M = 13.1$ m, $L_{PP}/\lambda = 2.27$, 1.67, and 1.25, $\zeta_a = 1$ m, and ruder angle $\delta_R = 35$ deg.

The results for both drag and lift show a constant magnitude as a function of the square of the speed, $V_R^2$. Small differences are encountered between tests in calm water which are similar for the cases of test in regular waves. The comparison of both results shows no practical influence of waves in the behaviour of the rudder.

The insignificant variation of the rudder behaviour in waves is not a conclusive nor a general statement. This is because the evaluation of the rudder behaviour in waves requires further attention, especially, at smaller rudder angles, low propeller rates, and combinations with drift angles and higher angles of wave encounter. At such conditions, a small change in the lift and drag forces might be important to accomplish the desired manoeuver. Such studies required further attention and remain as subject of future research.

# MANOEUVRING IN COASTAL WAVES



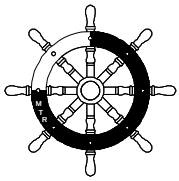

*The noblest pleasure is the joy of understanding.*
*Leonardo da Vinci*

# 6

# Model approach for manoeuvring in waves

## 6.1 Fluid phenomena: modelling challenges

### 6.1.1 General discussion

In Chapter 2 it has been shown that the equations of motion governing the ship's rigid body motions in six degrees of freedom, defined in the b-frame axes system, are given by:

$$\begin{aligned}
&m\big(\dot{u} - vr + wq - x_G(r^2+q^2) + y_G(pq-\dot{r}) + z_G(pr+\dot{q})\big) &&= X\\
&m(\dot{v} - wp + ur + x_G(pq+\dot{r}) - y_G(p^2+r^2) + z_G(qr-\dot{p})) &&= Y\\
&m\big(\dot{w} - uq + vp + x_G(pr-\dot{q}) + y_G(qr+\dot{p}) - z_G(p^2+q^2)\big) &&= Z\\
&\dot{h}_x + qh_z - rh_y + m\big(y_G\dot{w} - z_G\,\dot{v} + y_G(vp-uq) - z_G(ur-wp)\big) &&= K\\
&\dot{h}_y + rh_x - ph_z + m\big(z_G\dot{u} - x_G\dot{w} + z_G(wq-vr) - x_G(vp-uq)\big) &&= M\\
&\dot{h}_z + ph_y - qh_x + m\big(x_G\dot{v} - y_G\dot{u} + x_G(ur-wp) - y_G(wq-vr)\big) &&= N
\end{aligned} \tag{6.1}$$

The right hand side of Eq. (6.1) comprises the hydrodynamic forces applying on the ship's hull, the propeller forces, the rudder forces, and external force contributions such as wind and waves induced forces. The variables $X,Y,Z$ and $K,M,N$ represent the surge, sway, heave forces and the roll, pitch and yaw moments, respectively.

To summarise the expressions for the forces and moments, they are further written as bold capital letter $\boldsymbol{F} = [X, Y, Z, K, M, N]^T$, where the superscript $T$ represents the transpose of a matrix.

Equation (6.1) is a highly nonlinear equation. Finding a solution to it requires first an understanding of the hydrodynamic phenomena involved in the determination of $\boldsymbol{F}$. Concepts such as vorticity, viscosity, ideal fluids, cross flow effects, and turbulence flow are then necessary to comprehend the fluid phenomena, determine weak and relevant fluid effects, and possibly apply simplifications to the problem.

For instance, for a ship manoeuvring in calm water Figure 6.1 illustrates the relevant fluid phenomena generally considered in the modelling of the sway forces and yaw moments as a function of the drift angle $\beta$, see Ankudinov (1983), Oltmann and Sharma (1984), and Hooft (1994).

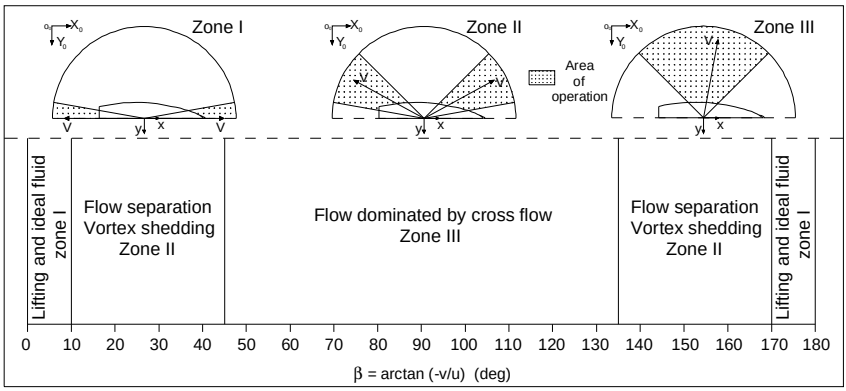


Figure 6.1 Sway force and yaw moment dominant flow phenomenon as function of the drift angle $\beta$.

Obviously, modelling $\boldsymbol{F}$ in general is quite complex and can be accomplished only by breaking the phenomenon up into a number of parts to be simulated separately. It is not surprising then to find in literature that due to this complexity the study of the ship dynamics has been subdivided in two independent fields, the manoeuvring in calm water studies and the seakeeping studies.

In seakeeping studies the aim is to investigate the ship's behaviour and responses to waves in open seas. For this purpose, it is accepted to assume that wave forces, moments and induced motions in irregular waves can be obtained by a superposition of the individual responses obtained from the analysis in regular waves which compose the given sea state, see Dennis and Pierson (1953).

Further, the ship is assumed to move with a constant forward speed $V$ in rectilinear trajectory and developed oscillatory motions varying harmonically about their mean position. Propeller forces, rudder forces, Coriolis forces, and centripetal forces are then all disregarded from Eq. (6.1) as their contribution is insignificant in contrast to wave forces and body reaction forces. These assumptions allow to express Eq. (6.1) directly in the inertial h-frame (moving at constant forward speed $V$), as:

$$\sum_{j=1}^{6}\left\{\left(M_{kj}+A_{kj}\right)\ddot{\xi}_{kj}+B_{kj}\dot{\xi}_{kj}+C_{kj}\xi_{kj}\right\}=F_k\,e^{i\omega_E t},\;\; k,j=1,\ldots,6 \qquad (6.2)$$

where $A_{kj}$ , $B_{kj}$ , $C_{kj}$ , $M_{kj}$ , $\xi_{kj}$ and $F_k$ are the added inertia coefficients, the damping coefficients, the restoring terms, the ship's inertial terms, the ship motions and the wave exciting forces, respectively (see Chapter 2).

In addition, by considering the flow as irrotational and inviscid, potential theory can be used to solve the Eq. (6.2). Examples of such potential studies are, for instance, the strip theory method of Salvesen et al., (1970) and the panel methods of Seo and Kim, (2011), and Chen, (2004).

The results from seakeeping analysis have certain limitations, for instance with respect to the viscous damping contribution to roll motions, which are deemed necessary and must be evaluated by other means. Large wave amplitudes and the more accurate solution of the forward speed problem are also still topics of continuous research; in spite of these limitations, seakeeping

studies applied taking into consideration the limited wave amplitude and up to moderate speeds can be considered quite satisfactory.

In manoeuvring in calm water the main objective is to investigate the ship performing manoeuvres in otherwise restricted waters. In here, different from seakeeping studies, the ship develops a more general curvilinear trajectory in response to its control devices.

The curvilinear motion introduces Coriolis and centripetal forces which are not only applied to the ship but also to the fluid disturbed by the ship motions. In addition, in a more general case, the ship's forward speed $V$ is not constant, drift angles $\beta$ are attained and different combinations of rudder angles and propeller rates are used. Other parameters such as the finite water depth $h$, and wind forces can also be taken into account.

The large number of parameters involved and the viscous characteristics of the flow limit the applicability of studies, as one for instance, cannot simply generalise the observations made at higher speeds and assume they remain applicable at lower speeds. Depending on the ship's forward speed, the drift angle, and the ship's yawing moment among other parameters, the flow around the hull and appendages will be more laminar or turbulent, vortices will appear and the characteristics of the boundary layer along the hull will vary.

Additional considerations in the modelling of manoeuvring ships in calm water are then necessary to further simplify the problem. For instance, assuming quasi-steady behaviour, and neglecting the ship's vertical motions and the wave generation at the free surface memory effects can be disregarded from the analysis. Thus, fluid forces can be assumed uniquely defined by the instantaneous ship velocities, $u$, $v$, $r$ and accelerations $\dot{u}$, $\dot{v}$, $\dot{r}$. The considerations mentioned above simplify the analysis greatly, however, obtaining a general expression for $\boldsymbol{F}$ which can be applied for any ship manoeuvre is yet far too complex.

Further simplifications of the manoeuvring problem have been applied by solving the latter under specific flow regimes which are a function of the ship speed and environmental conditions. Figure 6.2 shows for example the range of drift angles (dashed area inside the circle) attained as a function of the magnitude of the speed $V$ at two different manoeuvring conditions, in harbours and restricted waters, and when approaching a port.

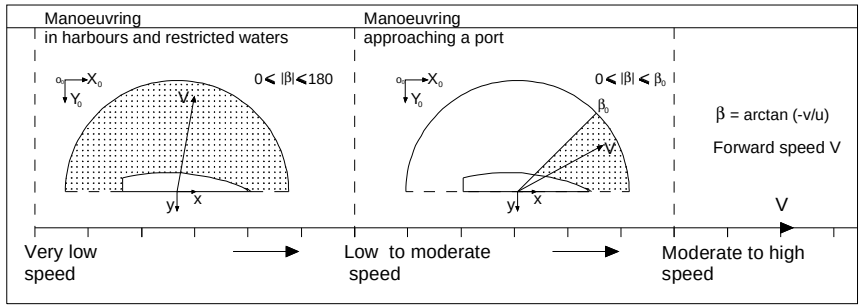


Figure 6.2 Ship velocity $\vec{V}$ and attained drift angles $\beta$ for manoeuvres performed in harbours/restricted waters and when approaching a port.

Mathematical models for $\boldsymbol{F}$ based on the Taylor series expansion, such as the one from Abkowitz (1964) are examples of manoeuvring models developed for moderate speed regions. These models are generally accepted because of the rather limited attained drift angles and yaw velocities at regime speed. This allows expressing further the fluid forces as polynomial functions of the velocity and acceleration terms.

It is important to notice that models as such the one proposed by Abkowitz (1964) (described as a 'black box models' by Ankudinov, 1983), however, do not suffice for more complex manoeuvres as the ones performed in harbours. In such conditions, the wide range of speeds (including zero speed, very low speed and moving backward) and the wide range of drift angles attained (including very large angles of drift) in combination with yaw velocities, makes it simply unsuitable to express the hydrodynamic forces as a Taylor series expansion. This type of manoeuvres has been studied separately from the full regime speed conditions, and can

be considered under the description of low speed manoeuvring models.

Low speed manoeuvring models have been developed to cover the most difficult manoeuvres the ship performs in ports and restricted waters where very low forward speeds are reached. In such conditions large drift angles are also attained. Manoeuvring models for $\boldsymbol{F}$ as such do not differ as a function of the range of speeds $V$ only, as shown Figure 6.2. For very low speed, it is also possible to distinguish sub-models but now as a function of the drift angle $\beta$, as proposed in Kobayashi (1987).

Even at low speed manoeuvres, the nature of the flow is very distinct from one drift angle to another, as shown in Figure 6.1. For instance, at small $\beta$ lift and ideal fluid effects are very important but at large $\beta$ cross flow effects are dominant. However, if one restricts the analysis to this speed range only, the nature of the flow can be considered similar for ship manoeuvres attaining the same hydrodynamics angles, $\beta$, $\gamma$, $\chi$, thus mathematical models with coefficients $\boldsymbol{F'}^{(\beta)}$, $\boldsymbol{F'}^{(\gamma)}$, $\boldsymbol{F'}^{(\chi)}$ depending only on these angles can be defined (see Chapter 2). Models as such are built then by arranging these coefficients in tabular form as function of $\beta$, $\gamma$, $\chi$, see e.g. Khattab (1987), Kobayashi (1987), Eloot and Vantorre (2003), and Delefortrie et al. (2016a).

The use of tabular models with coefficients $\boldsymbol{F'}^{(\beta)}$, $\boldsymbol{F'}^{(\gamma)}$, $\boldsymbol{F'}^{(\chi)}$ simplify the problem greatly as they require only the dependence on the hydrodynamic angles, but one should remind its limitations to slow and very slow forward speeds.

Taking into account the speed consideration, Kobayashi (1987) for example, proposed a mathematical model to cover all possible manoeuvring conditions (low speeds and regime speeds) by subdividing his model in two different sub models: one suited for manoeuvres at very low speeds ($Fn < 0.005$) and one suited for manoeuvres at regime speeds ($Fn > 0.010$). Interpolation between these models was conducted for speeds range in between these

limits. In Kobayashi (1987) the mathematical model proposed for very low speeds needed further subdivision but now as function of the drift angle $\beta$.

### 6.1.2 Ideal fluid effects for calm water manoeuvring

For the purpose of the present discussion, the general case of manoeuvring is considered where only horizontal motions are studied; in addition, the origin of the body fixed axis system is assumed to be located at the ship's centre of gravity, thus $x_G = y_G = z_G = 0$. Equation (6.1), taking into account ideal fluid effects, can now be written as:

$$\begin{aligned} m(\dot{u} - X_{\dot{u}}) - mvr &= X \\ m(\dot{v} - Y_{\dot{v}}) - Y_{\dot{r}}\dot{r} + mur &= Y \\ (I_{zz} - N_{\dot{r}})\dot{r} - N_{\dot{v}}\dot{v} &= N \end{aligned} \tag{6.3}$$

In the equation above, the ideal fluid forces have been transferred to the left hand side of the equation, they are given by $X_{\dot{u}}$, $Y_{\dot{v}}$, $Y_{\dot{r}}$, $N_{\dot{r}}$, and $N_{\dot{v}}$ coefficients. These terms are known as the added mass/moment coefficients.

In Kirchhoff (1869) it was shown that these terms are functions of the kinetic energy of the fluid ($T$, see Chapter 2) and the work done by the ship to change it. In general, it is accepted to consider that these coefficients remain constant for a ship moving with perturbation motions along its mean trajectory. The resulting coefficients are then found to be dependent of the geometric characteristics of the body only, see Kirchhoff (1869), Lamb (1945) and Milne-Thomson (1962).

The observation of Kirchhoff (1869) is in fact valid for any case of a body moving in an unbounded fluid. Because the steady wave generation at the free surface is neglected, Kirchhoff's analysis has been directly applied to the case of the ship by the double body, mirroring the hull with respect to the waterline.

The Kirchhoff approach has been of great advantage to the study of the problem of manoeuvring in calm water. It is important to recall, as discussed by Imlay (1961), that such ideal fluid forces

are always dependent on the kinetic energy of the flow, hence, the coefficients $X_{\dot{u}}$, $Y_{\dot{v}}$, $Y_{\dot{r}}$, $N_{\dot{r}}$, and $N_{\dot{v}}$ in Eq. (6.3) would remain constant as long as the flow along the ship hull remains the same.

To understand the nature of this problem, a sketch illustrating the flow streamlines along the ship moving in calm water is presented in Figure 6.3. Two types of motions are displayed, a rectilinear and a curvilinear motion. It can be observed that the flow along the ship in both scenarios is completely different, consequently the kinetic energy associated to both trajectories and the added mass coefficients differ. One cannot deny such a variation; therefore it should be carefully studied.

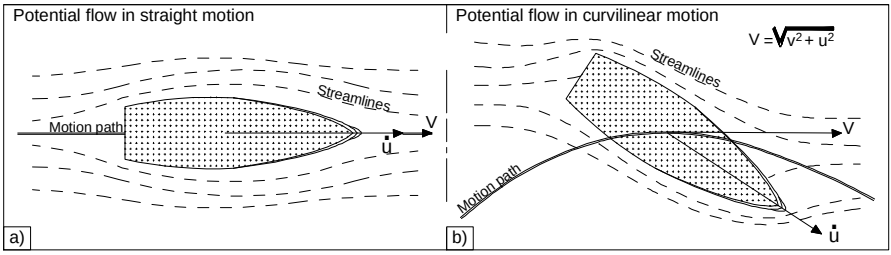


Figure 6.3 Ship manoeuvring in calm water. The potential flow described by the streamlines for (a) a rectilinear motion and (b) curvilinear motion both at constant forward speed.

The variation of the added mass coefficients has been already investigated and used in the mathematical models studied by Eloot (2006), and Delefortrie (2007). In their models the dependence of the added mass in sway, $Y_{\dot{r}}$, and added moment in yaw, $N_{\dot{r}}$, due to the drift angle $\beta$, for calm water manoeuvring, has been presented. Examples of such variation in the $Y_{\dot{r}}$ and $N_{\dot{r}}$ coefficients as function of the drift angle $\beta$ are shown in Figure 6.4 for three different under keel clearances (UKC), obtained from tests with the C0W model are compared.

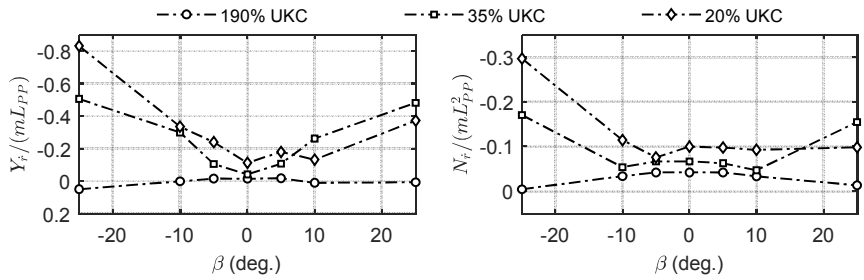


Figure 6.4 Ideal fluid coefficient in sway $Y_{\dot{r}}$ (left) and yaw $N_{\dot{r}}$ (right) as functions of the drift angle $\beta$ for container ship C0W at draft $T_m$ =15.2 m and at three different UKC.

From Figure 6.4 it can be observed that the change of the added inertia coefficients is of minor importance for smaller drift angles ($\beta < 25$) deg and higher UKC. In contrast, significant changes are found at relatively shallow water, especially for $Y_{\dot{r}}$. Similar results are seen for other ship types as presented in Eloot (2006).

The variation of $Y_{\dot{r}}$ and $N_{\dot{r}}$ coefficients as a function of the drift angle cannot be neglected. However, restricting the analysis to only small drift angles, for instance $\beta < 20$ deg, can simplify the problem as no significant change is encountered, hence, one can assume that added inertia terms remain constant. This would imply that the nature of the flow around the ship developed in different conditions would also remain the same.

The considerations stated above for smaller drift angles and the nature of the flow around the ship at such conditions has been assumed in the present study. Notice that if the ship is to move with larger drift angles, for instance $\beta > 25$ deg, this cannot be applied anymore as the flow around the ship is expected to change considerably.

It is important to notice that assuming the influence of the drift angles on the added inertia as negligible, is similar to as considering the ship performing a curvilinear trajectory to be moving in a set of short straight trajectories (composing the curvilinear path) with no drift angle $\beta = 0$ degrees. This would

resemble seakeeping studies and would allow applying the knowledge developed in this field in the manoeuvring analysis. Although this might be the case, one has to bear in mind other parameters such as the yaw rate and the wave characteristics before any final assumptions are taken into consideration.

### 6.1.3 Manoeuvring in waves in 6 DOF

When the ship manoeuvres in the presence of waves, the developed oscillatory motion will cause an additional phenomenon of wave generation at the free surface. Thus, the usual approach of manoeuvring in calm water which considers the fluid forces depending only on the instantaneously velocities and accelerations cannot be applied. Instead, the fluid forces will have an important contribution from the past events; this phenomenon is commonly known as *memory effects* and according to Newman (1979) have an important contribution, especially in shallow water.

As a consequence, certain modifications are without doubt deemed necessary in the formulation of the fluid forces $\boldsymbol{F}$. For studying the ship manoeuvring in waves, it is common to assume (see, e.g. Ankudinov,1983; Hooft and Pieffers, 1988; McCreight, 1991; Bailey et al., 1998, Lee, 2000) that the hydrodynamic forces on the hull can be decomposed in four main components: viscous forces, cross flow forces, lift, and ideal fluid forces:

$$\boldsymbol{F_H} = \boldsymbol{F_{Viscous}} + \boldsymbol{F_{Lift}} + \boldsymbol{F_{Cross\,flow}} + \boldsymbol{F_{id}} + \boldsymbol{F_W} \tag{6.4}$$

The viscous, lift, and cross flow terms remain the same in the hull forces as the ones estimated from manoeuvring in calm water. The introduction of memory effects are then introduced by modifying the ideal flow contribution only. The incorporation of memory effects in the study of manoeuvring will require the ideal forces described by constant coefficients in Eq. (6.3), to be expressed (see Cummins, 1962 and Bishop et al., 1977) as:

$$\boldsymbol{F_{id}} = [X_{id}\ Y_{id}\ Z_{id}\ K_{id}\ M_{id}\ N_{id}]^T = \boldsymbol{A\ddot{X}} + \boldsymbol{B\dot{X}} + \int_{-\infty}^{+\infty} \boldsymbol{H}(\boldsymbol{t}-\boldsymbol{\tau})\,\dot{\boldsymbol{X}}(\boldsymbol{\tau}) \tag{6.5}$$

In Eq. (6.5) $\boldsymbol{A}$, and $\mathbf{B}$ are added inertia and damping coefficients matrices, respectively. $\boldsymbol{H}$ is a matrix of impulse response functions (IRF), and $\ddot{\boldsymbol{X}}$ and $\dot{\boldsymbol{X}}$ refer to the instantaneous accelerations and velocities. It is important to stress that the matrices $\boldsymbol{A}$ in Eq. (6.5) should not be confused with the constant added inertia terms defined for calm water manoeuvring.

The major challenges when considering the implementation of Eq. (6.5) arise from the limitations depending on the flow characteristics developed along the hull; recall that for instance the added inertia term $\boldsymbol{A}$ and the IRF functions $\boldsymbol{H}$ at large drift angles will not remain the same, as the ones obtained at smaller drift angles, see 6.1.2. Other limitations when considering memory effects are associated to the speed dependence of $\boldsymbol{H}$. Which, requires a continuous evaluation because of the constantly changing forward speed while manoeuvring, see Skejic (2008).

When manoeuvring in coastal waves the finite water depth must be considered. In such operational areas, the ship will experience squat effects, sinking and trimming as a function of the ship speed and of the clearance between the ship's keel and the sea bottom. Taking into account squat effects and the ship motions due to waves, additional considerations might be required because of the continuously changing wetted surface of the ship. Thus, any forces depending on the latter would require also a continuous evaluation, hence, the assumption considered in Eq. (6.4) might not be applicable any longer.

From the discussion of calm water manoeuvring models, it has been concluded that the nature of the forces are different and strongly depending on the speed regimes, operational zones and the developed hydrodynamic angles at low speed. It is then clear that certain considerations and limitations in the analysis are needed. For instance, wave induced motions can only be considered large in rough to high sea states and consequently in up to moderate sea states the wetted surface can be considered as constant.

The study of the rudder and propeller forces in waves also deserves further attention. Variation of the wake factor can be expected to be significant, but only if amplitudes of motions and waves are large.

## 6.2 Scope of the mathematical model

### 6.2.1 Definition of manoeuvring in waves in 6 DOF

The discussion on the independency of the fields of manoeuvring in calm water and seakeeping has shown that to study and model the related complex fluid phenomena and their effects on the ship, firstly some level of simplification is required. These simplifications are based on the ship's behaviour and the environmental conditions which allowed defining weak and dominant fluid effects.

For studying manoeuvring in calm water, the complexity of the problem requires further additional consideration, and subdivision of the model in sub-models developed for manoeuvres at low speed and models developed for manoeuvres at regime speeds seems appropriate. The first type of models involves a wide range of drift angles, engine settings and propeller loading and rudder angle combinations. For models at regime speeds, the ship moves always forward, small drift angles are attained, and only positive propeller rates are employed. The first type of manoeuvres is commonly performed in harbours and restricted waters, hence, protected from the influence of waves. In contrast, waves will be always present for the second type of manoeuvres as they are performed in open waters.

Bearing in mind what has been stated above, the manoeuvres in waves in 6DOF can be then restricted to operational areas corresponding to ordinary speeds as discussed in Figure 6.2. However, one must notice that in these operational areas, common service speeds for ultra large container vessels (which is the case of the present study) are never reached, instead low to moderate speeds are used. Thus, for the purpose of the present study, the manoeuvring in waves model, with respect to the ship's forward speed, can be considered bounded between the limits of low to moderate positive forward speed. In addition, small drift angles, and positive propeller rates as mentioned before can be used as constraints.

### 6.2.2 General assumptions and limits of the model

To summarise, the main considerations taken in this study with respect to manoeuvring in waves are:

a) environmental conditions correspond to coastal waves;
b) the ship will always move with positive longitudinal speed $u$, and positive propeller rates $n$;
c) the ship speed $V$ can vary from low to intermediate speeds, e.g. Froude number $F_r < 0.125$;
d) the lateral velocity $v$ of the ship will always be small in contrast to the longitudinal speed $u$. Thus, only small angles of drift will be considered, e.g. $|\beta| < 20$ deg (see Figure 4.2).

In the present study, wave characteristics in the Belgian part of the North Sea have been taken into consideration. In this area waves have relatively limited amplitudes, and wave lengths are relatively small in comparison with the ship length of ultra large container vessels, see Chapter 1 and 4. Due to the relatively small wave amplitudes considered, also the amplitudes of the oscillatory ship motions are expected to be limited. Because the main objective of the present study is to implement a model for manoeuvres in waves in the simulator, the ship's vertical motions and the wave generation problem at the free surface must be accounted for. Although the ship motions are expected to be small and it would be a reasonable choice to neglect memory effects as well, according to Newman (1979) they are very important in shallow water, hence they deserve further attention in the present study.

It is important to precise that it is the purpose of the present study to include only memory effects arising from the wave generation problem at the free surface. Memory effects as result of vortex shedding will not be accounted, moreover, because of the restriction to positive forward speed, the ship will always travel away from its wake which is assumed to be the most important source of contribution to these phenomena.

# 6.3 Mathematical model

## 6.3.1 Modular approach

From the experimental study on the hull forces, in 5.2, it has been observed that during manoeuvring in waves they can be approximated by the individual contribution of two main components: a force as measured during manoeuvring in calm water, and a force induced by waves only. This approximation was also confirmed by comparing the oscillatory behaviour of the forces in 5.2.5, which provided a good agreement with the time records for all forces and moments.

The superposition of the calm water manoeuvring forces and wave forces on the hull was found to be suitable for waves characterised by a ship length to wave length ratio $L_{PP}/\lambda$ less than the 1. Because of the relative long ship length of ULCC ships, assuming the superposition of calm water forces and wave forces (mean drift and first order forces) on the hull can be applied without much restraint in coastal waves.

The study of the propeller and rudder revealed that when manoeuvring in waves (such as when approaching a port) the effects of waves can be neglected. Taking all these observations into consideration, manoeuvring in waves can be further studied by using the modular approach, as:

$$\boldsymbol{F} = \boldsymbol{F_H} + \boldsymbol{F_R} + \boldsymbol{F_P} + \boldsymbol{F_W} \tag{6.6}$$

The subscripts H, R, P, and W stand for hull, rudder, propeller, and wave contributions. $\boldsymbol{F_W}$ can be further subdivided approximately in:

$$\boldsymbol{F_W} = \boldsymbol{F_D} + \boldsymbol{F_{FK}} + \boldsymbol{F_{2nd}} \tag{6.7}$$

where $\boldsymbol{F_D}$, $\boldsymbol{F_{FK}}$ and $\boldsymbol{F_{2nd}}$ refer to the diffraction force, the Froude-Krylov force, and the mean second order wave forces.

Hydrostatic forces have not been mentioned in Eq. (6.6) but will be accounted together with the evaluation of the Froude-Krylov forces $\boldsymbol{F_{FK}}$ in Eq. (6.7).

Bear in mind, that the superposition approach does not necessarily mean that all hull forces as obtained in manoeuvring in calm water will remain approximately the same when manoeuvring in waves. Further considerations are yet needed and will be further discussed in the following subsections.

### 6.3.2 Hull forces

It has been stated that the hull forces $\boldsymbol{F_H}$ measured in calm water remain approximately the same when manoeuvring in waves. Although this has been generally accepted, it is important to take into account that $\boldsymbol{F_H}$ will require a further modification. This as the ship's oscillatory motions and the wave generation problem (arising due to the free surface) will need to be accounted properly. Recall that when the ship navigates in waves, added inertia terms are no longer constant and damping forces, neglected in calm water manoeuvring models, are present.

In the present work, to further proceed with the analysis of manoeuvring in waves in 6DOF in coastal waves, the hull forces are assumed to be decomposed (as discussed in subsection 6.1.3) as:

$$\boldsymbol{F_H} = \boldsymbol{F_S} + \boldsymbol{F_{id}} \tag{6.8}$$

where the steady components $\boldsymbol{F_S}$ comprise forces and moments arising from viscous, lift and cross flow phenomena, which can be treated independently from the body oscillation effects. Thus, any calm water manoeuvring model established for these fluid phenomena can be further used in the analysis.

The main change is regarding ideal fluid effects ($\boldsymbol{F_{id}}$) only. One might argue that models obtained from calm water incorporate already ideal fluid effects, such as the Munk's moment $(X_{\dot{u}} - Y_{\dot{v}})uv$. Therefore, they would require further corrections; which are,

however, not accounted for in the present work because no actual methods can estimate them accurately enough as they also depend on viscous effects.

The discussion of $\boldsymbol{F_S}$ in Eq. (6.8), and their respective variation during manoeuvres is considered in the following subsections. Squat effects in shallow water will also be discussed as part of the steady forces.

### *6.3.2.1Steady forces and moments*

As mentioned previously, fluid phenomena such as viscous, lift and cross flow can be estimated from calm water manoeuvring models. In the present study, following the works described in Delefortrie et al. (2014) and Delefortrie et al. (2016a), the tabular representation for the 6DOF manoeuvring model is used:

$$\begin{bmatrix} X_S \\ Y_S \\ Z_S \\ K_S \\ M_S \\ N_S \end{bmatrix} = \frac{1}{2}\rho L_{PP}^{s} T_M \begin{bmatrix} X'^{(\beta)} & X'^{(\gamma)} & X'^{(\chi)} \\ Y'^{(\beta)} & Y'^{(\gamma)} & Y'^{(\chi)} \\ Z'^{(\beta)} & Z'^{(\gamma)} & Z'^{(\chi)} \\ K'^{(\beta)} & K'^{(\gamma)} & K'^{(\chi)} \\ M'^{(\beta)} & M'^{(\gamma)} & M'^{(\chi)} \\ N'^{(\beta)} & N'^{(\gamma)} & N'^{(\chi)} \end{bmatrix} \begin{bmatrix} u^2 + v^2 \\ u^2 + v_{\mathrm{P}}^2 \\ v^2 + v_{\mathrm{P}}^2 \end{bmatrix} + \begin{bmatrix} 0 \\ 0 \\ 0 \\ K\mathrm{v} \\ 0 \\ 0 \end{bmatrix} \tag{6.9}$$

where $\rho$, $L_{\mathrm{PP}}$, and $T_M$ are the water density, the ship's length between perpendiculars and draft respectively. The exponent $s$ take the values of $s = 1$ for forces $X_H$, $Y_H$, $Z_H$, and $s = 2$ for moments $K_H$, $M_H$ $N_H$. $u$ and $v$, stand for the ship's linear velocities, and the reference lateral velocity $v_{\mathrm{P}}$ is given by $v_{\mathrm{P}} = rL_{PP}/2$, $r$ being the ship's yaw angular velocity. The viscous roll moment as a function of the ships forward speed is given by $K\mathrm{v}$.

In Eq. (6.9) $\beta$, $\gamma$, $\chi$ refer to the hydrodynamic angles, defined by:

$$\beta = \arctan\left(\frac{-v}{u}\right) \tag{6.10}$$

$$\gamma = \arctan\left(\frac{v_P}{u}\right) \tag{6.11}$$

$$\chi = \arctan\left(\frac{v_P}{v}\right) \tag{6.12}$$

The eighteen terms (e.g. $X'^{(\beta)}$ and $N'^{(\gamma)}$) in Eq. (6.9) are tabular coefficients expressed as functions of the hydrodynamic angles. They express phenomena such as lift, drag, and cross flow effects which are relevant for the horizontal forces. The roll $K'^{(\beta)}$, $K'^{(\gamma)}$, $K'^{(\chi)}$ and yaw $N'^{(\beta)}$, $N'^{(\gamma)}$, $N'^{(\chi)}$ moments are functions of the sway forces $Y'^{(\beta)}$, $Y'^{(\gamma)}$, $Y'^{(\chi)}$ and the respective positions of the application points (which are expected to change during manoeuvre). Similarly, the pitch moment $M'$ is a function of the surge ($X'$) and vertical ($Z'$) forces. Notices that the force $Z'$ will be the result of the projection in the vertical direction of the forces due to the pressures caused by the horizontal velocities on the hull surface.

To have a better idea of these parameters, in Figure 6.5 to Figure 6.7, result for surge, sway forces and yaw moments are presented as functions of their respective hydrodynamic angles. Three different water depths have been considered corresponding to deep, shallow and very shallow water. The results shown in here correspond to the test program 2016 described in Chapter 4.

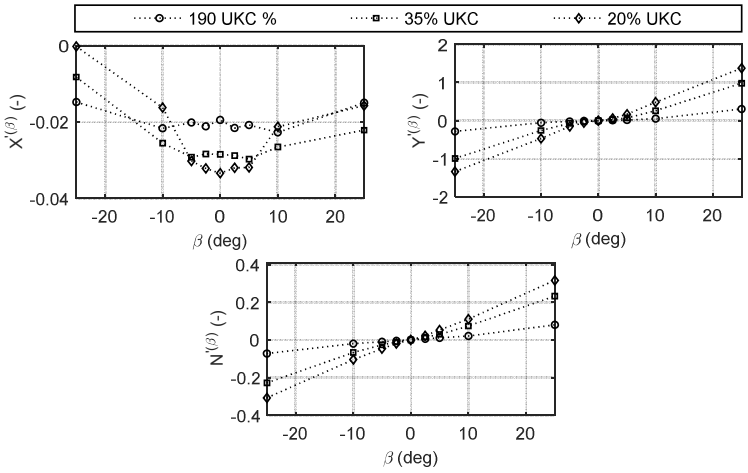


Figure 6.5 Surge $X'^{(\beta)}$ (top left), sway $Y'^{(\beta)}$ (top right) forces and yaw $N'^{(\beta)}$ (bottom) moment coefficients as function of the hydrodynamic angle $\beta$ for the C0W container ship model at three different UKC, at $T_M = 15.2$ m.

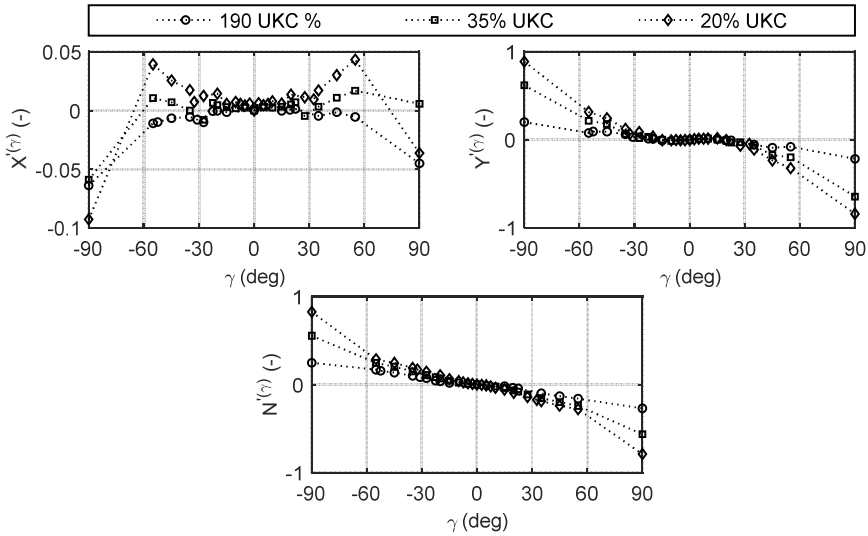


Figure 6.6 Surge $X'^{(\gamma)}$ (top left), sway $Y'^{(\gamma)}$ (top right) forces and yaw $N'^{(\gamma)}$ (bottom) moment coefficients as function of the hydrodynamic angle $\gamma$ for the C0W container ship model at three different UKC, at $T_M = 15.2$ m.

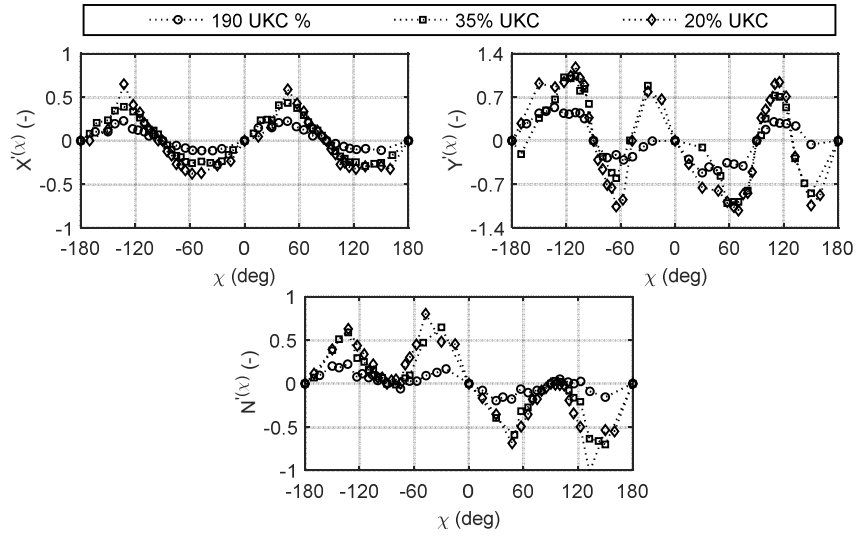


Figure 6.7 Surge $X'^{(\chi)}$ (top left), sway $Y'^{(\chi)}$ (top right) forces and yaw $N'^{(\chi)}$ (bottom) moment coefficients as function of the hydrodynamic angle $\chi$ for the C0W container ship model at three different UKC, at $T_M = 15.2$ m.

From the figures one can observe the relative small magnitude of the $X'$ coefficients. It seems then reasonable to assume that $X'$ forces coupled into $M'$ would yield a negligible trim compared to squat effects, see e.g. Figure 5.18 to Figure 5.20. Since the forces $X'$ are small and they are the result of the projection of the local hull forces on the longitudinal direction, there is no reason to believe that the vertical projection (the forces in $Z'$) should be significant, this in turns indicates that the total moments in $M'$ should be small as well.

Because of the small order of magnitudes of the forces $Z'$ and moments $M'$ and the large mass and longitudinal moment of inertia properties of the ship, it is reasonable to think that the induced sinkage and trim would be negligible. In any case, it is not possible to separate them from squat effects. In the present work, these forces $Z'$ and moments $M'$ are r assumed to be accounted for by squat effects.

It is important to mention that in the previous discussion in 5.1, it has been observed that forces and moments in calm water do not necessarily remain proportional to the square of the speed as proposed in Eq. (6.9). Slight variation in the coefficients could be obtained if only very low speeds are considered in their estimations. This was also seen in the study conducted in Vantorre and Eloot (1996), where for Froude numbers $F_r = 0.0173$ in contrast to larger ones a slight variation was observed.

The variation of this coefficient as a function of the square of the speed can be better understood if one considers the nature of the flow. For instance, notice that for a ship moving at a large drift angle, resembles a blunt body, for such shapes at very low speeds viscous forces are dominant but at larger speeds flow separation will occur and the pressure gradient will become more important. Because the present study is restricted to manoeuvres, such as when approaching a port, very low speeds are not the main concern, hence Eq. (6.9) remains suitable for the present study.

#### 6.3.2.1.1 Squat effects

Taking into account squat effects in Eq. (6.9) requires a careful distinction with respect to the definition the vertical coordinate, which is used as well for the estimation of restoring forces and moments. Experimental results show that during squat the ship attains a new position and orientation, but no change is observed in the ship's displacement. This is because, during squat, the water level along the hull drops as well.

Considering squat, sinkage and trim in Eq. (6.10) would require as well to model the exact water profile along the hull. This, however, is a more difficult task to achieve, if not accounted for correctly, hydrostatic forces will then compensate the new ship's position resulting in an unbalance between the ships displacement and buoyancy terms. For this reason, in the present work, squat effects will not be considered as an external force in Eq. (6.9), instead they will be addressed as a reduction of the water depth.

Squat has been investigated in 5.2.4 where semi captive tests were found to provide better estimations of the sinkage and trim. Moreover, their evaluations were found to be more practical by simply letting the ship free to sink and trim. For this reason, the present study will consider the simplified model as given by Tuck (1966).

$$Z'^{(\beta)} = z_{LCF}\frac{\mathrm{L}_{PP}^2}{\nabla T u_h} \tag{6.13}$$

$$M'^{(\beta)} = \theta_{LCF}\frac{\mathrm{L}_{PP}^3}{\nabla T u_h} \tag{6.14}$$

Examples of these coefficients for the results, presented in 5.2.4, are displayed in Figure 6.8. According to Tuck (1966) and Gourlay (2008), $Z'^{(\beta)}$ and $M'^{(\beta)}$ should be constant in open water and are only dependent on the ship's hull characteristics, which define the flow behaviour along the ship.

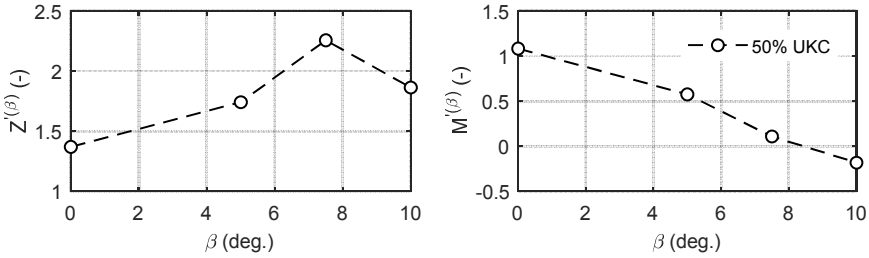


Figure 6.8 Squat sinkage $Z'^{(\beta)}$ (left) and trim $M'^{(\beta)}$ (right) coefficients as function of the hydrodynamic angle $\beta$ for the C0W container ship model at 50% UKC, ship's draught $T_m = 13.1$ m.

#### 6.3.2.1.2 Roll damping

The viscous roll moment $K_V$ presented in Eq. (6.9) can be obtained from the study of free decay tests. An example of such tests conducted with the C0W ship model are presented in Figure 6.9. Results obtained from two different tests conducted at 190% UKC and 20% UKC are presented.

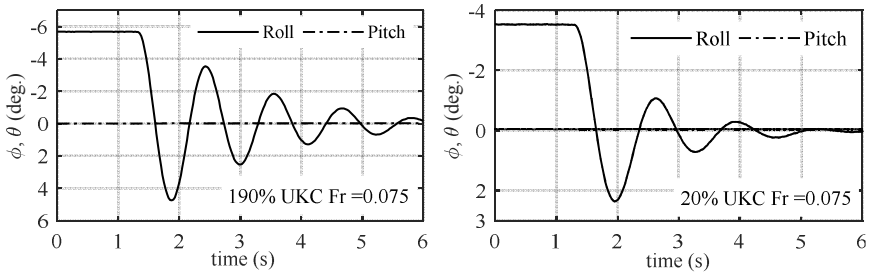


Figure 6.9 Example of roll and pitch motion at two different UKC at 190% UKC (left) and at 20% UKC (right), both results obtained at $F_r = 0.075$ for the C0W container ship model, ship's draught $T_m = 13.1$ m (full scale).

In general, the analysis of the roll viscous moment is conducted with a one degree of freedom (1DOF) model in the frequency domain. For this purpose, a constant potential added mass and damping coefficient obtained at the roll natural frequency are used. Taking into account these constraints of the analysis, analytical solutions are obtained from roll decay test results.

The analytical solution provides an equivalent linear viscous damping, which is best suited at the roll natural frequency only.

This is very convenient from the point of view of seakeeping studies which allows estimating roll responses in any given seas. Notice that if a nonlinear viscous roll damping is introduced spectral analysis in seakeeping studies could not be used.

Nevertheless the analysis in 1DOF, in the frequency domain, provides an analytical solution which is relatively simple and might provide acceptable results. The linear damping cannot be applied to real time simulations; a nonlinear approach for roll will be required. For this purpose, in the present study, the viscous contribution $K\mathrm{v}$ has been replaced by a linear $K\mathrm{v}_p$ and nonlinear $K\mathrm{v}_{p|p|}$ terms as suggested by Ikeda et al. (1977) and Himeno (1981).

$$K\mathrm{v} = K\mathrm{v}_p p + K\mathrm{v}_{p|p|} p|p| \tag{6.15}$$

where $p$ is the roll angular velocity.

To solve this problem, one cannot directly apply the frequency domain analysis any longer, instead the time domain approach is needed. For this purpose, the constant added inertia and damping coefficients assumed in the frequency domain studies require to be converted to their respective time domain responses, given by the impulse response function (IRF) $k_p$ and the infinite frequency limit for added inertia terms $k_{\dot{p}}^{\infty}$ , see Cummins (1962).

The $k_p$ and $k_{\dot{p}}^{\infty}$ parameters have been computed with the numerical software Hydrostar for the C0W container ship model at four different UKC, 190%, 35%, 20%, and 10%. The respective values for $k_{\dot{p}}^{\infty}$ are $k_{\dot{p}}^{\infty} = 42\%, 74\%, 100\%$ and 147% of the moment of inertia $I_{xx}$, and the IRF $k_p$ are shown in Figure 6.10.

The importance of the time domain representation from the point of view of the infinite added inertial term $k_{\dot{p}}^{\infty}$ and the incorporation of the impulse response function $k_p$ cannot be neglected. This is the case, especially, when shallow water is taken into account. From Figure 6.10 this is observed where the magnitudes of these functions increase as the UKC decreases.

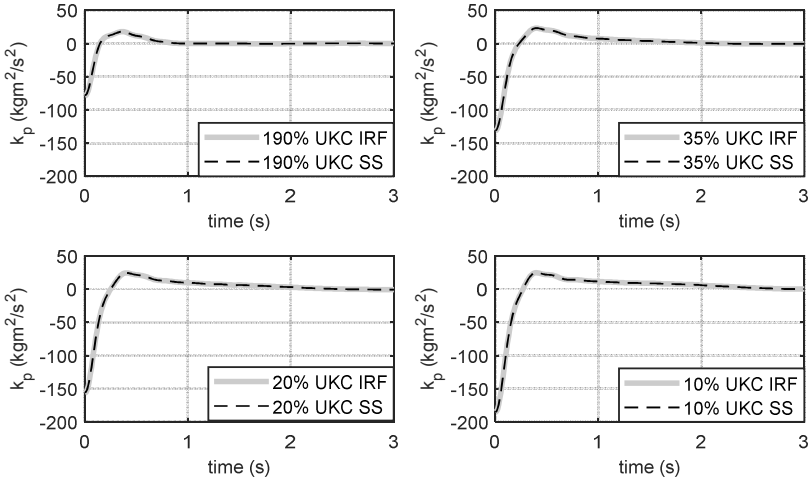


Figure 6.10 Roll impulse response function $k_p$ and its respective state space representation for four UKC obtained with Hydrostar for the C0W container ship model, ship's draught $T_m = 13.1$ m (full scale).

To proceed further with the analysis, the following 1DOF time domain model has been chosen:

$$K\mathrm{v} = \left(I_{xx} + k_{\dot{p}}^{\infty}\right)\dot{p} + K\mathrm{v}_p p + K\mathrm{v}_{p|p|} p|p| + \int_{-\infty}^{\infty} k_p(t-\tau)p(\tau)d\tau + C_{44}\phi \tag{6.16}$$

where, $C_{44}$ is the roll restoring coefficient given in Table 6.1.

Table 6.1 Ship's roll restoring coefficients at model scale.

| Item | Value | Units |
|---|---|---|
| $C_{44}$ | 360.4 | $Nm$ |

To obtain the viscous linear $K\mathrm{v}_p$ and nonlinear $K\mathrm{v}_{p|p|}$ coefficients, a nonlinear least square regression has been applied with the roll response obtained from the solution of Eq. (6.16) and results from experiments. To simplify the analysis, a state space representation of the convolution integral in Eq. (6.16) has been used. The state space fitting have been plotted in Figure 6.10 for comparison. Details on state space model can be found in Tello Ruiz et al. (2014).

Free decay tests have been performed for the four different UKC mentioned above, UKC, 190%, 35%, 20%, and 10%, see Chapter 4 for more detail on the experiments. Results obtained for the linear $Kv_p$ and nonlinear $Kv_{p|p|}$ coefficients are presented in Figure 6.11.

From Figure 6.11 it can be observed that the magnitudes for the nonlinear term $Kv_{p|p|}$ are very small, this in contrast to the linear terms. It can be also seen that the linear terms $Kv_p$ appears to be speed dependent.

In the case of relatively deep water, 190% UKC, a simplified model can be provided by a linear fitting given by:

$$Kv = Kv_p^* p + Kv_{up} up + Kv_{p|p|} p|p| \tag{6.17}$$

where $Kv_p^*$ and $Kv_{p|p|}$ are proportional to the roll angular velocity $p$, and $Kv_{up}$ in addition is also proportional to the longitudinal speed $u$. Despite the smaller values of $Kv_{p|p|}$ observed in Figure 6.11, this nonlinear term has been hold because it is believed to be important when larger initial heel angles are tested. Notice that during the tests the maximum initial heel angle was set at 6 deg.

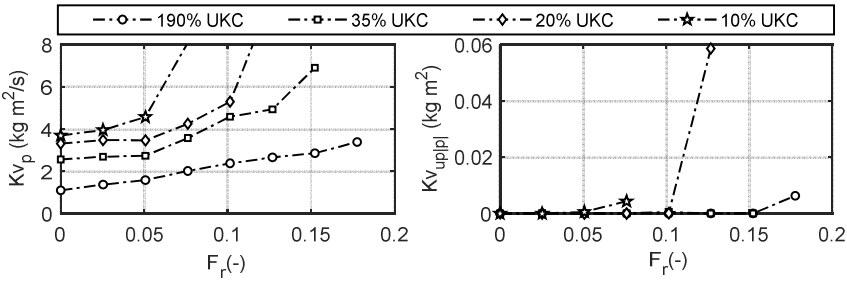


Figure 6.11 Linear $Kv_p$ (left) and nonlinear $Kv_{p|p|}$ (right) viscous damping coefficients for four different UKC obtained from tests with the C0W container ship model, ship's draught $T_m = 13.1$ m.

The study with a 1DOF model in the time domain can be considered as satisfactory if one takes into account for small roll angles only, for larger angles this model is no longer suitable because coupling between sway and roll will become more important. Recall that a pure roll motion does never occur and due

to bow-stern asymmetry of the hull, sway forces will be always present.

Taking into account larger roll angles, e.g. $\phi > 6$ degrees, nonlinear terms on $C_{44}$ will be introduced as well. This highly nonlinear analysis would be important for manoeuvring as well, especially for rounded midship section shape. This analysis is very important but is not discussed in the present work.

The study of the linear and nonlinear terms for the viscous roll moments in waves has not been conducted in the present study. It is believed, that waves would influence significantly the roll viscous contribution because vertical velocities of water particles (induced by the wave motion on the water surface) near the hull will be affected by the presence of the waves.

#### 6.3.2.2Body reaction forces ideal fluids

It has been discussed in Chapter 2 that the forces and moments on a body moving in an ideal fluid can be expressed differently, depending on the nature of the problem. For manoeuvring in calm water mostly acceleration terms are accounted for, terms related to velocities are neglected or assumed already included in other fluid phenomena. In seakeeping studies, because of the free surface, the wave generation problem is important, apart from acceleration terms, velocity terms are also incorporated.

For a ship moving with arbitrarily motions on the free surface, the resulting set of equations describing the ideal fluid forces are highly nonlinear (see Chapter 2), even when taking into account the ship's $xz$ −plane of symmetry. Important simplifications can be achieved if one recalls that the ship's oscillatory motions are small. Nonlinear terms of second order such as $\Omega \times \frac{\partial T}{\partial U}$, $\Omega \times \frac{\partial T}{\partial \varpi}$ and $U \times \frac{\partial T}{\partial U}$ (where $V$ and $\Omega$ are the linear and angular velocity of the b-frame, and $T$ is kinetic energy of the fluid associated to the potential flow $\phi$, see chapter 2 ), resulting from the translation and rotation of the b-frame, can be neglected.

The ideal fluid forces and moments, following the studies of Cummins (1962), Bishop et al. (1973) and Bailey et al. (1998), become then linear, and are given by:

$$\boldsymbol{F_{id}} = [\boldsymbol{X_{id}}\ \boldsymbol{Y_{id}}\ \boldsymbol{Z_{id}}\ \boldsymbol{K_{id}}\ \boldsymbol{M_{id}}\ \boldsymbol{N_{id}}]^T = \boldsymbol{A}\ddot{\boldsymbol{X}} + \boldsymbol{B}\dot{\boldsymbol{X}} + \int_{-\infty}^{+\infty} \boldsymbol{H^V}(\boldsymbol{t}-\boldsymbol{\tau})\,\dot{\boldsymbol{X}}(\boldsymbol{\tau})\boldsymbol{d\tau} \quad (6.18)$$

where $\boldsymbol{A}$ and $\boldsymbol{B}$ are constant added inertia and damping coefficients matrices, respectively. $\dot{\boldsymbol{X}}$ is the matrix of ship velocities and $\boldsymbol{H}$ is the matrix impulse response functions. These set of matrices are respectively given by:

$$\boldsymbol{A} = \begin{bmatrix} \tilde{X}_{\dot{u}}(\infty) & 0 & \tilde{X}_{\dot{w}}(\infty) & 0 & \tilde{X}_{\dot{q}}(\infty) & 0 \\ 0 & \tilde{Y}_{\dot{v}}(\infty) & 0 & \tilde{Y}_{\dot{p}}(\infty) & 0 & \tilde{Y}_{\dot{r}}(\infty) \\ \tilde{X}_{\dot{w}}(\infty) & 0 & \tilde{Z}_{\dot{w}}(\infty) & 0 & \tilde{Z}_{\dot{q}}(\infty) & 0 \\ 0 & \tilde{Y}_{\dot{p}}(\infty) & 0 & \tilde{K}_{\dot{p}}(\infty) & 0 & \tilde{K}_{\dot{r}}(\infty) \\ \tilde{X}_{\dot{q}}(\infty) & 0 & \tilde{Z}_{\dot{q}}(\infty) & 0 & \tilde{M}_{\dot{q}}(\infty) & 0 \\ 0 & \tilde{Y}_{\dot{r}}(\infty) & 0 & \tilde{K}_{\dot{r}}(\infty) & 0 & \tilde{N}_{\dot{r}}(\infty) \end{bmatrix} \quad (6.19)$$

$$\boldsymbol{B} = \begin{bmatrix} \tilde{X}_{u}(\infty) & 0 & \tilde{X}_{w}(\infty) & 0 & \tilde{X}_{q}(\infty) & 0 \\ 0 & \tilde{Y}_{v}(\infty) & 0 & \tilde{Y}_{p}(\infty) & 0 & \tilde{Y}_{r}(\infty) \\ \tilde{X}_{w}(\infty) & 0 & \tilde{Z}_{w}(\infty) & 0 & \tilde{Z}_{q}(\infty) & 0 \\ 0 & \tilde{Y}_{p}(\infty) & 0 & \tilde{K}_{p}(\infty) & 0 & \tilde{K}_{r}(\infty) \\ \tilde{X}_{q}(\infty) & 0 & \tilde{Z}_{q}(\infty) & 0 & \tilde{M}_{q}(\infty) & 0 \\ 0 & \tilde{Y}_{r}(\infty) & 0 & \tilde{K}_{r}(\infty) & 0 & \tilde{N}_{r}(\infty) \end{bmatrix} \quad (6.20)$$

$$\dot{\boldsymbol{X}} = [u \quad v \quad w \quad p \quad q \quad r]^T \quad (6.21)$$

$$\boldsymbol{H^V} = \begin{bmatrix} x_u^V & 0 & x_w^V & 0 & x_q^V & 0 \\ 0 & y_v^V & 0 & y_p^V & 0 & y_r^V \\ z_u^V & 0 & z_w^V & 0 & z_q^V & 0 \\ 0 & k_v^V & 0 & k_p^V & 0 & k_r^V \\ m_u^V & 0 & m_w^V & 0 & m_q^V & 0 \\ 0 & n_v^V & 0 & n_p^V & 0 & n_r^V \end{bmatrix} \quad (6.22)$$

The matrices $\boldsymbol{A}$, $\boldsymbol{B}$ and $\boldsymbol{H}$ are symmetric, see for instance $x_w = z_u$, $y_p = k_v$.

Equations (6.19) to (6.22) introduce to what is known as memory terms. This type of representation follows the extensive studies of Cummins (1962) and Bishop et al. (1973), on the independent fields of seakeeping and manoeuvring, respectively.

It should be stressed that the infinite values for $\boldsymbol{A}$ matrix in Eq. (6.19) should not be related to the ones as observed in seakeeping or to the ones from calm water manoeuvring studies, where frequency depended coefficients are used in the first, while a zero frequency constant value is used in the second. According to Cummins (1962) and Bishop et al. (1973) the seakeeping and manoeuvring coefficients are only a result of the simplification of Eq. (6.18) where $\dot{\boldsymbol{X}}$ is considered harmonically changing with time or constant.

An extensive discussion on these relationships for calm water manoeuvring added inertia terms was presented in Bishop et al. (1973), and subsequent works, Bishop et al. (1977) and Bishop et al. (1984). Their analysis and the study of Cummins (1962), however, did not provide any means of computing $\boldsymbol{H}$. In Ogilvie (1964) such relationships were investigated and a method to numerically compute $\boldsymbol{H}$ based on the frequency dependent coefficients obtained in seakeeping was proposed.

It is important to mention that in Ogilvie (1964) relationships are defined in the h-frame because the radiation problem is addressed from the point of view of seakeeping studies. Recall that Eq. (6.18) is defined in the b-frame, hence, transformations of the Ogilvie relationships are then required first in order to compute them in the b-frame. The investigation of this topic is extensively discussed in Chapter 7.

In Chapter 7, apart from the transformation of the axes, the IRF $\boldsymbol{H^V}$ defined in Eq. (6.19) has been split in two sub components, one constant function $\boldsymbol{H}$ independent of the forward speed and another one $\boldsymbol{H}^*$ proportional to the forward speed only.

$$\boldsymbol{H^V} = \boldsymbol{H}^* \boldsymbol{f}(\boldsymbol{V}) + \boldsymbol{H} \tag{6.23}$$

where $\boldsymbol{f}(\boldsymbol{V})$ describes the different relationships for each degree of freedom. See Chapter 7 for more detail.

Examples of the impulse response function are presented in Figure 6.12, Figure 6.13, and Figure 6.14. The numerical results have been computed with Hydrostar. The first plots present the results for the speed proportional function $\boldsymbol{H}^*$, while the second and third display the results for the constant functions $\boldsymbol{H}$. Notice that in Figure 6.12 to Figure 6.14, the state space representation has been also displayed, for illustration purposes.

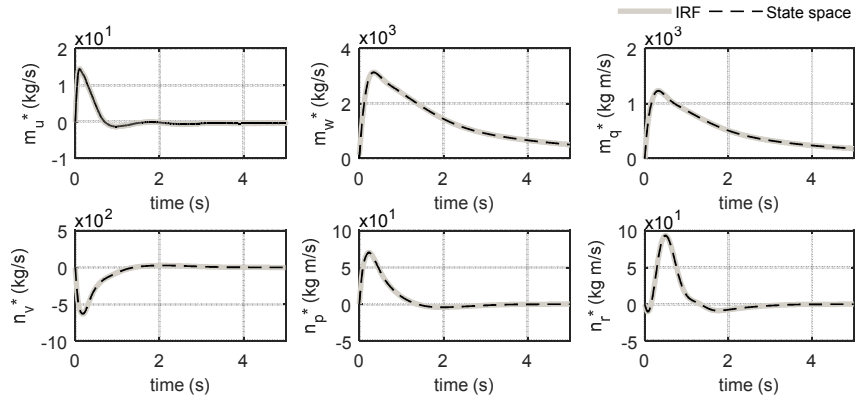


Figure 6.12 Pitch (top) and yaw (bottom) impulse response function (IRF) proportional to speed $V$ for the C0W container ship model, at 50% UKC, ($T_M = 13.1$ m at full scale). IRF shown in continuous grey line and state space representation in black dashed line.

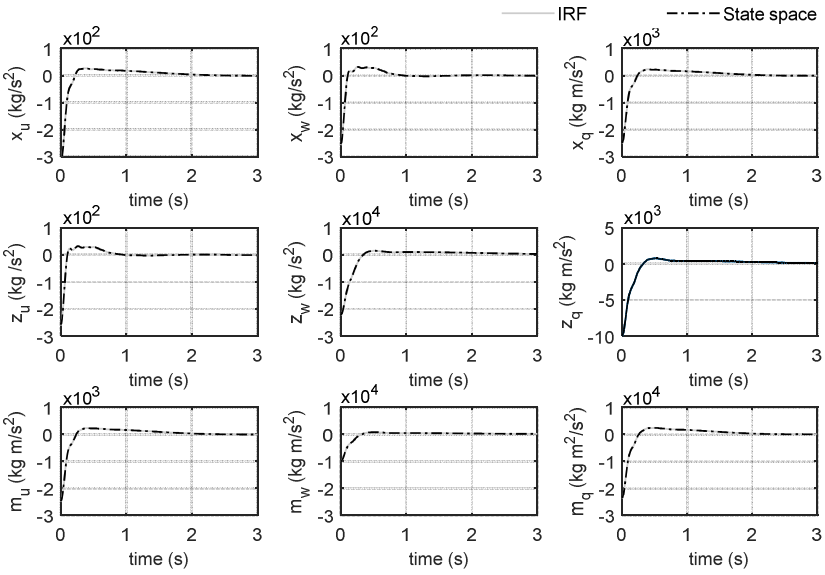


Figure 6.13 Speed independent impulse response function (IRF) for surge (top), heave (mid), and pitch (bottom) for the C0W container ship model at 50% UKC ($T_M = 13.1$ m at full scale). IRF shown in continuous grey line and state space representation in black dashed line.

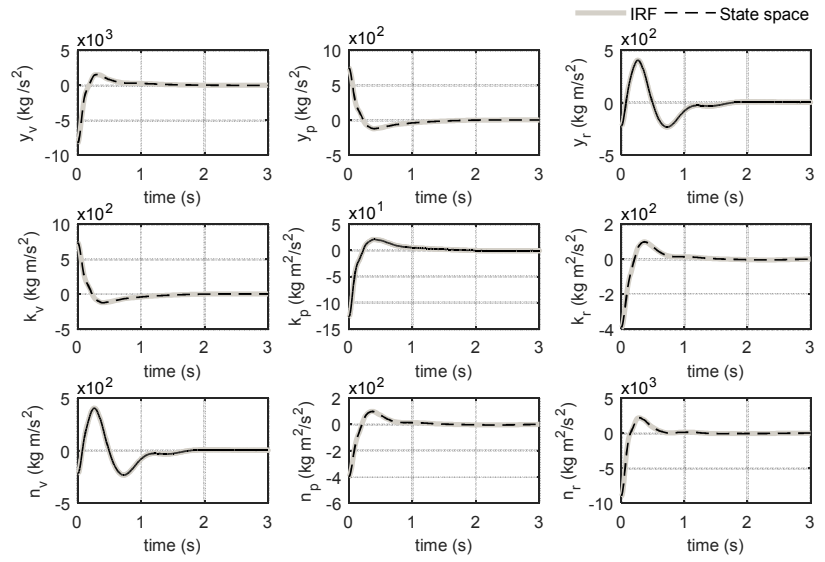


Figure 6.14 Speed independent impulse response function (IRF) for sway (top), roll (mid), and yaw (bottom) for the C0W container ship model, at 50% UKC ($T_M = 13.1$ m at full scale). IRF shown in continuous grey line and state space representation in black dashed line.

### 6.3.3 Wave forces

It has been observed in the discussion of experimental results in Chapter 5, that the superposition of wave forces to the manoeuvring forces can be applied under certain restrictions, e.g. for shorter wave lengths than the ship length, and smaller wave amplitudes. Bearing in mind these considerations wave forces on manoeuvring ships can be treated in a similar way as in seakeeping studies, as presented earlier in Eq. (6.7). Forces can be subdivided in three main components, the diffraction forces $F_D$, the Froude-Krylov forces $F_{FK}$, and the mean second order wave forces $F_{2nd}$. The first two are also known as the first order wave forces.

A discussion on their incorporation in the manoeuvring analysis will be presented in the following subsection. For better insight on the common approach in the assessment of each force see Chapter 2, and Chapter 7 for a modified analysis of the Froude-Krylov forces $F_{FK}$.

#### *6.3.3.1First order wave forces*

The first order wave forces $F_j^h$ on the ship can be written as the contribution of the diffraction forces $F_{Dj}^h$ and the Froude-Krylov forces $F_{FKj}^h$.

$$\boldsymbol{F_j^h = F_{Dj}^h + F_{FKj}^h} \tag{6.24}$$

The superscript $h$ indicates the frame of reference in which the forces are expressed. The subscript $j$ stands for the force component index, $j = 1,2,3$ for forces in surge, sway and heave and $j = 4,5,6$ for moments in roll, pitch and yaw, respectively.

Both forces result from the integration of the pressure on the hull surface due to the diffraction potential $\phi_D$ and incident wave potential $\phi_I$ . For an infinitesimal manoeuvring trajectory (rectilinear), they are given by:

$$\boldsymbol{F_{Dj}^h} = \left( -\rho \iint\limits_{S_0} \boldsymbol{n_j} \left( i\omega - V \frac{\partial}{\partial x} \right) \phi_D ds \right) \zeta_a e^{i\omega t} \tag{6.25}$$

$$\boldsymbol{F_{FKj}^{h}} = \left( -\rho \iint\limits_{S_0} \boldsymbol{n_j} \left( i\omega - V \frac{\partial}{\partial x} \right) \phi_I ds \right) \zeta_a e^{i\omega t} \tag{6.26}$$

$n_j$ is the normal vector to the differential surface $ds$, $\zeta_a$ is the wave amplitude, $\omega$ is the encounter frequency, $V$ is the ship forward speed, and $\rho$ is the water density. $S_0$ is the mean wetted surface.

Equation (6.26) can be further simplified by taking into account the incident wave potential, and the frequency of wave encounter which are defined by:

$$\phi_I = \frac{ig\zeta_a}{\omega_0} \frac{\cosh k(z+h)}{\cosh kh} e^{-i(kxcos\mu - kysin\mu)} \tag{6.27}$$

$$\omega = \omega_0 - kVcos\mu \tag{6.28}$$

Taking the partial derivative $\frac{\partial \phi_I}{\partial x}$, and the frequency of wave encounter relationship Eq. (6.28) in Eq. (6.26), yields:

$$\boldsymbol{F_{FKj}^{h}} = \left( -\rho i\omega_0 \iint\limits_{S_0} n_j \phi_I ds \right) \zeta_a e^{i\omega t} \tag{6.29}$$

The terms in parenthesis in Eq. (6.25) and Eq. (6.29) provide the means to compute the amplitude and phase of the first order forces over an infinitesimal manoeuvring trajectory. The term $e^{i\omega t}$ in both equations, however, requires further considerations. From Eq.(6.28), the expression $\omega t$ can be written as well as:

$$\omega t = \omega_0 t - k(X_0 cos\eta - Y_0 sin\eta) \tag{6.30}$$

where $\eta$ is the wave angle defined in the E-frame, see Chapter 2 for its definitions.

The right hand side from Eq. (6.30) should be used in Eq. (6.25) and Eq. (6.29) instead of $\omega t$. This is because $\omega$ will constantly change due to the change in ship's heading, consequently changing $\mu$ as well. It is important to recall that the right hand side terms in Eq. (6.30) are the arguments of the wave profile, see equation below:

$$\zeta = -\frac{1}{g}\frac{\partial\,\phi_I}{\partial t} = \zeta_a e^{-i(kX_0 cos\eta - kY_0 sin\eta - \omega_0 t + \alpha_W)}; \qquad at\ z = Z_0 = 0 \qquad (6.31)$$

The phase $\alpha_W$ has been introduced assuming the wave profile has an initial phase angle at t=0, and location $X_0 = Y_0 = 0$.

In order to incorporate the diffraction forces and the Froude-Krylov forces in the manoeuvring equation, they require first an axes transformation from the h-frame to the b-frame. This is achieved by the following relationships:

$$\boldsymbol{F_{Dj}^{b}} = R^{-1}(\Xi)R^{*}F_{Dj}^{h} \qquad (6.32)$$

$$\boldsymbol{F_{FKj}^{b}} = R^{-1}(\Xi)R^{*}\,F_{FKj}^{h} \qquad (6.33)$$

where $R_b^h(\Xi)$ is the rotation matrix from the b-frame to the h-frame, and $R^*$ is a matrix transforming the upright coordinates defined in seakeeping to the NED reference. They are given by:

$$\boldsymbol{R_b^h(\Xi)} = \begin{bmatrix} 1 & -\xi_6 & \xi_5 \\ \xi_6 & 1 & -\xi_4 \\ -\xi_5 & \xi_4 & 1 \end{bmatrix} \qquad (6.34)$$

$$R^{*} = \begin{bmatrix} 1 & 0 & 0 \\ 0 & -1 & 0 \\ 0 & 0 & -1 \end{bmatrix} \qquad (6.35)$$

$\xi_4, \xi_5, \xi_6$ , are the ship's roll, pitch and yaw, respectively, as observed from the h-frame.

#### 6.3.3.1.1 Tabular approach

$F_{Dj}^{h}$ and $F_{FKj}^{h}$ can be directly obtained from numerical potential software developed for seakeeping. A four dimension tabular function can be arranged such as:

$$\boldsymbol{F_{Dj}^{h}} = f_D(\omega_0\,, \mu, V, h) \qquad (6.36)$$

$$\boldsymbol{F_{FKj}^{h}} = f_{FK}(\omega_0\,, \mu, V, h) \qquad (6.37)$$

In practice, in coastal zones, the ship manoeuvres in access channels where the water depth will not change considerable.

Hence, once $h$ has been established, the number of interpolation parameters could be reduced by disregarding its effect for wave forces and moments only. With respect to the ship's forward speed $V$, although in waves it is expected to decrease, experimental results presented in section 5 show that the variation of forces in waves and in calm water can be less significant for the range of speeds considered in the present study. Thus, $V$ can be assumed to remain constant during the entire simulation for the estimation of wave forces and moments, which in turn could decrease significantly computing times.

#### 6.3.3.1.2 Nonlinear approach

The forces computed in Eq. (6.25) to Eq. (6.29) are regarded as linear because of their evaluation over the constant mean wetted surface $S_0$. A nonlinear approach can be used instead, by replacing $S_0$ by the actual wetted surface $S$. This approach is difficult to apply for the diffraction problem as it will require the evaluation of the $\phi_D$ on the constantly changing wetted surface. For the Froude-Krylov forces this task is relatively simpler to achieve, this is because $\phi_I$ is independent of the boundary value problem on the hull surface.

Keeping the diffraction forces as linear, a nonlinear analysis can be conducted by introducing the modification of the wetted surface only in the estimation of the Froude-Krylov forces. This approach has been conducted in the present work.

The Froude-Krylov force defined in Eq. (6.29) requires first to be redefined. For this purpose, recall that $\phi_I$ in Eq. (6.29) is defined in the $h$-frame, see Eq. (6.27), and that in $x$-axis of the $h$-frame, the following relationships hold true:

$$x = x_0 - Vt \qquad y = y_0 \tag{6.38}$$

Replacing these relationships in Eq. (6.29), and taking into account the frequency of wave encounter defined in Eq. (6.28), $F_{FKj}^h$ can be written as:

$$F_{FKj}^{h} = \rho \iint_{S} \boldsymbol{n_j} g\zeta_a \frac{\cosh k(z+h)}{\cosh kh} e^{-i(kx_0 cos\mu - ky_0 sin\mu - \omega_0 t + \alpha_W)} ds \tag{6.39}$$

Rewriting the above equation in the E-frame:

$$F_{FKj}^{E} = \iint_{S} \boldsymbol{N_j} \rho g\zeta_a \frac{\cosh k(z+h)}{\cosh kh} e^{-i(kX_0 cos\eta - ky_0 sin\eta - \omega_0 t + \alpha_W)} ds \tag{6.40}$$

In here, the normal vector $n_j$ defined in the $h-$frame has been replaced by the normal vector $N_j$ defined in the $E-$frame, and takes the form of:

$$\boldsymbol{N_j} = \begin{cases} \boldsymbol{N_j}, & j = 1,2,3 \\ \left(\boldsymbol{r_{O/O_0}} - \boldsymbol{r_{O'/O_0}}\right) \times \boldsymbol{N_i} & j = 4,5,6 \ ; i = j-3 \end{cases} \tag{6.41}$$

in here $N_j$, where j=1,2,3 refer to the directions in the $X_0$,$Y_0$, and $Z_0$ axes respectively. The notation employed in here, for instance for relative position $\boldsymbol{r_{O'/O_0}}$ (see also chapter 2) should be understood as the position of the point $O'$ with respect to the origin $O_0$.

Recalling that the wave dynamic pressure is given by:

$$p_W = \rho g\zeta_a \frac{\cosh k(z+h)}{\sinh kh} e^{-i(kX_0 cos\eta - kY_0 sin\eta - \omega_0 t + \alpha_W)} \tag{6.42}$$

Equation (6.40) can be expressed in a more compact form as:

$$\boldsymbol{F_{FKj}^{E}} = \iint_{S} \boldsymbol{N_j} p_W ds \tag{6.43}$$

Equation (6.43) can be then transformed in the b-frame by the following rotations:

$$F_{FKj}^{b} = R^{-1}(\Theta^*) R^{-1}(\Psi) R^* F_{FKj}^{E} \tag{6.44}$$

where $R_h^E(\Psi)$ is rotation matrix from the h-frame to the E-frame, and $R_h^b(\Theta^*)$ is the linear rotation matrix from the $h-$frame to the $b-$frame. These matrices are:

$$R_h^E(\Psi) = \begin{bmatrix} 1 & -sin\overline{\psi} & 0 \\ sin\overline{\psi} & ccos\overline{\psi} & 0 \\ 0 & 0 & 1 \end{bmatrix} \tag{6.45}$$

$$R_h^b(\Theta^*) = R_b^h(\Xi) \tag{6.46}$$

$R^*$ has been defined earlier in Eq. (6.35).

The variable $\overline{\psi}$ is the mean heading angle of the ship, which can be considered equal to $\psi$.

The current nonlinear approach does not extend only to the Froude Krylov forces, the hydrostatic forces can be already incorporated in the nonlinear analysis by modifying the pressure in Eq. (6.43) as:

$$p = p_W + p_H \tag{6.47}$$

where $p_H$ is given by:

$$p_H = \rho g(\zeta - Z_{c/O}) \tag{6.48}$$

in here, $\zeta$ and $Z_{c/O}$ are respectively the vertical coordinates of the wave profile and the panel surface for a given $X_0$, and $Y_0$, position; The notation employed for vertical coordinates $Z_{c/O}$ refer to the position of the panel centroid $c$ with respect to the Earth-frame's origin $O$.

When incorporating the hydrostatic forces, the forces and moments due to gravity and location of the ship mass in the ship should be accounted by:

$$\boldsymbol{F_G^E} = R^{-1}(\Theta^*)R^{-1}(\Psi)R^*\rho\boldsymbol{g}\nabla \tag{6.49}$$

$$\boldsymbol{M_G^E} = (\boldsymbol{r_{O/O_0}} - \boldsymbol{r_{O'/O_0}}) \times \boldsymbol{F_G^E} \tag{6.50}$$

The major challenge in estimating the nonlinear Froude-Krylov forces, and also the hydrostatic forces, are with respect to the numerical evaluation of the actual wetted surface $S$. An approach has been developed in the present study to compute the actual $S$ each time step, this has been extensively discussed in Chapter 7.

### *6.3.3.1Wave forces in irregular waves*

In an irregular wave system, where the wave profile $\zeta$ at a given location is expressed as function of a $N$ number components by:

$$\zeta = \sum_{n=1}^{n=N} \zeta_{a_n} e^{-i(k_n X_0 cos\eta_n - kY_0 sin\eta_n - \omega_{0_n} t + \alpha_{W_n})} \tag{6.51}$$

The diffraction forces and Froude-Krylov forces can be obtained by the superposition of each individual component. This can be expressed as:

$$\boldsymbol{F_{Dj}^h} = \sum_{n=1}^{n=N} \boldsymbol{F_{Dj_n}^h} \tag{6.52}$$

$$\boldsymbol{F_{FKj}^h} = \sum_{n=1}^{n=N} \boldsymbol{F_{FKj_n}^h} \tag{6.53}$$

The respective axes transformations, as presented in Eq. (6.32) and Eq. (6.44), are yet necessary before accounting for these forces in the manoeuvring equation.

### *6.3.3.2Second order wave forces*

The second order wave forces in shallow water $\boldsymbol{F_{2nd}}$ can be computed for all six forces and moments by the following expressions:

$$X_{2nd} = 2 \int_{-\pi}^{-\pi} \int_{0}^{\infty} \frac{X_D(V, \omega_0, \mu)}{\zeta_a^2} S_\zeta(\omega_0, \mu) d\omega_0 d\mu \tag{6.54}$$

$$Y_{2nd} = 2 \int_{-\pi}^{-\pi} \int_{0}^{\infty} \frac{Y_D(V, \omega_0, \mu)}{\zeta_a^2} S_\zeta(\omega_0, \mu) d\omega_0 d\mu \tag{6.55}$$

$$Z_{2nd} = 2 \int_{-\pi}^{-\pi} \int_{0}^{\infty} \frac{Z_D(V, \omega_0, \mu)}{\zeta_a^2} S_\zeta(\omega_0, \mu) d\omega_0 d\mu \tag{6.56}$$

$$K_{2nd} = 2 \int_{-\pi}^{-\pi} \int_{0}^{\infty} \frac{K_D(V, \omega_0, \mu)}{\zeta_a^2} S_\zeta(\omega_0, \mu) d\omega_0 d\mu \tag{6.57}$$

$$M_{2nd} = 2 \int_{-\pi}^{-\pi} \int_{0}^{\infty} \frac{M_D(V, \omega_0, \mu)}{\zeta_a^2} S_\zeta(\omega_0, \mu) d\omega_0 d\mu \tag{6.58}$$

$$N_{2nd} = 2 \int_{-\pi}^{-\pi} \int_{0}^{\infty} \frac{N_D(V, \omega_0, \mu)}{\zeta_a^2} S_\zeta(\omega_0, \mu) d\omega_0 d\mu \tag{6.59}$$

where $X_D$, $Y_D$, $Z_D$, $K_D$, $M_D$, and $N_D$ are surge, sway, heave, roll, pitch and yaw mean wave drift coefficients; $S_\zeta(\omega_0, \mu)$ is the directional wave spectrum.

The forces obtained in Eq. (6.54) to Eq. (6.59) would require first the transformation of axes frame, similarly conducted with the first order forces. These forces, in the manoeuvring frame are given by:

$$F_{2ndj}^b = R^{-1}(\Xi) R^* F_{2nd}^h \tag{6.60}$$

The rotation matrices $R(\Xi)$ and $R^*$ have been already given earlier in Eq. (6.34) and Eq. (6.35), respectively. Note as well that in general the computations of the mean forces are estimated in the up-right $h$ −frame, hence the required transformation $R^*$;

The drift coefficients are function of the ship forward speed $V$, the wave frequency $\omega_0$ and the wave angle of encounter $\mu$. These parameters can be computed in advance before any simulation starts. Interpolations can then be conducted for any speed, frequency, or incoming angles the ship encounters.

The mean wave drift coefficients can be obtained numerically or experimentally if a better accuracy is required. The experimental comparison conducted in Section 5 (see Figure 5.5 to Figure 5.8) showed that numerical estimations can give a good estimation for the short wave length range, which is especially the case encountered by ships of such large dimensions.

An example of the mean wave drift coefficients $X_D$, $Y_D$, $Z_D$, $K_D$, $M_D$, and $N_D$ have been computed with Hydrostar. These results are presented in Figure 6.15. The results have been estimated in the

NED $h-$frame. Hence, forces shown in figures below are plotted after the rotation $R^{*}F_{2nd}^{h}$.

From Figure 6.15 it can be observed that significant magnitudes of the wave drift forces and moments for the short wave length range are only obtained for sway and yaw, respectively. Other forces and moments remains small at such wave lengths. The latter, however, have a pick as the wave length increases meaning the relative motions between the ship and the waves are an important contribution to magnitudes. Recall that wave amplitude and lengths are considered moderate and short, respectively; hence, it seems then that some simplification can be made in order to estimate the wave second order effects. The latter, however, requires further experimental studies to verify this observations.

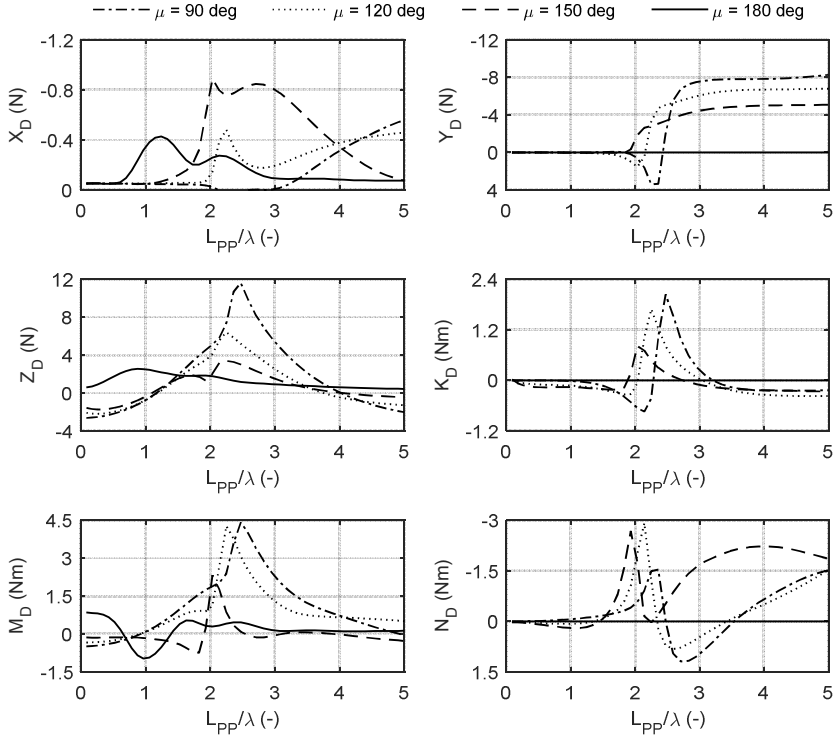


Figure 6.15 Numerical evaluation (with Hydrostar) of the mean wave drift forces for the container ship model C0W at Fr =0.100, 50% UKC ($T_M$ = 13.1 m at full scale) and $\zeta_a$ = 11.1mm.

# MANOEUVRING IN COASTAL WAVES



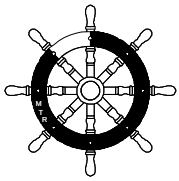

*One never notices what has been done; one can only see what remains to be done.*

*Marie Curie*

# 7

# Numerical approach

## 7.1 Overview

The present Chapter extends the brief discussion presented in Chapter 6 with respect to the two main aspects of the forces and moments acting on a ship in seakeeping studies: the ship body reaction forces (also known as the radiation forces), and the wave exciting forces and moments.

Section 7.2 comprises an extensive discussion of the manoeuvring coefficients regarding the radiation forces, further a relationship is developed with the respective coefficients derived in seakeeping studies. Bear in mind, however, that only potential contributions are accounted for.

In Section 7.3 a comprehensive discussion of a nonlinear method developed for the estimation of the wave exciting forces and moments in time domain will be presented.

## 7.2 Ideal fluid reaction forces

### 7.2.1 General discussion

Considering only ideal fluids, the frequency dependent radiation forces and moments in the frequency domain, expressed in the $b$ −frame, are given by:

$$\begin{bmatrix}\tilde{X}\\ \tilde{Z}\\ \tilde{M}\end{bmatrix} = \begin{bmatrix}\tilde{X}_{\dot{u}} & \tilde{X}_{\dot{w}} & \tilde{X}_{\dot{q}}\\ \tilde{Z}_{\dot{u}} & \tilde{Z}_{\dot{w}} & \tilde{Z}_{\dot{q}}\\ \tilde{M}_{\dot{u}} & \tilde{M}_{\dot{w}} & \tilde{M}_{\dot{q}}\end{bmatrix}\begin{bmatrix}\dot{u}\\ \dot{w}\\ \dot{q}\end{bmatrix} + \begin{bmatrix}\tilde{X}_{u} & \tilde{X}_{w} & \tilde{X}_{q}\\ \tilde{Z}_{u} & \tilde{Z}_{w} & \tilde{Z}_{q}\\ \tilde{M}_{u} & \tilde{M}_{w} & \tilde{M}_{q}\end{bmatrix}\begin{bmatrix}u\\ w\\ q\end{bmatrix} \tag{7.1}$$

$$\begin{bmatrix}\tilde{Y}\\ \tilde{K}\\ \tilde{N}\end{bmatrix} = \begin{bmatrix}\tilde{Y}_{\dot{v}} & \tilde{Y}_{\dot{p}} & \tilde{Y}_{\dot{r}}\\ \tilde{K}_{\dot{v}} & \tilde{K}_{\dot{p}} & \tilde{K}_{\dot{r}}\\ \tilde{N}_{\dot{v}} & \tilde{N}_{\dot{p}} & \tilde{N}_{\dot{r}}\end{bmatrix}\begin{bmatrix}\dot{v}\\ \dot{p}\\ \dot{r}\end{bmatrix} + \begin{bmatrix}\tilde{Y}_{v} & \tilde{Y}_{p} & \tilde{Y}_{r}\\ \tilde{K}_{v} & \tilde{K}_{p} & \tilde{K}_{r}\\ \tilde{N}_{v} & \tilde{N}_{p} & \tilde{N}_{r}\end{bmatrix}\begin{bmatrix}v\\ p\\ r\end{bmatrix} \tag{7.2}$$

and, in the h-frame, by:

$$\begin{bmatrix}H_1\\ H_3\\ H_5\end{bmatrix} = -\begin{bmatrix}A^V_{11} & A^V_{13} & A^V_{15}\\ A^U_{31} & A^U_{33} & A^V_{35}\\ A^U_{51} & A^U_{53} & A^U_{55}\end{bmatrix}\begin{bmatrix}\ddot{\xi}_1\\ \ddot{\xi}_3\\ \ddot{\xi}_5\end{bmatrix} - \begin{bmatrix}B^V_{11} & B^V_{13} & B^V_{15}\\ B^V_{31} & B^V_{33} & B^V_{35}\\ B^V_{51} & B^V_{53} & B^V_{55}\end{bmatrix}\begin{bmatrix}\dot{\xi}_1\\ \dot{\xi}_3\\ \dot{\xi}_5\end{bmatrix} \tag{7.3}$$

$$\begin{bmatrix}H_2\\ H_4\\ H_6\end{bmatrix} = -\begin{bmatrix}A^V_{22} & A^V_{24} & A^V_{26}\\ A^V_{42} & A^V_{44} & A^V_{46}\\ A^V_{62} & A^V_{64} & A^V_{66}\end{bmatrix}\begin{bmatrix}\ddot{\xi}_2\\ \ddot{\xi}_4\\ \ddot{\xi}_6\end{bmatrix} - \begin{bmatrix}B^V_{22} & B^V_{24} & B^V_{26}\\ B^V_{42} & A^V_{44} & B^V_{46}\\ B^V_{62} & B^V_{64} & B^V_{66}\end{bmatrix}\begin{bmatrix}\dot{\xi}_2\\ \dot{\xi}_4\\ \dot{\xi}_6\end{bmatrix} \tag{7.4}$$

The forces and moments in Equations (7.1) to (7.4) are proportional to ship velocities and accelerations with frequency dependent coefficients. The terms $u, v, w, p, q, r$ and $\dot{\xi}_1, \dot{\xi}_2, \dot{\xi}_3, \dot{\xi}_4, \dot{\xi}_5, \dot{\xi}_6$ are the surge, sway, heave, roll, pitch and yaw velocities, respectively, and their time derivatives yield the accelerations.

Equation (7.1) is decoupled from Eq. (7.2), similarly Eq. (7.3) from Eq. (7.4). Such a divided treatment of the 6DOF problem is only possible because of the axis-symmetry property of the ship hull form. A more complex geometry would require coupling between all degrees of freedom, as shown in Imlay (1961). Such analysis is, however, out of the scope of the present work.

To study manoeuvring in waves, it is then of great interest to unify the radiation expressions in the $b$ −frame, Eq. (7.1) and (7.2), with

the ones of the h-frame, Eq. (7.3) to (7.4). To the author's best knowledge, this analysis has been conducted first by Bailey et al. (1998). In their work Eq. (7.3) to (7.4) are correlated by using linearised kinematic transformation of the two axes-systems. Further, the non-zero forward speed hydrodynamic coefficients, given in the h-frame, were replaced by strip theory formulations, see e.g. Salvesen et al. (1970), Vugts (1965).

The following subsections, motivated by the work of Bailey et al. (1998), explore in detail the relationships between the coefficients of Eq. (7.1) to (7.4). Similar to their work, the non-zero forward speed added masses and damping coefficients were also taken from Salvesen et al. (1970).

The final results contain terms such as $V/\omega^2$ which introduces singularities at zero frequency for the pitch and yaw moments. These singularities, not discussed in Bailey et al. (1998), are important because frequencies ranging from zero to infinity are needed for the computation of the radiation forces and moments in the time domain. In this study, these singularities are addressed indirectly by using the fundamental properties of the Fourier transformation.

The radiation problem in the time domain is evaluated by convolving an IRF function (function of the hydrodynamic coefficients and forward speed $V$) with the instant ship velocity. This means intense computations to constantly update the IRF functions because of the variation of the forward speed $V$ while manoeuvring. In this work, the speed dependent IRF function has been split in two sub-IRFs, both independent of $V$. The final IRF functions are then obtained by their linear combination with one of them being multiplied by $V$. Moreover, further reduction of computing time has been attained by using the state space approach, see e.g. Yu and Falnes (1995), and Taghipour et al. (2008).

### 7.2.2 Frequency domain analysis

Taking into consideration the location of the h-frame's origin with respect to the b-frame (see Fig. 2.2) with coordinates $\vec{r}^{\,b}_{O'/O} = x_{O'}\hat{\imath} + y_{O'}\hat{\jmath} + z_{O'}\hat{k}$, the transformation of the forces in the h-frame to the b-frame is given by:

$$\begin{bmatrix}\tilde{X}\\ \tilde{Y}\\ \tilde{Z}\end{bmatrix} = R^{-1}(\Xi)\begin{bmatrix}H_1\\ H_2\\ H_3\end{bmatrix} = \begin{bmatrix}H_1\\ H_2\\ H_3\end{bmatrix} \tag{7.5}$$

and for the moments:

$$\begin{bmatrix}\tilde{K}\\ \tilde{M}\\ \tilde{N}\end{bmatrix} = R^{-1}(\Xi)\begin{bmatrix}H_4 + y_{O'}H_3 - z_{O'}H_2\\ H_5 + z_{O'}H_1 - x_{O'}H_3\\ H_6 + x_{O'}H_2 - y_{O'}H_1\end{bmatrix} = \begin{bmatrix}H_4 + y_{O'}H_3 - z_{O'}H_2\\ H_5 + z_{O'}H_1 - x_{O'}H_3\\ H_6 + x_{O'}H_2 - y_{O'}H_1\end{bmatrix} \tag{7.6}$$

The surge, sway, heave, roll, pitch and yaw forces and moments, $\tilde{X}$, $\tilde{Y}$, $\tilde{Z}$, $\tilde{K}$, $\tilde{M}$, $\tilde{N}$ and $H_1$, $H_2$, $H_3$, $H_4$, $H_5$, $H_6$ are given in the b-frame and h-frame, respectively.

Replacing the linearised kinematic relationships between the b-frame and the h-frame, see Eq. (2.63) to Eq. (2.64), in Eq. (7.3) and (7.4), and taking into account the coordinate transformation given by Eq. (7.5) and (7.6), the radiation forces and moments in the b-frame can be rewritten as:

$$\tilde{X} = -A^V_{11}\dot{u} - B^V_{11}u - A^V_{13}\dot{w} - B^V_{13}w - \left(A^V_{15} + V\frac{B^V_{13}}{\omega^2} + z_{O'}A^V_{11} - x_{O'}A^V_{13}\right)\dot{q}$$

$$- (B^V_{15} - VA^V_{13} + z_{O'}B^V_{11} - x_{O'}B^V_{13})q \tag{7.7}$$

$$\tilde{Y} = A^V_{22}\dot{v} - B^V_{22}v - (A^V_{24} - z_{O'}A^V_{22})\dot{p} - (B^V_{24} - z_{O'}B^V_{22})p$$

$$- \left(A^V_{26} - V\frac{B^V_{22}}{\omega^2} + x_{O'}A^V_{22}\right)\dot{r}$$

$$- (B^V_{26} + VA^V_{22} + x_{O'}B^V_{22})\,r \tag{7.8}$$

$$\tilde{Z} = -A^V_{31}\dot{u} - B^V_{31}u - A^V_{33}\dot{w} - B^V_{33}w - \left(A^V_{35} + V\frac{B^V_{33}}{\omega^2} + z_{O'}A^V_{31} - x_{O'}A^V_{33}\right)\dot{q}$$

$$- (B^V_{35} - VA^V_{33} + z_{O'}B^V_{31} - x_{O'}B^V_{33})q \tag{7.9}$$

$$\begin{aligned}\widetilde{K} = &-(A^V_{42} - z_{O'}A^V_{22})\dot{v} - (B^V_{42} - z_{O'}B^V_{22})v \\ &- \left(A^V_{44} - z_{O'}A^V_{42} - z_{O'}(A^V_{24} - z_{O'}A^V_{22})\right)\dot{p} \\ &- \left(B^V_{44} - z_{O'}B^V_{42} - z_{O'}(B^V_{24} - z_{O'}B^V_{22})\right)p \\ &- \left(A^V_{46} - V\frac{B^V_{42}}{\omega^2} + x_{O'}A^V_{42} - z_{O'}\left(A^V_{26} - V\frac{B^V_{22}}{\omega^2} + x_{O'}A^V_{22}\right)\right)\dot{r} \\ &- \left(B^V_{46} + VA^V_{42} + x_{O'}B^V_{42} - z_{O'}(B^V_{26} + VA^V_{22} + x_{O'}B^V_{22})\right)r\end{aligned} \tag{7.10}$$

$$\begin{aligned}\widetilde{M} = &-(A^V_{51} + z_{O'}A^V_{11} - x_{O'}A^V_{31})\dot{u} - (B^V_{51} + z_{O'}B^V_{11} - x_{O'}B^V_{31})u \\ &- (A^V_{53} + z_{O'}A^V_{13} - x_{O'}A^V_{33})\dot{w} - (B^V_{53} + z_{O'}B^V_{13} - x_{O'}B^V_{33})w \\ &- \left(A^V_{55} + V\frac{B^V_{53}}{\omega^2} - x_{O'}A^V_{53} + z_{O'}A^V_{51}\right)\dot{q} \\ &- z_{O'}\left(A^V_{15} + V\frac{B^V_{13}}{\omega^2} + z_{O'}A^V_{11} - x_{O'}A^V_{13}\right)\dot{q} \\ &+ x_{O'}\left(A^V_{35} + V\frac{B^V_{33}}{\omega^2} + z_{O'}A^V_{31} - x_{O'}A^V_{33}\right)\dot{q} \\ &- (B^V_{55} - VA^V_{53} - x_{O'}B^V_{53} + z_{O'}B^V_{51})q \\ &- z_{O'}(B^V_{15} - VA^V_{13} + z_{O'}B^V_{11} - x_{O'}B^V_{13})q \\ &+ x_{O'}(B^V_{35} - VA^V_{33} + z_{O'}B^V_{31} - x_{O'}B^V_{33})q\end{aligned} \tag{7.11}$$

$$\begin{aligned}\widetilde{N} = &-(A^V_{62} + x_{O'}A^V_{22})\dot{v} - (B^V_{62} + x_{O'}B^V_{22})v \\ &- \left(A^V_{64} - z_{O'}A^V_{62} + x_{O'}(A^V_{24} - z_{O'}A^V_{22})\right)\dot{p} \\ &- \left(B^V_{64} - z_{O'}B^V_{62} + x_{O'}(B^V_{24} - z_{O'}B^V_{22})\right)p \\ &- \left(A^V_{66} - V\frac{B^V_{62}}{\omega^2} + x_{O'}A^V_{62}\right)\dot{r} - x_{O'}\left(A^V_{26} - V\frac{B^V_{22}}{\omega^2} + x_{O'}A^V_{22}\right)\dot{r} \\ &- (B^V_{66} + VA^V_{62} + x_{O'}B^V_{62})r - x_{O'}(B^V_{26} + VA^V_{22} + x_{O'}B^V_{22})\,r\end{aligned}$$

Eq. (7.7) to Eq. (7.12) can be further rearranged considering the relationships between the zero and non-zero forward speed for the added masses and damping coefficients as described in Salvesen et al. (1970) (see subsection 2.5.5). Furthermore, a significant simplification can be achieved if we neglect the 'end' terms in the relationships in Salvesen et al. (1970). Considering this, Eq. (7.7) to (7.12) can be rewritten as:

$$\tilde{X} = -A_{11}^0\dot{u} - B_{11}^0 u - A_{13}^0\dot{w} - B_{13}^0 w - (A_{15}^0 + z_{O'}A_{11}^0 - x_{O'}A_{13}^0)\dot{q} - (B_{15}^0 + z_{O'}B_{11}^0 - x_{O'}B_{13}^0)q \tag{7.13}$$

$$\tilde{Y} = -A_{22}^0\dot{v} - B_{22}^0 v - (A_{24}^0 - z_{O'}A_{22}^0)\dot{p} - (B_{24}^0 - z_{O'}B_{22}^0)p - (A_{26}^0 + x_{O'}A_{22}^0)\dot{r} - (B_{26}^0 + x_{O'}B_{22}^0)r \tag{7.14}$$

$$\tilde{Z} = -A_{31}^0\dot{u} - B_{31}^0 u - A_{33}^0\dot{w} - B_{33}^0 w - (A_{35}^0 + z_{O'}A_{31}^0 - x_{O'}A_{33}^0)\dot{q} - (B_{35}^0 + z_{O'}B_{31}^0 - x_{O'}B_{33}^0)q \tag{7.15}$$

$$\begin{aligned}\tilde{K} = &-(A_{42}^0 - z_{O'}A_{22}^0)\dot{v} - (B_{42}^0 - z_{O'}B_{22}^0)v \\ &- \left(A_{44}^0 - z_{O'}A_{42}^0 - z_{O'}(A_{24}^0 - z_{O'}A_{22}^0)\right)\dot{p} \\ &- \left(B_{44}^0 - z_{O'}B_{42}^0 - z_{O'}(B_{24}^0 - z_{O'}B_{22}^0)\right)p \\ &- \left(A_{46}^0 + x_{O'}A_{42}^0 - z_{O'}(A_{26}^0 + x_{O'}A_{22}^0)\right)\dot{r} \\ &- \left(B_{46}^0 + x_{O'}B_{42}^0 - z_{O'}(B_{26}^0 + x_{O'}B_{22}^0)\right)r\end{aligned} \tag{7.16}$$

$$\widetilde{M} = -\left(A_{51}^0 + \frac{V}{\omega^2}B_{31}^0 + z_{O'}A_{11}^0 - x_{O'}A_{31}^0\right)\dot{u}$$
$$- (B_{51}^0 - VA_{13}^0 + z_{O'}B_{11}^0 - x_{O'}B_{31}^0)u$$
$$- \left(A_{53}^0 + \frac{V}{\omega^2}B_{33}^0 + z_{O'}A_{13}^0 - x_{O'}A_{33}^0\right)\dot{w}$$
$$- (B_{53}^0 - VA_{33}^0 + z_{O'}B_{13}^0 - x_{O'}B_{33}^0)w - \left(A_{55}^0 + \frac{V}{\omega^2}B_{53}^0\right)\dot{q}$$
$$+ x_{O'}\left(A_{53}^0 + \frac{V}{\omega^2}B_{33}^0 + A_{35}^0 + z_{O'}A_{31}^0 - x_{O'}A_{33}^0\right)\dot{q}$$
$$- z_{O'}\left(A_{51}^0 + \frac{V}{\omega^2}B_{31}^0 + A_{15}^0 + z_{O'}A_{11}^0 - x_{O'}A_{13}^0\right)\dot{q}$$
$$- (B_{55}^0 - VA_{53}^0)q$$
$$+ x_{O'}(B_{53}^0 - VA_{33}^0 + B_{35}^0 + z_{O'}B_{31}^0 - x_{O'}B_{33}^0)\,q \; - \; z_{O'}\,(B_{51}^0$$
$$- VA_{13}^0 + \; B_{15}^0 + z_{O'}B_{11}^0 - x_{O'}B_{13}^0)q \qquad (7.17)$$

$$\widetilde{N} = -\left(A_{62}^0 - \frac{V}{\omega^2}B_{22}^0 + x_{O'}A_{22}^0\right)\dot{v} - (B_{62}^0 + VA_{22}^0 + x_{O'}B_{22}^0)v$$
$$- \left(A_{64}^0 - \frac{V}{\omega^2}B_{24}^0\right)\dot{p} + z_{O'}\left(A_{62}^0 - \frac{V}{\omega^2}B_{22}^0\right)\dot{p}$$
$$- x_{O'}(A_{24}^0 - z_{O'}A_{22}^0)\dot{p} - (B_{64}^0 + VA_{24}^0)p + z_{O'}(B_{62}^0 + VA_{22}^0)p$$
$$- x_{O'}(B_{24}^0 - z_{O'}B_{22}^0)p - \left(A_{66}^0 - \frac{V}{\omega^2}B_{62}^0\right)\dot{r}$$
$$- x_{O'}\left(A_{62}^0 - \frac{V}{\omega^2}B_{22}^0\right)\dot{r} - x_{O'}(A_{26}^0 + x_{O'}A_{22}^0)\dot{r}$$
$$- (B_{66}^0 + VA_{62}^0)r - x_{O'}(B_{62}^0 + VA_{22}^0)r$$
$$- x_{O'}(B_{26}^0 + x_{O'}B_{22}^0)r \qquad (7.18)$$

The relationships between the radiation coefficients expressed in the b-frame and the h-frame can be obtained now by comparing Eq. (7.13) to (7.18) with Eq. (7.1) to (7.2). These are shown in Table 7.1, for surge, sway, heave, and roll forces and moments, and in Table 7.2 and Table 7.3 for the pitch and yaw moments, respectively.

Table 7.1 Surge, sway, heave and roll frequency domain radiation coefficients given in manoeuvring coordinates.

| Item | In b-frame | Item | In b-frame |
|---|---|---|---|
| $\tilde{X}_{\dot{u}} =$ | $-A_{11}^0$ | $\tilde{Y}_{\dot{v}} =$ | $-A_{22}^0$ |
| $\tilde{X}_{u} =$ | $-B_{11}^0$ | $\tilde{Y}_{v} =$ | $-B_{22}^0$ |
| $\tilde{X}_{\dot{w}} =$ | $-A_{13}^0$ | $\tilde{Y}_{\dot{p}} =$ | $-A_{24}^0 + z_{O'}A_{22}^0$ |
| $\tilde{X}_{w} =$ | $-B_{13}^0$ | $\tilde{Y}_{p} =$ | $-B_{24}^0 + z_{O'}B_{22}^0$ |
| $\tilde{X}_{\dot{q}} =$ | $-A_{15}^0 - z_{O'}A_{11}^0 + x_{O'}A_{13}^0$ | $\tilde{Y}_{\dot{r}} =$ | $-A_{26}^0 - x_{O'}A_{22}^0$ |
| $\tilde{X}_{q} =$ | $-B_{15}^0 - z_{O'}B_{11}^0 + x_{O'}B_{13}^0$ | $\tilde{Y}_{r} =$ | $-B_{26}^0 - x_{O'}B_{22}^0$ |
| $\tilde{Z}_{\dot{u}} =$ | $-A_{31}^0$ | $\tilde{K}_{\dot{v}} =$ | $-A_{42}^0 + z_{O'}A_{22}^0$ |
| $\tilde{Z}_{u} =$ | $-B_{31}^0$ | $\tilde{K}_{v} =$ | $-B_{42}^0 + z_{O'}B_{22}^0$ |
| $\tilde{Z}_{\dot{w}} =$ | $-A_{33}^0$ | $\tilde{K}_{\dot{p}} =$ | $-A_{44}^0 + z_{O'}(A_{42}^0 + A_{24}^0) - z_{O'}^2A_{22}^0$ |
| $\tilde{Z}_{w} =$ | $-B_{33}^0$ | $\tilde{K}_{p} =$ | $-B_{44}^0 + z_{O'}(B_{42}^0 + B_{24}^0) - z_{O'}^2B_{22}^0$ |
| $\tilde{Z}_{\dot{q}} =$ | $-A_{35}^0 - z_{O'}A_{31}^0 + x_{O'}A_{33}^0$ | $\tilde{K}_{\dot{r}} =$ | $-A_{46}^0 + z_{O'}A_{26}^0 - x_{O'}A_{42}^0 + x_{O'}z_{O'}A_{22}^0$ |
| $\tilde{Z}_{q} =$ | $-B_{35}^0 - z_{O'}B_{31}^0 + x_{O'}B_{33}^0$ | $\tilde{K}_{r} =$ | $-B_{46}^0 + z_{O'}B_{26}^0 - x_{O'}B_{42}^0 + x_{O'}z_{O'}B_{22}^0$ |

Table 7.2 Pitch radiation frequency domain coefficients given in manoeuvring coordinates.

| Item | Zero speed terms in b-frame | Speed terms in b-frame |
|---|---|---|
| $\tilde{M}_{\dot{u}} =$ | $-A_{51}^0 - z_{O'}A_{11}^0 + x_{O'}A_{31}^0$ | $-V\left(\frac{B_{31}^0}{\omega^2}\right)$ |
| $\tilde{M}_{u} =$ | $-B_{51}^0 - z_{O'}B_{11}^0 + x_{O'}B_{31}^0$ | $+V(A_{13}^0)$ |
| $\tilde{M}_{\dot{w}} =$ | $-A_{53}^0 - z_{O'}A_{13}^0 + x_{O'}A_{33}^0$ | $-V\left(\frac{B_{33}^0}{\omega^2}\right)$ |
| $\tilde{M}_{w} =$ | $-B_{53}^0 - z_{O'}B_{13}^0 + x_{O'}B_{33}^0$ | $+V(A_{33}^0)$ |
| $\tilde{M}_{\dot{q}} =$ | $-A_{55}^0 - z_{O'}(A_{51}^0 + A_{15}^0) + x_{O'}(A_{53}^0 + A_{35}^0) + x_{O'}z_{O'}(A_{31}^0 + A_{13}^0) - z_{O'}^2A_{11}^0 - x_{O'}^2A_{33}^0$ | $-V\left(\frac{B_{53}^0}{\omega^2} - x_{O'}\frac{B_{33}^0}{\omega^2} + z_{O'}\frac{B_{31}^0}{\omega^2}\right)$ |
| $\tilde{M}_{q} =$ | $-B_{55}^0 - z_{O'}(B_{51}^0 + B_{15}^0) + x_{O'}(B_{53}^0 + B_{35}^0) + x_{O'}z_{O'}(B_{31}^0 + B_{13}^0) - z_{O'}^2B_{11}^0 - x_{O'}^2B_{33}^0$ | $+V(A_{53}^0 - x_{O'}A_{33}^0 + z_{O'}A_{13}^0)$ |

Table 7.3 Yaw radiation frequency domain coefficients given in manoeuvring coordinates.

| Item | Zero speed terms in b-frame | Speed terms in b-frame |
|---|---|---|
| $\widetilde{N}_{\dot{v}} =$ | $-A_{62}^0 - x_{O'}A_{22}^0$ | $+V\left(\frac{B_{22}^0}{\omega^2}\right)$ |
| $\widetilde{N}_{v} =$ | $-B_{62}^0 - x_{O'}B_{22}^0$ | $-V(A_{22}^0)$ |
| $\widetilde{N}_{\dot{p}} =$ | $-A_{64}^0 + z_{O'}A_{62}^0 - x_{O'}A_{24}^0 + x_{O'}z_{O'}A_{22}^0$ | $+V\left(\frac{B_{24}^0}{\omega^2} - z_{O'}\frac{B_{22}^0}{\omega^2}\right)$ |
| $\widetilde{N}_{p} =$ | $-B_{64}^0 + z_{O'}B_{62}^0 - x_{O'}B_{24}^0 + x_{O'}z_{O'}B_{22}^0$ | $-V(A_{24}^0 - z_{O'}A_{22}^0)$ |
| $\widetilde{N}_{\dot{r}} =$ | $-A_{66}^0 - x_{O'}(A_{62}^0 + A_{26}^0) - x_{O'}^2A_{22}^0$ | $+V\left(\frac{B_{62}^0}{\omega^2} + x_{O'}\frac{B_{22}^0}{\omega^2}\right)$ |
| $\widetilde{N}_{r} =$ | $-B_{66}^0 - x_{O'}(B_{62}^0 + B_{26}^0) - x_{O'}^2B_{22}^0$ | $-V(A_{62}^0 + x_{O'}A_{22}^0)$ |

### *7.2.2.1 Infinite frequency Coefficients*

For further evaluation of the radiation problem in the time domain, the infinite frequency values are required. Replacing $\omega = \infty$ in the results shown in Table 7.1 to Table 7.3, these coefficients are obtained. They are displayed in Table 7.4, to Table 7.6.

Table 7.4 Surge, sway, heave and roll radiation coefficients at infinite frequency in manoeuvring coordinates.

| Item | In b-frame | Item | In b-frame |
|---|---|---|---|
| $\tilde{X}_{\dot{u}}(\infty) =$ | $-A_{11}^0(\infty)$ | $\tilde{Y}_{\dot{v}}(\infty) =$ | $-A_{22}^0(\infty)$ |
| $\tilde{X}_{\dot{w}}(\infty) =$ | $-A_{13}^0(\infty)$ | $\tilde{Y}_{\dot{p}}(\infty) =$ | $-A_{24}^0(\infty) + z_{O'}A_{22}^0(\infty)$ |
| $\tilde{X}_{\dot{q}}(\infty) =$ | $-A_{15}^0(\infty) - z_{O'}A_{11}^0(\infty) + x_{O'}A_{13}^0(\infty)$ | $\tilde{Y}_{\dot{r}}(\infty) =$ | $-A_{26}^0(\infty) - x_{O'}A_{22}^0(\infty)$ |
| $\tilde{X}_{u}(\infty) =$ | $0$ | $\tilde{Y}_{v}(\infty) =$ | $0$ |
| $\tilde{X}_{w}(\infty) =$ | $0$ | $\tilde{Y}_{p}(\infty) =$ | $0$ |
| $\tilde{X}_{q}(\infty) =$ | $0$ | $\tilde{Y}_{r}(\infty) =$ | $0$ |
| $\tilde{Z}_{\dot{u}}(\infty) =$ | $-A_{31}^0(\infty)$ | $\tilde{K}_{\dot{v}}(\infty) =$ | $-A_{42}^0(\infty) + z_{O'}A_{22}^0(\infty)$ |
| $\tilde{Z}_{\dot{w}}(\infty) =$ | $-A_{33}^0(\infty)$ | $\tilde{K}_{\dot{p}}(\infty) =$ | $= -A_{44}^0(\infty) + 2z_{O'}A_{42}^0(\infty) - z_{O'}^2A_{22}^0(\infty)$ |
| $\tilde{Z}_{\dot{q}}(\infty) =$ | $-A_{35}^0(\infty) - z_{O'}A_{31}^0(\infty) + x_{O'}A_{33}^0(\infty)$ | $\tilde{K}_{\dot{r}}(\infty) =$ | $-A_{46}^0(\infty) + z_{O'}A_{26}^0(\infty) - x_{O'}A_{42}^0(\infty) + x_{O'}z_{O'}A_{22}^0(\infty)$ |
| $\tilde{Z}_{u}(\infty) =$ | $0$ | $\tilde{K}_{v}(\infty) =$ | $0$ |
| $\tilde{Z}_{w}(\infty) =$ | $0$ | $\tilde{K}_{p}(\infty) =$ | $0$ |
| $\tilde{Z}_{q}(\infty) =$ | $0$ | $\tilde{K}_{r}(\infty) =$ | $0$ |

Table 7.5 Pitch radiation coefficients at infinite frequency in manoeuvring coordinates.

| Item | In b-frame |
|---|---|
| $\widetilde{M}_{\dot{u}}(\infty) =$ | $-A^0_{51}(\infty) - z_{O'}A^0_{11}(\infty) + x_{O'}A^0_{31}(\infty)$ |
| $\widetilde{M}_{u}(\infty) =$ | $+V(A^0_{13}(\infty))$ |
| $\widetilde{M}_{w}(\infty) =$ | $-A^0_{53}(\infty) - z_{O'}A^0_{13}(\infty) + x_{O'}A^0_{33}(\infty)$ |
| $\widetilde{M}_{w}(\infty) =$ | $+V(A^0_{33}(\infty))$ |
| $\widetilde{M}_{\dot{q}}(\infty) =$ | $-A^0_{55}(\infty) - 2z_{O'}A^0_{51}(\infty) + 2x_{O'}A^0_{53}(\infty) + 2x_{O'}z_{O'}A^0_{31}(\infty) - z^2_{O'}A^0_{11}(\infty) - x^2_{O'}A^0_{33}(\infty)$ |
| $\widetilde{M}_{q}(\infty) =$ | $+V\left(A^0_{53}(\infty) - x_{O'}A^0_{33}(\infty) + z_{O'}A^0_{13}(\infty)\right)$ |

Table 7.6 Yaw radiation coefficients at infinite frequency in manoeuvring coordinates.

| Item | In b-frame |
|---|---|
| $\widetilde{N}_{\dot{v}}(\infty) =$ | $-A^0_{62}(\infty) - x_{O'}A^0_{22}(\infty)$ |
| $\widetilde{N}_{v}(\infty) =$ | $-V(A^0_{22}(\infty))$ |
| $\widetilde{N}_{\dot{p}}(\infty) =$ | $-A^0_{64}(\infty) + z_{O'}A^0_{62}(\infty) - x_{O'}A^0_{24}(\infty) + x_{O'}z_{O'}A^0_{22}(\infty)$ |
| $\widetilde{N}_{p}(\infty) =$ | $-V(A^0_{24}(\infty) - z_{O'}A^0_{22}(\infty))$ |
| $\widetilde{N}_{\dot{r}}(\infty) =$ | $-A^0_{66}(\infty) - 2x_{O'}A^0_{62}(\infty) - x^2_{O'}A^0_{22}(\infty)$ |
| $\widetilde{N}_{r}(\infty) =$ | $-V(A^0_{62}(\infty) + x_{O'}A^0_{22}(\infty))$ |

### 7.2.3 Time domain analysis

Following the works by Cummins (1962), Bishop et al. (1984), and Bishop et al. (1977), the radiation forces in the time domain can be expressed as a function of constant coefficients proportional to the ship's accelerations and velocities, together with a convolution of a IRF function with the ship velocity. These relationships, as presented by Bishop, and given in the b-frame are shown in Eq. (7.19) to Eq. (7.24).

In Bishop et al. (1984), and Bishop et al. (1977) the m-terms such as $X^m_{\dot{u}}$ are written as $X^\infty_{\dot{u}}$. Because such symbolic representation might be confused with the ones employed by Cummins (1962) in the h-frame, the symbol '$m$' is kept in here.

$$\mathrm{X(t)} = \int_{-\infty}^{t} x_u(t-\tau)u(\tau)d\tau + \int_{-\infty}^{t} x_w(t-\tau)w(\tau)d\tau + \int_{-\infty}^{t} x_q(t-\tau)q(\tau)d\tau$$
$$+ X_{\dot{u}}^{m}\dot{u} + X_{u}^{m}u + X_{\dot{w}}^{m}\dot{w} + X_{w}^{m}w + X_{\dot{q}}^{m}\dot{q} + X_{q}^{m}q \qquad (7.19)$$

$$\mathrm{Y(t)} = \int_{-\infty}^{t} y_v(t-\tau)v(\tau)d\tau + \int_{-\infty}^{t} y_p(t-\tau)p(\tau)d\tau + \int_{-\infty}^{t} y_r(t-\tau)r(\tau)d\tau$$
$$+ Y_{\dot{v}}^{m}\dot{v} + Y_{v}^{m}v + Y_{\dot{p}}^{m}\dot{p} + Y_{p}^{m}p + Y_{\dot{r}}^{m}\dot{r} + Y_{r}^{m}r \qquad (7.20)$$

$$\mathrm{Z(t)} = \int_{-\infty}^{t} z_u(t-\tau)u(\tau)d\tau + \int_{-\infty}^{t} z_w(t-\tau)w(\tau)d\tau + \int_{-\infty}^{t} z_q(t-\tau)q(\tau)d\tau$$
$$+ Z_{\dot{u}}^{m}\dot{u} + Z_{u}^{m}u + Z_{\dot{w}}^{m}\dot{w} + Z_{w}^{m}w + Z_{\dot{q}}^{m}\dot{q} + Z_{q}^{m}q \qquad (7.21)$$

$$\mathrm{K(t)} = \int_{-\infty}^{t} k_v(t-\tau)v(\tau)d\tau + \int_{-\infty}^{t} k_p(t-\tau)p(\tau)d\tau + \int_{-\infty}^{t} k_r(t-\tau)r(\tau)d\tau$$
$$+ K_{\dot{v}}^{m}\dot{v} + K_{v}^{m}v + K_{\dot{p}}^{m}\dot{p} + K_{p}^{m}p + K_{\dot{r}}^{m}\dot{r} + K_{r}^{m}r \qquad (7.22)$$

$$\mathrm{M(t)} = \int_{-\infty}^{t} m_u(t-\tau)u(\tau)d\tau + \int_{-\infty}^{t} m_w(t-\tau)w(\tau)d\tau + \int_{-\infty}^{t} m_q(t-\tau)q(\tau)d\tau$$
$$+ M_{\dot{u}}^{m}\dot{u} + M_{u}^{m}u + M_{\dot{w}}^{m}\dot{w} + M_{w}^{m}w + M_{\dot{q}}^{m}\dot{q} + M_{q}^{m}q \qquad (7.23)$$

$$\mathrm{N(t)} = \int_{-\infty}^{t} n_v(t-\tau)v(\tau)d\tau + \int_{-\infty}^{t} n_p(t-\tau)p(\tau)d\tau + \int_{-\infty}^{t} n_r(t-\tau)r(\tau)d\tau$$
$$+ N_{\dot{v}}^{m}\dot{v} + N_{v}^{m}v + N_{\dot{p}}^{m}\dot{p} + N_{p}^{m}p + N_{\dot{r}}^{m}\dot{r} + N_{r}^{m}r \qquad (7.24)$$

It is important to mention that the representation of the radiation forces by Bishop et al. (1977) differs from the one by Cummins (1962) only in the incorporation of terms proportional to the ship motions. This sort of restoring terms as shown in Cummins (1962), represented by the symbol $C_{ij}^{m}$, are non-zero in the h-frame only for $C_{55}^{m}$ and $C_{66}^{m}$ as shown by the author in Tello Ruiz et al. (2015). Such coefficients $C_{ij}^{m}$ are zero for all modes of motion in the b-frame, thus they are omitted in Eq. (7.20) to Eq. (7.24).

To define the radiation problem in the time domain the m-terms coefficients and the IRF in Eq. (7.20) to Eq. (7.24) have to be obtained. The analysis for their determination is presented in the following subsection.

### 7.2.4 Frequency and time domain relationships

To illustrate better the relationships between time domain and the frequency domain parameters, the radiation force in heave due to heave motions from Eq. (7.21) is chosen as an example. This is given by:

$$\mathrm{Z(t)} = Z_{\dot{w}}^{m}\dot{w}(t) + Z_{w}^{m}w(t) + \int z_w(t-\tau)w(\tau)d\tau \tag{7.25}$$

where $Z_{\dot{w}}^{m}$ and $Z_{w}^{m}$ are the acceleration and velocity coefficients, respectively, and $z_w$ is the IRF function (also known as the impulse response function, IRF).

During harmonic oscillations Eq. (7.25) can be expressed in terms of constant oscillatory coefficients as:

$$\mathrm{Z(t)} = \tilde{Z}_{\dot{w}}(\omega)\dot{w}(t) + \tilde{Z}_{w}(\omega)w(t) \tag{7.26}$$

To find the relationships between both expressions, the Fourier transformation is applied to both Eq. (7.25) and Eq. (7.26). For Eq. (7.25) this results in:

$$\mathcal{F}\{\mathrm{Z(t)}\} = \left\{i\left(\omega Z_{\dot{w}}^{m} + I_{w}^{z}(\omega)\right) + \left(Z_{w}^{m} + R_{w}^{Z}(\omega)\right)\right\}\mathcal{F}\{w(t)\} \tag{7.27}$$

and for Eq. (7.26) in:

$$\mathcal{F}\{\mathrm{Z(t)}\} = \{i\,\omega\tilde{Z}_{\dot{w}}(\omega) + \tilde{Z}_{w}(\omega)\}\mathcal{F}\{w(t)\} \tag{7.28}$$

Comparing both equations, real and imaginary parts, the following relationships are found:

$$\omega\tilde{Z}_{\dot{w}}(\omega) = \omega Z_{\dot{w}}^{m} + I_{w}^{z}(\omega) \tag{7.29}$$

$$\tilde{Z}_{w}(\omega) = Z_{w}^{m} + R_{w}^{Z}(\omega) \tag{7.30}$$

Because both the imaginary $I_w^z$ and the real part $R_w^Z$ have to exist (meaning that $z_w$, $I_w^z$ and $R_w^Z$ are Fourier pairs), the relationships above must be valid for every frequency $\omega$, including infinity, $\omega = \infty$. Evaluating Eq. (7.29) and (7.30) at this frequency, and recalling that $I(\infty) = R(\infty) = 0$ (see appendix), the m-terms of the time domain radiation are found to be related to the frequency domain coefficients by:

$$Z_{\dot{w}}^m = \tilde{Z}_{\dot{w}}(\infty) \tag{7.31}$$

$$Z_w^m = \tilde{Z}_w(\infty) \tag{7.32}$$

Now that the m-terms have been found, the $m$ superscript in the time domain coefficients will be replaced by the symbol ∞.

Taking into account Eq. (7.29) to (7.32) and the Fourier inverse transformation (see appendix), the IRF function $z_w(t)$ can be found by:

$$z_w(t) = \begin{cases} \frac{2}{\pi}\int_0^\infty \left(\tilde{Z}_w(\omega) - Z_w^\infty\right)\cos(\omega t)\, d\omega & t > 0 \\ z_w(0^+) & t = 0 \end{cases} \tag{7.33}$$

Considering the relationships described in Table 7.1 and Table 7.4 the heave radiation forces in the b-frame can be rewritten as:

$$z_w(t) = \begin{cases} = \frac{2}{\pi}\int_0^\infty \left(-B_{33}^0\right)\cos(\omega t)\, d\omega = -h_{33}(t) & \\ z_w(0^+) & t = 0 \end{cases} \tag{7.34}$$

where $Z_w^\infty = -B_{33}^0(\infty) = 0$.

The same transformations can be applied for all force components of the radiation force. For instance, for those including the position coordinates $x_{O'}, y_{O'}, z_{O'}$ such as the roll moment due to yaw the transformation yields:

$$k_r(t) = -h_{46}(t) + z_{O'}h_{26}(t) - x_{O'}h_{42}(t) + x_{O'}z_{O'}h_{22}(t) \tag{7.35}$$

where $\tilde{K}_r(\omega) = -B_{46}^0 + z_{O'}B_{26}^0 - x_{O'}B_{42}^0 + x_{O'}z_{O'}B_{22}^0$, $K_{\dot{r}}^\infty = \tilde{K}_{\dot{r}}(\infty)$ and $K_r^\infty = \tilde{K}_r(\infty)$, see Table 7.1 and Table 7.4.

#### 7.2.4.1 Speed terms

The transformation as obtained in Eq. (7.34) cannot be directly obtained for the pitch $M$ and yaw $N$ moments. This complexity arises from the incorporation of the speed coefficients of the form $U/\omega^2$ (see Table 7.2 and Table 7.3) and their integration including the zero frequency values in Eq. (7.33), yielding undefined results.

To get a better idea on how these speed terms are related to the IRF functions, the pitch moment due to heave is taken as example. Rewriting Eq. (7.29) and (7.30), the following is obtained:

$$I_w^m(\omega) = \omega\widetilde{M}_{\dot{w}}(\omega) - \omega\widetilde{M}_{\dot{w}}(\infty) \tag{7.36}$$

$$R_w^m(\omega) = \widetilde{M}_w(\omega) - \widetilde{M}_w(\infty) \tag{7.37}$$

The equivalent representation of frequency domain coefficients $\widetilde{M}_{\dot{w}}$ and $\widetilde{M}_w$ in the b-frame (see Table 7.2) are:

$$\widetilde{M}_{\dot{w}} = -A_{53}^0 - z_{O'}A_{13}^0 + x_{O'}A_{33}^0 - V\left(\frac{B_{33}^0}{\omega^2}\right) \tag{7.38}$$

$$\widetilde{M}_w = -B_{53}^0 - z_{O'}B_{13}^0 + x_{O'}B_{33}^0 + V(A_{33}^0) \tag{7.39}$$

replacing them in Eq. (7.36) and (7.37) respectively, the imaginary and real part of the IRF function $m_w$ are:

$$I_w^m(\omega) = (A_{53}^0(\infty) - A_{53}^0)\omega + z_{O'}(A_{13}^0(\infty) - A_{13}^0)\omega - x_{O'}(A_{33}^0(\infty) - A_{33}^0)\omega - V\left(\frac{B_{33}^0}{\omega}\right) \tag{7.40}$$

$$R_w^m(\omega) = \left(-B_{53}^0 - z_{O'}B_{13}^0 + x_{O'}B_{33}^0 + V(A_{33}^0 - A_{33}^0(\infty))\right) \tag{7.41}$$

From Eq. (7.40) and (7.41) the terms independent of the forward speed can be solved as shown previously for the roll moment, see Eq. (7.35).

For the case of the speed terms, let's assume that the real part, $V(A_{33}^0 - A_{33}^0(\infty))$, and the imaginary part, $-V\left(\frac{B_{33}^0}{\omega}\right)$, are respectively the real and imaginary components of the function $F(\omega)$, such that

$F(\omega) = R_w^{m^V}(\omega) + iI_w^{m^V}(\omega)$. Then, an IRF function $m_w^V$ can also be defined, where $m_w^V$ and $F(\omega)$ are Fourier pairs. Taking this into account and applying the property of the Fourier transformation for the derivative of a function, it is found that:

$$\frac{dm_w^V(t)}{dt} = \frac{1}{2\pi}\int_{-\infty}^{\infty} \mathrm{i}\omega F(\omega)\, \mathrm{e}^{\mathrm{i}\omega t} d\omega = -\omega I_w^{m^V}(\omega) + \mathrm{i}\omega R_w^{m^V}(\omega) \tag{7.42}$$

and replacing $R_w^{m^V} = V(A_{33}^0 - A_{33}^0(\infty))$, and $I_w^{m^V} = -V\left(\frac{B_{33}^0}{\omega}\right)$ in the equation above, yields:

$$\frac{dm_w^V(t)}{dt} = V\left(\frac{1}{2\pi}\int \left(+B_{33}^0 + \mathrm{i}\omega(A_{33}^0 - A_{33}^0(\infty))\right)\mathrm{e}^{\mathrm{i}\omega t} d\omega\right) \tag{7.43}$$

Recall that for the force in heave due to heave motion, applying the relationships obtained in Table 7.1, Table 7.4, Eq. (7.29) and Eq. (7.30), the real and imaginary parts of the Fourier transformations of the IRF function $z_w$ are:

$$I_w^z(\omega) = \omega(A_{33}^0(\infty) - A_{33}^0) \tag{7.44}$$

$$R_w^z(\omega) = -B_{33}^0 \tag{7.45}$$

Applying the inverse Fourier transform to (7.44) and (7.45), $z_w$is defined by:

$$z_w(t) = \frac{1}{2\pi}\int_{-\infty}^{\infty} F(\omega)\, \mathrm{e}^{\mathrm{i}\omega t} d\omega = \frac{1}{2\pi}\int_{-\infty}^{\infty} \left(-B_{33}^0 - i\omega(A_{33}^0 - A_{33}^0(\infty))\right) \mathrm{e}^{\mathrm{i}\omega t} d\omega$$

$$= -h_{33}(t) \tag{7.46}$$

Eq. (7.46) is similar to Eq. (7.43). Comparing both equation yields:

$$\frac{dm_w^V(t)}{dt} = -z_w(t) = h_{33}(t) \qquad \text{hence} \quad m_w^V(t) = \int h_{33}^0(t) dt \tag{7.47}$$

Now, the final IRF function for the moment in pitch due to heave can be written as:

$$m_w(t) = -h_{53}(t) - z_{O'}h_{13}(t) + x_{O'}h_{33}(t) + V\int h_{33}^0(t) dt \tag{7.48}$$

Applying the above obtained relationships, the IRF functions for all forces and moments can be found. They are shown in Table 7.7.

Table 7.7 IRF functions of the radiation forces given in the b-frame for all six degrees of freedom.

| Item | In b-frame |
|---|---|
| $x_u(t) =$ | $-h^0_{11}(t)$ |
| $x_w(t) =$ | $-h^0_{13}(t)$ |
| $x_q(t) =$ | $-h^0_{15}(t) - z_{O'}h^0_{11}(t) + x_{O'}h^0_{13}(t)$ |
| $y_v(t) =$ | $-h^0_{22}(t)$ |
| $y_p(t) =$ | $-h^0_{24}(t) + z_{O'}h^0_{22}(t)$ |
| $y_r(t) =$ | $-h^0_{26}(t) - x_{O'}h^0_{22}(t)$ |
| $z_u(t) =$ | $-h^0_{31}(t)$ |
| $z_w(t) =$ | $-h^0_{33}(t)$ |
| $z_q(t) =$ | $-h^0_{35}(t) - z_{O'}h^0_{31}(t) + x_{O'}h^0_{33}(t)$ |
| $k_v(t) =$ | $-h^0_{42}(t) + z_{O'}h^0_{22}(t)$ |
| $k_p(t) =$ | $-h^0_{44}(t) + z_{O'}(h^0_{42}(t) + h^0_{24}(t)) - z^2_{O'}h^0_{22}(t)$ |
| $k_r(t) =$ | $-h^0_{46}(t) + z_{O'}h^0_{26}(t) - x_{O'}h^0_{42}(t) + x_{O'}z_{O'}h^0_{22}(t)$ |
| $m_u(t) =$ | $-h^0_{51} - z_{O'}h^0_{11}(t) + x_{O'}h^0_{31}(t) + V\int h^0_{31}(t)dt$ |
| $m_w(t) =$ | $-h_{53}(t) - z_{O'}h_{13}(t) + x_{O'}h_{33}(t) + V\int h^0_{33}\,dt$ |
| $m_q(t) =$ | $-h^0_{55} - z_{O'}(h^0_{51} + h^0_{15}) + x_{O'}(h^0_{53} + h^0_{35}) + x_{O'}z_{O'}(h^0_{31} + h^0_{13})$ $- z^2_{O'}h^0_{11} - x^2_{O'}h^0_{33}$ $+ V\left(\iint h^0_{53}\,dt - x_{O'}\int h^0_{33}\,dt + z_{O'}\int h^0_{13}\,dt\right)$ |
| $n_v(t) =$ | $-h^0_{62} - x_{O'}h^0_{22} - V\int h^0_{22}\,dt$ |
| $n_p(t) =$ | $-h^0_{64} + z_{O'}h^0_{62} - x_{O'}h^0_{24} + x_{O'}z_{O'}h^0_{22} - V\left(\iint h^0_{24}\,dt - z_{O'}\int h^0_{22}\,dt\right)$ |
| $n_r(t) =$ | $-h^0_{66} - x_{O'}(h^0_{62} + h^0_{26}) - x^2_{O'}h^0_{22} - V\left(\iint h^0_{62}\,dt + x_{O'}\int h^0_{22}\,dt\right)$ |

### 7.2.5 State space representation

The implementation of the radiation forces as given in Eq. (7.19) to (7.24) requires the convolution integral equation to be computed every time step from $-\infty$ to $t$. This demands large computing times which are costly from the point of view of real time simulations. Hence, an alternative solution is needed.

The simplification in the evaluation of the convolution integral is not an uncommon practice within the field of hydrodynamics. In many applications the convolution integral is replaced by a system of ordinary differential equations (ODE), better suited for numerical simulation (see Kristiansen et al., 2005). The new representation is also known as state space (SS) realization. The state space realization has been largely employed in control engineering and in hydrodynamic problems, see Taghipour et al. (2008), Kristiansen et al., (2005), and Yu and Falnes (1995).

Taking the convolution integral of the radiation force in heave due to heave from Eq. (7.21) as an example:

$$f_z(t) = \int_{-\infty}^{\infty} z_w(t-\tau)w(\tau)d\tau \tag{7.49}$$

Its respective state space realization will be given by:

$$\begin{aligned} \dot{X}(t) &= AX(t) + Bw(t) \\ Y(t) &= CX(t) + Dw(t) \end{aligned} \tag{7.50}$$

where $X$ is the state variable, $A$, $B$, $C$ and $D$ are the state, input, output, and transmission matrix, respectively.

The solution to (7.50) is:

$$\begin{aligned} X(t) &= e^{A(t-t_0)}X(t_0) + \int_{t_0}^{t} e^{A(t-\tau)}Bw(\tau)d\tau \\ Y(t) &= Ce^{A(t-t_0)}X(t_0) + \int_{t_0}^{t} Ce^{A(t-\tau)}Bw(\tau)d\tau + Dw(t) \end{aligned} \tag{7.51}$$

where $X(t_0) = \int_{-\infty}^{t_0} e^{A(t-\tau)}Bw(\tau)d\tau$, and $Y(t) = f_z(t)$.

Now taking into account the causality of the radiation force:

$$\begin{aligned} f_z(t) &= \int_0^t h_R(t-\tau)\dot{z}(\tau)d\tau, \left\{ \begin{matrix} w(t) = 0 \\ z_w(t) = 0 \end{matrix} \middle| t < 0 \right\} \\ X(t_0) &= 0 \end{aligned} \tag{7.52}$$

Equations (7.49) and (7.51) are then related to each other by:

$$Y(t) = f_z(t) = \int_0^t Ce^{A(t-\tau)}Bw(\tau)d\tau + Dw(t) = \int_0^t z_w(t-\tau)w(\tau)d\tau \qquad (7.53)$$

To obtain the equivalence between the $A$, $B$, $C$ and $D$ matrices with the $z_w$ IRF function different methodologies can be applied: the impulse response curve fitting, the realization theory and the regression in the frequency domain (see Taghipour et al. (2008)).

The curve fitting method requires that the transmission matrix $D$ to be set to zero yielding the following equivalence:

$$Ce^{A(t)}B = h_R(t) \qquad (7.54)$$

Then the IRF function is fitted to a set of coefficients distributed over a companion matrix. To find the matrix coefficients, the least square method is used minimizing the error between the estimated IRF and the given one.

$$E = \sum_{k=1}^{n} G(t_k)\left(h_R(t_k) - Ce^{A(t)}B\right)^2 \qquad (7.55)$$

where $G(t_k)$) is the weight function.

The curve fitting by companion matrices has been investigated in more detail in Tello Ruiz et al. (2014). Other methods applied using the realization theory and the regression in the frequency domain exist in literature. Perhaps, the most suitable and ready to use is the MATLAB function IMP2SS, which gives the continuous state space model. The latter requires further discretization and model reduction can be achieved by using an additional MATLAB function, BALMR, from the Robust Control Toolbox.

## 7.3 Nonlinear wave forces and moments

### 7.3.1 General discussion

Wave forces are estimated based on the linear contribution of two potentials, the incident wave potential $\phi_I$ and the diffraction potential $\phi_D$. The first is already defined from the wave theory, while the second requires first the solution of the boundary value problem (BVP) on the free surface and the hull surface.

Generally, the solution of the BVP is obtained by taking into account three main considerations: (a) incident wave amplitudes and (b) body oscillatory motions must be of small amplitude relative to the wave length, and (c) assume all phenomena oscillating harmonically with the encounter frequency.

Taking into consideration items (a) and (b), one can assume the ship's hull wetted surface approximately constant during each oscillation. If now one considers (c), the potential depending on the BVP can be solved linearly and independently of time. Hence, indirect solutions in the frequency domain solution can be derived as in Salvesen et al. (1970) and Ogilvie (1964).

When the ship develops large oscillatory motions the constant wetted surface assumption is not valid. The BVP on the hull surface changes each time step and the solution of the diffraction potentials with it. These types of nonlinearity makes the study in the frequency domain impossible; hence a different approach is required. For container ships with large bow-flare even small to moderate ship motions can introduce similar nonlinear effects. An additional source of this type of nonlinearity can be associated to squat effects in shallow water. The induced trim will change the mean position of the ship, hence the hull form being subjected to wave exciting forces. The nonlinear treatment of the wave forces is then necessary.

The nonlinear BVP requires a more complex analysis. The complete solution of the nonlinear problem, however, might not be necessary. In Fonseca and Guedes Soares (1998) an

approximate estimation of these forces and moments has been conducted by considering the nonlinearity of the problem associated to hydrostatic and Froude-Krylov forces (incident wave forces and moments) only, thus improving significantly the results. The diffraction problem is then regarded as linear.

Figure 7.1 illustrates the main differences between the linear and the nonlinear approach.

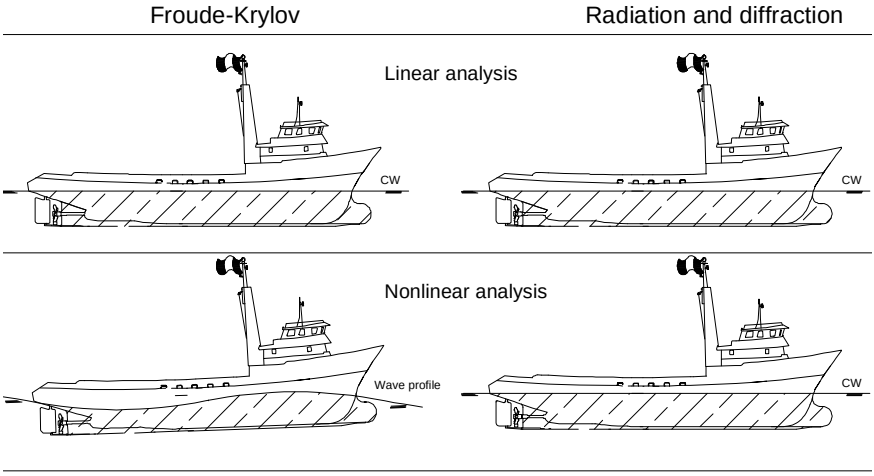


Figure 7.1 Hull wetted surface taken into account by the linear analysis (top figure) and the nonlinear analysis (bottom figure) of the Froude-Krylov forces.

Taking into account the Froude-Krylov and hydrostatic forces only (hence no diffraction is considered) simplifies the analysis significantly. Recall that the incident wave potential is already defined and does not depend on the BVP on the hull surface. Hence, the analysis is reduced to the correct estimation of these two forces on the actual wetted surface.

To estimate the actual hydrostatic and Froude-Krylov forces requires to obtain the pressure distribution on the submerged part of the hull. This will need first to determine the ship's position and orientation in space, in addition to a numerical scheme to re-compute the submerged part of the hull each time step.

In the present study, the numerical scheme considers an approximation of the three-dimensional hull surface by using flat panels. It is worth noticing, that in the process of redefining the wetted surface each time step, in some cases, panels above the mean water level will be included. This requires further care for the evaluation of wave pressure, valid only up to the mean water level ($z = 0$). The numerical scheme and the considerations taken in the present nonlinear approach are discussed in the following subsections.

### 7.3.2 Froude-Krylov forces and moments

It has been shown in chapter 6 that the Froude-Krylov forces and moments can be obtained by:

$$\boldsymbol{F}_{\boldsymbol{FKj}}^{\boldsymbol{E}} = \iint_{S} \boldsymbol{N}_{\boldsymbol{j}} p_W ds \tag{7.56}$$

where $\boldsymbol{N}_{\boldsymbol{j}}$ is the normal vector to the surface area $ds$, and the wave pressure $p_W$ is given by:

$$p_W = \rho g \zeta_a \frac{\cosh k(z+h)}{\sinh kh} e^{-i(kX_0 cos\eta - kY_0 sin\eta - \omega_0 t + \alpha_W)} \tag{7.57}$$

The hydrostatic contribution can be included in the computation as well by adding to the dynamic pressure $p_W$ the hydrostatic pressure as:

$$p = p_W + p_H \tag{7.58}$$

where $p_H$ is given by:

$$p_H = \rho g \left(\zeta - Z_{c/O}\right) \tag{7.59}$$

#### *7.3.2.1* Dynamic wave pressure above mean water level

During computations, the actual wetted surface will incorporate panels located above the mean water level ($Z_0 = 0$). For such panel locations Eq. (7.57) cannot be directly used to compute the wave pressure because $\phi_I$ (found by using the linearization of the free surface boundary condition, see Journée and Massie (2001)), has

been defined up to the mean water surface $Z_0 = 0$. A simple method to calculate the wave pressure above the mean water level is hydrostatically (Dean and Dalrymple, 1991) by:

$$p_W = \rho g(\zeta - Z_{c/O}) \tag{7.60}$$

A widely used method is the stretching approach (Wheeler, 1969)). This method applies a correction to the potential flow by stretching the negative $Z_0$-axis up to the water surface. A variation of this method is the vertical extrapolation, and the tangential extrapolation methods. For this type of method a stretching factor $E(z)$ applied to the potential $\phi_I$ is given by:

$$E(Z_O) = \frac{\cosh\big(k(Z_O + h)\big)}{\sinh(kh)} \tag{7.61}$$

In the vertical extrapolation approach, the potential above the mean water level is assumed equal to the one defined at the mean water level. Thus $Z_O$ in Eq. (7.61) is set to:

$$Z_O = 0 \tag{7.62}$$

In the Wheeler (1969) approach the potential flow at the actual water surface is the same as the one obtained at the mean water level. For any other intermediate position, the potential is found by modifying the vertical axis $Z_O$ in Eq. (7.61) by:

$$Z_O' = \frac{h(Z_O - \zeta)}{h + \zeta} \tag{7.63}$$

The Wheeler method in literature is recommended for waves with smaller slopes, and its use should be avoided for steep waves.

Finally, in the tangential extrapolation method, the derivative of $E(Z_O)$ is required at the mean water level. Then for every point, the potential is modified by:

$$E(z) = E(Z_O = 0) + Z_O \left.\frac{dE}{dz}\right|_{Z_O=0} \tag{7.64}$$

Figure 7.2 illustrates the main differences between the three stretching approaches.

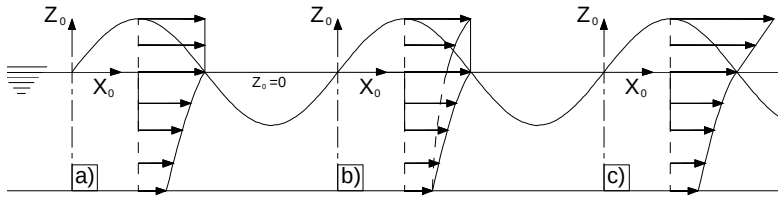


Figure 7.2 Stretching methods, (a) the vertical extrapolation, (b) the Wheeler approach, and (c) the tangential extrapolation.

According to Grue et al. (2003) the Wheeler method can provide reasonable results for smaller wave slopes but in general in literature no preference is found between the methods.

Considering the further extension to irregular waves, it is clear that the stretching approach will require more computational time, as the extrapolations has to be conducted for every single wave component. As a first step in the present study, the hydrostatic approach is used. This is the simplest method, but offers a robust and minimal computing time analysis.

### 7.3.3 Wetted surface analysis

At a given time, panels located above the mean water level will be also part of the wetted surface. Thus, the initial discretization of the hull surface should include panels located above the mean water level. Figure 7.3 shows an example of such discretisation for a ship with constrained motion modes in irregular waves.

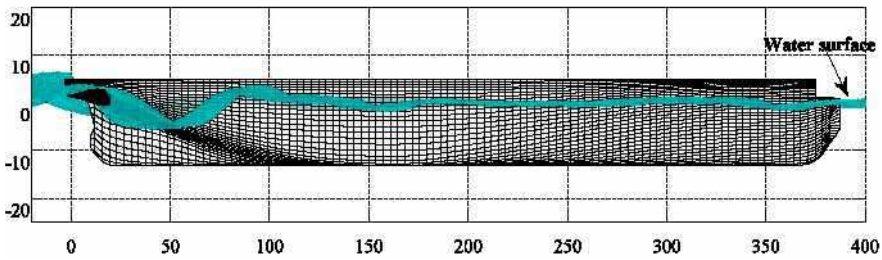


Figure 7.3 Panel discretisation below and above the mean water level.

The waterline will intersect panels defining new shapes that need to be investigated. To further proceed with the study three main conditions are required:

a) waves should not break as they propagate along the hull surface,
b) moderate wave amplitudes, and
c) the panel's main dimensions should be relatively small compared to the smaller wave length considered in the analysis.

These requirements allow the approximation of the water surface along each panel to be defined as a simple plane. This finally reduces the study to the intersection of two planes, one defined by the hull surface's panel and the other one defined by the variation of the water surface along that panel.

#### *7.3.3.1 Panel cutting cases*

The analysis yields five different cases. These are hereafter referred to as: C0, CI, CII, CIII, and CIV. The names make reference to the number of vertices above the local water line, e.g. CII indicates two vertices above the water line. In Figure 7.4 a sketch illustrates the different intersections between the water surface and the hull surface panels.

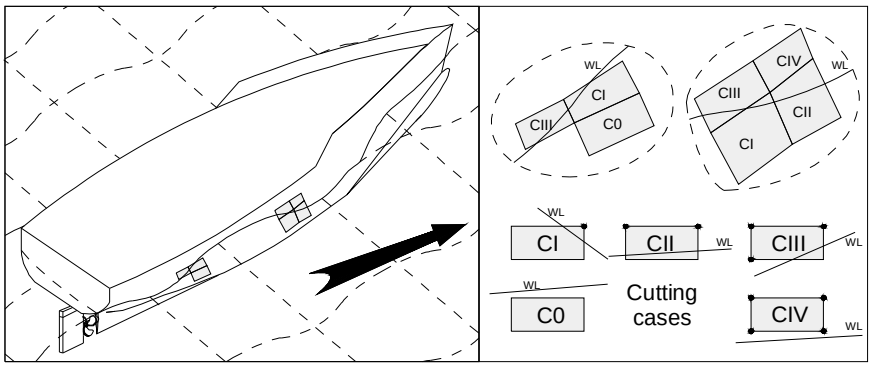


Figure 7.4 The five different cutting cases depending on the relative position between the panel and the water level.

From all of the cutting cases, the CIV case is omitted from the analysis conducted in the current time-step because the panel is completely located above the water surface. The C0 case is also skipped from the re-shaping analysis but an update of the panel coordinates (due to the ship motions) is required. The flow chart in Figure 7.5 describes the process for the re-meshing analysis.

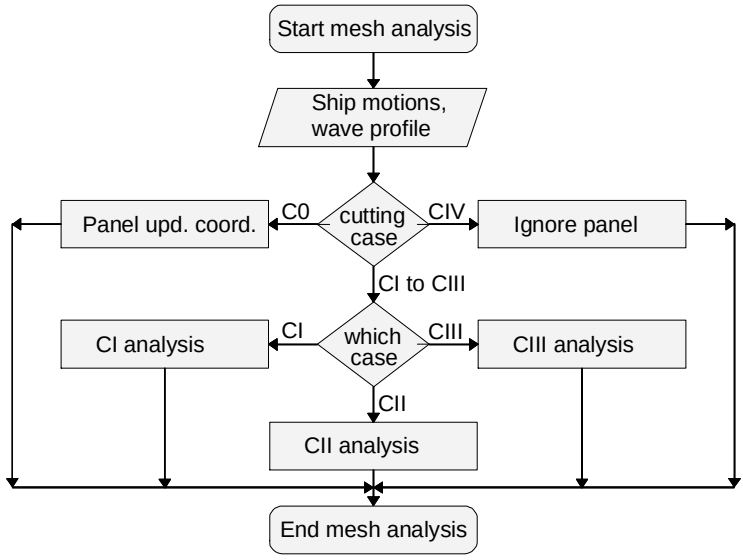


Figure 7.5 Flow chart of the numerical analysis for re-meshing the wetted surface.

### *7.3.3.2 Numerical algorithm*

The panel's vertices are ordered clockwise, as seen from the fluid domain. Each panel has four vertices defining a quadrilateral shape; in some cases two vertices might coincide yielding a triangular shape. For all panels (hereafter named as faces), the vertices $V$, the area $A$ and the centroid $c$ are given in the Earth axes system, the E-frame. See Figure 7.6 for better illustration.

All vertices and the resulting faces are further arranged in two different sets of matrices. These are named the $\boldsymbol{V}$ and $\boldsymbol{f}$ matrices. The $\boldsymbol{V}$ matrix contains the three spatial coordinates and is arranged in such a way that each row gives the position in space of a given vertex. The $\boldsymbol{f}$ matrix's rows contain a sequence of four

vertices (row indexes of the $\boldsymbol{V}$ matrix) which define a given face. In Table 7.8 the two matrices are presented for better illustration.

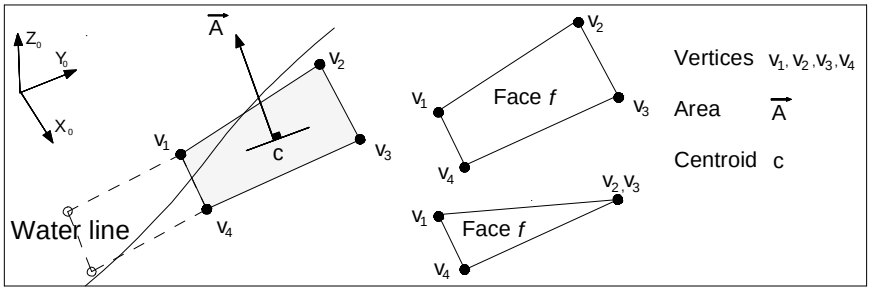


Figure 7.6 Panel vertices, sign conventions and general arrangement.

Table 7.8 The $\boldsymbol{V}$ and the $\boldsymbol{f}$ matrices used to describe the hull.

| Face matrix | Vertices matrix |
|---|---|
| $\boldsymbol{f} = \begin{bmatrix} f_1 \\ \vdots \\ f_R \end{bmatrix} = \begin{bmatrix} V_{m_1 1}\ V_{m_2 1}\ V_{m_3 1}\ V_{m_4 1} \\ \vdots \\ V_{m_1 R}\ V_{m_2 R}\ V_{m_3 R}\ V_{m_4 R} \end{bmatrix}_{r\times 4}$ | $\boldsymbol{V} = \begin{bmatrix} V_1 \\ \vdots \\ V_N \end{bmatrix} = \begin{bmatrix} X_{01}\ Y_{01}\ Z_{01} \\ \vdots \\ X_{0N}\ Y_{0N}\ Z_{0N} \end{bmatrix}_{n\times 3}$ |
| $r = 1,2,\dots,R \qquad m_{1,2,3,4} = 1,2,\dots,N$ | $n = 1,2,3,\dots,N$ |

The letters $R$ and $N$ in Table 7.8 indicate the total number of faces and vertices, respectively.

To determine whether a face is located below or above the water surface a first comparison is made between the vertical coordinates of a face and the respective vertical position of the water surface.

For this analysis, the three-dimensional points for all panels are rearranged in three separate matrices describing the longitudinal, transversal, and vertical positions, distributed in the $\boldsymbol{x_f}$, $\boldsymbol{y_f}$, and $\boldsymbol{z_f}$ matrices, respectively.

$$\boldsymbol{x_f} = \begin{bmatrix} X_{0f_1} \\ \vdots \\ X_{0f_R} \end{bmatrix} = \begin{bmatrix} X_{0V_{m_1 1}} & X_{0V_{m_2 1}} & X_{0V_{m_3 1}} & X_{0V_{m_4 1}} \\ & \vdots & \vdots & \\ X_{0V_{m_1 R}} & X_{0V_{m_2 R}} & X_{0V_{m_3 R}} & X_{0V_{m_4 R}} \end{bmatrix} \tag{7.65}$$

$$\boldsymbol{y}_f = \begin{bmatrix} Y_{0f_1} \\ \vdots \\ Y_{0f_R} \end{bmatrix} = \begin{bmatrix} Y_{0V_{m_1}1} & Y_{0V_{m_2}1} & Y_{0V_{m_3}1} & Y_{0V_{m_4}1} \\ & \vdots & \vdots & \\ Y_{0V_{m_1}R} & Y_{0V_{m_2}R} & Y_{0V_{m_3}R} & Y_{0V_{m_4}R} \end{bmatrix} \tag{7.66}$$

$$\boldsymbol{z}_f = \begin{bmatrix} Z_{0f_1} \\ \vdots \\ Z_{0f_R} \end{bmatrix} = \begin{bmatrix} Z_{0V_{m_1}1} & Z_{0V_{m_2}1} & Z_{0V_{m_3}1} & Z_{0V_{m_4}1} \\ & \vdots & \vdots & \\ Z_{0V_{m_1}R} & Z_{0V_{m_2}R} & Z_{0V_{m_3}R} & Z_{0V_{m_4}R} \end{bmatrix} \tag{7.67}$$

Eq. (7.65) and Eq. (7.66) can be used to find the respective vertical position of the water surface, $\boldsymbol{z_w}$ by introducing the $\boldsymbol{x_f}$ and $\boldsymbol{y_f}$ matrices in the wave equation:

$$\boldsymbol{z_w} = \zeta(\boldsymbol{x_f}, \boldsymbol{y_f}, t, k, \mu, \zeta_a) \tag{7.68}$$

Comparing the two matrices $\boldsymbol{z_w}$and $\boldsymbol{z_f}$, yield a matrix of indexes $\boldsymbol{I_f}$, which can be summarised to five representative combinations:

$$\boldsymbol{I_f} = \boldsymbol{z_f} > \boldsymbol{z_w} \quad \begin{array}{ll} = [0,0,0,0] & \text{Case C0} \\ = [0,0,0,1] & \text{Case CI} \\ = [0,0,1,1] & \text{Case CII} \\ = [0,1,1,1] & \text{Case CIII} \\ = [1,1,1,1] & \text{Case CIV} \end{array}$$

Each case corresponds to all possible combinations yielding the same number of vertices above the local water level. To be more clear, For instance, the case CI summarise four different results such as $[1,0,0,0]$, $[0,1,0,0]$, $[0,0,1,0]$, $[0,0,0,1]$.

The faces are then separated based on the results obtained in the $\boldsymbol{I_f}$ matrix and treated independently (as shown in Figure 7.5). Each case requires a particular analysis which is described in the following subsections.

#### 7.3.3.2.1 Case CI

In this case the local water line intersects the panel in two different points, *a* and *b*, see Figure 7.7 left. The line defined by these two points is further used to redefine the panel in two sub panels, one above and one below the water level.

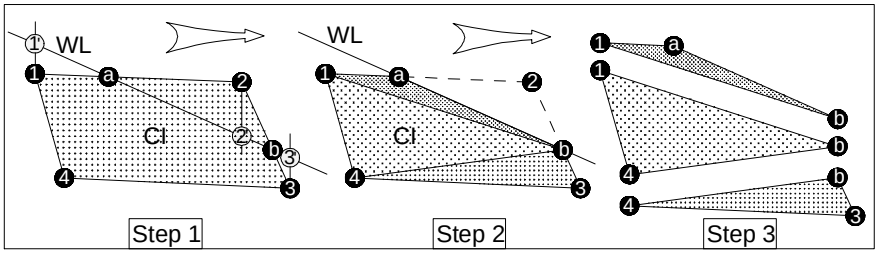


Figure 7.7 CI panel analysis procedure.

To redefine the panels, first, these new two vertices *a* and *b* must be obtained. In the present study this approach comprises four main steps:

a) First, based on the index corresponding to the unit value in the $\boldsymbol{I_f}$ matrix for the face $\boldsymbol{f_r}$, the vertex located above the water line is identified (see vertex *2* in Figure 7.7).
b) Using the vertex *2* place in the matrix $\boldsymbol{I_f}$, the adjacent vertices, *1* and *3* are also identified.
c) Then, the $X_0$ and $Y_0$ coordinates of the vertices *1* and *3*, together with the surface function $\zeta$, are used to define the new points *1'* and *3'* in space.
d) Finally, point *a* is obtained from the intersection between the lines defined by the points *1'* and *3'* with the ones defined by the points *1* to *2.* Point *b* is found in a similar way to point *a,* but with the line defined by points *2* and *3*.

As an example of the last step in the analysis, the estimation of point *a* is discussed here. The vertices 1 ($V_1$) and 2 ($V_2$), and points 1' ($P_{1'}$) and 2' ($P_{2'}$) define the lines $\mathrm{l_V}$ and $\mathrm{l_P}$, respectively. The coordinates $(X_0, Y_0, Z_0)$ for any given point located within the respective limits, defined for each line, can be defined as:

$$(X_0, Y_0, Z_0)_{l_V} = \mathrm{V_1} + s_{\mathrm{l_V}}(\mathrm{V_2} - \mathrm{V_1}) \qquad s_{\mathrm{l_V}} = [0\ 1] \tag{7.69}$$

$$(X_0, Y_0, Z_0)_{l_P} = P_{1'} + s_{\mathrm{l_P}}(P_{2'} - P_{1'}) \qquad s_{\mathrm{l_P}} = [0\ 1] \tag{7.70}$$

here the subscripts make reference to the lines which the respective coordinates belong. The scalar parameters $s_{\mathrm{l_V}}$ and $s_{\mathrm{l_P}}$ can vary between zero and one.

Because both lines are coplanar ($V_1$ and $V_2$ with respect to points $P_1$, and $P_2$, differ only in their vertical coordinates) their intersection will occur when $s_{\mathrm{l_V}} = s_{\mathrm{l_P}} = s$. Replacing $s$ for $s_{\mathrm{l_V}}$ and $s_{\mathrm{l_P}}$ in Eq.(7.69) and Eq. (7.70) and equating both, yields:

$$s = \frac{V_1 - P_1,}{(V_2 - V_1) - (P_2, - P_1,)} \qquad s = [0\ 1] \tag{7.71}$$

where s varies between zero and one also.

Using Eq. (7.71) the intersection point *a* (see Figure 7.7 left) can be obtained by simply replacing $s$ for $s_{l_V}$ in Eq. (7.69) or for $s_{l_P}$ in Eq. (7.70). A similar approach is conducted to obtain the intersection point *b*.

Once both intersection points *a* and *b* are obtained, reshaping the panel from case CI is conducted by defining three new triangular shapes as shown in Figure 7.7 right. Care should be taken when defining the new faces in order to keep the clockwise orientation (seen from the fluid domain). This is of relevance for further evaluation of the normal vectors to the surface.

#### 7.3.3.2.2 Case CII

In the case CII, first, the two points located above the waterline are first identified. Then the adjacent points are obtained from the matrix of indexes $\boldsymbol{I_f}$. With the identification of these vertices, the intersections *a* and *b* are found by using the same mathematical procedure described above for the CI case. However, in this case, the points 1 and 4, and 2 and 3 define the new intersection edges.

The redefined shape of the panel is then finally composed of two triangles, as shown in Figure 7.8 right. As in the CI case care is taken to redefine the face of the panels for further analysis.

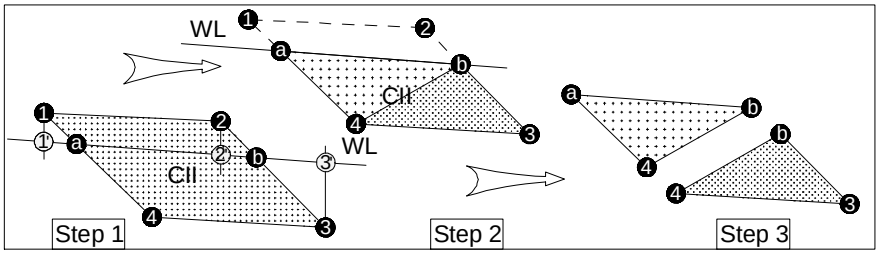


Figure 7.8 CII panel analysis procedure.

#### 7.3.3.2.3 Case CIII

In the case CIII, different from the other cases, first the index of the vertex located below the water surface is identified from the matrix $\boldsymbol{I_f}$, and then the adjacent vertices are also obtained.

The procedure to find the intersection points *a* and *b* is similar to the one followed in the CI case. Once these points are found the panel is redefined by only one triangular shape as shown in Figure 7.9. As stated above, it is important to keep the clockwise orientation for the vertices in the definition of the new face.

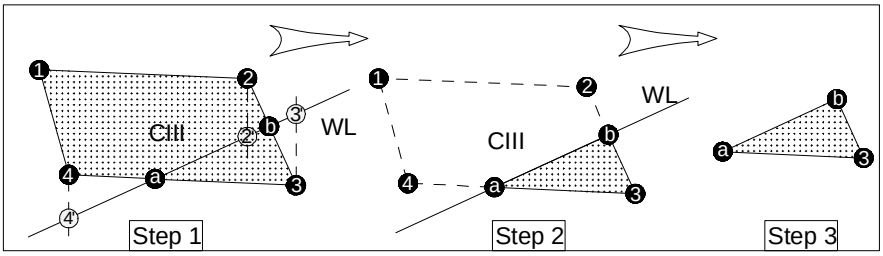


Figure 7.9 CIII panel analysis procedure.

#### 7.3.3.2.4 Centroid and normal vector for triangular geometry

Redefining the panels with triangular shapes simplifies the analysis because the evaluation of their geometrical characteristics such as areas and centroids is relatively simpler.

These two main characteristics are needed to compute the local forces and their points of application on the panel. Figure 7.10 sketches the triangular shape with the centroid's location and the counter clockwise convention for the area vector definition.

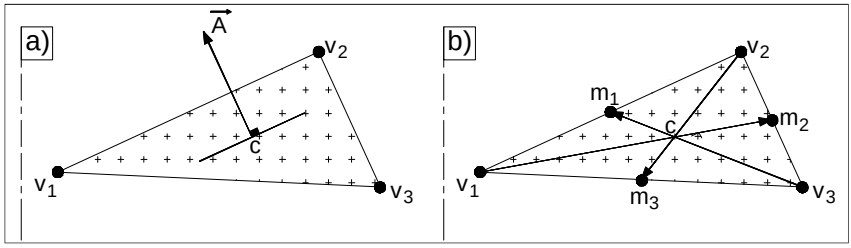


Figure 7.10 (a) Triangular shape with vertices $V_1$ , $V_2$ , $V_3$, normal vector $\vec{\mathbf{A}}$, and centroid $c$, and (b) the geometrical location of the centroid c.

For a triangular shape, the centroid $c$ is defined by the intersection of the medians $\mathrm{V_1m_2}$, $\mathrm{V_2m_3}$, and $\mathrm{V_3m_1}$. This is illustrated in Figure 7.10 (b). Any point ($X_0$, $Y_0$, $Z_0$) located within each meridian can be defined as:

$$(X_0, Y_0, Z_0)_{\mathrm{V_1m_2}} = \mathrm{V_1} + s_{\mathrm{V_1m_2}}(\mathrm{m_2} - \mathrm{V_1}) \qquad s_{\mathrm{V_1m_2}} = [0\ 1] \qquad (7.72)$$

$$(X_0, Y_0, Z_0)_{V_2\mathrm{m_3}} = \mathrm{V_2} + s_{V_2\mathrm{m_3}}(\mathrm{m_3} - \mathrm{V_2}) \qquad s_{V_2\mathrm{m_3}} = [0\ 1] \qquad (7.73)$$

$$(X_0, Y_0, Z_0)_{V_3\mathrm{m_1}} = \mathrm{V_3} + s_{V_3\mathrm{m_1}}(\mathrm{m_1} - \mathrm{V_3}) \qquad s_{V_3\mathrm{m_1}} = [0\ 1] \qquad (7.74)$$

The points $m_1$, $m_2$, and $m_3$ can be found by simply averaging the vertices in between, e.g. $m_2 = (\mathrm{V_2} + \mathrm{V_3})/2$ and $m_3 = (V_3 + \mathrm{V_1})/2$. The intersection between the medians can be obtained by equating for instance Eq. (7.72) and Eq. (7.73):

$$(X_0, Y_0, Z_0)_{\mathrm{V_1m_2}} = (X_0, Y_0, Z_0)_{V_2\mathrm{m_3}} \qquad (7.75)$$

Substituting the $m$ coordinates as function of the vertices, yields the following equation:

$$\left(2 - s_{\mathrm{V_1m_2}} - s_{V_2\mathrm{m_3}}\right)\mathrm{V_2} + \mathrm{V_1}\left(s_{V_2\mathrm{m_3}} + 2s_{\mathrm{V_1m_2}} - 2\right) + \mathrm{V_3}\left(s_{V_2\mathrm{m_3}} - s_{\mathrm{V_1m_2}}\right) = 0 \qquad (7.76)$$

For the intersection to be unique, the terms in the parenthesis must be zero, hence:

$$s_{\mathrm{V_1m_2}} = s_{V_2\mathrm{m_3}} = \frac{2}{3} \qquad (7.77)$$

Replacing $s_{\mathrm{V_1 m_2}} = 2/3$ in Eq. (7.72), the centroid can be found as function of the vertices by:

$$\mathrm{C} = \frac{\mathrm{V}_1 + V_2 + \mathrm{V}_3}{3} \tag{7.78}$$

The area $\mathbf{A}$ can be found by the cross product of the vectors defined by vertices $\mathrm{V}_1$, $\mathrm{V}_2$, and $\mathrm{V}_3$ as, $\overline{\mathrm{V}_1\mathrm{V}_2}$ and $\overline{\mathrm{V}_1\mathrm{V}_3}$. The normal vector $\boldsymbol{n}$ can be obtained by the normalisation of the vector area. These two quantities can be obtained respectively by:

$$\mathbf{A} = \frac{1}{2}\overline{\mathrm{V}_1\mathrm{V}_2} \times \overline{\mathrm{V}_1\mathrm{V}_3} \tag{7.79}$$

$$\mathbf{n} = \frac{\mathbf{A}}{|\mathbf{A}|} \tag{7.80}$$

# MANOEUVRING IN COASTAL WAVES



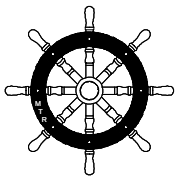

*Every new beginning comes from some other beginning's end.*

*Seneca*

# 8

# Conclusions and future work

## 8.1 General discussion

The investigation of the manoeuvring problem in waves required first a comprehensive literature study and the identification of the state of the art methods. The large amount of research available in literature can be, to some extent, overwhelming because of the significant progress conducted in the independent fields of seakeeping and manoeuvring in calm water.

From the literature review two state of the art methods for manoeuvring in waves have been identified, the two-time scale method and the unified method. The first one is solved in two separate modules, one identical to the manoeuvring in calm water and the other identical to the seakeeping model. Information is exchanged from one model to another each (or at any other previously chosen interval) time step. The second one, however, requires a more complex treatment of the hydrodynamic problem because the main goal is to merge the formulations applied in both fields, seakeeping and manoeuvring in calm water. Hence, in

the unified method a more consistent analysis of the physics is involved.

The main goal of the project is to develop a 6DOF manoeuvring model in coastal waves; hence, vertical motions need to be included in the analysis. The latter is neglected in the two-time scale method, which simplifies the problem considerably. Moreover, because the ship is to manoeuvre in real seas, the ship motions will not necessarily be harmonically oscillating; hence, the treatment of the radiation problem in manoeuvring by constant zero frequency coefficients (or replacing them by constant values at a given frequency) cannot be applied. The latter is, however, indifferently used in the two-time scale method.

The radiation problem in a more consistent analysis (the unified method) introduces the use of convolutions integrals. Researchers, e.g. Skejic and Faltinsen (2008) and Seo and Kim (2011), however, argue that the dependency of the convolution terms on the ship speed and variant encounter frequency (because they are found based on frequency dependent added masses and damping coefficients) is the main constraint to their application, hence models such as the one proposed in Bailey et al. (1998) were not further used, and the two time scale method was preferred.

It is important to recall that the present model is intended for implementation on a manoeuvring simulator at FHR. Hence, a more realistic scenario of ship manoeuvring in waves is desired. Because of this, and a more consistent analysis of the physics involved, the unified method was further investigated in the present work.

To investigate further the effect of waves two main possibilities are available in literature, Experimental Fluid Dynamic (EFD) analysis and Computational Fluid Dynamic (CFD) analysis. CFD studies were not used in the present work because of the computational and time demanding resources even when solving the ship's steady responses in deep water. Because of the

complexity of the flow when the ship manoeuvres in waves, and considering the shallow water restrictions, in the present work, EFD was preferred.

## 8.2 Experimental studies

For the evaluation of wave effects on the manoeuvring of the ship a scale model of an ultra large container carrier was used. Several test parameters were varied, such as the water depth, the ship's draft, the ship's forward speed, the drift angle, the wave amplitude and length, the wave's angle of encounter, the propeller rate, and the rudder angle. Two different test types were also used, harmonic oscillating yaw tests and steady straight-line tests. In addition, to investigate the influence of ship motions on the results, two different beam frames were used which allowed to perform fully captive and semi-captive models tests.

In fully captive tests, all forces and moments were measured, as well as the ship's horizontal position along the tank. In semi-captive tests only horizontal forces and the yaw moment were obtained; in addition, the ship motions in heave, roll and pitch were obtained. During the tests, wave profiles were recorded by a wave gauge ahead the ship and at positions fixed along the tank.

The combination of all the parameters considered resulted in an approximate of +3000 tests per test campaign. Four test campaigns were executed in the scope of the present work. Due to problems encountered in the initial programs the analysis of the results are restricted to the discussion of the most extensive one. In the course of the present work, the test procedures and post processing analysis methods have been improved.

### 8.2.1 Hull forces and moments

#### *8.2.1.1First order wave forces and moments*

From the experimental results obtained for the forces in surge and heave and the pitch moment, the influence of the drift angle was found to be negligible. All results were found to overlap to each other. The results where further compared against numerical

computations carried out with Hydrostar. In general a fair agreement was found. Only slightly larger differences were obtained in following waves at higher speed.

These results were also compared against the contribution of the Froude-Krylov (FK) forces and moments only; insignificant differences were obtained indicating a minor advantage when considering the diffraction problem for the tested conditions. This, however, should be carefully considered because at larger angles of wave encounter the diffraction problem, especially for the short wave lengths under study, could be relevant.

#### *8.2.1.2 Second order wave forces*

When measuring the second order forces, their small order of magnitude was found to be a critical problem in the experimental study. The noise in the gauges, the interferences due to the limitations of the towing tank itself were found to be the main constraint. It should be then of great importance to specify the uncertainties on these quantities, however, due to the amount of variables to be accounted for in such analysis was not conducted. Instead, only the precision uncertainty was study for steady test which was assumed to be representative for all test conducted with the model fully captive (frame B). Nevertheless, the results, although influenced by such limitations, are still of relevance to investigate trends that can allow the identification of the main wave effects on manoeuvring.

##### 8.2.1.2.1 Wave added resistance

From the experimental result of the added wave resistance the findings can be summarised as:

a) larger magnitudes were encountered in head waves in contrast to following waves. In following waves the added wave resistance seems to be rather negligible for all wave lengths considered;
b) their magnitudes were found to be slightly affected by ship's forward speed and motions for waves shorter than 0.5 $L_{PP}$;

c) results were found to confirm the square of the wave amplitude dependence of the added wave resistance, except for the case of the lower forward speed where a slight spreading was found between the results obtained from the two different wave amplitudes;

Recall that the added wave resistance has been estimated by subtracting the resistance obtained in waves from the value measured in calm water. Because of the proportionality with respect to the square of the wave amplitude holds for the two wave amplitudes, it can be inferred that waves do not alter significantly any of the components of the ship resistance as observed in calm water; hence, added wave resistance can be assumed as an additional component to the calm water problem.

The results were also compared against the estimations of the added wave resistance carried out in Hydrostar. In head waves a fair agreement was found for wave lengths smaller than 0.4 $L_{PP}$ only. For longer waves an overprediction is found with, in some cases, twice the experimental values. To the author's opinion the latter can be associated to the differences in the estimations of the ship motions. In following waves, however, because of the smaller magnitudes of the results the comparison is rather inconclusive, however, this is of a minor importance because of the same smaller obtained magnitudes.

#### 8.2.1.2.2 Mean second order wave forces and moments

The evaluation of the mean second order wave forces at large incoming wave angles was investigated by performing fully captive model tests. Although the suitability of the towing tank at FHR is limited for such tests, the investigation was still carried out by selecting a time window of a harmonic yaw test conducted at very low forward speed.

The result showed only significant magnitudes for the forces in surge, sway, and heave; the moments, however, were found to be rather negligible. Similarly to what has been found for the added wave resistance, the forces are found to be proportional to the

square of the wave amplitude. The comparisons against the numerical results, obtained from Hydrostar, show a fair agreement for surge and sway forces; heave forces, however, were found to be underpredicted.

#### *8.2.1.3Steady forces and moments*

The investigation of the wave effects was further carried out by the evaluation of the steady forces as measured in calm water and their comparison against the ones obtained in waves.

The results obtained for surge and sway forces, and the yaw moment, from the model in fully and semi captive modes, showed no significant differences, which confirms the insignificant influence of the oscillatory motions.

With respect to the influence of waves, their effects on the steady forces and moments were found to decrease as the speed increases. For surge forces, wave effects were found to be slightly larger in following waves but overall their magnitudes were rather small. In contrast, only at very low speeds the influence of waves seems to be of great relevance.

With respect to the steady heave forces and pitch moments, it was possible to compare both tested conditions, semi-captive and fully captive, by the non-dimensionalisation based on the Tuck parameter. The results, however, show to be different, especially for the pitch moment. To the author's opinion this is rather expected as the hydrostatic equilibrium in the case of the fully captive test is not satisfied. Regarding the wave effect in both tested conditions, however, no significant variations with respect to the calm water results were obtained.

### 8.2.2 Ship motions

The results obtained from tests conducted at different drift angles showed no significant differences. This was observed for all forward speeds and wave angles of encounter considered. When comparing the results against numerical estimations (computed in Hydrostar), the major discrepancies were found for heave in

following wave conditions. Discrepancies were also found to increase as the speed increases. In spite of these differences, in general a fair agreement was found.

### 8.2.3 Propeller and rudder effects

Model tests with and without waves have also been conducted with the propeller and rudder working. Tests were conducted with the model semi-captive, thus allowing the ship to oscillate freely in heave, pitch and roll.

Bear in mind that the present evaluation was limited to a few scenarios of propeller rates and rudder angles (first quadrant). However, the present conditions are believed to be of relevance for the purpose of manoeuvres performed along the access channels in the presence of waves.

Oscillatory thrust forces and torque moments were found when the propeller operates in waves; they were found to be relatively small compared to the average value. Further evaluation was conducted by the thrust and torque identity methods to evaluate the wake in waves. Additionally the evaluation of the thrust deduction factor was also studied. From the study of the wake, no significant differences were found between the tests in calm water and in waves, a slightly larger variation was found with the thrust identity method but they remain negligible. In the case of the thrust deduction factor, wave effects were also found to have a negligible influence.

With respect to the rudder, an oscillatory behaviour was observed for the normal and tangential forces, only for the tangential force the order of magnitude of the oscillations was found to be significant. The mean of the rudder forces were then further evaluated by comparing the drag and lift coefficients obtained in calm water and in waves. No significant differences were found.

### 8.2.4 The superposition principle

The superposition of the wave forces in calm water with numerical estimations of the first and second order (only mean forces) forces

and moment obtained from Hydrostar were compared against experimental results obtained in waves. For this purpose, harmonic yaw tests were executed in calm water and in waves with and without the influence of drift angles. The comparison showed a fair agreement between the superposed values and the results obtained in waves. This was observed for both tendency and magnitudes, for all forces and moments, even for tests where a drift angle was used. Results were found to be more suitable for wave lengths smaller than 0.5 $L_{PP}$ than for longer waves.

For longer waves an oscillatory behaviour of the sway force and yaw moment was found (better seen at zero drift angle) when the ship attains a condition similar to head waves (wave parallel to the speed of the ship). To the author's opinion this can be addressed due to the fact the for longer waves the required time for one wave oscillation was comparable to the time needed for a significant change in ship's heading, hence the ship never reaches a steady condition where waves are parallel to the ship heading. Bear in mind that for the present study, an ULCC navigating in the Belgian part of the North Sea, these limitations are however out of the scope of the present work; hence, the superposition of the wave forces can be considered as a valid approach for further analysis of the ULCC manoeuvring in waves.

## 8.3 A unified radiation problem

The radiation problem (expressed differently in the fields of seakeeping and the manoeuvring) requires a single representation that can unify them. An important progress on this need was presented by Bailey et al. (1998). However, their final results contained terms such as $V/\omega^2$ which introduced singularities at zero frequency for the pitch and yaw moments. These singularities were not further discussed in Bailey et al. (1998), but they are relatively important because frequencies ranging from zero to infinity are needed for the evaluation of the respective Impulse Response Functions (IRFs). These singularities were solved in the present work by differential and integral calculus and extending

additional relationships between the IRFs in heave and yaw to the ones in surge and sway, respectively.

The radiation problem in the time domain is expressed by convolution integral equations where the IRFs are convolved with the instantaneous ship velocities. Because the IRFs depend as well of the ship's speed through the variant encounter frequency (recall they are estimated based on the frequency domain coefficients intense computations to constantly update the IRFs are a major problem. In the present study, constant IRFs where found by separating the IRFs in two sub-IRFs. The final IRFs are then obtained by their linear combination, with one of them being directly proportional to $V$.

In spite of the simplifications achieved with respect to the speed dependence of the IRFs, the lengthy computations when using convolution integral can be a major drawback for simulation purposes. This, however, does not represent a further problem because they can be further simplified by using their state space representation. This methodology transforms the convolution integral into a set of ordinary differential equations that are generally better suited for numerical purposes.

## 8.4 A nonlinear method for wave forces

A numerical tool has also been developed for the evaluation of the nonlinear forces and moments due to the Froude-Krylov phenomena. In addition, the nonlinear approach has been extended to the hydrostatic problem by adding the hydrostatic pressure to the hydrodynamic pressure due to waves. Hence, if this approach is used, additional restoring terms in the dynamic equation are no longer required.

It is important to mention that in seakeeping studies, hydrostatic and Froude-Krylov forces and moments computed on the hull wetted surface above the mean water level are regarded as second order effects. Hence, it can be stated that the present method does also account, partially, for second order forces and moments.

This tool is of practical application because it can be used to estimate wave forces in regular and irregular waves directly in the time domain. At this stage, however, the diffraction problem has not been accounted for. Although its influence was found to be small for head and following waves, the diffraction problem are believed to be important specially for beam waves (waves approaching from the side of the ship) and should be included in the analysis. Its implementation is, however, considered a future topic of research.

## 8.5 A 6DOF manoeuvring model

### 8.5.1 Overview

The experimental study revealed that the wave effects (within the limits of the present study) do not affect significantly the steady forces and moments as obtained from manoeuvring in calm water. It was also observed that forces and moments due to wave action are indifferent to the influence of the drift angle. Hence, the superposition approach was found to be a good assumption to proceed with the analysis of forces and moments when the ship manoeuvres in waves, especially at higher speeds.

### 8.5.2 Equations of motion

The equations of motion are expressed in a body fixed coordinate system, of which the origin is fixed amidships, with its x-axis positive towards the bow, the y-axis positive starboard and the z-axis positive downwards. The dynamic equation of the ship as a rigid body then yields:

$$\boldsymbol{F} = \begin{bmatrix} m\big(\dot{u} - vr + wq - x_G(r^2 + q^2) + z_G(pr + \dot{q})\big) \\ m(\dot{v} - wp + ur + x_G(pq + \dot{r}) + z_G(qr - \dot{p})) \\ \big(\dot{w} - uq + vp + x_G(pr - \dot{q}) - z_G(p^2 + q^2)\big) \\ \dot{h}_x + qh_z - rh_y + m\big(-z_G\,\dot{v} - z_G(ur - wp)\big) \\ \dot{h}_y + rh_x - ph_z + m\big(z_G\dot{u} + z_G(wq - vr) - x_G(\dot{w} + vp - uq)\big) \\ \dot{h}_z + ph_y - qh_x + m\big(x_G\dot{v} + x_G(ur - wp)\big) \end{bmatrix} \quad (8.1)$$

$\boldsymbol{F}$ is column matrix representing all forces and moments.

### 8.5.3 A modular approach

The proposed mathematical considers also that hydrodynamic forces and moments $\boldsymbol{F}$ can be expressed by a modular approach as:

$$\boldsymbol{F} = \boldsymbol{F_H} + \boldsymbol{F_R} + \boldsymbol{F_P} + \boldsymbol{F_W} \quad (8.2)$$

assuming that no other external forces act on the ship except for waves. The subscripts H, R, P, and W stand for hull, rudder, propeller, and wave contributions, respectively.

Note that because of indifference to wave action of the propeller and rudder, their respective model can be assumed to be the same as the ones obtained from calm water studies.

The wave induced forces $\boldsymbol{F_W}$ can be further subdivided as:

$$\boldsymbol{F_W = F_D + F_{FK} + F_{2nd}} \tag{8.3}$$

$\boldsymbol{F_D}$, $\boldsymbol{F_{FK}}$ and $\boldsymbol{F_{2nd}}$ refer to the diffraction, the Froude-Krylov, and the mean second order wave forces and moments.

Forces arising due to $\boldsymbol{F_D}$ and $\boldsymbol{F_{FK}}$ are also known as linear first order forces and moments. In the present work, a nonlinear $\boldsymbol{F_{FK}}$ method has been developed which incorporates, partially, second order effects. Further work is yet required in order to incorporate the diffraction problem.

The hull forces $\boldsymbol{F_H}$ are assumed to be decomposed as:

$$\boldsymbol{F_H = F_S + F_{id}} \tag{8.4}$$

$\boldsymbol{F_S}$ comprise forces arising from viscous, lift and cross flow phenomena, which can be treated independently from the body oscillation forces. Thus, any calm water manoeuvring model found for these fluid phenomena can be further used in the analysis.

The main change is regarding ideal fluid effects ($\boldsymbol{F_{id}}$) only. The ideal fluid forces and moments, following the studies of Cummins (1962), Ogilvie (1964), Bishop et al. (1973) and (Bailey et al., 1998), can be expressed, linearly, as:

$$\boldsymbol{F_{id} = A\ddot{X} + B\dot{X} + \int_{-\infty}^{+\infty} H^V(t-\tau)\,\dot{X}(\tau)d\tau} \tag{8.5}$$

$\boldsymbol{A}$ and $\mathbf{B}$ are composed of the high frequency limit for the added inertia and damping coefficients, $\boldsymbol{\dot{X}}$ expresses the ship velocities and $\boldsymbol{H}$ contains the impulse response functions. These matrices are respectively given by, considering $y_G = 0$:

$$\boldsymbol{A} = \begin{bmatrix} \tilde{X}_{\dot{u}}(\infty) & 0 & \tilde{X}_{\dot{w}}(\infty) & 0 & \tilde{X}_{\dot{q}}(\infty) & 0 \\ 0 & \tilde{Y}_{\dot{v}}(\infty) & 0 & \tilde{Y}_{\dot{p}}(\infty) & 0 & \tilde{Y}_{\dot{r}}(\infty) \\ \tilde{X}_{\dot{w}}(\infty) & 0 & \tilde{Z}_{\dot{w}}(\infty) & 0 & \tilde{Z}_{\dot{q}}(\infty) & 0 \\ 0 & \tilde{Y}_{\dot{p}}(\infty) & 0 & \tilde{K}_{\dot{p}}(\infty) & 0 & \tilde{K}_{\dot{r}}(\infty) \\ \tilde{X}_{\dot{q}}(\infty) & 0 & \tilde{Z}_{\dot{q}}(\infty) & 0 & \tilde{M}_{\dot{q}}(\infty) & 0 \\ 0 & \tilde{Y}_{\dot{r}}(\infty) & 0 & \tilde{K}_{\dot{r}}(\infty) & 0 & \tilde{N}_{\dot{r}}(\infty) \end{bmatrix} \tag{8.6}$$

$$\boldsymbol{B} = \begin{bmatrix} \tilde{X}_{u}(\infty) & 0 & \tilde{X}_{w}(\infty) & 0 & \tilde{X}_{q}(\infty) & 0 \\ 0 & \tilde{Y}_{v}(\infty) & 0 & \tilde{Y}_{p}(\infty) & 0 & \tilde{Y}_{r}(\infty) \\ \tilde{X}_{w}(\infty) & 0 & \tilde{Z}_{w}(\infty) & 0 & \tilde{Z}_{q}(\infty) & 0 \\ 0 & \tilde{Y}_{p}(\infty) & 0 & \tilde{K}_{p}(\infty) & 0 & \tilde{K}_{r}(\infty) \\ \tilde{X}_{q}(\infty) & 0 & \tilde{Z}_{q}(\infty) & 0 & \tilde{M}_{q}(\infty) & 0 \\ 0 & \tilde{Y}_{r}(\infty) & 0 & \tilde{K}_{r}(\infty) & 0 & \tilde{N}_{r}(\infty) \end{bmatrix} \tag{8.7}$$

$$\dot{\boldsymbol{X}} = [u \quad v \quad w \quad p \quad q \quad r]^T \tag{8.8}$$

$$\boldsymbol{H^V} = \begin{bmatrix} x_u^V & 0 & x_w^V & 0 & x_q^V & 0 \\ 0 & y_v^V & 0 & y_p^V & 0 & y_r^V \\ z_u^V & 0 & z_w^V & 0 & z_q^V & 0 \\ 0 & k_v^V & 0 & k_p^V & 0 & k_r^V \\ m_u^V & 0 & m_w^V & 0 & m_q^V & 0 \\ 0 & n_v^V & 0 & n_p^V & 0 & n_r^V \end{bmatrix} \tag{8.9}$$

The matrices $\boldsymbol{A}$, $\boldsymbol{B}$, and $\boldsymbol{H^V}$ are symmetric, see for instance $x_w = z_u$, $y_p = k_v$. The IRF matrix $\boldsymbol{H^V}$ has been split in two sub components, one constant function $\boldsymbol{H}$ independent of the forward speed and another one $\boldsymbol{H}^*$ proportional to the forward speed only.

$$\boldsymbol{H^V} = \boldsymbol{H} + \boldsymbol{f}(\boldsymbol{V})\boldsymbol{H}^* \tag{8.10}$$

where $\boldsymbol{f}(\boldsymbol{V})$ describes the different relationships for each degree of freedom.

The expression for the IRF $\boldsymbol{H}$ and $\boldsymbol{f}(\boldsymbol{V})\boldsymbol{H}^*$ are summarised in following Table 8.1 and Table 8.2, respectively. Notice that they are given in the b-frame as a function of the IRFs obtained from seakeeping studies. The coordinates, $x_{O'}$ and $z_{O'}$, make reference to the position of origin of the b-frame (body-fixed axes frame) with respect to the origin of the h-frame (horizontal axes frame).

Table 8.1 IRFs for the speed independent term $\boldsymbol{H}$.

| Item | In b-frame |
|---|---|
| $x_u =$ | $-h_{11}^0(t)$ |
| $x_w =$ | $-h_{13}^0(t)$ |
| $x_q =$ | $-h_{15}^0(t) - z_{O'}h_{11}^0(t) + x_{O'}h_{13}^0(t)$ |
| $y_v =$ | $-h_{22}^0(t)$ |
| $y_p =$ | $-h_{24}^0(t) + z_{O'}h_{22}^0(t)$ |
| $y_r =$ | $-h_{26}^0(t) - x_{O'}h_{22}^0(t)$ |
| $z_u =$ | $-h_{31}^0(t)$ |
| $z_w =$ | $-h_{33}^0(t)$ |
| $z_q =$ | $-h_{35}^0(t) - z_{O'}h_{31}^0(t) + x_{O'}h_{33}^0(t)$ |
| $k_v =$ | $-h_{42}^0(t) + z_{O'}h_{22}^0(t)$ |
| $k_p =$ | $-h_{44}^0(t) + z_{O'}(h_{42}^0(t) + h_{24}^0(t)) - z_{O'}^2h_{22}^0(t)$ |
| $k_r =$ | $-h_{46}^0(t) + z_{O'}h_{26}^0(t) - x_{O'}h_{42}^0(t) + x_{O'}z_{O'}h_{22}^0(t)$ |
| $m_u =$ | $-h_{51}^0 - z_{O'}h_{11}^0(t) + x_{O'}h_{31}^0(t)$ |
| $m_w =$ | $-h_{53}(t) - z_{O'}h_{13}(t) + x_{O'}h_{33}(t)$ |
| $m_q =$ | $-h_{55}^0 - z_{O'}(h_{51}^0 + h_{15}^0) + x_{O'}(h_{53}^0 + h_{35}^0) + x_{O'}z_{O'}(h_{31}^0 + h_{13}^0) - z_{O'}^2h_{11}^0 - x_{O'}^2h_{33}^0$ |
| $n_v =$ | $-h_{62}^0 - x_{O'}h_{22}^0$ |
| $n_p =$ | $-h_{64}^0 + z_{O'}h_{62}^0 - x_{O'}h_{24}^0 + x_{O'}z_{O'}h_{22}^0$ |
| $n_r =$ | $-h_{66}^0 - x_{O'}(h_{62}^0 + h_{26}^0) - x_{O'}^2h_{22}^0$ |

Table 8.2 IRFs proportional to the forward speed $\boldsymbol{f(V)H^*}$.

| Item | In b-frame |
|---|---|
| $m_u^* =$ | $+V\int h_{31}^0(t)dt$ |
| $m_w^* =$ | $+V\int h_{33}^0\,dt$ |
| $m_q^*$ | $+V\left(\int h_{53}^0\,dt - x_{O'}\int h_{33}^0\,dt + z_{O'}\int h_{13}^0\,dt\right)$ |
| $n_v^* =$ | $-V\int h_{22}^0\,dt$ |
| $n_p^* =$ | $-V\left(\int h_{24}^0\,dt - z_{O'}\int h_{22}^0\,dt\right)$ |
| $n_r^* =$ | $-V\left(\int h_{62}^0\,dt + x_{O'}\int h_{22}^0\,dt\right)$ |

### 8.5.4 A note on the model of the steady term $F_S$

One of the main objectives is the implementation of the mathematical model at FHR simulator. For this main purpose, as a model for calm water manoeuvres in 6DOF in shallow water has been proposed in Delefortrie et al. (2014), this model is advised by the author for the estimation of $F_S$. However, some modifications are required for the present proposal of manoeuvring in waves, which yields to the following formulation:

$$\begin{bmatrix} X_S \\ Y_S \\ Z_S \\ K_S \\ M_S \\ N_S \end{bmatrix} = \frac{1}{2}\rho L_{PP}^{s} T_M \begin{bmatrix} X'^{(\beta)} & X'^{(\gamma)} & X'^{(\chi)} \\ Y'^{(\beta)} & Y'^{(\gamma)} & Y'^{(\chi)} \\ Z'^{(\beta)} & Z'^{(\gamma)} & Z'^{(\chi)} \\ K'^{(\beta)} & K'^{(\gamma)} & K'^{(\chi)} \\ M'^{(\beta)} & M'^{(\gamma)} & M'^{(\chi)} \\ N'^{(\beta)} & N'^{(\gamma)} & N'^{(\chi)} \end{bmatrix} \begin{bmatrix} u^2 + v^2 \\ u^2 + v_{\mathrm{P}}^2 \\ v^2 + v_{\mathrm{P}}^2 \end{bmatrix} + \begin{bmatrix} 0 \\ 0 \\ 0 \\ K\mathrm{v} \\ 0 \\ 0 \end{bmatrix} \tag{8.11}$$

where $\rho$, $L_{PP}$, and $T_M$ are the water density, the ship's length and draft, respectively. The exponent $s$ is $s = 1$ for forces $X_S$, $Y_S$, $Z_S$, and $s = 2$ for moments $K_S$, $M_S$ $N_S$. $u$ and $v$, stand for the ship's longitudinal and lateral velocity components, respectively, and the reference lateral velocity $v_{\mathrm{P}}$ due to yaw is given by:

$$v_{\mathrm{P}} = rL_{PP}/2 \tag{8.12}$$

$r$ being the ship's yaw angular velocity, and $\beta$, $\gamma$, $\chi$ refer to the hydrodynamic angles, defined by:

$$\beta = \arctan\left(\frac{-v}{u}\right) \tag{8.13}$$

$$\gamma = \arctan\left(\frac{v_P}{u}\right) \tag{8.14}$$

$$\chi = \arctan\left(\frac{v_P}{v}\right) \tag{8.15}$$

Eighteen terms in Eq. (8.11), i.e. $X'(\beta)$ to $N'(\chi)$, are tabular coefficients expressed as function of the hydrodynamic angles $\beta$, $\gamma$, and $\chi$. They express phenomena such as lift, drag, and cross flow effects which are believed to be relevant for the horizontal forces and moments.

To the author's opinion the tabular coefficients in Eq. (8.11) for roll, $K'(\beta)$, $K'(\gamma)$, $K'(\chi)$ and yaw, $N'(\beta)$, $N'(\gamma)$, and $N'(\chi)$, moments are functions of the sway forces, $Y'(\beta)$, $Y'(\gamma)$, $Y'(\chi)$, and their respective positions of their application points. Similarly, the pitch moments $M'(\beta)$, $M'(\gamma)$, and $M'(\chi)$ are functions of the surge forces $X'(\beta)$, $X'(\gamma)$, $X'(\chi)$ and the vertical forces $Z'(\beta)$, $Z'(\gamma)$, $Z'(\chi)$ and their respective application points. Surge and vertical forces, however, contrary to sway forces are expected to be of small order of magnitude because of the streamline design of the ship. It seems then reasonable to assume that they can be neglected or assumed to be already accounted for by squat effects.

In shallow water squat effects are an important phenomenon to be considered. They are of different hydrodynamic nature than the forces described above, they depend on the hydrostatic equilibrium reached as a function of the ship speed and initial bottom clearance. Because the flow is accelerated at the small bottom clearance, the water surface will drop accordingly to satisfy the conservation of mass along the hull, thus inducing a sinkage and trim.

Taking into consideration what has been stated above, at the present stage, the forces in heave and the moments in pitch in Eq. (8.11) are set to zero. This reduced the eighteen terms depending on the hydrodynamic angles in Eq. (8.11) to only twelve. In any case, it is not possible to separate forces and moments arising from the coupling of surged forces in Eq. (8.11) to the ones obtained from squat effects. Hence, these couple forces and moments can be assumed to be accounted for by squat estimation.

Squat dependence on $\gamma$, and $\chi$ are believed to be insignificant, since the lateral velocity is always expected to be small, especially for the case of manoeuvring in waves in access channels. Hence, they influence have been neglected. Bear in mind that they require yet further studies to confirm these assumptions. In the case of

squat effect dependence on $\beta$ a strong influence was found which confirms its importance in the model.

Another important remark resulting from the present study is with respect to the estimation of squat based on the fully captive and semi captive model test. Different results were obtained for the sinkage and trim, with major differences obtained in the trim results. To the authors opinion such differences arose mainly from the fact that the new hydrostatically equilibrium required was not satisfied in the fully captive test. Thus, for the purpose of the evaluation of squat, tests with the model semi-captive is highly advised.

The modelling of squat then followed the practical approach proposed in Tuck (1966), where the sinkage $z_{LCF}$ and trim $\theta_{LCF}$ expressions, given at the longitudinal centre of flotation (LCF) are:

$$Z'^{(\beta)} = z_{LCF}\frac{\mathrm{L}_{PP}^2}{\nabla T u_h} \tag{8.16}$$

$$M'^{(\beta)} = \theta_{LCF}\frac{\mathrm{L}_{PP}^3}{\nabla T u_h}, \tag{8.17}$$

Taking into account that the longitudinal centre of flotation (LCF) is smaller compared to the ship length $L_{PP}$ ($\mathrm{LCF} \ll L_{PP}$), $z_{LCF}$ and $\theta_{LCF}$ can be assumed to be equal to $z$ and $\theta$, as given at the b-frame's origin. In Eq. (8.16) and Eq. (8.17) $\nabla$ is the ship displacement and $L_{PP}$ is the ship length between perpendiculars. The Tuck's parameter $Tu_h$ can be estimated by:

$$Tu_h = \frac{F_{rh}^2}{\sqrt{1-F_{rh}^2}} \tag{8.18}$$

$F_{rh} = V/\sqrt{gh}$ is the depth-based Froude number, $g$ the acceleration of gravity, and $h$ the water depth.

It is important to mention that although squat effects can be referred as forces and moments by hydrostatic equilibrium, to the author's opinion, such representations should not be included in

the solution of the dynamic equation if the modelling of the water level drop has not been accounted for. This is because when the ship attains a new hydrostatic equilibrium a change in the restoring coefficients will be expected, which is, however, not the actual case.

Modelling forces and moments as a function of a hydrostatic change has however worked well; this is because in their analysis, no updates on the hydrostatic forces and moments are conducted taking into account the actual wetted surface; instead constant restoring forces and moments are used. The latter cannot be applied for many reasons to the case of manoeuvring in waves, this is because the squat induced trim and the ship motion will induce a constant change of the wetted surface that needs to be computed each time step. For these main reasons, in the present work, squat effects are suggested to be modelled as an external source of reducing the water depth. The modelling of such a phenomenon in the simulator is still a subject for further research.

With respect to the viscous roll moment, $K\mathrm{v}$ in Eq. (8.11), it has been modelled as suggested in Himeno (1981) by:

$$K\mathrm{v} = K\mathrm{v}_p p + K\mathrm{v}_{p|p|} p|p| \tag{8.19}$$

where $K\mathrm{v}_p$ and $K\mathrm{v}_{p|p|}$ are the linear and nonlinear viscous damping coefficients, respectively, and $p$ is the roll angular velocity.

The nonlinear term was found to be small, and the linear terms speed dependent. These coefficients were not studied in waves, which are believed to have an important contribution, this because the vertical velocities of the flow near the hull (which are important for roll viscous roll moments) will be affected by oscillatory motion of the waves.

## 8.6 Further work

The radiation problem has been simplified and separated in two constant IRF function terms, one being proportional to the ship forward speed. The validation and further evaluation of the relative importance for this function has not been carried out. It should be noticed that these relationships are independent of the ULCC considered for the present study, and can be applied to any other ship type. To the author's opinion this could be better investigated by a comparative analysis of the ULCC and a smaller ship.

From the point of view of the evaluation of the manoeuvring characteristics of the ship, the unified representation of the radiation problem can be further compared against the zero frequency calm water manoeuvring coefficients to evaluate the importance of the change from constant coefficients to the convolution integral representations. Further evaluations with respect to the manoeuvring capability are to compute directional stability, turning cicle ability and zigzag manoeuvres in waves and compare them to their respective estimations in calm water. Changes in the main characteristics of these manoeuvres can be then estimated.

During the development of the experimental program several problems where encountered due to the limitations of the tank main dimensions. Although they have been studied and reduced throughout the process of the present work, they were still present and could not be totally removed. For this main reason, it is of relevant importance to conduct additional experiments in a wider tank to define clear limits and constraints of problems such as tank side wall interaction, which is especially of great significance for the right estimation of the second order forces and moments.

The evaluation of the propeller and rudder operation in waves has been investigated in the present study. However, the analysis was restricted to a few possible combinations of propeller rates and rudder angles that were focused in the characteristics of full

propeller loading condition and maximum rudder angle. To have a broader picture of the propeller and rudder working under the influence of waves, further investigations will require a wider range of propeller loading and rudder angles to cover all possible and relevant combinations.

Experimental studies will be of great use to be extended also for larger angles of wave encounter, to incorporate, for instance, beam waves in the analysis. Such tests were not possible to be conducted in the present study because of the restricted dimensions of the current towing tank at FHR. Experimental analysis with free running models such as turning cicle and zigzag manoeuvres are also of great interest. The above mentioned can be performed in the new facilities of FHR to be ready to use by the years 20209-2021.

A numerical tool for the estimation of wave forces and moments has been developed. However, the diffraction problem has not yet been accounted for and remains a further work. The incorporation of which can be achieved by taking into account the experimental observations. For instance, for the ULCC ship, the motion responses have been found to be irrelevant for second order forces and moments. This can be used to incorporate theoretical simplifications such as the one conducted in the asymptotic theory of Faltinsen et al. (1980).

Moreover, additional studies can be further extended to other ship types and dimensions which will definitely require more insight in their analysis. Notice that the present representation of the unified model is valid for any ship model type and size.

# MANOEUVRING IN COASTAL WAVES



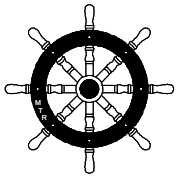

*A scientist in his laboratory is not a mere technician: he is also a child confronting natural phenomena that impress him as though they were fairy tales.*

*Marie Curie*

# 9

# Bibliography

**Abkowitz, M. A.,** 1964. *Lectures on Ship Hydrodynamics – Steering and Manoeuvrability*. Lyngby, Denmark.

**Akimoto, H.,** 2010. *On the Prediction of Ship Performance in Actual Sea Condition Using Computational Fluid Dynamics*. In: proceedings of The International Conference on Marine technology MARTEC 2010, Dhaka, Bangladesh.

**Ankudinov, V.,** 1983. *Simulation Analysis of Ship Motion in Waves.* In: Proceedings of the International Workshop on Ship and Platform Motions. Berkeley, California.

**Araki, M., Umeda, N., Hashimoto, H., and Matsuda, A.,** 2011. *An Improvement of Broaching Prediction With a Nonlinear 6 Degrees of Freedom Model*. Journal of the Japan Society of Naval Architects and Ocean Engineers, 14, 85-96.

**Ayaz, Z., Vassalos, D., and Spyrou, K. J.,** 2006a. *Manoeuvring Behaviour of Ships in Extreme Astern Seas*. Ocean Engineering, 33(17–18), 2381–2434.

**Ayaz, Z., Vassalos, D., and Turan, O.,** 2006b. *Parametrical Studies of a New Numerical Model for Controlled Ship Motions in Extreme Astern Seas*. Journal of Marine Science and Technology, 11(1), 19–38.

**Bailey, P. A., Price, W. C., and Temarel, P.,** 1998. *A Unified Mathematical Model Describing the Manoeuvring of a Ship Travelling in a Seaway*. RINA, 140, 131–149.

**Benjamin, T. B., and Feir, J. E.,** 1967. *The Disintegration of Wave Trains on Deep Water Part 1 Theory*. Journal of Fluid Mechanics, 27(3), 417–430.

**Bishop, R. E. D., Burcher, R. K., and Price, W. G.,** 1973. *The Fifth Annual Fairey Lecture: on the Linear Representation of Fluid Forces and Moments in Unsteady Flow*. Journal of Sound and Vibration, 29(1), 113–128.

**Bishop, R. E. D., Parkinson, A. G., and Price, W. G.,** 1977. *On the Nature of Slow Motion Derivatives*. Journal of Sound and Vibration, 51(1), 111–116.

**Bishop, R. E. D., Price, W. G., and Temarel, R.,** 1984. *A Functional Representation of Fluid Actions on Ships*. International Shipbuilding Progress, 31(361), 239–250.

**Brix, J.,** 1993. *Manoeuvring Technical Manual*. Hamburg: Seehafen-Verlag.

**Bureau Veritas,** 2012. *HYDROSTAR for Experts User Manual.*

**Carrica, P. M., Ismail, F., Hyman, M., Bhushan, S., and Stern, F.,** 2012. *Turn and Zigzag Maneuvers of a Surface Combatant Using a URANS Approach with Dynamic Overset Grids*. Journal of Marine Science and Technology, 18(2), 166–181.

**Carrica, P. M., Mofidi, A., Eloot, K., and Delefortrie, G.,** 2016. *Direct Simulation and Experimental Study of Zigzag Maneuver of KCS in Shallow Water*. Ocean Engineering, 112, 117–133.

**Chen, X.,** 2004. *Hydrodynamics in Offshore and Naval Applications – Part I*. In 6th International Conference on Hydrodynamics, Perth, Australia. pp. 1–28.

**Chen, X.,** 2007. *Middle-Field Formulation for the Computation of Wave-Drift Loads*. Journal of Engineering Mathematics. 59 (1), pp 61–82.

**Cummins, W. E.,** 1962. *The Impulse Response Function and Ship Motions*. Schiffstechnik, 9, 101–109.

**Daugaard, E.,** 1972. *Generation of Regular Waves in The Laboratory*. Technical University of Denmark. PhD thesis.

**Dean, R. G., and Dalrymple, R. A.** 1991. *Water Wave Mechanics for Engineers and Scientists*. World Scientific.

**Delefortrie, G.,** 2007. *Manoeuvring Behaviour of Container Vessels in Muddy Navigation Areas*. Ghent University. Faculty of Engineering. PhD thesis.

**Delefortrie, G., Eloot, K., Vos, S., Peeters, P., and Mostaert, F.,**

2014. *Estuary navigation: 6 DOF Manoeuvring model*. Version 4_0. WL Rapporten, 12_106, FHR: Antwerp, Belgium.

**Delefortrie, G., Eloot, K., Lataire, E., Van Hoydonck, W., and Vantorre, M.,** 2016a. *Captive Model Tests Based 6 DOF Shallow Water Manoeuvring Model*. In 4th MASHCON. Hamburg, Germany, pp. 273–286.

**Delefortrie, G., Geerts, S., and Vantorre, M.,** 2016c. *The Towing Tank for Manoeuvres in Shallow Water*. In 4th MASHCON , Hamburg, Germany, pp. 226–235.

**Delefortrie, G., Tello Ruiz, M., Vantorre, M., Suzuki, T., Peeters, P., and Mostaert, F**., 2016b. *Effect of Wave Induced Phenomena on Manoeuvring of Ships in Shallow Water: Determination of the Transfer Function of the Wave Maker in the Towing Tank for Manoeuvres in Shallow Water*. Version 5.0. FHR Reports, 12_034. Antwerp, Belgium.

**Eloot, K.,** 2006. *Selection, Experimental Determination and Evaluation of a Mathematical Model for Ship Manoeuvring in Shallow Water*. Ghent University. Faculty of Engineering. PhD thesis.

**Eloot, K., & Vantorre, M.,** 2003. *Development of a Tabular Manoeuvring Model for Hull Forces Applied to Full and Slender Ships in Shallow Water*. In MARSIM 2003, pp. RC(18)–1–RC(18)–9

**Faltinsen, O. M., and Løken, A. E.,** 1979. *Slow Drift Oscillations of a Ship in Irregular Waves*. Applied Ocean Research, 1(1), 21–31.

**Faltinsen, O. M., Minsaas, K., Liapis, N., and Skjørdal, S. O.,** 1980. *Prediction of Resistance and Propulsion of a Ship in a Seaway*. In The 13th Symp. on Naval Hyd., Tokyo, Japan. pp. 505–529.

**Fonseca, N., and Guedes Soares, C.,** 2004. *Validation of a Time-Domain Strip Method to Calculate the Motions and Loads on a Fast Monohull*. Applied Ocean Research, 26(6), 256–273.

**Fonseca, N., and Guedes Soares, C.,** 1998. *Time-Domain Analysis and Wave Loads of Large-Amplitude Vertical Ship Motions*. Journal of Ship Research, 42(2), 139–153.

**Fontanet, P.,** 1961. *Théorie de la génération de la houle cylindrique par un batteur plan*. La Houille Blanche, 16(1–2). (In French).

**Gourlay, T.,** 2008. *Slender-Body Methods for Predicting Ship Squat*. Ocean Engineering, 35(2), 191–200.

**Guo, B. J., Steen, S., and Deng, G. B.,** 2012. *Seakeeping Prediction of KVLCC2 in Head Waves with RANS*. Applied Ocean Research, 35, 56–67.

**Grue, J., Clamond, D., Huseby, M., and Jensen, A.,** 2003. *Kinematics of Extreme Waves in Deep Water*. Applied Ocean Research, 25(6), 355–366.

**Hamamoto, M., and Kim, Y.,**1993. *A New Coordinate System and the Equations Describing Manoeuvring Motion of a Ship in Waves*. Journal of the Society of Naval Architectures of Japan, 173, 209–220.

**Hansen, J. B., and Svendsen, I. A.,** 1974. *Laboratory Generation of*

*Waves of Constant Form*. Coastal Engineering, 321–339.

**Himeno, Y.,** 1981. *Prediction of Ship Roll Damping State of the Art*. Ann Arbor, Michigan, USA.

**Hirano, M., Takashina, J., Takeshi, K., and Saruta, T.,** 1980. *Ship Turning Trajectory in Regular Waves*. Transaction of West-Japan Society of Naval Architects, 60, 17–31.

**Hirayama, T., and Kim, S.,** 1994. *Manoeuvrability of a Full Ship in Directional Spectrum Waves of Short Wave Length*. Journal of the Society of Naval Architects of Japan, 129–136.

**Hooft, J. P.,** 1994. *The Cross-Flow Drag on a Manoeuvring Ship*. Ocean Engineering, 21(3), 329–342.

**Hooft, J. P., and Pieffers, J. B. M**., 1988. *Maneuverability of Frigates In Waves*. Marine Technology, 25(4), 262–271.

**Ikeda, Y., Himeno, Y., and Tanaka, N.,** 1977. *On Eddy Making Component of Roll Damping Force on Naked Hull*. Journal of the Society of Naval Architects of Japan, 1977(142), 54–64.

**Imlay, F. H.,** 1961. *The Complete Expressions for "Added Mass" of a Rigid Body Moving in an Ideal Fluid*. David Taylor Model Basin (DTMB) Report 1528.

**Inoue, S., Hirano, M., Kijima, K., and Takashina, J.,** 1981. *A Practical Calculation Method of Ship Maneuvering Motion*. International Shipbuilding Progress, 28(325), 207–222.

**ITTC,** 2011a. *Dictionary of Hydromechanics Alphabetic*. 26th International Towing Tank Conference, 1–144.

**ITTC,** 2011b. ITTC – *Recommended Procedures and Guidelines. Seakeeping Experiments,* 26th International Towing Tank Conference, 1–8.

**ITTC,** 2014. Manoeuvring committee. In Proceedings of the 27th International Towing Tank Conference.

**Journée, J. M. J., and Massie, W. W.,** 2001. *Offshore Hydromechanics.* Delft University of Technology. First Edition.

**Khattab, O.,** 1987. *Ship Handling in Harbours Using Real Time Simulations*. In International Conference on Ship Manoeuvrability–Prediction and Achievement. Gatwick, UK: The Royal Institution of Naval Architects.

**Kijima, K.,** 1987. *Manoeuvrability Of Ship In Confined Water*. In International Conference on Ship Manoeuvrability, London, UK, p. 1–15.

**Kirchhoff, G.,** 1869. *Ueber die Bewegung Eines Rotationskörpers in Einer Flüssigkeit.* Journal Für Die Reine Und Angewandte Mathematik, 71, 237–262.

**Kobayashi, E.,** 1987. *A Simulation Study on Ship Manoeuvrability at Low Speeds*. In International Conference on Ship Manoeuvrability–Prediction and Achievement. Gatwick, UK: The Royal Institution of Naval Architects.

**Kristiansen, E., Hjulstad, Å., and Egeland, O.,** 2005. *State–Space Representation of Radiation Forces in Time–Domain Vessel Models*. Ocean Engineering, 32(17–18), 2195–2216.

**Lamb, S. H.,** 1945. *Hydrodynamics*. Dover Publication, Sixth Edit.

New York, USA.

**Lataire, E.,** 2014. *Experiment Based Mathematical Modelling of Ship-Bank*. Ghent University. Faculty of Engineering. PhD thesis.

**Lee, S.-K.,** 2000. *The Calculation of Zig-Zag Maneuver in Regular Waves with Use of the Impulse Response Functions*. Ocean Engineering, 27(1), 87-96.

**Letki, L., and Hudson, D. A.,** 2005. *Simulation Of Ship Manoeuvring Performance In Calm Water And Waves*. University of Southampton.

**LLoyd, A. R. J. M.,** 1989. *Seakeeping: Ship Behaviour in Rough Weather*. Ellis Horwood Series in Marine technology.

**Madsen, O. S.**, 1971. *On the Generation of Long Waves*. Journal of Geophysical Research, 76(36), 8672-8683.

**Mansuy, M., Tello Ruiz, M., Delefortrie, G., and Vantorre, M.,** 2017. *Post Processing Techniques Study for Seakeeping Tests in Shallow Water*. In the 5th International Conference on Advance Model Measurement Technology for the Maritime Industry Glasgow, UK, pp. 460-473.

**Maruo, H.**, 1957. *The Excess Resistance of a Ship in a Rough Seas*. International Shipbuilding Progress, 4 (35).

**Maruo, H.,** 1960. *the Drift of a Body Floating on Waves*. Journal of Ship Research, 4, 1-10.

**McCreight, W. R.,** 1986. *Ship Manoeuvring in Waves*. In:

Proceedings of the 16th Symposium on Naval Hydrodynamics, 456–469.

**McCreight, W. R.,** 1991. *A Mathematical Model for Surface Ship Maneuvering*. Maryland, Technical Report, David Taylor Research Center, USA.

**Milne-Thomson, L. M.,** 1962. *Theoretical Hydrodynamics*. Fourth edition, Macmillan, London.

**Motora, S., Sugiura, M., Fujino, M., and Suaita, M.,** 1971. *Equivalent Added Mass of Ships in Collisions*. Journal of the Society of Naval Architects of Japan, 7, 138–148.

**Mousaviraad, S. M., Bhushan, S., and Stern, F.,** 2012. *CFD Prediction of Free-Running SES/ACV Deep and Shallow Water Maneuvering in Calm Water and Waves*. In MARSIM2012. Singapore.

**Munk, M.,**1924. *Remarks on the Pressure Distribution Over the Surface of an Ellipsoid, Moving Translationally Through a Perfect Fluid*. NACA Technical Note, (196), 151–160.

**Newman, J. N.,** 1967. *The Drift Force and Moment on Ships in Waves*. Journal of Ship Research, 11, 51–60.

**Newman, J. N.,** 1977. *Marine Hydrodynamics*. MIT Press Cambridge, Mass.

**Newman, J. N.,** 1979. *Theoretical Methods in Ship Manoeuvring*. Proceedings of the Symposium on Advances in Marine Technology, Trondheim.

**Nishimura, K., and Hirayama, T.** 2003. *Manoeuvring and Motion Simulation of a Small Vessel in Waves*. In MARSIM2003, pp. RC-10(1)-RC-10(9).

**Norrbin, N. H.,** 1971. *Theory and Observations on the Use of a Mathematical Model for Ship Manoeuvring in Deep and Confined Waters*. Göteborg, Sweden: Publication of the Swedish State Shipbuilding Experimental Tank.

**Norrbin, N. H.,** 1978. *A Method for the Prediction of the Manoeuvring Lane of a Ship in a Channel of Varying Width*. In Symposium on Aspects of Navigability, Delft, The Netherlands, Vol. 3, pp. 1-18.

**Ogawa, A., and Kasai, H.,** 1978. *On the Mathematical Model of Manoeuvring Motion of Ships*. International Shipbuilding Progress, 25(259), 306-319.

**Ogilvie, T.,** 1964. *Recent Progress Toward the Understanding and Prediction Of Ship Motions*. 5th Symposium on Naval Hydrodynamics.

**Oltmann, P., and Sharma, S. D.,** 1984. *Simulation of Combined Engine and Rudder Maneuvers Using an Improved Model of Hull-Propeller-Rudder Interactions*. 15th Symposium on Naval Hydrodynamics,1-24.

**Ottoson, P., and Bystrom, L.,** 1991. *Simulation of the Dynamics of a Ship Manoeuvring in Waves*. Transaction SNAME, 99, 281-298.

**Otzen, J. F., and Simonsen, C. D.,** 2012. *Development of a Mathematical Model of a High Speed Catamaran Ferry for*

*Simulations in Hard Weather During Arrival Based on PMM and Seakeeping Model Tests*. In International Conference on Marine Simulation and Ship Manoeuvrability, MARSIM2012. Singapore.

**PIANC,** 2012. *Capability of Ship Manoeuvring Simulation Models for Approach Channels and Fairways In Harbours*.

**Salvesen, N., Tuck, E. O., and Faltinsen, O. M.,** 1970. *Ship Motion and Sea Loads*. Transactions SNAME, 78.

**Schoop-zipfel, J., and Abdel-maksoud, M.,** 2011. *A Numerical Model to Determine Ship Manoeuvring Motion in Regular Waves*. In: International Conference on Computational Methods in Marine Engineering MARINE2011. Lisbon, Portugal.

**Seo, M.-G., and Kim, Y.,** 2011. *Numerical Analysis on Ship Maneuvering Coupled with Ship Motion in Waves*. Ocean Engineering, 38(17–18), 1934–1945.

**Shäffer, H. A.,** 1996. *Second-Order Wavemaker Theory for Irregular Waves*. Ocean Engineering, 23(1), 47–88.

**SIMMAN,** 2008, http://www.simman2008.dk/kcs/container.html.

**Skejic, R.,** 2008. *Maneuvering and Seakeeping of a Single Ship and of Two Ships in Interaction*. Norwegian University of Science and Technology. PhD thesis.

**Skejic, R.,** 2013. *Ships Maneuvering Simulations in Seaway- How Close are We to Reality?.* In International Workshop on Next Generation Nautical Traffic Models. Delft, The Netherlands.

**Skejic, R., and Faltinsen, O. M.,** 2008. *A Unified Seakeeping and Maneuvering Analysis of Ships in Regular Waves*. Journal of Marine Science and Technology, 13(4), 371–394.

**Söding, H.,** 1982. *Prediction of Ship Steering Capabilities*. Schifftechnik, 29, 3–29.

**St. Denis, M., and Pierson, W. J.,** 1953. *On the Motions of Ships in Confused Seas*. Transactions of the Society Naval Architects Marine Engineers, 61, 280–357.

**Subramanian, R., and Beck, R. F.,** 2015. *A Time-Domain Strip Theory Approach to Maneuvering in a Seaway*. Ocean Engineering, 104, 107–118.

**Sung, Y. J., Lee, H., Lee, T., and Kim, S.,** 2012. *Captive Model Test and Numerical Simulation on the Manoeuvring Forces in Waves*. In STAB2012, Athens, Greece, pp. 865–876.

**Sutulo, S., and Guedes Soares, C.,** 2006a. *A Unified Nonlinear Mathematical Model for Simulating Ship Manoeuvring and Seakeeping in Regular Waves*. In MARSIM 2006. Terschelling, The Netherlands.

**Sutulo, S., and Guedes Soares, C.,** 2006b. *Numerical Study of Ship Rolling in Turning Manoeuvres*. In STAB 2006. Rio de Janeiro, Brazil.

**Sutulo, S., and Guedes Soares, C.,** 2008. *A Generalized Strip Theory for Curvilinear Motion In Waves*. In Proc. of the 27th International Conference on Offshore Mechanics and Arctic Engineering OMAE2008, Estoril, Portugal., pp. 1–10.

**Taghipour, R., Perez, T., and Moan, T.,** 2008. *Hybrid Frequency–Time Domain Models for Dynamic Response Analysis of Marine Structures*. Ocean Engineering, 35(7), 685–705.

**Tasai, F.,** 1961. *Damping Force and Added Mass of Ships in Heaving and Pitching*. Trans. of the West Japan Society of Naval Architects, 21.

**Taskar, B.,** 2017. *The Effect of Waves on Marine Propellers and Propulsion*. Norwegian University of Science and Technology. PhD thesis.

**Tello Ruiz, M., Mansuy, M., Delefortrie, G., and Vantorre, M.,** 2018. *Manoeuvring Study of a Container Ship in Shallow Water Waves*. In OMAE2018 (paper accepted).

**Tello Ruiz, M., Vantorre, M., and Delefortrie, G.,** 2016a. *Induced Wave Forces on a Ship Manoeuvring in Coastal Waves*. Ocean Engineering 12, 472–491.

**Tello Ruiz, M., Van Hoydonck, W., Delefortrie, G., and Vantorre, M.,** 2017. *Side Wall Effects of Ship Model Tests in Shallow Water*. In 20th Numerical Towing Tank Symposium, Wageningen, The Netherlands, pp. 193–198.

**Tello Ruiz, M., Vantorre, M., Delefortrie, G., Peeters, P., and Mostaert, F.,** 2014. *Effect on Wave Induced Phenomena on Manoeuvring of Ships in Shallow Water: First Progress Report*: February 2014–November 2014. Version 4.0, 14_034. FHR: Antwerp, Belgium.

**Tello Ruiz, M., Vantorre, M., Delefortrie, G., Peeters, P., and Mostaert, F.,** 2015. *Effect of Wave Induced Phenomena on*

*Manoeuvring of Ships in Shallow Water: Second Progress Report: November 2014 – October 2015*. Version 6.0. FHR: Antwerp, Belgium.

**Tello Ruiz, M., Vantorre, M., Van Zwijnsvooorde, T., and Delefortrie, G.,** 2016b. *Challenges With Ship Model Tests in Shallow Water*. In Proceedings of The 12th International Conference on Hydrodynamics, ICHD2016, Egmond aan Zee, The Netherlands, pp.1-10.

**Tuck, E. O.,** 1966. *Shallow-Water Flows Past Slender Bodies*. Journal of Fluid Mechanics, 26, 81-95.

**Ueno, M., Nimura, T., and Miyazaki, H.,** 2003. *Experimental Study on Manoeuvring Motion of a Ship in Waves*. In MARSIM2003. Kanazawa, Japan.

**Ueno, M., Nimura, T., Miyazaki, H., and Nonaka, K.,** 2000. *Steady Wave Forces and Moment Acting on Ships in Manoeuvring in Short Waves*. Journal of the Society of Naval Architects of Japan, 188, 163-172.

**Vantorre, M.,** 1989. *Nauwkeurigheidsoverwegingen en Optimalisatie van de Parameterkeuze bij Gedwongen Maneuvreerproeven met Scheepsmodelen*. Ghent, Belgium: Ghent University.

**Vantorre, M.,** 1997. Genereren, valideren en uitwerken van gedwongen manoeuvreer- en zeegangsproeven. Ghent, Belgium: Ghent University.

**Vantorre, M., and Eloot, K.,** 1996. *Hydrodynamic Phenomena Affecting Manoeuvres at Low Speed in Shallow Navigation*

*Areas*. In 11th International Harbour Congress Antwerp, Belgium: Royal Flemish Society of Engineers, pp. 535–546.

**Vantorre, M., Eloot, K., and Delefortrie, G.,** 2012. *Probabilistic Regulation for Inland Vessels Operating at Sea as an Alternative Hinterland Connection for Coastal Harbours*. European Journal Of Transport And Infrastructure Research, 12(12), 111–131.

**Vantorre, M., and Journée, J.,** 2003. *Validation of the Strip Theory Code SEAWAY by Model tests in Very Shallow Water*. Flanders Hydraulics Research, Numerical Modelling Colloquium.

**Van Zwijnsvooorde, T., Tello Ruiz, M., Delefortrie, G., and Vantorre, M.,** 2018. *Sailing in Shallow Water Waves with the DTC Container Carrier: Open Model Test Data for Validation Purposes*. In 5th International Conference on Ship Manoeuvring in Shallow and Confined Water. Ostend, Belgium. (paper accepted).

**Verwilligen, J., Vantorre, M., Peeters, P., and Mostaert, F.,** 2014. *Vergelijking en Optimalisatie Toegankelijkheidstools Schelde: Deelrapport 3 – AIS-Analyse 2012-2013*. WL Rapporten, 13_015. Waterbouwkundig Laboratorium/Universiteit Gent: Antwerpen.

**Vugts, J. H.,** 1965. *The Hydrodynamic Forces and Ship Motions in Waves*. Delft University Technology. PhD thesis.

**Wang, J., and Wan, D**., 2018. *Direct Simulations of Turning Circle Manoeuver in Waves Using Rans-Overset Method*. In OMAE2018 (paper accepted).

**Wheeler, J. D.,** 1969. *Method for Calculating Forces Produced by Irregular Waves*. Preprints 1969 Offshore Technology Conference, 1(1007), I-83-I-94.

**Yasukawa, H.,** 2006a. *Simulation of Ship Maneuvering in Waves (1st Report: Turning Motion)*. Journal of the Japan Society of Naval Architects and Ocean Engineers, 4, 127-136.

**Yasukawa, H.,** 2006b. *Simulation of Wave-Induced Motions of a Turning Ship*. Journal of the Japan Society of Naval Architects and Ocean Engineers, 4, 117-126.

**Yasukawa, H.,** 2015. *Maneuvering Simulation of A KVLCC2 Tanker in Irregular Waves*. In MARSIM2015. Newcastle, UK.

**Yasukawa, H., and Adnan, F. A.,** 2006. *Experimental Study on Wave-Induced Motions and Steady Drift Forces of an Obliquely Moving Ship*. Journal of the Japan Society of Naval Architects and Ocean Engineers, 3, 133-138.

**Yasukawa, H., and Nakayama, Y.,** 2009. *6-DOF Motion Simulations of a Turning Ship in Regular Waves*. In MARSIM2009. Panama.

**Yu, Z., and Falnes, J.,** 1995. *State-Space Modelling of a Vertical Cylinder in Heave*. Applied Ocean Research, 17, 265-275.

**Zakharov, V. E., and Ostrovsky, L. a.,** 2009. *Modulation Instability: The Beginning*. Physica D: Nonlinear Phenomena, 238(5), pp. 540-548.

**Zhang, W., Zou, Z. J., and Deng, D. H.,** 2017. *A Study on Prediction of Ship Maneuvering in Regular Waves*. Ocean Engineering, 137, 367-381.

# MANOEUVRING IN COASTAL WAVES



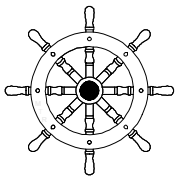

*To know what you know and what you do not know, that is true knowledge.*

*Confucius*

# A

# Appendices

## A.1 The convolution integral

### A.1.1 Mathematical definition

The convolution of a function $x(t)$ with the delta Dirac function $\delta(t)$ results in the same function $x(t)$

$$x(t) = \int_{-\infty}^{+\infty} x(\tau)\,\delta(t-\tau)d\tau \tag{A.1}$$

$$x(t) = \sum_{p=-\infty}^{+\infty} x(n_p)\delta(t-n_p)\Delta n \tag{A.2}$$

Eq. (A.1) and Eq. (A.2) show the continuous and discrete representations of this particular property. This can be also expressed in a more convenient form as:

$$\delta(t) \rightarrow h(t) = h(t) * \delta(t) = h(t) \tag{A.3}$$

where $\int_{-\infty}^{+\infty} \delta(t)dt = 1$.

Hence, $h(t) * \delta(t)$ represents the convolution of $h(t)$ with $\delta(t)$.

Now, if one considers a linear system $h(t)$ where the principle of superposition is valid as depicted in Figure A.1, and using as input to the linear system the expanded version of the discrete representation of $x(t)$, in terms of the convolution as given by:

$$x(t) = \cdots + x(n_p)\delta(t - n_p)\Delta n + x(n_{p+1})\delta(t - n_{p+1})\Delta n + \cdots \quad \text{(A.4)}$$

where $\delta(0)\Delta n = 1$

Then the convolution of $h(t)$ with $x(t)$ can be expressed as:

$$h(t) * x(t) = h(\ldots + x(n_p)\delta(t - n_p)\Delta n + x(n_{p+1})\delta(t - n_{p+1})\Delta n + \cdots) \quad \text{(A.5)}$$

The right hand side expression, $x(n_p)$, $x(n_{p+1})$, are constant discrete values of $x(t)$. Now taking into account the superposition principle of a linear system, the equation above can be written as:

$$h(t) * x(t) = \cdots + x(n_p)h\left(\delta(t - n_p)\right)\Delta n + x(n_{p+1})h\left(\delta(t - n_{p+1})\right)\Delta n$$

$$+ \cdots = \sum_{p=-\infty}^{+\infty} x(n_p)h\left(\delta(t - n_p)\right)\Delta n$$

$$= \sum_{p=-\infty}^{+\infty} x(n_p)h(t - n_p)\Delta n \quad \text{(A.6)}$$

And by taking the limits we have:

$$h(t) * x(t) = \lim_{\Delta n \to 0} \sum_{p=-\infty}^{+\infty} x(n_p)h(t - n_p)\Delta n = \int_{-\infty}^{+\infty} x(\tau)\, h(t - \tau)d\tau \quad \text{(A.7)}$$

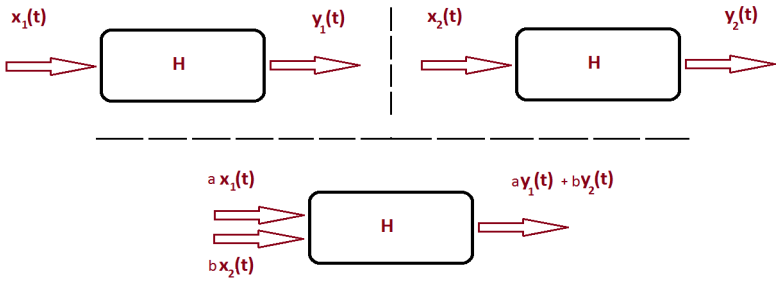


Figure A.1 Sketch illustrating the representation of a linear system.

### A.1.2 The impulse response function

The Fourier pairs applied to the impulse response function can be written as:

$$h_{kj}(t) = \frac{1}{2\pi}\int_{-\infty}^{+\infty} F(\omega)\, e^{i\omega t} d\omega \qquad F(\omega) = \int_{-\infty}^{+\infty} h_{kj}(t)\, e^{-i\omega t} dt \quad \text{(A.8)}$$

Considering the Fourier relationships displayed in (A.8), the real and imaginary parts of $F(\omega)$in the frequency domain are:

$$R(\omega) = +\int_{-\infty}^{\infty} h_{kj}(t)\cos(\omega t)\, dt \quad \text{(A.9)}$$

$$X(\omega) = -\int_{-\infty}^{\infty} h_{kj}(t)\sin(\omega t)\, dt \quad \text{(A.10)}$$

where is given by $F(\omega) = R(\omega) + iX(\omega)$.

From the relationships above, the following condition applies to the real and imaginary frequency components:

$$R(-\omega) = R(\omega) \qquad \text{(even)} \quad \text{(A.11)}$$

$$X(-\omega) = -X(\omega) \qquad \text{(odd)} \quad \text{(A.12)}$$

Introducing Eq. (A.11) and (A.12) in the inverse Fourier transform of function $h_{kj}(t)$, the relationship can be reduced to:

$$h_{kj}(t) = \frac{1}{\pi}\int_{0}^{+\infty} (R(\omega)cos(\omega t) - X(\omega)\sin(\omega t))d\omega \quad \text{(A.13)}$$

Now, considering that any real function can be expressed as a sum of an even ($he$) and odd ($ho$) functions, hence, $h_{kj}(t)$ can be rewritten as:

$$h_{kj}(t) = he_{kj}(t) + ho_{kj}(t) \quad \text{(A.14)}$$

Where: $he$ and $ho$ are given by:

$$he_{kj}(t) = \frac{h_{kj}(t) + h_{kj}(-t)}{2} \quad \text{(A.15)}$$

$$ho_{kj}(t) = \frac{h_{kj}(t) - h_{kj}(-t)}{2} \tag{A.16}$$

Note that $h_{kj}(-t) = 0$ because $h_{kj}(t)$ is a real and causal function ($\forall\, t < 0 : h_{kj}(t) = 0$), thus:

$$h_{kj}(t) = 2he_{kj}(t) = 2ho_{kj}(t) \tag{A.17}$$

Recall that for even and odd functions, as described for $R(\omega)$ and $X(\omega)$ in Eq. (A.11) and (A.12), the following properties apply:

$$he_{kj}(-t) = he_{kj}(t) \qquad ho_{kj}(-t) = -\,ho_{kj}(t) \tag{A.18}$$

Using these relationships, real and imaginary components of the Fourier transforms of $he_{kj}$ and $ho_{kj}$ can be expressed as follows:

$$R_{he}(\omega) = +\int_{-\infty}^{\infty} he_{kj}(t)\cos(\omega t)\,dt = 2\int_{0}^{\infty} he_{kj}(t)\cos(\omega t)\,dt \tag{A.19}$$

$$X_{he}(\omega) = -\int_{-\infty}^{\infty} he_{kj}(t)\sin(\omega t)\,dt = 0 \tag{A.20}$$

$$R_{ho}(\omega) = +\int_{-\infty}^{\infty} ho_{kj}(t)\cos(\omega t)\,dt = 0 \tag{A.21}$$

$$X_{ho}(\omega) = -\int_{-\infty}^{\infty} ho_{kj}(t)\sin(\omega t)\,dt = -2\int_{0}^{\infty} he_{kj}(t)\sin(\omega t)\,dt \tag{A.22}$$

and the respective time domain pairs, using the inverse Fourier transform, are expressed as:

$$he_{kj}(t) = \frac{1}{2\pi}\int_{-\infty}^{+\infty} R_{he}(\omega)\,e^{i\omega t}d\omega = +\frac{1}{\pi}\int_{0}^{+\infty} R_{he}(\omega)\cos(\omega t)d\omega \tag{A.23}$$

$$ho_{kj}(t) = \frac{1}{2\pi}\int_{-\infty}^{+\infty} iX_{ho}(\omega)\,e^{i\omega t}d\omega = -\frac{1}{\pi}\int_{0}^{+\infty} X_{ho}(\omega)\sin(\omega t)d\omega \tag{A.24}$$

Recall that $h_{kj}(t) = he_{kj}(t) + ho_{kj}(t)$, hence $h_{kj}(t)$ can be expressed as the sum:

$$h_{kj}(t) = \frac{1}{\pi}\int_{0}^{+\infty} R_{he}(\omega)\cos(\omega t)d\omega - \frac{1}{\pi}\int_{0}^{+\infty} X_{ho}(\omega)\sin(\omega t)d\omega \tag{A.25}$$

Previous analysis showed, see Eq. (A.13):

$$h_{kj}(t) = \frac{1}{\pi}\int_0^{+\infty} R(\omega)cos(\omega t)d\omega - \frac{1}{\pi}\int_0^{+\infty} X(\omega)\sin(\omega t)\,d\omega \tag{A.26}$$

Comparing the similar terms in Eq. (A.25) and (A.26): $R(\omega) = R_{he}(\omega)$, $X(\omega) = X_{ho}(\omega)$. Now, introducing this in Eq. (A.24) and taking into $h_{kj}(t)$ can be expressed as $h_{kj}(t) = 2he_{kj} = 2ho_{kj}(t)$, see Eq. (A.17). The following relationship is obtained:

$$h_{kj}(t) = +\frac{2}{\pi}\int_0^{+\infty} R(\omega)\cos(\omega t)d\omega = 2he_{kj}(t) \tag{A.27}$$

$$h_{kj}(t) = -\frac{2}{\pi}\int_0^{+\infty} X(\omega)\sin(\omega t)d\omega = 2ho_{kj}(t) \tag{A.28}$$

$$h_{kj}(0^+) = h_{kj}(0^+) \tag{A.29}$$

It is important to remember that $h_{kj}(t)$ is now entirely defined for all $t$ because of its causality (see below). In addition, based on the relationship described above, the relevant values of the frequency components $R(\omega)$ and $X(\omega)$ at zero and infinite frequency can be described:

$$h_{kj}(t) = \begin{cases} h_{kj}(t), & x \geq 0 \\ 0, & x < 0 \end{cases} \tag{A.30}$$

$$R(\omega) = \begin{cases} R(0), & \omega = 0 \\ \approx 0, & \omega = \infty \end{cases} \tag{A.31}$$

$$X(\omega) = \begin{cases} 0, & \omega = 0 \\ \approx 0, & \omega = \infty \end{cases} \tag{A.32}$$

# List of Figures

# List of Tables